# Cooperative Science and Monitoring Initiative (CSMI) Lake Ontario 2018

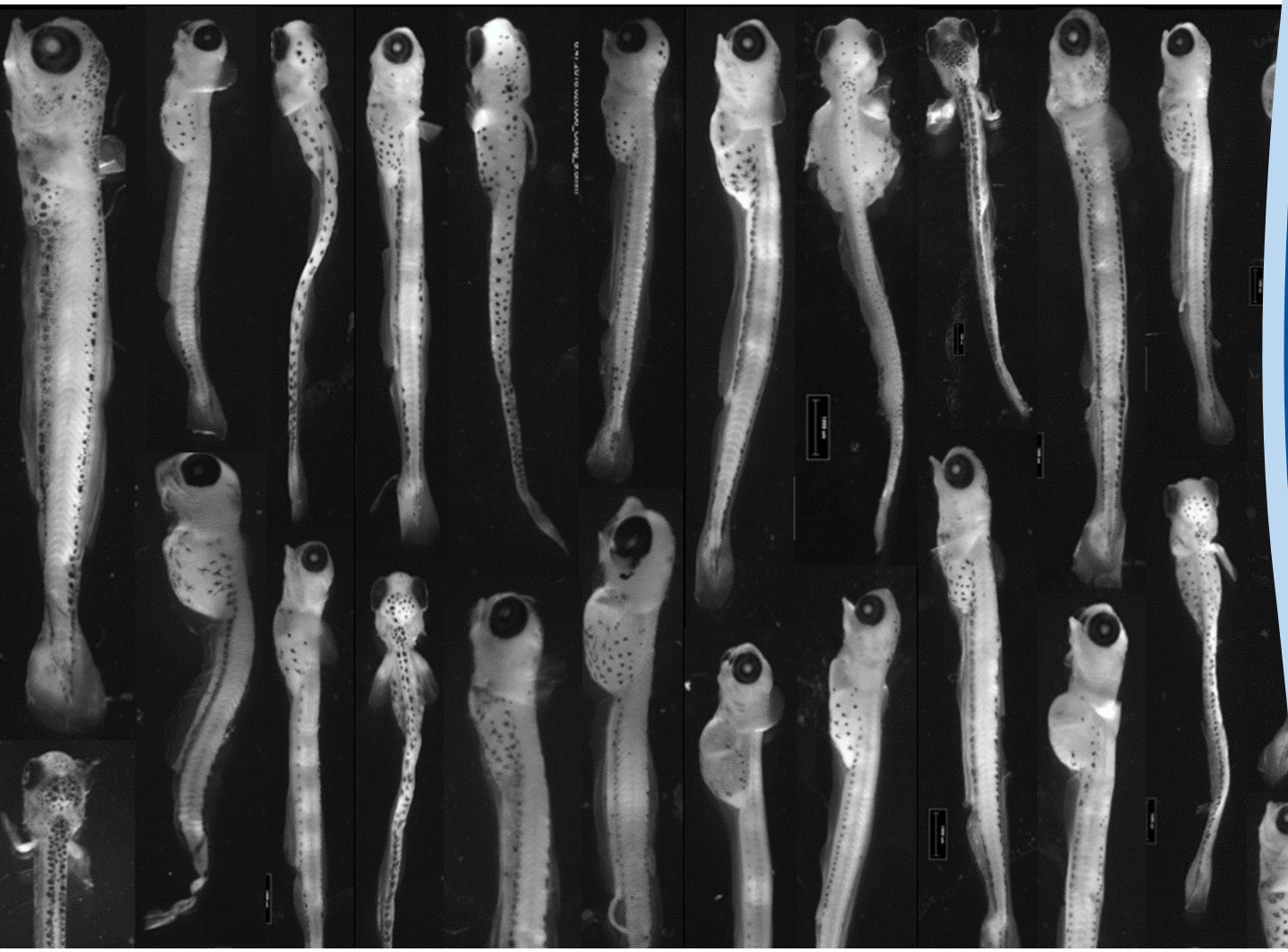

*Photo : Taylor Brown, Cornell University*

CSMI Lake Ontario

www.nyseagrant.org

**Report Edited by:**


Stacy Furgal
Great Lakes Fisheries & Ecosystem Health Specialist
New York Sea Grant
SUNY Oswego, Penfield 4
Oswego, NY 13126
Phone: 315.312.3045
slf85@cornell.edu

Paris Collingsworth
Great Lakes Ecosystem Specialist
Illinois-Indiana Sea Grant
Purdue University
195 Marsteller Street
West Lafayette, IN 47907-2033
Phone: 312.886.7449
pcolling@purdue.edu


Sea Grant New York

NOAA National Oceanic and Atmospheric Administration U.S. Department of Commerce

Sea Grant ILLINOIS-INDIANA

# Table of Contents

## Executive Summary

S. Furgal New York Sea Grant and P. Collingsworth IL/IN Sea Grant

The Cooperative Science and Monitoring Initiative (CSMI) is a binational effort to provide enhanced monitoring and research activities across the Laurentian Great Lakes that addresses the science priorities of the Lake Partnerships established under the Lakewide Management Annex of the 2012 Great Lakes Water Quality Agreement (GLWQA). The Lake Ontario Partnership is a collaborative team of natural resource managers from federal, state, provincial and municipal governments, tribal governments, and watershed management agencies that is charged with developing long term ecosystem-based management strategies for protecting and restoring the Lake Ontario ecosystem. On a practical level, CSMI offers the Lake Partnerships an opportunity to collect timely information about the health and status of the lake in a way that will help them better manage the lake ecosystem. The following is an executive summary of the 2018 research results from Lake Ontario and the associated white paper containing reports with more specific information on individual research projects. These results represent primarily GLRI-funded efforts by US partners.

A main goal of the Lake Ontario Partnership in setting the 2018 Lake Ontario CSMI priorities was to collect information to improve understanding of nutrient loading impacts and aquatic invasive species impacts on water quality and the aquatic food web at a lake-wide scale to inform management decisions, including the 2020-2021 Great Lakes Water Quality Agreement (GLWQA) Nutrients Annex review of phosphorus substance objectives for Lake Ontario. The scope of the 2018 CSMI priorities included the Niagara River, Lake Ontario, and the Upper St. Lawrence River.

The following science and monitoring priorities were developed by the Lake Partnership for 2018 CSMI:

1) Characterize nutrient concentrations in nearshore and offshore waters and loadings from tributaries, point and non-point sources.
2) Improve understanding of nearshore nutrient-related problems, including the role of internal phosphorus loadings in driving Cladophora biomass and production and the characterization of triggers of cyanobacterial blooms in nearshore and embayment areas.
3) Evaluate aquatic food web status, including lake-wide assessments of primary production, phytoplankton, zooplankton, mysids, and Dreissenid mussels and other benthic organisms.
4) Improve understanding of fish dynamics, including nearshore fish ecology, evaluation of methods to quantify prey fish distribution during critical life history periods, expanded use of existing techniques and technologies (e.g., acoustic telemetry, angler surveys) to fill knowledge gaps.
5) Characterize LAMP critical and emerging contaminants (i.e., PCBs, Mercury, DDT, Mirex, Dieldrin/Aldrin, Dioxin) in atmospheric deposition, water, fish tissue, biota, and sediment.

6) Evaluate coastal wetland status, including status of Lake Ontario LAMP coastal wetland indictors.

The main results from GLRI-funded 2018 CSMI efforts to address these priorities are summarized in the following sections by major CSMI priority theme. Full reports from the primarily GLRI-funded research groups that participated in 2018 CSMI investigations are included in this synthesis report, after the executive summary.

## Nutrient Concentrations and Nearshore Delineation

One of the primary knowledge gaps in Lake Ontario is how spatial differences in tributary nutrient loading affects water quality and food web processes in nearshore and offshore habitats. Previous studies have estimated that more than half of Lake Ontario's nutrient loads enter the lake via the Niagara River, where the prevailing winds and along-shore currents in the western basin of the lake tend to entrain these nutrients into nearshore habitats along Lake Ontario's south shore to the detriment of nearshore water quality. Further to the west, in Ontario's "Golden Horseshoe" area, the large and rapidly growing urban areas that spread along the western shore of Lake Ontario are a source of elevated nutrients that drive localized negative impacts on nearshore water quality. High nutrient levels can have a negative impact on food webs and water quality in nearshore areas, as evidenced by reports of increasing nuisance levels of the benthic algae *Cladophora* in nearshore areas of Lake Ontario. In contrast to the nutrient surplus issues that define nearshore habitats, the offshore waters of Lake Ontario are oligotrophic. Lake Ontario spring mean open water total phosphorus concentrations have been below the 10 µg/L GLWQA interim substance objective for almost two decades. Low nutrient levels in offshore habitats have led to concern among fisheries managers that the biomass of phytoplankton and zooplankton at the base of the offshore food web have declined to the point where Lake Ontario may soon risk losing its ability to support desirable fisheries.

In the Great Lakes, study areas are often categorized as nearshore and offshore, however, the transition zone between these two extremes is dynamic. Understanding what defines the boundaries of these zones is extremely important for creating and calibrating models, but often relies on traditional sampling methods that can be limited spatially, temporally, or both. In 2018, an autonomous glider was used to assess water quality parameters in southern Lake Ontario between the Niagara River and Rochester, NY. The glider was deployed twice, each for a three-week sampling time period. Sensors collected data for temperature, conductance, Chl-a, optical backscatter and colored dissolved organic matter CDOM concentration. Each deployment resulted in the collection of over 3000 vertical water profiles. Findings indicate that two parameters, water temperature and Chl-a, can be used for defining the boundaries of the coastal nearshore and the offshore zones. In the early summer, the boundary is defined by elevated surface Chl-a at the thermal front where nearshore waters (stratified by temperature) interact with offshore waters that are isothermal (completely mixed). In the late summer, the boundary is defined by elevated Chl-a below the thermocline, and the formation of the deep chlorophyll layer in offshore waters.

Based on data collected, the transition zone between nearshore and offshore regions was determined to occur over a coastal zone that extended 10-15 km from shore. By using a glider, observations of water quality parameters were made across a much larger spatial scale than could have been achieved using traditional sampling techniques. Deploying the glider for a long duration of time allowed for a more comprehensive and nuanced view of the boundary zone between the nearshore and offshore zones as it fluctuated throughout the sampling period.

## Aquatic Food Web Status

### *Phytoplankton*

Phytoplankton are the base of the food web in aquatic ecosystems and community composition at this trophic level can serve as an indicator of ecosystem health. In 2018, CSMI researchers sampled phytoplankton in Lake Ontario by collecting integrated water column samples in shallow, nearshore habitats and deeper offshore locations during the months of April and August, in conjunction with the EPA Great Lakes Biology Monitoring Program surveys, to characterize spring and summer conditions. During the summer, additional samples were collected in deeper areas of the lake that were targeted to collect phytoplankton in the deep chlorophyll layer (DCL). This layer of deep primary production is understudied in the Great Lakes but may be an important source of food for zooplankton in the offshore waters of oligotrophic lakes, such as the Great Lakes.

Overall phytoplankton abundance was higher in the summer than in the spring, a phenomenon that is becoming increasingly common in the Great Lakes. The spring phytoplankton community in nearshore habitats of Lake Ontario was largely comprised of centric diatoms and chrysophytes whereas the offshore phytoplankton community was dominated by large-celled dinoflagellates. During the summer, integrated water column samples indicated that the phytoplankton communities in both nearshore and offshore waters were comprised primarily of cyanobacteria, but both habitats also contained a mixture of dinoflagellates, cyanophytes, cryptophytes and pennate diatoms. While phytoplankton composition of the nearshore and offshore was similar in summer integrated samples, the phytoplankton community in the DCL was comprised mostly of pennate diatoms and cryptophytes and had a notably lower cyanophyte biovolume, possibly a result of their buoyancy that did not allow them to sink into the DCL. Overall, results from CSMI suggest that the phytoplankton community is relatively healthy, but the diminished spring bloom and a high biovolume of cyanophytes during the summer indicate that the potential for food web disruption exists in the system.

### *Zooplankton*

Further up the food chain, grazing and predator zooplankton and macroinvertebrates represent an important link between primary production and higher trophic level consumers such as fish. Zooplankton and mysid samples were collected from the EPA R/V Lake Guardian lake-wide surveys in April, June, August, and September and from the CCG Limnos lakewide survey in July during 2018, with seasonal sampling of one transect in the far west. The New York State Department of Environmental Conservation (NYSDEC) Biomonitoring Program performed monthly (April-October) nearshore and offshore sampling on the southern shore using traditional

nets as well as high resolution Laser Optical Plankton Counter methods. Overall, the status of offshore zooplankton within Lake Ontario can be classified as "good". There was a decline in biomass from 1997-2018, however at this time, the amount of zooplankton biomass in offshore waters is still sufficient to support higher trophic levels. Like the upper Great Lakes, the zooplankton species community has shifted from predominately cladocerans and cyclopoid copepods to predominately calanoid copepods. Density of mysids over the time series remains high and stable compared to Lakes Michigan and Huron.

The 2018 CSMI sampling effort for zooplankton and mysids was spatially and temporally extensive, providing more insight to the seasonal development of zooplankton biomass than is possible from the April and August US EPA GLNPO Great Lakes Biology Monitoring Program sampling design. The timing of dreissenid mussel veliger release was identified as October of 2018, with the greatest density in the western basin. Peak abundances of invasive predatory cladocerans, *Bythotrephes* and *Cercopagis*, occurred in July and September, respectively. Other rare catches of note include the discovery of two nonnative microcrustacean species new to Lake Ontario; the benthic harpacticoid copepod species *Schizopera borutzkyi* and *Heteropsyllus nunni*, neither of which had been documented in the lake prior to this 2018 sampling event.

### *Benthic Community*

Similar to zooplankton in the water column, benthic invertebrates in the sediment can reveal information about the health of a lake ecosystem and the food webs that are supported therein. To help assess overall ecosystem health in Lake Ontario, a lake-wide survey of benthic macroinvertebrates was conducted as part of the CSMI field year in 2018. Overall, 87 taxa (species, genera or higher taxa) of benthic macroinvertebrates were sampled in Lake Ontario, with the most diverse taxa being Oligochaeta, Chironomidae, Malacostraca, and Bivalvia. By far, the most widely abundant species throughout the lake was the invasive bivalve *Dreissena r. bugensis*, which was found at all of the 55 benthic stations sampled. Other widely distributed taxa included Oligochaeta, *Mysis*, and chironomids. The current distribution of benthic organisms revealed major long-term changes in densities of benthic macroinvertebrates in Lake Ontario. For example, there were major declines in *Diporeia* and Sphaeriidae across all depth zones sampled in 2018. These declines started in the mid-1990s, following a period of elevated densities in the late 1980s – early 1990s that was likely driven by a period of eutrophication in Lake Ontario. Similar to Lakes Michigan and Huron, *Diporeia* is only present in Lake Ontario in the deepest parts of the lake (>90 m) and the remnant populations that exist are at extremely low densities (<1 $m^{-2}$). The highest densities of Oligochaeta were observed in 1964 (approximately 10,000 $m^{-2}$), and they declined in the 1970s and 1980s, mostly due to the large decrease in pollution-tolerant Tubificid oligochaetes in shallow zones. Oligochaeta are another taxa that have experienced fluctuations in population densities through the decades in Lake Ontario, reaching peak densities in the 1960's, followed by declines in the 1970's and 1980's and then increasing again during the 1990s after the establishment of dreissenids. They declined somewhat in the late 2000s, but their densities have again been increasing over the past decade. The only benthic taxa that showed long-term increases in density were *Dreissena* and Chironomidae, which have increased significantly at intermediate (>30 – 90 m) depths.

### *Dreissenid Mussels*

The lake-wide average *Dreissena* biomass in 2018 was the highest ever observed in Lake Ontario (at 25.2±3.3 g $m^{-2}$ of ash-free dry tissue weight). During the 2018 CSMI benthic survey for Lake Ontario, videos from 59 Ponar stations and 57 benthic sled tows were collected from the EPA R/V Lake Guardian and used to estimate *Dreissena* distribution in the lake and were compared to results from standard Ponar sampling. The results from this effort indicate that *Dreissena* coverage was higher at intermediate depths (between 30 and 100 m) than at both shallow (< 30 m) and deep (> 100 m) areas. One of the drawbacks of using video to sample *Dreissena* is that very small mussels (< 10 mm) were difficult to detect in underwater images, resulting in lower *Dreissena* densities in sled tow videos compared to Ponar grabs when high abundances of small mussels were present. However, *Dreissena* biomass estimated from Ponar grabs and video transects were almost identical. Moreover, at the larger scale (i.e. depth zones), difference in density and biomass estimations were non-significant between sled tow videos and Ponar grabs. These results underscore the value that may be added to *Dreissena* monitoring efforts by incorporating underwater video imagery in monitoring, especially in areas where Ponar sampling is not possible (e.g. rocky bottom habitats).

Quagga mussel body condition was calculated using samples collected from 12 sites during the 2018 CSMI benthic survey. These sites were representative of different lake depths and basins. Length-weight relationships were used to determine body condition. Significant depth-specific length-weight relationships were discovered, with the heaviest mussels occurring at < 30 m, the lightest mussels at 51-90 m, and intermediate weight mussels at >90 m, these measurements allowed researchers to update lake-wide estimates of quagga mussel body condition.

An *in-situ* experiment was used to quantify year-round dreissenid mussel growth in Lake Ontario. This was part of a multi-year, multi-lake study that also included Lake Michigan and Lake Huron. Experimental cages at three locations were attached to moorings at three different depths (15 m, 45 m, 90 m) in southeastern Lake Ontario near Oswego, NY. Moorings were deployed in June 2018, serviced in November 2018, and retrieved in May 2019. Key results include that quagga mussel growth potential was correlated to depth, with mussels having high growth potential at 15 m, intermediate growth potential at 45 m, and lowest growth potential at 90 m. Initial shell length was correlated with mussel growth at 15 m, but not the other depths. Differences recorded in water temperature and chlorophyll, even when small, led to significant differences in mussel growth. This experiment provided approximately one full year of growth data, which included data from the often-understudied fall and winter periods.

Mussels in the shallowest sampling locations were the heaviest and had the highest growth potential, indicating these locations provide the most favorable conditions for growth.

## Understanding of Fish Dynamics:

The re-establishment of healthy native fish communities is one of the primary goals of fisheries managers across the Great Lakes Basin. Coregonines, a group of native planktivores that were once common across the Great Lakes, are of particular interest in these efforts and knowledge about existing stocks of coregonines in Lake Ontario was an important priority of the

2018 CSMI field year. The lake-wide sampling effort in 2018 was the largest and most spatially comprehensive survey of larval coregonines (cisco and lake whitefish) ever undertaken. Partners in the U.S. and Canada conducted lake-wide sampling that included sites in the nearshore and offshore zones on both the northern and southern shores. Larval fish densities in ichthyoplankton tows were used as a proxy to provide a metric of regional spawning success. Species-specific environmental drivers were evaluated using models to hypothesize which factors contribute to successful coregonine recruitment to the larval stage.

Catches from the 1000+ ichthyoplankton tows completed over the 34-day sampling period revealed that the highest catch per unit effort (CPUE) of coregonine larvae was found in the eastern basin of the lake, however, the presence of larvae in other locations indicates that successful spawning is occurring in other locations as well, just at much lower densities. Over half of all coregonine larvae captured came from a single location, Chaumont Bay, in the NY waters of the eastern basin of the lake. Genetic barcoding was successfully used to differentiate cisco from lake whitefish. The coregonine larvae caught were almost entirely cisco, with only 6% identified as lake whitefish. All coregonine larvae were collected at nearshore locations. Among other species, notable catches of burbot and deepwater sculpin larvae were made, which have never been collected in larval samples in Lake Ontario before. They are both native species of conservation interest. Results from modeling indicated that day of year, distance to shore, and ice cover duration were most strongly supported as being associated with larval cisco catches. For larval lake whitefish catches, water temperature, site depth, and ice cover duration were most strongly supported by the models as drivers of larval catch. Results from this project have been used to inform coregonine management and have served as the catalyst for current and pending projects aimed at coregonine habitat assessment and restoration efforts.

## Critical and Emerging Pollutants

An intensive sampling campaign was performed during the 2018 CSMI field year as part of the Great Lakes Fish Monitoring and Surveillance Program (GLFMSP) to quantify paired contaminant/food web markers in an effort to assess the contaminant levels in ambient waters and contaminant burdens in macroinvertebrates, prey and top predator fish species The overarching goal of this effort was to assess biomagnification of legacy contaminants and chemicals of emerging concern in the food web to quantify impacts to the aquatic ecosystem.

Mercury concentrations followed a traditional bioaccumulation trend with levels increasing with trophic level at the Oswego and North Hamlin GLFMSP sampling sites. Lake trout contained the highest mercury levels (87$\pm$ 14 µg/kg and 114 $\pm$ 37 µg/kg, respectively) followed by deepwater sculpin, alewife, round goby and rainbow smelt, respectively. Concentrations were greater at the Oswego site for prey fish while lake trout contained higher concentrations at the North Hamlin site.

Dissolved per- and polyfluoroalkyl substances (PFAS) in surface waters were measured in 2018 at the North Hamlin site only. The shorter chain (more water soluble) carboxylic acids perfluorobutanoic (PFBA), perfluoroheptanoic (PFHpA) and perfluorooctanoic (PFOA) acids were found at 2.7 $\pm$ 0.28 ng/L, 2.1 $\pm$ 0.10 ng/L and 2.8 $\pm$ 0.6 ng/L, respectively. Several perfluoroalkyl sulfonic acids including, perfluorobutane (PFBS), perfluorohexane (PFHxS) and

perfluorooctane (PFOS) sulfonic acids were observed at 1.2 ± 0.1 ng/L, 1.57 ± 0.04 ng/L, and 2.6 ± 0.5 ng/L, respectively. The longer chain (less water soluble) perfluoroalkyl carboxylic acids (> 11 carbons) and perfluoroalkyl sulfonic acids (>10 carbons) were below detection limits. In general, the level of PFAS measured in 2018 were about an order of magnitude lower than values reported by Martin (2004).

Perfluorooctane sulfonic acid (PFOS) was detected in all of the sampled seston, macroinvertebrates (pelagic and benthic) and fish in 2018. The sulfonic acids accounted for > 60% of the PFAS, with PFOS as the dominant component. Among all of the fish species collected, the highest total PFAS concentration (∑PFAS) was observed in deepwater sculpin and not the top predator (lake trout) in Lake Ontario, contrary to what would be expected for traditional bioaccumulative contaminants (i.e., mercury above). The deepwater sculpin PFOS concentrations observed at North Hamlin and Oswego sites were still lower than reported in previous studies. After deepwater sculpin then lake trout, ∑PFAS values decreased from prey fish (alewife, rainbow smelt, and round goby) to invertebrates such as *Mysis* and zooplankton.

## Coastal Wetland Status

Coastal wetlands are valuable, multi-functional resources that have historically provided large numbers of important ecosystem goods and services in the Great Lakes. However, many of the coastal wetlands have been degraded by altered hydrological regimes that promote dense and aggressive infestations by cattails (*Typha* spp). Long-term management of these wetland resources that would support the historical plant structure and ecological function of these degraded ecosystems requires timely and accurate monitoring. Traditional surveying and mapping of coastal wetlands has been accomplished using field-based surveys and/or photointerpretation, but these methods tend to be resource- and cost-intensive. In 2018, CSMI researchers tested remote sensing applications using hyperspectral imagery and high-resolution true-color imagery to provide updated wetland classifications for Lake Ontario coastal wetlands. Remote sensing data was compared to existing field-collected vegetation survey data from the EPA Great Lakes Coastal Wetland Monitoring Program (GLCWMP) to generate wetland classification data with a high level of precision.

With further refinement, the methods developed in this study hold promise for efficient inventorying and monitoring of Great Lake coastal wetland resources across the basin and may be used to assess the effectiveness of adaptive management strategies. Reliable and recent field data and GLCWMP data played a key role as part of the training dataset for this study. This work demonstrates how existing data from monitoring programs can be leveraged in the development of new wetland assessment and classification methods.


## Acknowledgement:

Funding for this report was provided by the Great Lakes Restoration Initiative through a grant to IISG from NOAA.

# Autonomous underwater glider observations in southern Lake Ontario and Niagara plume

**Paul McKinney, Tom Hollenhorst, Joel Hoffman U.S. EPA**

## Abstract

We assessed alongshore and cross-shore gradients in water quality parameters in southern Lake Ontario in early and late summer 2018 using data acquired during two three-week Slocum autonomous glider deployments. Each deployment resulted in over 3000 vertical profiles of the water column. The early summer cross-shore temperature gradient between nearshore (2 km from shore and less than 40m water depth) and offshore (20 km from shore and greater than 100m water depth) zones was characterized by elevated surface chlorophyll concentration at the frontal zone between stratified conditions closer to shore and unstratified conditions. In the late summer, vertical variability was highest within 10km of shore, whereas in offshore region further from shore was characterized by a layer below the thermocline with elevated chlorophyll *a* concentration. Alongshore and cross shore gradients in conductance indicated the fate of Niagara River and distribution of lower conductance Lake Erie water as it mixed alongshore and offshore Lake Ontario. Variability of nearshore conductance was due to winds that enhanced mixing between the nearshore and offshore regions. The high-resolution sub-surface glider observations provide a detailed view of spatio-temporal variability across a dynamic coastal zone and demonstrate the utility of autonomous gliders for characterizing and monitoring distinct water quality zones in the Great Lakes.

## Introduction

In large aquatic systems such as the Great Lakes, observations that identify and characterize patterns of water quality and biota are fundamental for model development and provide a spatial framework for monitoring (Yurista et al. 2016). Current understanding of spatio-temporal patterns in Great Lakes is largely based on traditional observing approaches, such as infrequent and spatially coarse sampling from ship-based programs or high temporal resolution observations from a limited number of fixed locations. More recently, satellite remote sensing has been used to delineate water quality zones over broader scales based on optical characteristics or temperature (Warren et al., 2018; Fichot et al., 2019), however, detection is limited to near-surface conditions (Bennion et al., 2019) and clouds frequently interfere, reducing its effectiveness. Towed sensor arrays make direct, high resolution observations of subsurface conditions across large spatial areas (e.g., Scofield et al., 2020), but these are generally limited to favorable weather conditions because they are ship-based. In contrast, autonomous underwater gliders also profile nearly the entire water column over large spatial areas, with the advantage that they can remain deployed for weeks at a time, collecting data in all weather conditions (Austin, 2012). The quantity of subsurface data acquired during routine glider deployments of several weeks provides a more statistically robust dataset than datasets with more sparse observations and increases the probability for detection of finer scale features including hotspots, or anomalous conditions, that can be targeted for subsequent intensive investigation using traditional methods.

Here, we report basic water quality parameters measured during two three-week glider deployments in southern Lake Ontario during the summer of 2018, with emphasis on the utility of these autonomous platforms for identifying and monitoring the transition zone between the nearshore and offshore. The nearshore zone, located between the surrounding landscape and the open lake, has received increased attention because of increasingly eutrophic conditions, which is in contrast with the increasingly oligotrophic conditions offshore, a situation which is not unique to Lake Ontario (Dove and Chapra, 2015). The glider-based work reported here compliments previous work in Lake Ontario's nearshore, which was focused on the identifying landscape and tributary contributions to nearshore water quality.

For example, Yurista et al. (2016) conducted a high-resolution survey of coastal waters by following the shoreline at the 20m contour, and Makarewicz et al. (2012) investigated water quality in the vicinity of selected tributaries. The observations were in support of a hydrodynamic model of the nearshore that extended to 5km from shore and up to 70m water depth (Atkinson et al. 2012). This is typically considered the width of the nearshore zone in the Great Lakes, based largely on horizontal gradients in surface layer water quality parameters. For example, Warren et al. (2018) analyzed gradients of remotely sensed chlorophyll concentrations in Lake Michigan in spring and estimated the average width of the nearshore zone was 4.5 km, although it was wider in several cases due to wind driven exchange processes. Their findings were consistent with the description of the coastal boundary layer presented by Rao and Schwab (2007) which includes an inshore component within 3km of shore where alongshore currents are strongest, and an offshore component to 15 km from shore over which conditions adjust to open lake conditions. An important and distinguishing characteristic of Lake Ontario's southern coastal region is the input of the Niagara River, which flows from Lake Erie. With typical discharge of 7,000 $m^3s^{-1}$, the river forms a large dynamic plume, visible in satellite imagery, that typically veers to the right and hugs the southern shore of the lake (Horner-Devine et al., 2008; Vodacek, 2012). Here we present glider observations focused on the southern shore from the Niagara River eastward to characterize the width of the nearshore zone and the transition to offshore conditions.

## Methods

### *Sampling plan*

We deployed a Teledyne Webb Research G2 Slocum Glider as part of its CSMI research since 2015. Gliders are autonomous, battery powered submersibles capable of carrying a wide range of scientific instrumentation on deployments lasting up to 90 days, depending on battery configuration. As a result of their modular design, portability and relatively low operating cost, gliders are now widely used tools in the coastal and open ocean and are increasingly applied to Great Lakes studies (Austin, 2013).

The U.S. Environmental Protection Agency (EPA) glider 'Nokomis' was deployed May 23-June 12 and July 27-Aug 14, 2018, as part of the 2018 Lake Ontario Coordinated Science and Monitoring Initiative (CSMI). In both deployments, the glider was deployed near the mouth of the Niagara River, and completed a series of alongshore and cross shore segments along the southern (US) coast to Rochester, NY. Alongshore segments approximately followed the 30m contour and cross-shore segments initiated near the mouths of selected tributaries and geographic landmarks and extended to approximately 20km offshore (Figure 1). The west-to-east direction of travel in the alongshore segments corresponded to the expected current direction to minimize the risk of glider being swept ashore. In the early summer deployment, the glider turned offshore after reaching its easternmost waypoint near Rochester and then returned to the western end of the lake, where it was recovered near its starting point. Near the conclusion of the second deployment, scheduling changes required a revision of the sampling plan, and instead of returning to its starting point, the glider repeated a triangle shaped pattern in the offshore near Rochester, NY where it was eventually recovered.

The glider was configured to dive to 6m above the bottom, up to maximum dive depth of 150m, and climb to within 3m of the surface. Dive/climb angle was set to 26 degrees, which resulted in horizontal to vertical distance travelled ratio of 2:1 for each profile and nominal speed over ground of .25 m $s^{-1}$ (approximately 1 km $hr^{-1}$).

### *Glider science configuration*

The glider was outfitted with a Seabird pumped CTD, Aanderaa dissolved oxygen optode and WetLabs FLBBCD Environmental Characterization Optics (ECO) optical sensor. The optical sensor measures in situ fluorescence at excitation/emission wavelengths of 470/695 nm, and 370/460 nm, and converts the intensities of the detected fluorescence signals to concentration of Chlorophyll *a* (Chl-a) and colored dissolved organic matter (CDOM) using factory-set calibration standards (Huot and Babin, 2010). The optical sensor also measures optical backscatter at wavelength 700 nm (Boss et al., 2004). Water depth

was calculated onboard the glider while underway as the sum of altimeter and pressure readings. All sensors were calibrated by the manufacturer, and factory calibration completed at the conclusion of the 2018 field season confirmed sensors were functioning properly. The glider is deployed in the (freshwater) Great Lakes only, and a typical season includes 4 deployments and 60- 90 sampling days, thus biofouling common in saltwater glider deployments (e.g., Cetinic et al., 2009) is generally absent.

### *Data Processing*

Dissolved oxygen is reported by the optode in units of percent saturation in % and concentration in $\mu M\ l^{-1}$. Here we report percent saturation following Scofield et al. (2017), who used it to identify regions of active photosynthesis. Values are calculated internally by the optode and temperature compensated using an integrated thermistor. The optode response time is slow compared to the response time of the CTD pressure sensor used to calculate depth and the mismatch between the two requires correction. We followed the procedure outlined in Kohut et al. (2014) and adjusted the optode observations by 26 seconds, so that visual comparison of successive downcast-upcast pairs showed they were equivalent. Conductivity values reported by the glider are not temperature compensated and were converted to specific electrical conductance (hereafter 'conductance') at the reference temperature of 25 °C using correction factors reported in Radtke et al. (2005). Chl-a concentration is calculated internally by an optical sensor based on detection of fluorescence; however, due to non-photochemical quenching (NPQ) cells exposed to daylight require correction for daytime values in the photic zone (Bennion et al., 2019). In offshore areas, this daytime correction can be accomplished by comparing successive day-night ratios of fluorescence to optical backscatter, which is primarily due to phytoplankton. Because our data also covers optically complex nearshore areas, no correction was applied, and we report Chl-a values using night-time (local sundown to sunup) sampling only.

The continuous data was divided into individual vertical profiles by identifying inflection points in the pressure record. The glider profiles the water column at an angle, not vertically, and therefore the horizontal variability at the scale of individual profiles was compressed. Data collected during both dives and climbs was retained for analysis. Individual profiles were assigned the time and location corresponding to its midpoint. Profiles were linearly interpolated to a vertical pressure grid with 0.5m spacing and a low pass filter was applied to minimize noise. Distance to shore was calculated from the gridded profile location.

### *Data analysis*

We compared the vertical distribution of water quality parameters along gradients of water depth, distance offshore, and longitude using the gridded data. The epilimnion was defined as the layer extending from the surface to bottom of the surface mixed layer (mixed layer depth (MLD)), which was calculated for each gridded profile as the shallowest depth where the temperature gradient exceeds 1 °C per meter following Watkins et al. (2015). The metalimnion was defined as extending from the bottom of epilimnion to the deepest depth where potential density was less than 1000 kg $m^{-3}$. The hypolimnion was defined as the layer below the metalimnion.

We defined the deep chlorophyll layer (DCL) as the region below the MLD where Chl-a concentration exceeded a threshold of 2 $\mu g\ l^{-1}$ following Scofield et al. (2017). The deep chlorophyll maximum (DCM) was defined as the maximum concentration of Chl-a within the DCL, and the depth of the DCM was defined as the depth of the maximum value.

To assess nearshore to offshore gradients of water quality parameters, distance to shore for each of the profiles in cross-shore segments was linearly fit to a horizontal grid with spacing of 0.5 km. The average of profiles within each 0.5 km bin was retained for analysis, and a 2d smoothing filter was applied using a moving mean over 5 levels in the vertical and 5 levels in the horizontal. The result of the filtering was to smooth small-scale variability; various filter settings were compared and did not qualitatively change the results. Individual cross-shore segments were averaged by distance to shore to produce an average nearshore – offshore gradient for each parameter for each deployment.

Alongshore variability from the Niagara River eastward was assessed using profiles from the periods when the glider was travelling parallel to shore. A filter was applied so that only profiles located within 5 km from shore and in water less than 50 m deep were included in the analysis. The alongshore observations were evaluated with respect to wind speed and direction measured at the National Data Center Buoy (NDBC) station id YGNN6, which is located at the Niagara Coast Guard Station at the mouth of the Niagara River, and near the starting point of the glider deployments. The wind data was downloaded from the NDBC website.

## Results

Early and late summer deployments were completed over a combined total of 38 days that included over 3,000 vertical profiles covering approximately 1000 km (Table 1). Each deployment included alongshore segments within 2 km of the coast, and several nearshore to offshore transects between 2 and 20km from shore (Figure 1). Despite the difference in the glider's route due to the scheduling change, the distribution of water depths and distances to shore were approximately equivalent between the two deployments and provide a large dataset of nearshore and offshore vertical profiles for comparison (Table 2). In the early summer deployment, seasonal density stratification was established in nearshore areas and median temperature in the epilimnion was 12 °C (Table 3). Deeper offshore areas had either weak stratification or had not yet stratified at the time of the early summer deployment, whereas in late summer deployment, stratification was established lakewide, except for a small number of profiles in shallow water that were uniformly warm to the bottom. Median epilimnetic temperature in the A regional scale pattern in epilimnetic conductance was observed in both deployments and highlighted the strong influence of the Niagara River on Lake Ontario's nearshore (Figure 2). The plume itself was evident by low conductance and warm temperature that extended to the bottom in 30m of water just west of where the river enters the lake. In addition to the large-scale regional pattern, the high-resolution glider observations revealed horizontal and vertical variability at finer sales than achievable with traditional sampling methods. Changes in the vertical distribution of parameters between the two deployments emphasized the effect of seasonal stratification (Figure 3). Early season Chlor-a concentration was highest in the surface, at the interface between nearshore stratified and offshore vertically mixing water masses. In the late season, the peak was observed offshore, below the MLD, consistent with observations of Lake Ontario's deep chlorophyll layer (Scofield et al. 2017). Chlor-a outlier values (not shown), ranged to over 20 $\mu g\ l^{-1}$ in the early summer deployment in each of the depth bins, consistent with vertical mixing at the thermal bar front (Rao and Schwab, 2007). Outlier values in late summer were lower and were under 5 $\mu g\ l^{-1}$ in each depth bin. The vertical distribution of optical backscatter was similar to that of Chl-a, highlighting the contribution of plankton. An exception was higher late summer backscatter values in the epilimnion compared to the metalimnion. This likely included backscatter associated with the runoff of the Genesee River following a rain event on which presumably included higher concentrations of suspended sediment. Dissolved oxygen levels varied similarly to Chl-a, suggesting the fluorescence is associated with actively photosynthesizing plankton. Although we report only nighttime Chl-a concentrations, we assumed the general pattern measured at night and shown in Figure 3 persisted during the daylight hours. Conductance (SEC) showed a similar pattern in both deployments with lower values in the epilimnion reflecting the influence of Lake Erie runoff on the nearshore region of southern Lake Ontario. The highest conductance in both deployments was measured in the hypolimnion and showed little variability, indicative of Lake Ontario's lakewide mean. Metalimnetic conductance values were consistently intermediate between the surface and deep-water values. Epilimnetic CDOM values were lower in the late summer than in early summer, likely due to the combined influence of reduced CDOM values in the Niagara River runoff and the stronger stratification, which would reduce vertical mixing and promote photodegradation of epilimnetic CDOM.

Comparison of depth integrated values within 5 km of shore to values 15km or greater from shore showed differences in median values as well as differences in variability between the two zones (Figure 4). Nearshore values were more variable, reflecting the complex mixing that includes bottom water within

the nearshore zone, whereas offshore values were dominated by hypolimnetic values due to the greater proportion of hypolimnetic water per vertical profile in the offshore. Mixed layer depth was deeper and more variable in coastal areas, and visual examination of MLD with distance to shore suggested a breakpoint at roughly 10 km between the nearshore zone where the range of MLD values was greater and the offshore zone where values were more uniform (Figure 5).

## Discussion

The glider data suggested two biological markers for describing the spatial extent of coastal versus offshore waters. In the early summer, the boundary was indicated at the surface by elevated Chl-a at the thermal front where nearshore stratified water interacted with offshore isothermal water, and in the late summer, the boundary was indicated by elevated Chl-a levels below the thermocline, and formation of the deep chlorophyll layer between 14.5 and 25m deep (Figure 6). The distance to these features corresponds to the transition zone between the inshore component of the coastal boundary layer and the open lake beyond 15 km from shore (Rao Schwab, 2007), and also the transition between more variable nearshore MLD and more stable offshore MLD (Figure 5). A recent method developed by Warren et al. 2018 used satellite remote sensed Chl-a to delineate the coastal nearshore in Lake Michigan and although they found an average nearshore zone width of 4.5km, they noted several cases where the width was greater due to wind-driven offshore advection of nearshore water. Assuming the width of the nearshore zone in their study describes surface Chl-a patterns in Lake Ontario as well, there were several wind events during the glider deployments (discussed below) that may have expanded the width across the coastal boundary transition zone, while also causing upwelling and downwelling of the MLD.

For a closer examination of possible wind effects, the alongshore gradients of conductance and temperature, were plotted against longitude (Figure 7). As discussed above, Niagara River water signal of relatively lower conductance and higher temperature characterizes the western end of the plot, whereas the eastern end is closer to the lakewide mean value. Both deployments show an increase in conductance moving towards the east, and the gradient is less steep in the early summer when stratification was limited to the nearshore areas, and the thermal bar inhibited mixing between nearshore and offshore regions. The steeper gradient in late summer suggests lower conductance Niagara River water was carried offshore more rapidly later in the summer. Over smaller scales, there were sharp increases in values suggesting increased rates of mixing between nearshore and offshore within the coastal boundary layer (Rao and Murthy, 2001). Selecting the dates surrounding these fluctuations and comparing to the wind data (Figure 8) shows the fluctuations occurred during wind shifts that drive exchange.

The Niagara River contributes over half of the annual nutrient load to Lake Ontario and is also a major source of pollutants (Environment and Climate Change Canada, 2020), thus the fate of the plume after it enters lake has implications for both nearshore and offshore food webs and overall health of the lake's ecosystem functioning. Of all the Great Lakes, Lake Ontario has the highest conductance (Cai and Reavie, 2018) and observations presented here show the relatively lower conductance of Lake Erie water is a useful tracer for the fate of Niagara River after it enters the coastal waters of southern Lake Ontario. The low conductance signal extended offshore as well as alongshore within the coastal boundary layer in both deployments and delineated a broader transition zone between nearshore and offshore regions than is typically investigated. Our use of conductance to identify regional scale differences contrasts with earlier work by Yurista et al. (2012) and others who studied variability within a narrower coastal zone and local impacts of relatively small tributaries (Yurista et al., 2012; Makarewicz et al., 2012). They identified high conductance observations in shallow areas close to shore as tributary runoff and linked the high conductance to elevated nutrient levels that drive local eutrophication. The high-resolution glider observations showed the small-scale variability within a few km of shore occurred within a larger regional pattern that extended 10-15 km from shore.

We used Chl-a concentration reported by the glider for delineating patterns of Chl-a abundance, following the common practice of estimating the distribution and variability of phytoplankton using in vivo fluorescence of chlorophyll *a*, even though the relationship between the pigment and biomass varies

between species, and within species, based on environmental factors (Cloern et al., 1995). In addition, the glider-reported concentration values depend on a factory loaded calibration standard which may be inappropriate for Lake Ontario (Roesler et al. (2017). On the other hand, the values reported by the glider are within the ranges of several previous investigators in Lake Ontario (Watkins et al., 2015; Scofield et al., 2017) and so we feel they adequately represent the spatio-temporal pattern of Chl-a variability, which is our primary goal. For assessment of Chl-a values measured with the glider, future deployments should include side-by-side comparison with ship-based sampling.
Variability in optical backscatter is typically associated with plankton abundance in offshore regions (Boss et al., 2004; Bennion et al., 2019), and suspended sediment from tributary runoff and resuspension in nearshore regions. In contrast to western Lake Superior, where glider-based optical backscatter levels routinely exceed the sensor limit due to resuspension of bottom sediment (Austin, 2013), the highest values observed in the two Lake Ontario deployments were within the observational range of the sensor and were measured in the epilimnion. Backscatter values were lower in the hypolimnion in both deployments compared to western Lake Superior and may be due to differences in surrounding soil types and bottom sediment character as well as the high mussel densities in Lake Ontario, which reduced resuspension.

## Summary

The transition zone between nearshore and offshore regions in the Great Lakes is a dynamic region where landscape inputs are incorporated into the open lake and where observations are needed for model development and calibration. In 2018, water quality parameters were assessed using an autonomous glider deployed in Southern Lake Ontario between the Niagara River and Rochester, NY. Gradients in temperature, conductance, Chl-a, optical backscatter and CDOM concentration extended alongshore and between the nearshore and offshore. Cross shore variability in mixed layer depth and water quality parameters, and changes in the alongshore gradient of conductance that correlated with wind speed variability suggested the transition zone between nearshore and offshore regions occured over a coastal zone that extended 10-15 km from shore. The use of the glider allowed for sustained period of observation that provided an extensive dataset and increased the probability of capturing these events over a larger spatial area than would have normally been accomplished using traditional techniques.

## References

Atkinson, J.F., Edwards, W.J. and Feng, Y., 2012. Physical measurements and nearshore nested hydrodynamic modeling for Lake Ontario nearshore nutrient study. J. Great Lakes Res. 38:184-193. doi.org/10.1016/j.jglr.2012.07.003

Austin, J., 2012. Resolving a persistent offshore surface temperature maximum in Lake Superior using an autonomous underwater glider. Aquat. Ecosys. Health Manage. 15:316-321. doi.org/10.1016/j.jglr.2013.01.004

Austin, J., 2013. The potential for autonomous underwater gliders in large lake research. J. Great Lakes Res. 39:8-13. doi.org/10.1016/j.jglr.2013.01.004

Bennion, D.H., Warner, D.M., Esselman, P.C., Hobson, B. and Kieft, B., 2019. A comparison of chlorophyll a values obtained from an autonomous underwater vehicle to satellite-based measures for Lake Michigan. J. Great Lakes Res. 45: 726-734. doi.org/10.1016/j.jglr.2019.04.003

Boss, E., D. Stramski, T. Bergmann, W.S. Pegau, and M. Lewis. 2004. Why should we measure the optical backscattering coefficient? Oceanogr. 17:44–49. doi.org/10.5670/oceanog.2004.46

Cai, M. and Reavie, E.D., 2018. Pelagic zonation of water quality and phytoplankton in the Great Lakes. Limnology. 19: 127-140. doi.org/10.1007/s10201-017-0526-y

Cloern, J.E., Grenz, C. and Vidergar-Lucas, L., 1995. An empirical model of the phytoplankton chlorophyll: carbon ratio-the conversion factor between productivity and growth rate. Limnol. Oceanogr. 40:1313-1321. doi.org/10.4319/lo.1995.40.7.1313

Cetinić, I., Toro-Farmer, G., Ragan, M., Oberg, C. and Jones, B.H., 2009. Calibration procedure for Slocum glider deployed optical instruments. Optics Express, 17:15420-15430.

Environment and Climate Change Canada and the U.S. Environmental Protection Agency. 2018. *Lake Ontario Lakewide Action and Management Plan*, *2018-2022*. [online]. Available from https://binational.net/wp-content/uploads/2019/04/2018-Lake-Ontario-For-Public-Comment-APRIL-2019.pdf [accessed January, 2020].

Dove, A. and Chapra, S.C., 2015. Long-term trends of nutrients and trophic response variables for the G reat Lakes. Limnol. Oceanogr. 60:696-721. doi.org/10.1002/lno.10055

Horner-Devine, A.R., Fong, D.A. and Monismith, S.G., 2008. Evidence for the inherent unsteadiness of a river plume: Satellite observations of the Niagara River discharge. Limnol. Oceanogr. 53:2731-2737. doi.org/10.4319/lo.2008.53.6.2731

Huot, Y. and Babin, M., 2010. Overview of fluorescence protocols: theory, basic concepts, and practice. In *Chlorophyll a fluorescence in aquatic sciences: Methods and applications* (pp. 31-74). Springer, Dordrecht.

Kohut, J., Haldeman, C. and Kerfoot, J., 2014. *Monitoring Dissolved Oxygen in New Jersey Coastal Waters Using Autonomous Gliders. US Environmental Protection Agency, Washington, DC.* EPA/600/R-13/180.

Makarewicz, J.C., Lewis, T.W., Pennuto, C.M., Atkinson, J.F., Edwards, W.J., Boyer, G.L., Howell, E.T. and Thomas, G., 2012. Physical and chemical characteristics of the nearshore zone of Lake Ontario. J. Great Lakes Res. 38, pp.21-31. doi.org/10.1016/j.jglr.2011.11.013

Radtke, D.B., Davis, J.V. and Wilde, F.D., 2005. *Specific electrical conductance* (No. 09-A6. 3). US Geological Survey.

Rao, Y.R. and Murthy, C.R., 2001. Nearshore currents and turbulent exchange processes during upwelling and downwelling events in Lake Ontario. J. Geophys. Res. 106(C2):2667-2678. doi.org/10.1029/2000JC900149

Rao, Y.R. and Schwab, D.J., 2007. Transport and mixing between the coastal and offshore waters in the Great Lakes: a review. J. Great Lakes Res. 33: 202-218. doi.org/10.3394/0380-1330(2007)33[202:TAMBTC]2.0.CO;2

Scofield, A.E., Watkins, J.M., Weidel, B.C., Luckey, F.J. and Rudstam, L.G., 2017. The deep chlorophyll layer in Lake Ontario: extent, mechanisms of formation, and abiotic predictors. J. Great Lakes Res. 43:782-794. doi.org/10.1016/j.jglr.2017.04.003

Scofield, A. E., Watkins, J. M., & Rudstam, L. G. (2020). Heterogeneity in zooplankton distributions and vertical migrations: Application of a laser optical plankton counter in offshore Lake Michigan. J. Great Lakes Res. doi.org/10.1016/j.jglr.2020.01.005

Vodacek, A., 2012. Linking year-to-year Cladophora variability in Lake Ontario to the temperature contrast between nearshore and offshore waters during the spring. J. Great Lakes Res. 38:85-90. doi.org/10.1016/j.jglr.2012.02.013

Warren, G.J., Lesht, B.M. and Barbiero, R.P., 2018. Estimation of the width of the nearshore zone in Lake Michigan using eleven years of MODIS satellite imagery. J. Great Lakes Res. 44: 563-572. doi.org/10.1016/j.jglr.2017.11.011

Watkins, J.M., Weidel, B.C., Rudstam, L.G. and Holeck, K.T., 2015. Spatial extent and dissipation of the deep chlorophyll layer in Lake Ontario during the Lake Ontario lower foodweb assessment, 2003 and 2008. Aquat. Ecosyst. Heal. Manage. 18:18-27. doi.org/10.1080/14634988.2014.937316

Yurista, P.M., Kelly, J.R., Miller, S. and Van Alstine, J., 2012. Lake Ontario: Nearshore conditions and variability in water quality parameters. J. Great Lakes Res. 8: 133-145. doi.org/10.1016/j.jglr.2011.09.002

Yurista, P.M., Kelly, J.R. and Scharold, J.V., 2016. Great Lakes nearshore–offshore: Distinct water quality regions. J. Great Lakes Res. 42: 375-385. doi.org/10.1016/j.jglr.2015.12.002

Tables

| Start | End | Days | Distance (km) | Profiles | Stratified profiles | ML depth (m) |
|---|---|---|---|---|---|---|
| 23-May | 12-Jun | 20 | 543 | 3402 | 2286 | 7 |
| 27-Jul | 14-Aug | 18 | 445 | 3185 | 3176 | 11 |

**Table 1.** Deployments data. The average mixed layer (ML) depth is reported for stratified profiles.

| Spatial category | Number of profiles | | Minimum water depth (m) | | Maximum water depth (m) | | Median water depth (m) | |
|---|---|---|---|---|---|---|---|---|
| Alongshore | 1913 | 1559 | 14 | 26 | 93 | 76 | 41 | 36 |
| Cross-shore | 1071 | 1046 | 18 | 16 | 207 | 189 | 92 | 98 |
| Offshore | 423 | 582 | 41 | 39 | 191 | 209 | 169 | 167 |

**Table 2.** Water depths sampled in deployments 1 (left column) and 2 (right column). Alongshore segments were parallel to shore within 5km of shore. Cross shore segments transited from 2km to 20km from shore.

| Parameter | units | Epilimnion | | Metalimnion | | Hypolimnion | |
|---|---|---|---|---|---|---|---|
| Temperature | (°C) | 11.97 | 22.66 | 8.01 | 12.11 | 4.89 | 4.66 |
| Chlor-a | ($\mu g\ l^{-1}$) | 1.27 | 1.10 | 1.52 | 1.78 | 0.54 | 0.39 |
| Backscatter* | ($m^{-1}\ sr^{-1}$) | 10.75 | 6.68 | 9.86 | 7.80 | 4.85 | 2.87 |
| Dissolved Oxygen | (% saturation) | 97.04 | 90.67 | 93.49 | 90.46 | 86.67 | 82.50 |
| Specific Conductance | ($\mu S\ l^{-1}$) | 295.02 | 300.90 | 302.79 | 307.16 | 308.81 | 311.81 |
| CDOM | (ppb) | 3.64 | 2.33 | 3.74 | 3.16 | 3.58 | 3.35 |

**Table 3.** Parameter median values by vertical depth stratum for deployment 1 (left column) and deployment 2 (right column). Asterisk indicates backscatter values are multiplied by $10^3$.

Figures

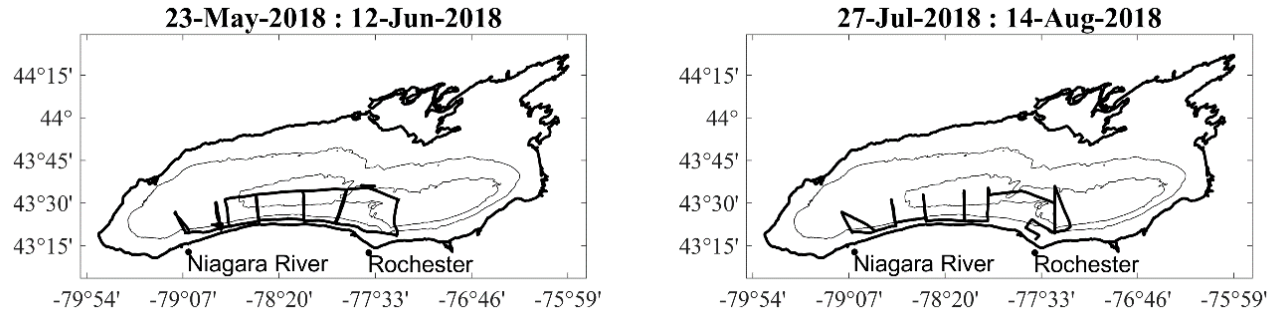


**Figure 1.** Course followed by the autonomous glider in Lake Ontario deployment 1 (left) and deployment 2 (right) during summer, 2018. Both deployments started in the west where the Niagara River enters the lake. Light gray lines indicate water depth of 80 m and 160 m.

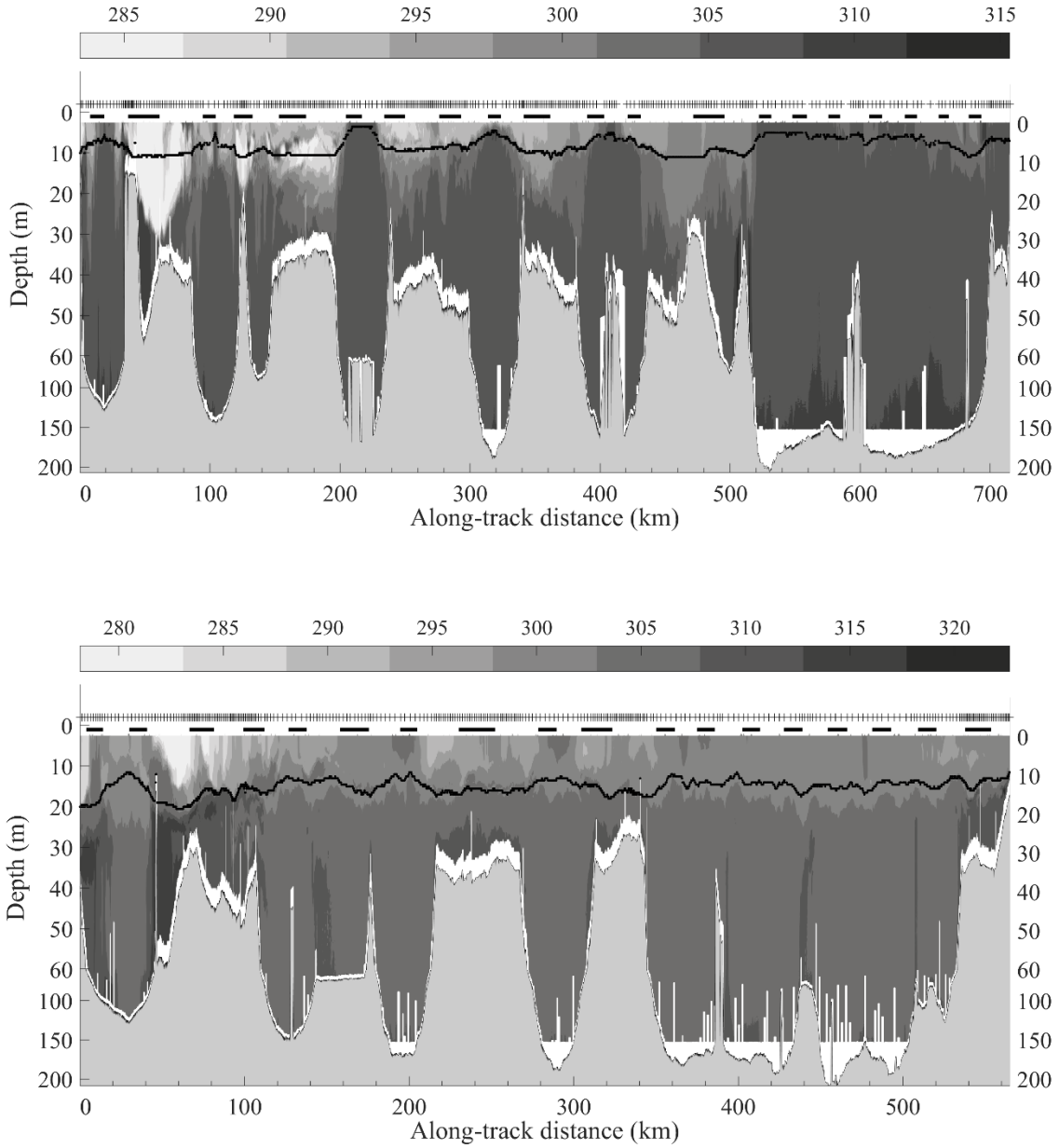


**Figure 2.** Conductance measured in early summer (top) and late summer (bottom) glider deployments in Lake Ontario. Vertical axis enlarged in the top 60 meters to emphasize variability near the surface. Solid black line indicates mixed layer depth described in the text. Horizontal black lines above indicate nighttime periods and are included to show the spatial distribution of profiles used in analysis of Chl-a concentration. Each vertical hash mark above represents 10 vertical casts. Higher spatial density of profiles in shallow water is due to the glider's undulating glide path.

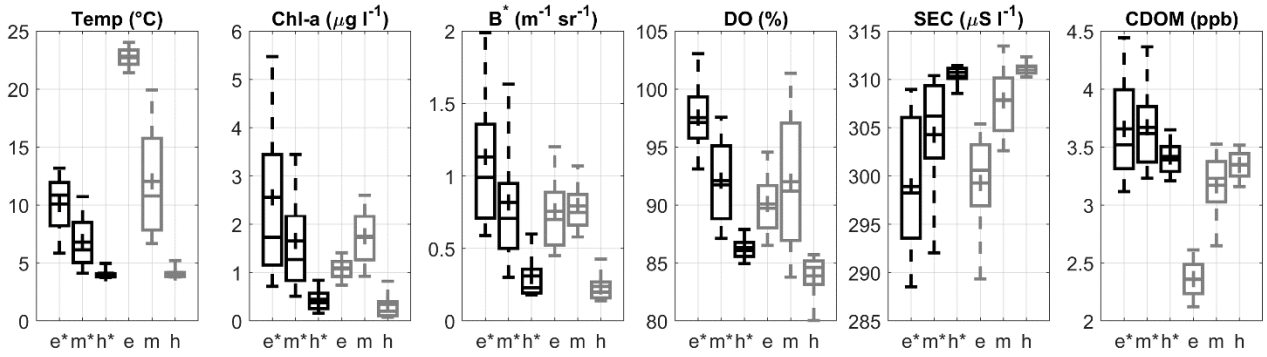


**Figure 3.** Box and whisker plots for early summer (black) and late summer (gray) parameters measured in the epilimnion (e), metalimnion (m) and hypolimnion (h). Asterisks indicate early summer depth ranges are fixed depths of 10m, 25m and bottom as explained in the text. Mean values are represented by cross +, median values represented by line -, interquartile range represented by box edges, whiskers extend to 9$^{th}$ and 91$^{st}$ percentiles. Parameters from left to right are temperature, chlorophyll *a*, optical backscatter, dissolved oxygen saturation, conductance, CDOM. Chlor-a values are from nighttime sampling only. The asterisk indicates backscatter values are multiplied by $10^3$.

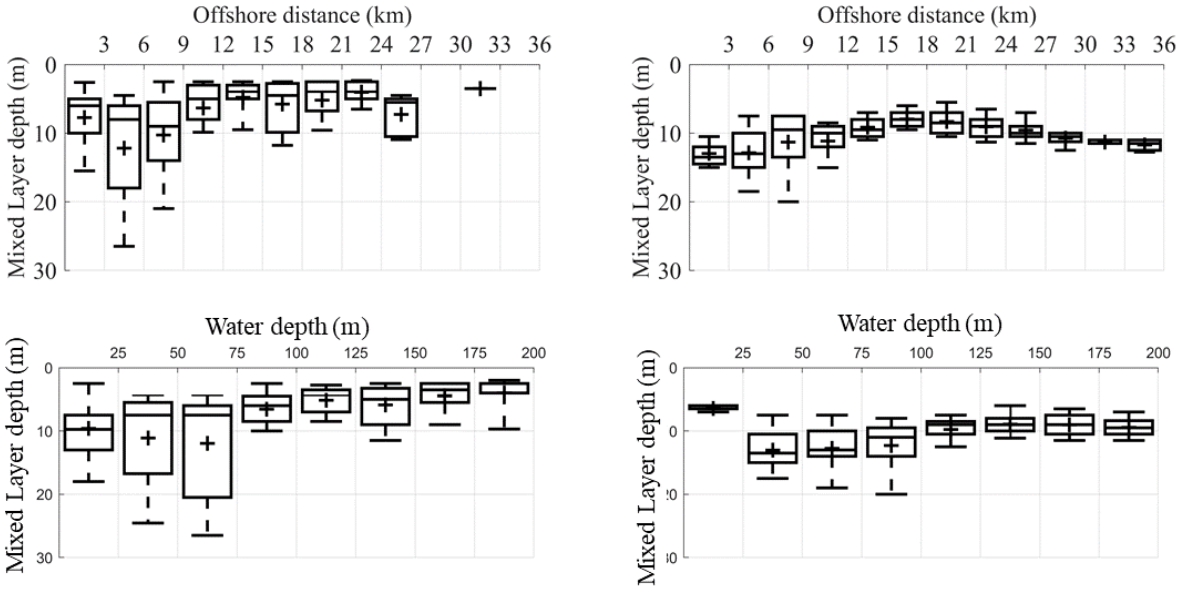


**Figure 4.** Box and whisker plots of mixed layer depth by distance to shore (top) and water depth (bottom) for the early summer (left column) and late summer (right column) deployments. Mean values are represented by cross +, median values represented by line -, interquartile range represented by box edges, whiskers extend to 9$^{th}$ and 91$^{st}$ percentiles.

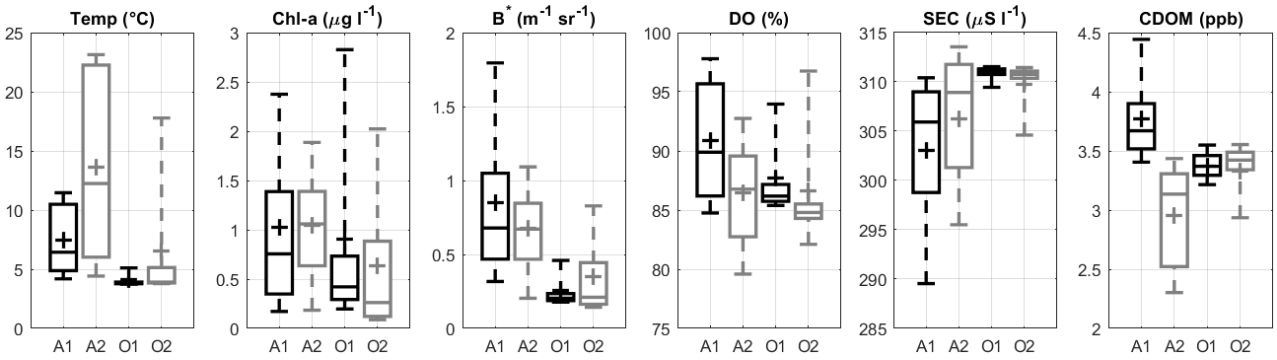


**Figure 5.** Box and whisker plots of whole water column values in alongshore (A) and offshore (O) areas in early summer (1) and late summer (2). Mean values are represented by cross +, median values represented by line -, interquartile range represented by box edges, whiskers extend to 9$^{th}$ and 91$^{st}$ percentiles. Parameters from left to right are temperature, chlorophyll *a*, optical backscatter, dissolved oxygen saturation, specific conductance, CDOM. The asterisk for optical backscatter indicates values are multiplied by $10^3$.

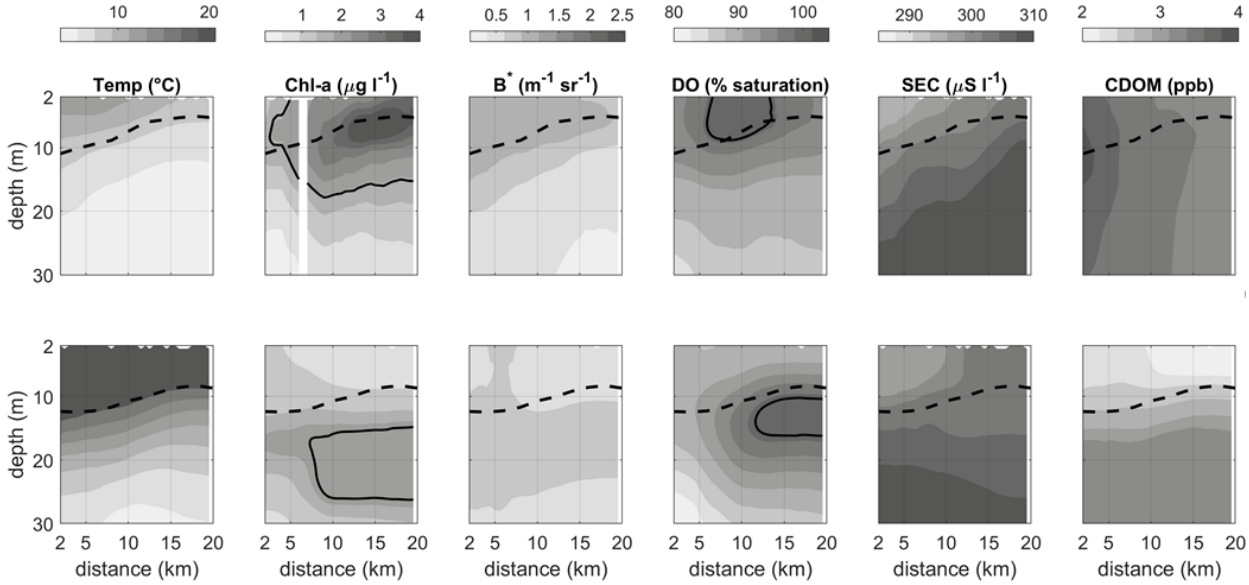


**Figure 6.** Average cross shore patterns of glider-measured parameters in the early summer (top) and late summer (bottom) glider deployments. Parameters from left to right are temperature, chlorophyll a, optical backscatter, dissolved oxygen, specific electrical conductance, CDOM. Asterisk indicates optical backscatter values are multiplied by $10^3$. The dashed line is the average mixed layer depth as defined in the text. Areas with missing data (0-2 km from shore and 0-2 m depth) were omitted for clarity. The solid contour line on Chl-a plot indicates concentration of 2 µg l$^{-1}$, corresponding to deep chlorophyll layer threshold value described in text. Solid line contour in DO indicates 100% saturation level.

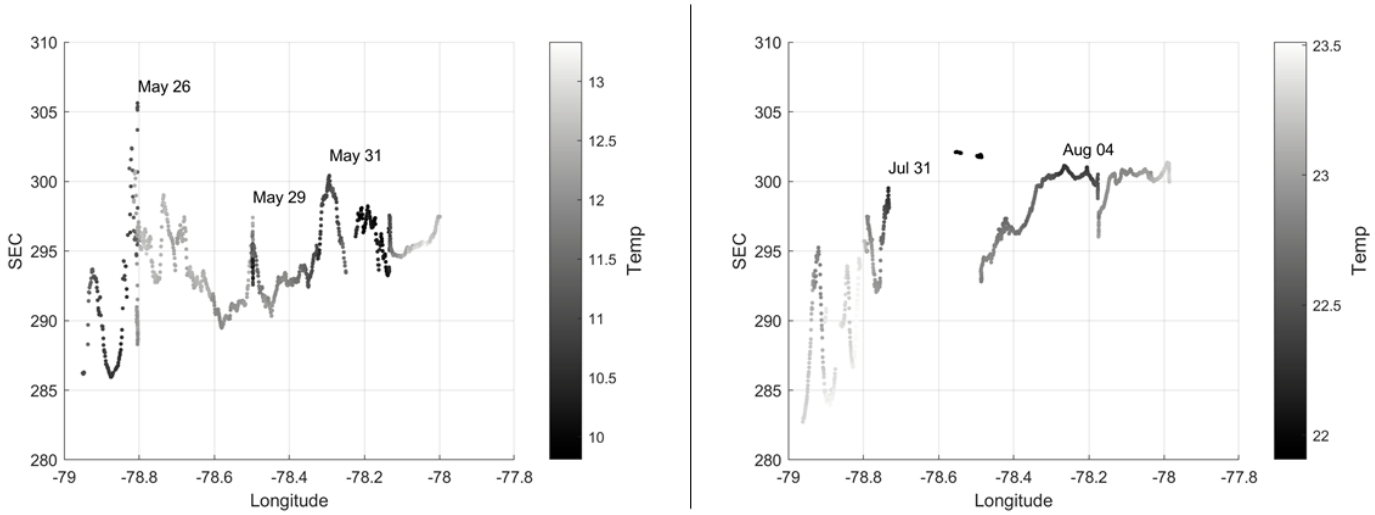


**Figure 7.** Mean surface (<10 meters depth) nearshore values of conductance (SEC) (yaxis) and temperature (gray scale), plotted against longitude (x axis) for southern Lake Ontario. The Niagara River enters the lake at longitude -79. Dated spikes in temperature and conductance correspond to wind events indicated in Figure 8.

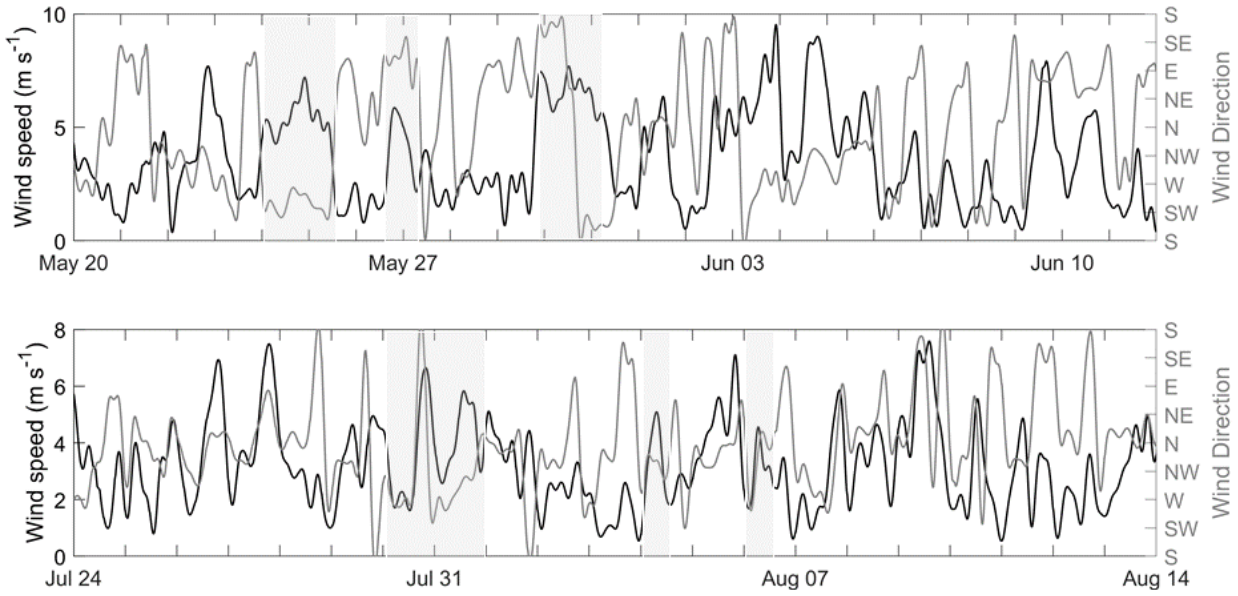


**Figure 8.** Wind data from NDBC station YGNN6 for period of the early summer (top) and late summer (bottom) glider deployments. Shaded areas correspond to periods rapid nearshore temperature and conductance change corresponding to peaks in Figure 7.

## Lake Ontario CSMI results for phytoplankton, 2018

**E. Reavie, Universtiy of Minnesota**

**Euan D. Reavie, Natural Resources Research Institute, University of Minnesota Duluth, Duluth, MN 55811**

CSMI phytoplankton sampling in Lake Ontario comprised integrated sampling of the homogeneous water column in shallow, nearshore and deepwater, offshore locations in spring (April) and summer (August). Summer sampling further included collection of a discrete deep chlorophyll layer (DCL) sample. Greater details of sampling protocols are provided by Reavie et al. (2014). Nearshore samples represent collections at stations with water column depth of approximately 30 m.

Volumetrically, phytoplankton abundance tended to be higher in summer when compared to spring (Figure 1), a phenomenon that is commonly observed in the upper Great Lakes (Reavie et al. 2014). In the spring phytoplankton biovolume in offshore samples was dominated by large-celled dinoflagellates (*Peridinium* dominant), while nearshore samples were dominated by centric diatoms (*Stephanodiscus* and *Aulacoseira* dominant) and chrysophytes (largely haptophytes). In terms of cell density offshore summer phytoplankton communities were dominated by cyanobacteria, though algal biovolume reveals a mixture of dinoflagellates (mainly *Peridinium* and *Ceratium hirundinella*), cyanophytes (mainly *Dolichospermum*, formerly identified as *Anabaena*), cryptophytes (mainly *Cryptomonas*) and pennate diatoms (*Fragilaria crotonensis*). Summer integrated samples had higher phytoplankton biovolumes than nearshore. While phytoplankton composition was similar in summer sample types, DCL samples had a notably lower cyanophyte biovolume, possibly a result of their buoyancy (Bramburger & Reavie 2016), and a larger abundance of pennate diatoms and cryptophytes.

Though not specifically focused on CSMI efforts, long-term monitoring from 2001 through 2018 in the pelagic waters (Reavie et al. 2014, plus more recent data) indicate that spring phytoplankton abundance is increasing slightly and becoming represented to a greater degree by dinoflagellates. Summer phytoplankton abundance is also increasing to include larger numbers of cyanophytes. Paleolimnological records of chlorophyll *a* based on deepwater cores (Reavie et al. 2021) indicated that eutrophication trends that began in the mid-20$^{th}$ century were alleviated by the 1990s, however sediments from the most recent decade indicate a slight uptick in chlorophyll deposition, potentially corresponding with our long-term monitoring observations.

### REFERENCES

Bramburger, A.J., E.D. Reavie 2016. A comparison of phytoplankton communities of the deep chlorophyll layers and epilimnia of the Laurentian Great Lakes. *Journal of Great Lakes Research* 42(5): 1016-1025.

Reavie, E.D., R.P. Barbiero, L.E. Allinger, G.J. Warren 2014. Phytoplankton trends in the Great Lakes: 2001-2011. *Journal of Great Lakes Research* 40(3): 618-639.

Reavie, E.D., M. Cai, J.P. Werne, C. Meyer-Jacob, J.P. Smol 2020. Long-term productivity trends in the Laurentian Great Lakes: a comparison of geochemical methods. *Journal of Paleolimnology* (in press).

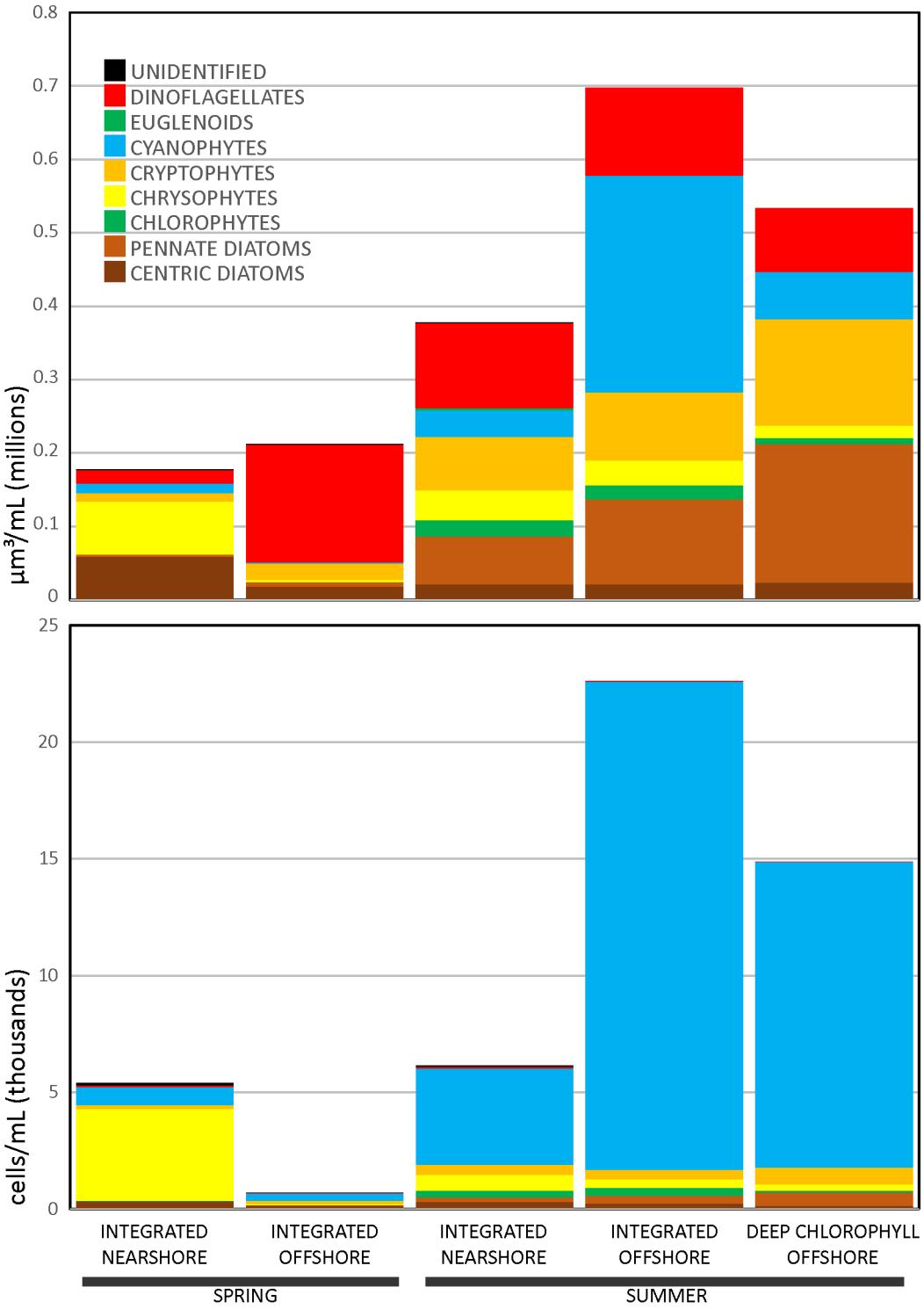


Figure 1. Basin-wide sample averages of phytoplankton abundance in Lake Ontario in 2018. Abundance data are summarized for spring and summer for algal biovolume (top) and density (bottom). Nearshore, offshore and summer deep chlorophyll maximum sample data are presented separately as stacked histograms of broad algal groups. Integrated samples represent combined samples from throughout the homogeneous upper water column (spring = whole water column; summer = epilimnion).

# Lake Ontario 2018 Coordinated Science and Monitoring Initiative (CSMI) Quagga Mussel Growth Experiment and a Lake-wide Quagga Mussel Condition Assessment

**Ashley K. Elgin*, NOAA GLERL, Paul W. Glyshaw, NOAA GLERLBrian C. Weidel, U.S. Geological Survey (USGS), Lake Ontario Biological Station**

*Contact: ashley.elgin@noaa.gov; 231-755-7699

Lake Michigan Field Station

1431 Beach St.

Muskegon, MI 49441

## Project Overview

We conducted a year-long quagga mussel (*Dreissena rostriformis bugensis*) growth field experiment to complement long-term studies on dreissenid mussels, which are considered to be a major driver of change in Lake Ontario. In this study we also report on a lake-wide assessment of quagga mussel body condition, as measured by length-weight regressions, conducted during the whole-lake benthic survey aboard the EPA R/V Lake Guardian in September 2018.

This project addresses Lake Ontario Management Partnership (LAMP) Science Priority #3: "Evaluate aquatic food web status" (Environment and Climate Change Canada and the U.S. Environmental Protection Agency 2018). Further, it aligns closely with the following prescribed activity under Priority #3: "For dreissenid mussels, assessing overall changes in distribution, a better understanding of dreissenid growth and reproductive rates in deeper, colder waters is needed in order to fully understand the impacts this benthic species is having on the Lake Ontario aquatic food web."

The complete findings from the growth experiment will be published in the Journal of Great Lakes Research Special Issue on Lake Ontario 2018 CSMI. The quagga mussel body condition data were used to calculate mussel tissue biomass, as reported in Karatayev et al. (Early View, Journal of Great Lakes special issue), and will be released in 2021 as a data paper and archived by the NOAA National Centers for Environmental Information (NCEI). GLERL also assisted with the collection of samples and preparation and interpretation of data from the whole-lake benthic survey led by Buffalo State College and the U.S Environmental Protection Agency (EPA). The results from the benthic survey are reported in manuscripts by Burlakova et al. and Karatayev et al. (both Early View, JGLR Special Issue).

## Study Highlights

- Quagga mussels have high growth potential at 15 m, intermediate at 45 m, and low at 90 m.
- Quagga mussel shell length growth was highly dependent on initial starting shell length at 15 m, but not at 45 m or 90 m.
- We found that even modest differences in temperature and chlorophyll, such as the conditions observed between the 45 m and 90 m sites, lead to significant differences in mussel growth.

- We updated lake-wide estimates of quagga mussel body condition, based on length-weight relationships. Mussel tissue ash-free dry weight was highest at sites < 30 m, intermediate at depths > 90 m, and lowest at mid-depth sites (51 - 90 m).
- Tissue ash-free dry weight increased significantly from 2013 to 2018 at depth zones of < 30 m and 51 - 90 m, but not at > 90 m.

## Quagga Mussel Growth Experiments

### *Overview*

We conducted an *in situ* quagga mussel growth experiment to improve year-round estimates of mussel growth and to better understand dreissenid population trends. This experiment in Lake Ontario was Phase 3 of a multi-year cross-lake study that included Lakes Michigan and Huron. We produced growth estimates spanning nearly a full year that include the often-unstudied fall through winter period.

## Methods

We deployed moorings at three locations in south eastern Lake Ontario near Oswego, New York in coordination with the USGS Lake Ontario Biological Station: LO15, LO45, and LO90 (Table 1, Fig. 1). The moorings were deployed on June 13, 2018 and retrieved on May 7, 2019. We serviced the moorings on November 15, 2018 to switch out instruments and collect mussel cages to assess seasonal growth, but these samples were compromised, and we are unable to present those findings. Each mooring was equipped with two thermistors (Hobo Tidbit v2) to log temperature hourly and one fluorometer (Seabird Scientific ECO-FL) to record chlorophyll *a* every 6 hours (herein: chlorophyll). Thermistor data from June 13 to November 14, 2018 was lost, so we incorporated temperature data from other sources. For LO15, we used water intake temperature (~12 m depth) from the nearby Monroe County water treatment plant. For LO45 and LO90 we used bottom temperatures from trawls conducted by USGS adjacent to the experimental sites in July and October; values in-between trawl dates were linearly extrapolated. We calculated daily means for temperature and chlorophyll). We also calculated cumulative values of temperature and chlorophyll exceeding 0 ℃ and 0 µg/L through the duration of the experiment, with the exception of cumulative chlorophyll at 15 m due to instrument failure on February 25, 2019.

We included two types of cages in the experimental design, each with a specific approach for measuring mussel growth. The “Group” cages (n = 6 cages at 15 m and 45 m and 5 cages at 90 m) contained 10 mussels within a consistent size range (11.0 - 13.0 mm shell length) to produce a robust growth estimate for comparison across sites and control for the effect of mussel size on growth. We chose this size range based on the assumption that smaller mussels had higher growth potential and these sizes were the smallest mussels available in sufficient numbers for the experiment. Growth for the group cages was determined as a difference between mean starting length and mean final length within each cage. The other, “individual” cages (n = 6 cages per depth) contained 10 individually labeled mussels so that we could track individual, size-specific growth rates across a broad initial size range (8.5 - 21.9 mm shell length). Due to limited availability of mussels near LO45 and LO15, all mussels used to populate the cages were collected by Ponar grab in the vicinity of LO90 (depth range: 90 -150 m).

One-way ANOVA and Tukey HSD post-hoc tests were used to examine differences in depth for shell growth among the group cages. The relationships between change in shell length and initial shell length was examined using ANCOVA; post-hoc comparisons of least square means were completed using Tukey's HSD. When analyzing change in shell length by initial shell length, we addressed violations of normality by removing values with high Cook's D values, but the results of the statistics did not change. Herein, we report using the full range of values. The data for change in wet weight vs. initial wet weight violated the assumptions of normality, but neither removing a large number of outlier variables nor performing log transformations was sufficient to correct this violation. As a result, we do not present statistics for change in weight. All statistical analysis was completed using the R statistical package (R Core Team, 2019); post-hoc tests were calculated with the lsmeans package (Lenth, 2016).

## Results and Discussion

Quagga mussel growth was strongly depth-dependent. There was a significant depth difference among the group cages (ANOVA: $F_{2,12}$= 417.2, $p < 0.001$), with LO15 exhibiting the greatest mean increase in shell length (10.2 mm ± 0.8), followed by LO45 (5.9 mm ± 0.2), and LO90 (0.7 mm ± 0.4; Fig. 2). Change in shell length was also significant among depths for mussels in the individual cages (ANCOVA: $F_{2,120}$= 60.21, $p < 0.001$), where initial shell length covaried with length change ($F_{1,120}$= 33.32, p = $p < 0.001$), and a significant interaction between depth and initial shell length ($F_{2,120}$= 10.8, $p < 0.01$) illustrates that shell growth was most strongly size-dependent at LO15 (Fig. 3A). Change in wet weight followed a different pattern; the magnitude of change increased with initial wet weight at LO15 and LO45 (Fig. 3B). This is because of the non-linear relationship between length and weight, where increases in length for larger mussels are associated with much greater gains in weight. Mussels from LO90 expressed low levels of weight change across all initial values, which corresponds with the low level of shell length change observed. Differences in growth among stations was most evident among mussels with shell lengths <10 mm. Faster growth is particularly important for smaller mussels because it allows them to attain sizes associated with sexual maturity and refuge from goby predation (Foley et al. 2017). Mussel growth at LO15 was strongly size-dependent and therefore differences in growth among sites was dampened at higher starting shell lengths.

Mussel mortality was notably higher at the 15 m (30%) and 45 m (45%) sites, compared to 90 m, where only 5% of mussels died over the course of 11 months. According to the final shell lengths of the dead mussels, they grew a modest amount before dying. Based on data from the Group cages and assuming a starting shell length of 12 mm, the dead mussels grew, on average, 4.3 mm at 15 m, 3.4 mm at 45 mm, and 0.2 mm at 90 m. These levels of growth represent 42%, 73%, and 29% of the total growth achieved by the live mussels at these three depths, respectively.

Cumulative temperature and chlorophyll results show how conditions varied between sites (Fig. 4). Mussels at 15 m experienced the highest cumulative temperature ( daily sum = 2982 ℃) and chlorophyll (daily sum =718 µg/L); these conditions led to the highest growth rates of the experiment. Mussels at 90 m had the lowest growth rates, along with the lowest cumulative temperature (1408 ℃) and chlorophyll (166 µg/L). Cumulative temperature (1770 ℃) and chlorophyll (339 µg/L) conditions at 45 m were intermediate, as were growth rates at this depth. While these results do not allow us to separate out the different effects of temperature and chlorophyll on growth, they show that even

modest differences in temperature and chlorophyll, such as conditions observed between 45 m and 90 m, can lead to significant differences in mussel growth.

## Quagga Mussel Lake-wide Length-weight Analysis

### *Overview*

We analyzed length-weight relationships at 12 stations in Lake Ontario representing different depth zones. This analysis allows for depth-specific calculations of mussel biomass. We resampled several sites that were visited in 2013, which allowed us to examine temporal changes in length-weight relationships by depth.

## Methods

During the R/V Lake Guardian cruise, GLERL researchers collected quagga mussels from 12 stations for length-weight analysis (Table 1, Fig. 5). The overall goal was to collect mussels from sites that represent different depth zones and basin regions. The mussels were processed as described by Nalepa et al. 2020. Briefly, the soft tissue was removed from 25 individuals (target shell length: 10 mm-25 mm), dried at 60 $C^o$ for at least 48 h, then ashed at 550 $C^o$ for 1 h. Ash-free dry weight (AFDW) was calculated as the difference between dry weight and post-ashed weight. Overall, a total of 300 individual *D. r. bugensis* from 12 sites were weighed and measured. Measured AFDWs and shell lengths (SL) were used to develop length-weight relationships according to the allometric equation:

$$\log_e \text{AFDW (mg)} = b + m * \log_e \text{SL (mm)}$$

Relationships were developed for pooled sites within three different depth intervals: $\leq$ 30 m, 51-90 m, and > 90 m (Table 2). The parameters reported here will differ from what is reported for 2018 in Karatayev et al. (Early View) because those regressions were based on the depth categories as measured in 2013 and here we use the 2018 depth values. Two of the sites shifted depth categories between 2013 and 2018 (ON29 from 31-50 m to <30 m and ON94 from 31-50 m to 51-90 m). We used ANCOVA (response variable: ln AFDW; covariate: ln shell length) to analyze (1) differences among depth zones in 2018 and (2) temporal differences between the subset of five sites that were sampled in both 2013 (Nalepa and Baldridge 2016) and 2018. Post-hoc pairwise and other comparisons of least square means were completed using Tukey's HSD. All statistical analysis was completed using the R statistical package (R Core Team, 2019); post-hoc tests were calculated with the lsmeans package (Lenth, 2016).

## Results and Discussion

Mussels from Lake Ontario exhibited significant depth-specific length-weight patterns (ANCOVA: depth, $F_{2,296} = 101.0$, $p < 0.001$) and shell length covaried with AFDW ($F_{1,296} = 2208.1$, $p < 0.001$). There was no significant interaction between shell length and depth zone ($F_{2,294} = 1.1$, $p = 0.33$). Mussels were relatively heavier at 16 - 30 m, lightest at 51 - 90 m, and intermediate at > 90 m (all post-hoc pairwise comparisons $p < 0.001$) (Fig. 6). There were also depth-specific changes in relative tissue weight over time. The effects of depth and year, as well as their interaction were significant (ANCOVA: depth, $F_{2,235} = 20.0$, $p < 0.001$; year, $F_{1,235} = 28.4$, $p < 0.001$; interaction, $F_{2,235} = 17.7$, $p < 0.001$ ; Fig. 7) for the five stations that were sampled in both 2013 and 2018. Pairwise comparisons between years within each depth zone revealed significant increases between 2013 and 2018 in tissue AFDW at depths of < 30 m

and 51 – 90 m only (both $p < 0.01$). These increases in relative body tissue weight between 2013 and 2018 indicate that the mussels are not experiencing increasing food limitation over time, as has been observed in Lake Michigan (Glyshaw et al. 2015). However, when food is not limiting, the ash-free tissue weight of a 15 mm mussel generally exceeds 8 mg (Nalepa et al. 1995 for *D. polymorpha*). In our study, only mussels found at depths <30 m were above this threshold (Table 2), so food limitation may be impacting mussel populations in deeper regions of Lake Ontario.

Comparing these results with mussel data from the whole lake benthic surveys of 2013 and 2018 reveals some interesting connections. Both density and biomass of quagga mussels in the < 30 m and > 90 m depth zones increased, while slight declines in density at 51 – 90 m were paired with increases in biomass (Karatayev et al. Early View). The general lake-wide trend of the increase in mussel biomass outpacing the increase in density can be attributed to the mussels themselves being larger on average than in 2013 (Karatayev et al. Early View). Our findings offer the additional explanation that mussels < 90 m are individually heavier after controlling for size. Counter to the expectation that mussel body condition would decline in regions where mussel density is increasing (Stanczykowska et al. 1975), we did not find an association between density trajectory and body condition. Potential connections between changes in tissue weight and mussel population trajectories (specific to different regions and depth zones) is an area that warrants further study.

## Acknowledgements

We thank the vessel, administrative, and science support staff at the USGS Lake Ontario Biological Station, and M. Wensman and G. Carter from the Cooperative Institute for Great Lakes Research at NOAA GLERL. Any use of trade, product, or firm names is for descriptive purposes only and does not imply endorsement by the U.S. Government.

## Literature Cited

Burlakova, L. E., A.Y. Karatayev, A.Y. Hrycik, S.E. Daniel, K. Mehler, L.G. Rudstam, J.M. Watkins, R. Dermott, J. Scharold, A.K. Elgin, T.F. Nalepa. Early View. Six decades of Lake Ontario ecological history according to benthos. Journal of Great Lakes Research.

Environment and Climate Change Canada and the U.S. Environmental Protection Agency. 2018. Lake Ontario Lakewide Action and Management Plan, 2018-2022.

Foley, C.J., S.R. Andree, S.A. Pothoven, T.F. Nalepa, and T.O. Höök. 2017. Quantifying the predatory effect of round goby on Saginaw Bay dreissenids. Journal of Great Lakes Research 43:121-131.

Glyshaw, P.W., C.M. Riseng, T.F. Nalepa, and S.A. Pothoven. 2015. Temporal trends in condition and reproduction of quagga mussels (*Dreissena rostriformis bugensis*) in southern Lake Michigan. Journal of Great Lakes Research 41(Supplement 3):16-26.

Karatayev, A.Y., L. E. Burlakova, K. Mehler, A. K. Elgin, L. G. Rudstam, J. M. Watkins, and M. Wick. Early View. Dreissena in Lake Ontario 30 years post-invasion. Journal of Great Lakes Research https://doi.org/10.1016/j.jglr.2020.11.010

Karatayev, A.Y., L.E. Burlakova, K. Mehler, S.E. Daniel, and A.R. Hrycik. 2021. Lake Ontario Benthos Survey Cooperative Science and Monitoring Initiative 2018. Technical Report. USEPA-GLRI GL00E02254. Great Lakes Center, SUNY Buffalo State, Buffalo, NY. Available at: https://greatlakescenter.buffalostate.edu/sites/greatlakescenter.buffalostate.edu/files/uploads/Documents/Publications/LakeOntarioBenthosSurveyCSMI2018FinalReport.pdf

Lenth, R.V., 2016. Least-Squares Means: The *R* Package **lsmeans**. J. Stat. Softw. 69. https://doi.org/10.18637/jss.v069.i01

Nalepa, T.F., Wojcik, J.A., Fanslow, D.L., Lang, G.A., 1995. Initial colonization of the zebra mussel (*Dreissena polymorpha*) in Saginaw Bay, Lake Huron: population recruitment, density and size structure. Journal of Great Lakes Research 21:417–434.

Nalepa, T.F., A.K. Baldridge., 2016. Benthos. Lake Ontario Cooperative Science and Monitoring Initiative (CSMI) 2013. Summary Report.

Nalepa, T.F., L.E. Burlakova, A.K. Elgin, A.Y. Karatayev, G.A. Lang, and K. Mehler. 2020. NOAA Tech memo GLERL-175. Abundance and biomass of benthic macroinvertebrates in Lake Michigan in 2015, with a summary of temporal trends. Technical Memo, NOAA Great Lakes Environmental Research Laboratory, NOAA Great Lakes environmental Research Laboratory, Ann Arbor MI.

Stanczykowska, A. H.J. Schenker, Z. Fafara. 1975. Comparative characteristics of populations of *Dreissena polymorpha* (Pall.) in 1962 and 1972 in 13 Mazurian lakes. Bulletin de L'Académie Polonaise des sciences 23:383-390.

## Tables and Figures

Table 1. Station information for the three-growth experiment and 12 length-weight stations. The coordinates and 2018 depths correspond with Table A1 from Karatayev et al. (2021). 2013 depths for the length-weight stations are according to Nalepa and Baldridge (2016). Stations marked with an asterisk were used to compare mussel length-weight changes between 2013 and 2018. Data not available are represented by an "NA".

| Station | Basin | Latitude | Longitude | 2013 Depth (m) | 2018 depth (m) |
|---|---|---|---|---|---|
| Growth Experiment Stations | | | | | |
| LO15 | East | 43.532 | -76.374 | NA | 15 |
| LO45 | East | 43.535 | -76.447 | NA | 45 |
| LO90 | East | 43.563 | -76.468 | NA | 90 |
| Length-Weight Survey Stations | | | | | |
| ON28* | West | 43.77517 | -78.8546 | 65.0 | 60.6 |
| ON29* | West | 43.81742 | -78.86992 | 32.0 | 29.5 |
| ON32 | Central | 43.78277 | -78.4377 | 79.0 | 75.3 |
| ON34* | West | 43.46135 | -78.75918 | 135.0 | 134.7 |
| ON35 | West | 43.36185 | -78.729 | 27.0 | 27.0 |
| ON37 | Central | 43.39145 | -78.03646 | 23.5 | 21.7 |
| ON39 | Central | 43.48562 | -77.99746 | 146.0 | 152.7 |
| ON55* | East | 43.4439 | -77.4389 | 187.0 | 198.0 |
| ON61* | East | 43.78645 | -77.15828 | 47.0 | 51.3 |

| | | | | | |
|---|---|---|---|---|---|
| ON72 | East | 43.54915 | -76.52569 | 112.5 | 106.6 |
| ON74 | East | 43.74834 | -76.51604 | 68.9 | 67.3 |
| ON94 | East | 43.32509 | -77.21652 | 45.0 | 52.4 |

Table 2. Relationship between shell length (SL in mm) and tissue ash-free dry weight (AFDW in mg) for *D. r. bugensis* collected from multiple depth intervals in 2018 in Lake Ontario. Regression constants (m, b) are derived from the linear regression: $\log_e AFDW = b + m*\log_e SL$; n = total number of mussels used to derive the relationship. Also given is the tissue AFDW of a standard 15 mm individual as calculated from the corresponding regression.

| **Depth Zone** | **b** | **M** | **$R^2$** | ***P*** | **n** | **15-mm mussel tissue AFDW (mg)** |
|---|---|---|---|---|---|---|
| < 30 m | -4.510 | 2.454 | 0.855 | <0.001 | 75 | 8.5 |
| 51 - 90 m | -5.464 | 2.622 | 0.938 | <0.001 | 125 | 5.1 |
| > 90 m | -5.446 | 2.658 | 0.850 | <0.001 | 100 | 5.8 |

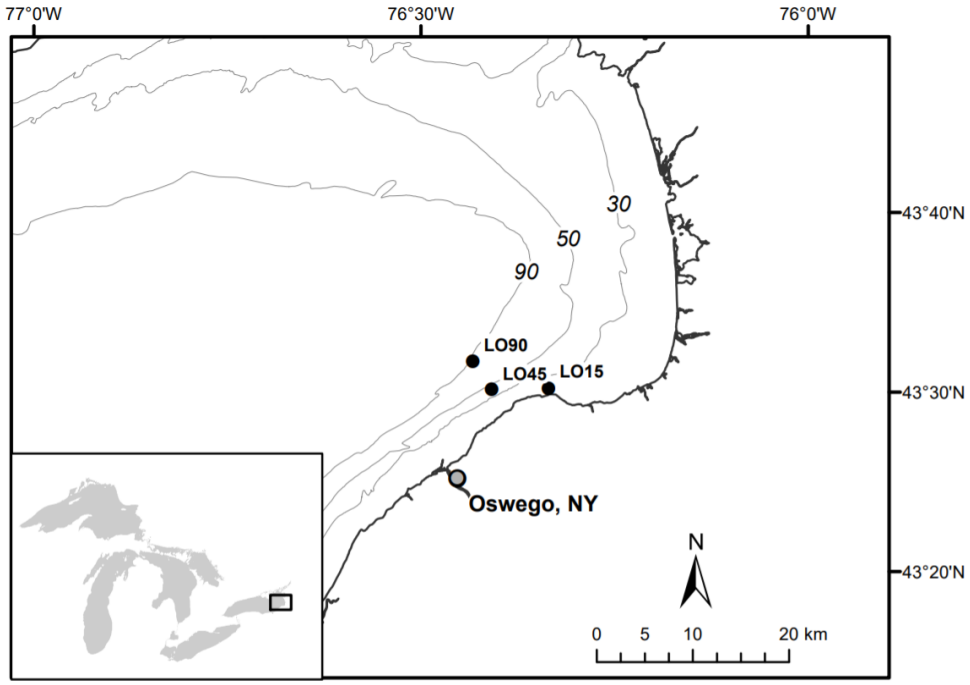


Figure 1: Map of the growth experiment study area in eastern Lake Ontario. Inset shows location within the Great Lakes region. Approximate distances between sites: 5.9 km between LO15 and LO45 and 3.4 km between LO45 and LO90.

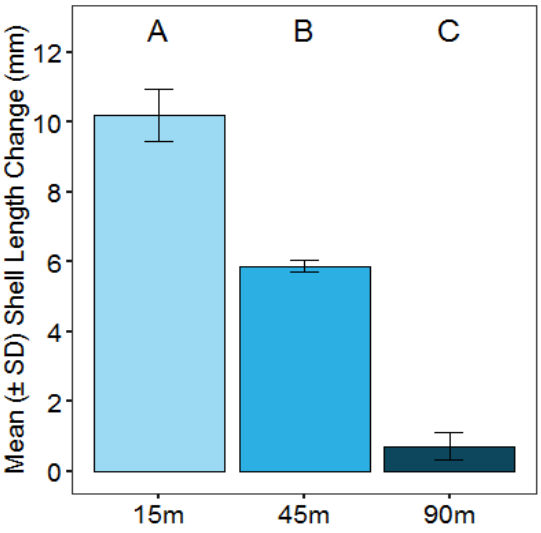


Figure 2: Mean growth (± SD) of quagga mussels grown in group cages at three depths in Lake Ontario. Growth is measured by the mean change in shell length per cage. Mean starting shell length per cage was ~12 mm. Categories with different letters differ significantly ($p < 0.05$), according to pairwise comparisons.

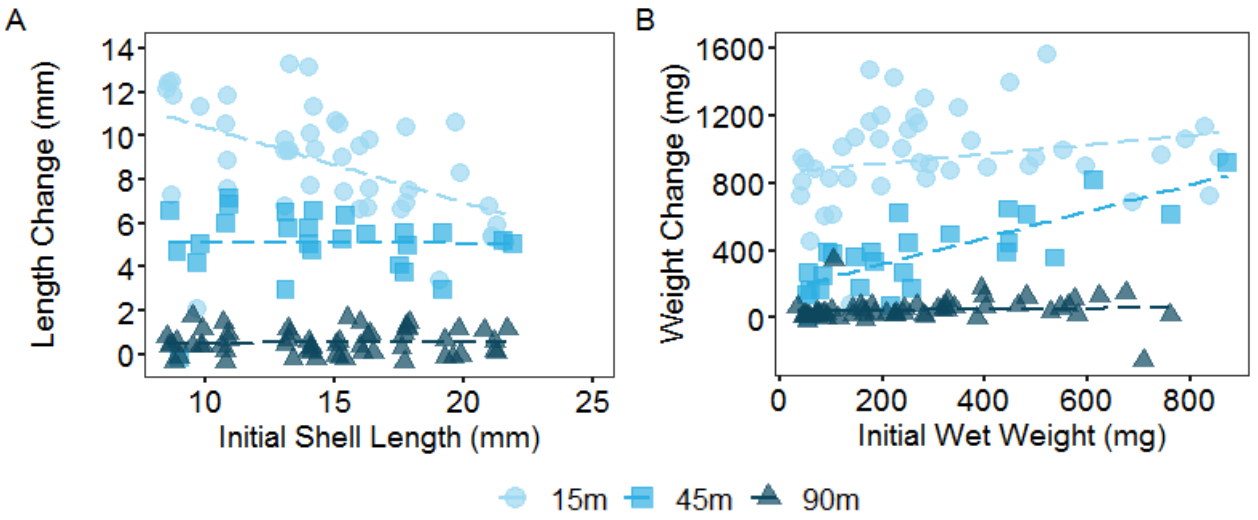


Figure 3: Length change as a function of initial shell length (A) and whole mussel wet weight change (B) for quagga mussels grown in individual cages at three depths in Lake Ontario. Each datum represents an individual mussel. Trendlines are shown for all relationships, even if not significant.

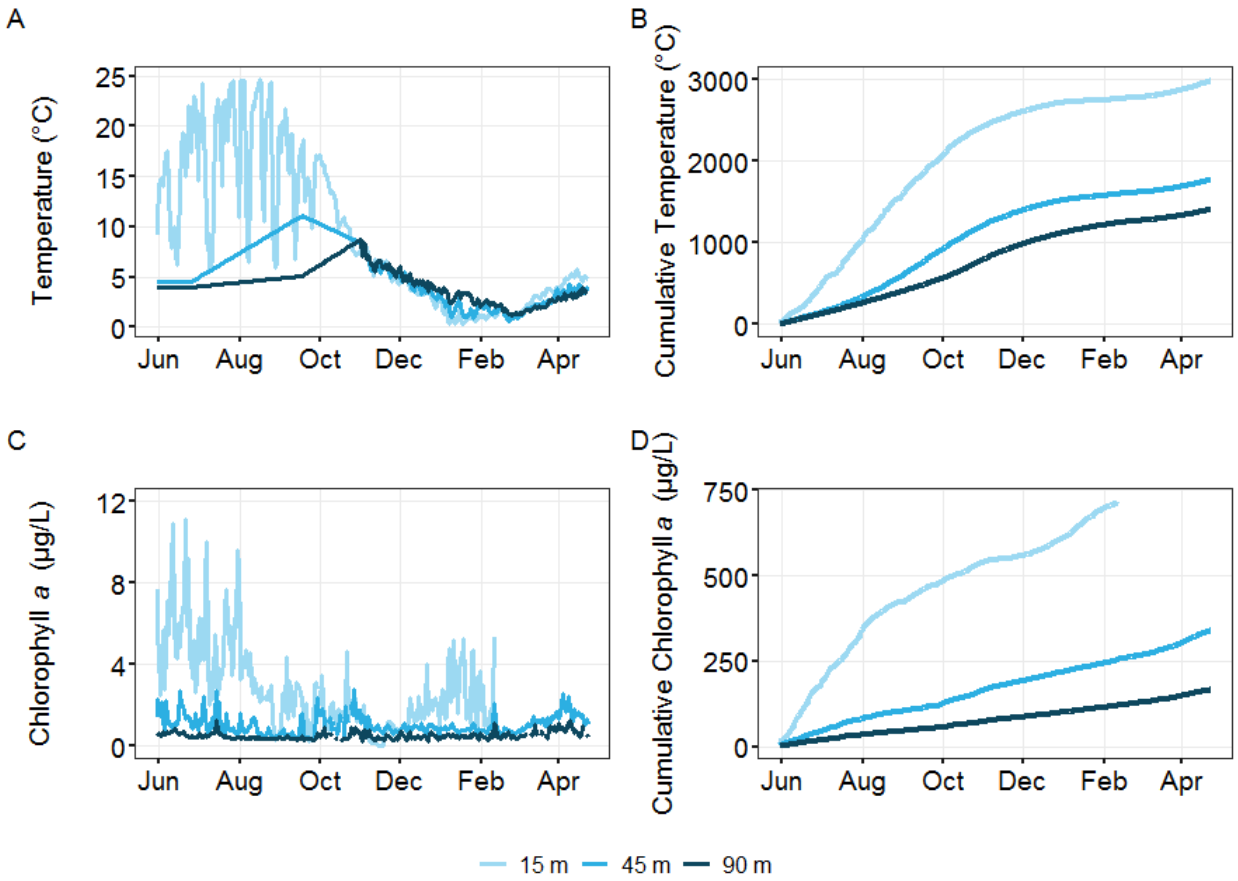


Figure 4. Daily mean temperature (A) and chlorophyll *a* (C) as measured by instruments mounted <0.5 m from the lake bed. Cumulative values (B, D) are shown through May 7, 2019, with the exception of cumulative chlorophyll *a* at site 15 m due to instrument failure on February 25, 2019.

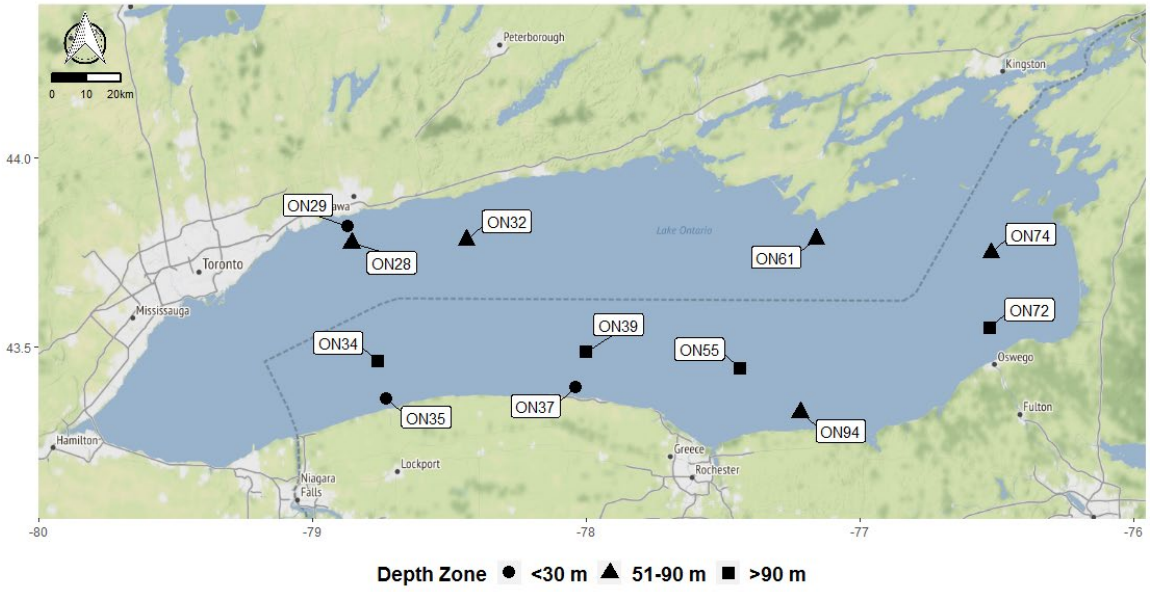


Figure 5. Stations in Lake Ontario where quagga mussels were collected for whole-lake length-weight analysis. Station depth zone is indicated by symbol shape.

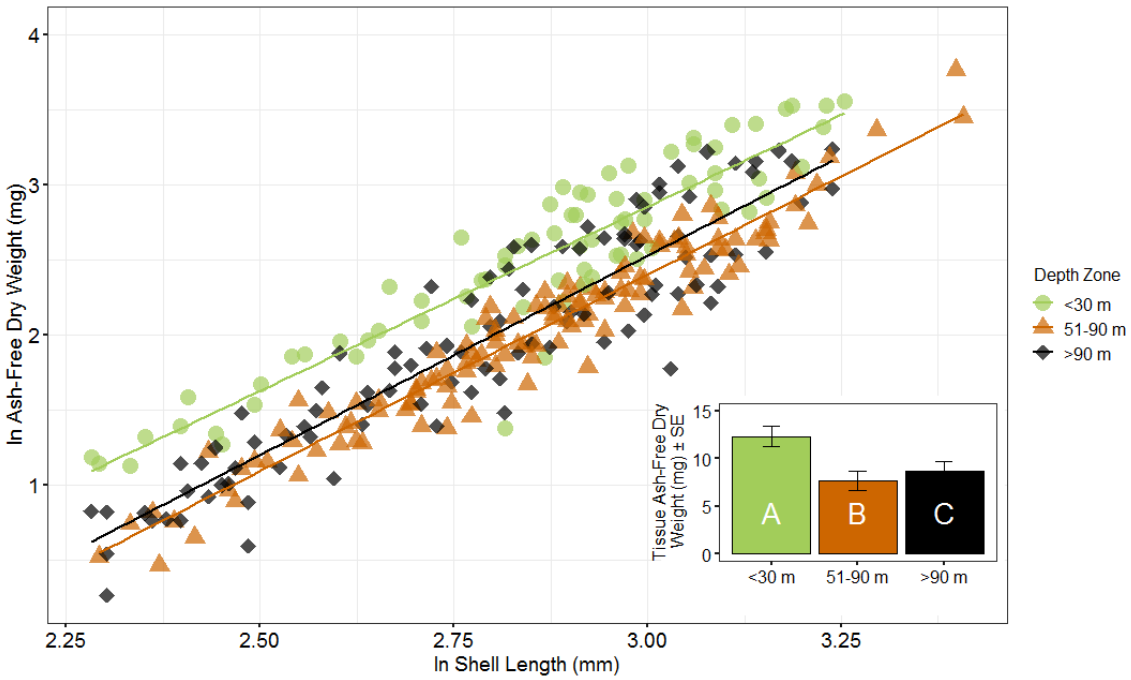


Figure 6. Lake Ontario 2018 quagga mussel body condition by depth zone. Refer to Fig. 5 for station locations and depth categories. The main figure shows tissue ash-free dry weight (ln AFDW) as a function of shell length (ln mm) for quagga mussels collected from three depth zones: <30 m (green circles); 51-90 m (orange triangles); and >90 m (black diamonds). Figure inset displays quagga mussel tissue AFDW by depth zone, expressed as least square means from ANCOVA, adjusted for corresponding

shell length. Categories with different letters differ significantly ($p < 0.05$), according to pairwise comparisons.

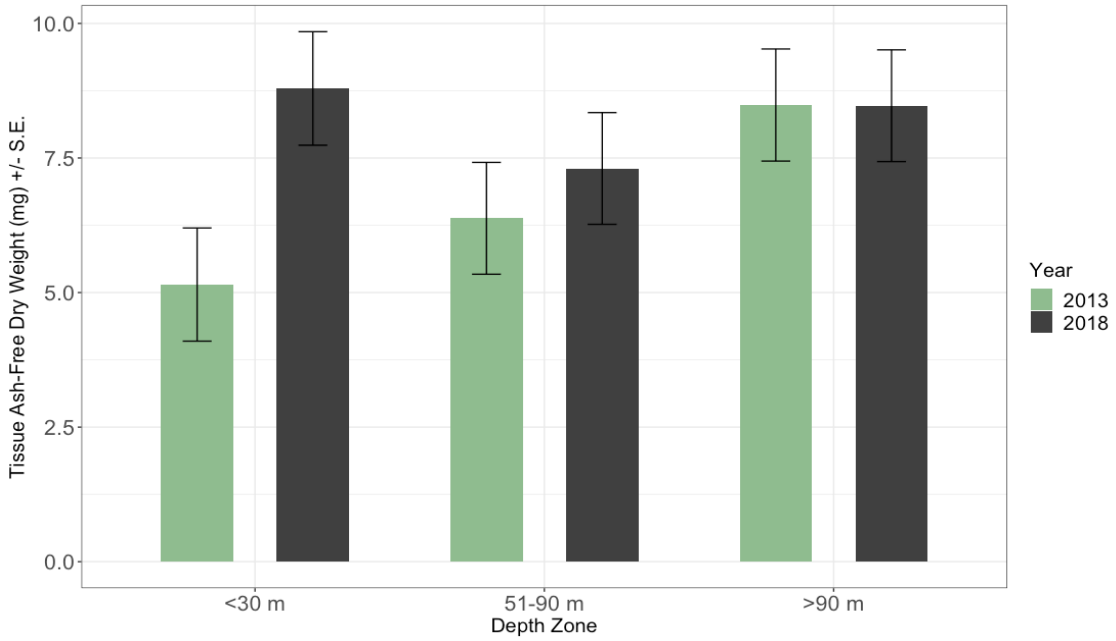


Figure 7. Quagga mussel tissue ash-free dry weight over time, by depth zone, for a subset of five stations that were sampled in both 2013 and 2018 (< 30 m- ON29; 51 - 90 m- ON28 and ON61; > 90 m- ON34 and ON55; refer to Fig. 5 for locations). Values are least square means from ANCOVA, adjusted for corresponding shell length, for all mussels pooled within each depth zone. There was a significant difference between years at the depth zones of < 30 m and 51 - 90 m, but not at > 90 m.

# Lake Ontario Benthos Survey Cooperative Science and Monitoring Initiative 2018

**Alexander Y. Karatayev, Lyubov E. Burlakova, Knut Mehler, Susan E. Daniel, and Allison R. Hrycik, Great Lakes Center, SUNY Buffalo State, Buffalo, New York**

## CHAPTER 1. MAJOR FINDINGS FROM THE CSMI BENTHIC MACROINVERTEBRATE SURVEY IN LAKE ONTARIO IN 2018 WITH AN EMPHASIS ON TEMPORAL TRENDS

### INTRODUCTION

In this report, we present results of a benthic survey of Lake Ontario conducted as part of the United States Environmental Protection Agency (U.S. EPA) Great Lakes National Program Office (GLNPO) Great Lakes Biology Monitoring Program (GLBMP). The benthic monitoring component of GLBMP includes sample collections from a number of long-term monitoring stations (9 - 16 depending on the lake) sampled every year for each of the five Great Lakes and a much more intensive lake-wide survey conducted on each lake every 5 years as part of the Cooperative Science and Monitoring Initiative (CSMI). Consistent with the sampling scheme of previous CSMI benthic surveys, a lake-wide benthic survey was conducted in 2018 at 61 stations in Lake Ontario to assess the status of the benthic macroinvertebrate community. The primary focus of this survey was the status of benthic community, including the invasive zebra mussels (*Dreissena polymorpha*) and quagga mussels (*D. rostriformis bugensis*) in comparison with historic data.

This report contains detailed descriptions of benthic communities in Lake Ontario in 2018, including information on sampling design (station locations, sampling and laboratory procedures) and the taxonomy and abundance of benthic invertebrates. Primary information (number and biomass of each taxon in each replicate sample) can be requested from U.S. EPA GLNPO. Detailed analysis of results obtained within this study are provided in the peer-reviewed publications submitted to the special issue of the *Journal of Great Lakes Research* "Lake Ontario 2020" (Appendices 2, 3).

## METHODS

### *Station Locations and Field Procedures*

Samples for benthic macroinvertebrates were collected from August - September 2018 at 61 stations located throughout Lake Ontario (Fig. 1.1, Appendix 1), including historically sampled sites. Stations were sampled aboard the U.S. EPA R/V *Lake Guardian* using a regular Ponar grab (sampling area 0.0523 $m^2$, coefficient used to calculate density per $m^2$ = 19.12), including 9 stations sampled during the summer Long-term Monitoring (LTM) survey in August and 52 stations during the CSMI survey in September. Three replicate Ponar samples were successfully collected at 55 of the planned 61 stations, excluding 6 stations (#29, 42, 43, 62, 66, and 71B) where samples were not collected due to hard substrate. A total of 165 samples were analyzed for benthos and *Dreissena* population assessment.

Upon collection, each sample was placed separately into an elutriation device and then washed through a 500-µm mesh screen. All retained organisms and sediments were placed into a collection jar and preserved with neutral buffered formalin with Rose Bengal stain to a final concentration of 5 – 10%. Detailed methods are described in the EPA GLNPO Standard Operating Procedure for Benthic Invertebrate Field Sampling (SOP LG406, Revision 12, March 2018).

### *Laboratory Procedures*

All organisms found in each replicate sample at the 55 Ponar stations were sorted, identified, counted, and weighted (total wet weight). Organisms were separated under low magnification using a dissecting microscope. Oligochaetes and chironomids were mounted on slides and identified using a compound microscope; other organisms were identified using a dissecting microscope. Adult oligochaetes were identified to species; immature Tubificidae, Lumbriculidae, Naididae and Enchytraeidae were identified to the lowest taxonomic level possible, usually family, and included in density and biomass estimates. Counts of oligochaete fragments were excluded from density analyses but fragment weight was considered in the determination of biomass. Immature Oligochaeta (in cocoons) were recorded but excluded both from density and biomass calculations for comparison with historic data. Chironomids were identified to the lowest practical taxonomic level, usually genus. Other invertebrates were identified to species, when possible.

*Dreissena* from all samples were identified to species, measured to the nearest millimeter with a caliper, counted, and the whole sample was weighed to the nearest 0.0001 g after being blotted dry on absorbent paper (total wet weight of tissue and shell, WW); details are described in the EPA GLNPO Standard Operating Procedure for Benthic Invertebrate Laboratory Analysis (SOP LG407, Revision 09, April 2015). All *Dreissena* collected during this survey were quagga mussels.


**Figure 1.1.** Location of stations in Lake Ontario sampled for *Dreissena* during August – September 2018. Please find information on station locations and depths in Appendix 1.

## RESULTS AND DISCUSSION

### *Benthic Taxonomy, Density and Biomass*

We found 76 species and higher taxa of benthic macroinvertebrates in Lake Ontario in 2018. The most diverse were Oligochaeta (33 species and higher taxa), Insecta (Chironomidae, 28), Malacostraca (6 species: 5 Amphipoda and 1 Mysida), and Bivalvia (3). Other classes were represented by less than 3 taxa, or were not identified to species level (e.g., Trepaxonemata, Hirudinea, Hydrozoa, Nemertea). Among Oligochaeta, the most diverse were Tubificidae (18 species and higher taxa), and Naididae (13).

The most widely occurred species throughout the lake was exotic bivalve *Dreissena r. bugensis*, found at 98% of all 55 benthic stations sampled, followed by Oligochaeta (immature tubificids: 83%, immature lumbriculids: 78%, lumbriculid *Stylodrilus heringianus*: 60%, and tubificid *Limnodrilus hoffmeisteri*: 56%), *Mysis* (56%), and chironomids (*Micropsectra* sp.: 47%, *Heterotrissocladius subpilosus* group: 44%, and *Procladius* sp.: 36%). All other species were found in less than 50% of the samples.

*Dreissena r. bugensis* comprised a large percentage of lake-wide benthos densities (67%), followed by Oligochaeta (28%), and by Chironomida (5%). Contribution of other groups (Amphipoda, Gastropoda, Hirudinea, etc.) to total benthos density was less than 1% each. Among Oligochaeta, the most numerous were Tubificidae (79%) and Lumbriculidae (19%). *Dreissena r. bugensis* dominated lake-

wide benthos by biomass (99.8% of total wet biomass) (Table 1.1). The remaining benthic biomass was represented by Oligochaeta (0.15%) and Chironomidae (0.02%) (Table 1.1).

**Table 1.1.** Average (± standard error) density (ind. $m^{-2}$) and wet biomass (g $m^{-2}$) of major taxonomic groups of benthic invertebrates collected in Lake Ontario in 2018 averaged by depth zones and lake-wide. In 2018 benthos was collected at 55 stations. n.r. – not recorded. Number of stations given in parentheses.

| **Taxa** | **0 - 30m (13)** | **>30 - 50m (3)** | **>50 - 90m (16)** | **>90m (23)** | **Lake-wide (55)** |
|---|---|---|---|---|---|
| Amphipoda (ind. $m^{-2}$) | 33±16 | n.r. | 2±1 | n.r. | 8±4 |
| (g $m^{-2}$) | 0.08±0.04 | n.r. | 0.01±0.01 | n.r. | 0.02±0.01 |
| Chironomidae (ind. $m^{-2}$) | 569±116 | 74±49 | 408±90 | 88±29 | 294±48 |
| (g $m^{-2}$) | 0.44±0.07 | 0.05±0.02 | 0.25±0.06 | 0.08±0.02 | 0.21±0.03 |
| *Diporeia* (ind. $m^{-2}$) | n.r. | n.r. | n.r. | 0.3±0.3 | 0.1±0.1 |
| (g $m^{-2}$) | n.r. | n.r. | n.r. | 0.002±0.002 | 0.001±0.001 |
| *Dreissena* (ind. $m^{-2}$) | 5037±2133 | 4587±1965 | 4749±532 | 3554±501 | 4308±566 |
| (g $m^{-2}$) | 1432±455 | 1007±228 | 1931±236 | 539±112 | 1181±156 |
| Sphaeriidae (ind. $m^{-2}$) | n.r. | n.r. | 2±2 | 18±5 | 8±2 |
| (g $m^{-2}$) | n.r. | n.r. | <0.01 | 0.02±0.01 | 0.010±0.004 |
| Gastropoda (ind. $m^{-2}$) | 57±57 | n.r. | n.r. | n.r. | 14±14 |
| (g $m^{-2}$) | 0.15±0.15 | n.r. | n.r. | n.r. | 0.03±0.03 |
| Hirudinea (ind. $m^{-2}$) | 2±2 | n.r. | n.r. | n.r. | 0.5±0.5 |
| (g $m^{-2}$) | <0.001 | n.r. | n.r. | n.r. | <0.001 |
| Mysidae (ind. $m^{-2}$) | 1±1 | n.r. | \|}16±4 | 40±10 | 21±5 |
| (g $m^{-2}$) | 0.004±0.004 | n.r. | 0.19±0.05 | 0.62±0.24 | 0.31±0.11 |
| All Oligochaeta (ind. $m^{-2}$) | 3681±940 | 5494±4300 | 1516±263 | 426±79 | 1789±367 |
| (g $m^{-2}$) | 1.87±0.63 | 2.68±1.73 | 2.56±0.42 | 1.07±0.28 | 1.78±0.25 |
| Others (ind. $m^{-2}$) | 16±8 | 36±19 | 14±4 | 5±2 | 12±3 |
| (g $m^{-2}$) | 0.04±0.03 | 0.03±0.02 | 0.04±0.01 | 0.02±0.01 | 0.03±0.01 |
| Turbellaria (ind. $m^{-2}$) | 5±3 | 21±13 | 6±2 | 1±1 | 4±1 |
| (g $m^{-2}$) | 0.001±0.001 | 0.003±0.002 | 0.001±0.001 | <0.001 | 0.001±0.0002 |
| All benthos (ind. $m^{-2}$) | 9401±2919 | 10212±6256 | 6711±665 | 4131±580 | 6459±845 |
| (g $m^{-2}$) | 1435±456 | 1009±229 | 1934±237 | 541±112 | 1183±156 |
| All benthos w/o *Dreissena* (ind. $m^{-2}$) | 4364±978 | 5626±4295 | 1964±259 | 577±88 | 2151±384 |
| (g $m^{-2}$) | 2.58±0.72 | 2.76±1.73 | 3.05±0.42 | 1.81±0.49 | 2.4±0.31 |

### *Long-Term Trends in Benthos*

This section contains a brief description of trends for all major groups of benthic invertebrates in the last 50 years (except for *Dreissena*, for which trends are described in the "*Dreissena* Spatial and Temporal Trends" section of this report). This analysis is based on data from 13 lake-wide benthic surveys conducted in Lake Ontario over the course of 54 years (1964, 1972, 1977, 1990, 1994, 1995, 1997-1999, 2003, 2008, 2013 and 2018) (Hiltunen, 1969; Nalepa and Thomas, 1976; Golini, 1979; Lozano et al., 2001; Dermott and Geminiuc, 2003; Watkins et al., 2007; Birkett et al., 2015; Nalepa and Baldridge, 2016, Appendix 2). Due to different sampling locations over time, historical comparisons were performed using densities in each depth zone (<30 m, >30 – 50 m, >50 – 90 m, and >90 m) and lake-wide as a weighted average using means of stations located at 4 depth zones considering the proportion of the total lake area represented by each zone (21.6, 11.7, 18.5, and 48.2%, respectively) (Appendix 2). Detailed analysis of long-term trends in benthos is provided in the peer-reviewed publications submitted to the special issue of the Journal of Great Lakes Research "Lake Ontario 2020" (Appendices 3, 4).

Among the major long-term trends in densities of benthic macroinvertebrates in Lake Ontario, the most important were the decline in *Diporeia* (Spearman $\rho = -0.50$, $P < 0.001$) and in Sphaeriidae ($\rho = -0.40$, $P < 0.001$) at all depth zones starting in the mid-1990s, which followed a period of elevated densities at depths >30 m in late 1980s – early 1990s (Fig. 2, Appendix 2). Similar trends in *Diporeia* densities were observed in lakes Michigan (Nalepa et al., 2017) and Huron (Karatayev et al., 2020). Currently, *Diporeia* is only present at depths >90 m at very low densities (<1 $m^{-2}$). Total oligochaete density significantly declined in the shallow zone (<30 m) in the past several decades ($\rho = -0.14$, $P < 0.001$); the highest observed densities on record (app. 10,000 $m^{-2}$) occurred in 1964 and 1990, after which densities decreased to <1000 $m^{-2}$ by 2008. However, there has been an increase in the last five years (2013 – 2018), with densities rebounding to 2,000 – 4,000 $m^{-2}$ (Fig. 2, Appendix 2). These long-term trends were mostly driven by large changes in pollution-tolerant Tubificidae ($\rho = -0.22$, $P < 0.001$), which comprise 20 to 95% of all Oligochaeta densities. Tubificidae underwent the most dramatic changes in the shallow zone ($\rho = -0.42$, $P < 0.001$), declining over ten-fold from their peak densities in 1960s and 1990s (~9,000 $m^{-2}$) to 765±276 $m^{-2}$ in 2008, and then increased again to ~ 3,000 $m^{-2}$ in 2013 – 2018. Amphipoda (excluding *Diporeia*), Gastropoda, Hirudinea, and Trichoptera densities all peaked in the shallow zone in mid-1990s, likely positively affected by aggregations of zebra mussels, and then declined (Appendix 2).

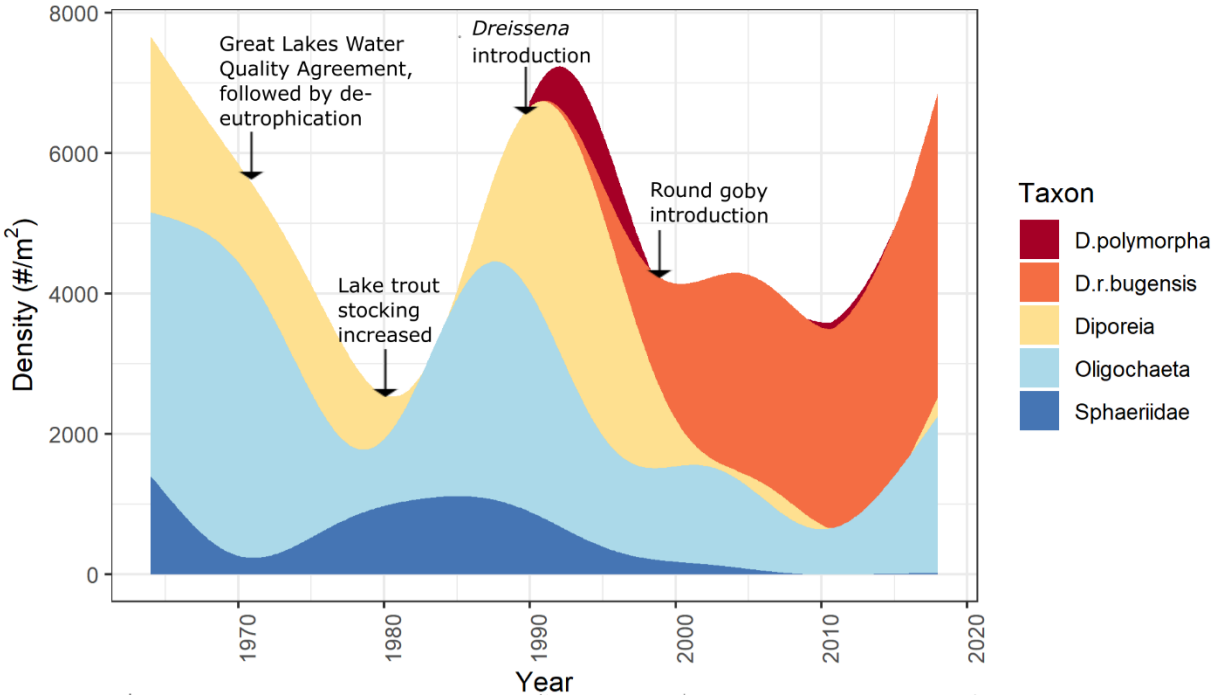


**Figure 1.2.** Average densities of major taxonomic groups that were consistently counted over time for the entire Lake Ontario with major events highlighted. The following years in our data set were excluded due to incomplete data: 1994 and 2003. Missing data were simulated using splines, then all data were smoothed with a general additive model (GAM) function. See Appendix 2 for data.

The only taxa that showed increasing density trends with time were *Dreissena* (lake-wide $\rho$ = 0.71, P <0.001) and Chironomidae ($\rho$ = 0.20, P <0.001), with the strongest increases occurring at intermediate depths (>30 – 90 m) (*Dreissena*: $\rho$ = 0.84, P <0.001; Chironomidae: $\rho$ >0.30, P <0.01). As a result of mixed increasing and decreasing trends across individual taxa, total benthos density did not exhibit clear overall trends lake-wide ($\rho$ = 0.07, P = 0.04). However, total benthos (excluding *Dreissena*) declined lake-wide ($\rho$ = -0.29, P <0.001). The decline in native species densities was most pronounced at depths >90 m ($\rho$ = -0.45; P <0.0001), primarily due to the large declines in *Diporeia* and Sphaeriidae.

### *Dreissena Spatial and Temporal Trends*

Among the deep Great Lakes (all lakes except Lake Erie), Lake Ontario has the longest history of dreissenid invasion (since 1989 for zebra mussels, Griffiths et al., 1991, and since 1990 for quagga mussels, Mills et al., 1993); therefore, trends observed in Lake Ontario may provide insight into the potential long-term dynamics of *Dreissena* populations across depth zones in other deep lakes of North America and Europe.

To document long-term trends in *Dreissena* population dynamics in Lake Ontario, we compiled a dataset of *Dreissena* spp. densities by station and depth for 1990, 1995, 1997, 1998, 1999, 2003, 2008, and 2013 (Dermott and Geminiuc, 2003; Lozano et al., 2001; Watkins et al., 2007; Birkett et al., 2015; Nalepa and Baldridge, 2016) to complement the data from 2018 presented here. To increase the spatial resolution of the 2003, 2008, and 2013 surveys, we added data from the U.S. EPA Great Lakes National Program Office (GLNPO) long-term monitoring stations (9 to 10 stations per survey, Burlakova et al., 2018). Detailed analysis of this database is provided in a paper submitted to the Special Issue of the Journal of Great Lakes Research "Lake Ontario 2020" (Appendix 3). Below is a brief analysis of *Dreissena* spp. population dynamics in Lake Ontario over the last 30 years.

Previous studies in Lake Ontario have shown that quagga mussels reached their population maximum in the shallow (0 – 30 m) to mid (>30 – 50 m) depth zone by 2003, 13 years after the first detection in Lake Ontario, and then declined (Table 1.2; Birkett et al., 2015; Nalepa and Baldridge, 2016; Karatayev et al., accepted). Such a decline may be expected if quagga mussels in shallow to mid-depth water had increased to densities greater than their carrying capacity. Similar declines in dreissenid densities in the nearshore zone, along with a shift of the maximum density to deeper areas, were also observed in lakes Michigan and Huron (Nalepa et al., 2020; Karatayev et al., 2020; Mehler et al., 2020). At depths <50 m, the decline in density occurred mainly from 2003 to 2008, and there were no significant changes from 2008 to 2018. Mussel densities in >50 – 90 m steadily declined from 2003 to 2018, but densities in deep water and lake-wide have significantly increased (Table 1.2). The increases in mussel density at depths >90 m have a strong influence on lake-wide values because by area, 48% of the lake bottom is >90 m deep.

The recent increases in lake-wide density were unexpected considering the substantial population decline recorded from 2003 to 2008 (Table 1.2). Based on observed declines in lake-wide *Dreissena* density in Michigan in 2015, 18 years after the first record of quagga mussels in the lake (Nalepa et al., 2020), we had expected the 2018 Lake Ontario surveys to indicate further declines in quagga mussel populations as well, especially given that the mussels have been present in Lake Ontario for 30 years. Contrary to our prediction, we found significant increases in *Dreissena* lake-wide density and biomass, suggesting that the mussel population in Lake Ontario is still increasing. The lake-wide average of *Dreissena* biomass was the highest observed in Lake Ontario to date at 25.2±3.3 g $m^{-2}$ of ash-free dry tissue weight (Karatayev et al., accepted).

**Table 1.2.** Long-term dynamics of *Dreissena polymorpha* and *D. rostriformis bugensis* density ($m^{-2}$) in Lake Ontario. Average ± standard errors. Lake-wide densities were calculated as weighted averages from four depth zones. Sample size given in parenthesis.

| Depth / Species | 1990 (25) | 1995 (41) | 1997 (68) | 1998 (114) | 1999 (67) | 2003 (46) | 2008 (58) | 2013 (55) | 2018 (55) |
|---|---|---|---|---|---|---|---|---|---|
| **0 - 30 m** | | | | | | | | | |
| *D. polymorpha* | 14±9 | 3108±1118 | 1259±697 | 2394±1259 | 126±59 | 38±36 | 0 | 0 | 0 |
| *D. r. bugensis* | 0 | 1798±1078 | 774±390 | 3472±1022 | 1786±335 | 7724±2936 | 2366±1074 | 2651±1177 | 5037±2132 |
| Both species | 14±9 | 4906±1716 | 2033±757 | 5867±1972 | 1913±333 | 7762±2931 | 2366±1074 | 2651±1177 | 5037±2133 |
| **>30 - 50 m** | | | | | | | | | |
| *D. polymorpha* | 0 | 29±29 | 46±39 | 27±11 | 9±9 | 0 | 0 | 0 | 0 |
| *D. r. bugensis* | 0 | 15±9 | 1271±608 | 1748±517 | 3899±1057 | 10315±4289 | 3536±1741 | 5385±1301 | 4587±1964 |
| Both species | 0 | 44±37 | 1317±619 | 1776±513 | 3907±1060 | 10315±4289 | 3536±1741 | 5385±1301 | 4587±1965 |
| **>50 - 90 m** | | | | | | | | | |
| *D. polymorpha* | 0 | 4±4 | 28±26 | 1±1 | 3±3 | 1±1 | 0 | 0 | 0 |
| *D. r. bugensis* | 5±5 | 7±5 | 122±55 | 282±114 | 4484±1397 | 7338±1835 | 6854±993 | 5355±566 | 4749±532 |
| Both species | 5±5 | 11±6 | 150±77 | 283±114 | 4487±1397 | 7339±1835 | 6854±993 | 5355±566 | 4749±532 |
| **>90 m** | | | | | | | | | |
| *D. polymorpha* | 2±2 | 0 | 0 | >1±>1 | 0 | 0 | 0 | 0 | 0 |
| *D. r. bugensis* | 7±7 | 0 | 1±1 | 2±1 | 35±24 | 840±479 | 594±329 | 1909±398 | 3554±501 |
| Both species | 9±9 | 0 | 1±1 | 2±1 | 35±24 | 840±479 | 594±329 | 1909±398 | 3554±501 |
| **Lake-wide** | | | | | | | | | |
| *D. polymorpha* | 4±2 | 676±242 | 283±151 | 521±272 | 29±13 | 8±8 | 0 | 0 | 0 |
| *D. r. bugensis* | 4±4 | 391±233 | 339±111 | 1008±230 | 1688±296 | 4638±907 | 2479±393 | 3114±368 | 4216±577 |
| Both species | 8±5 | 1067±371 | 621±179 | 1528±431 | 1717±296 | 4646±906 | 2479±393 | 3114±368 | 4216±577 |

## REFERENCES


Birkett, K., Lozano, S.J., Rudstam, L.G., 2015. Long-term trends in Lake Ontario's benthic macroinvertebrate community from 1994-2008. Aquat. Ecosystem Health Manag. 18, 78-88.

Burlakova, L.E., Barbiero, R.P., Karatayev, A.Y., Daniel, S.E., Hinchey, E.K., Warren, G., 2018. The benthic community of the Laurentian Great Lakes: analysis of spatial gradients and temporal trends from 1998-2014. J. Great Lakes Res. 44, 600-617.

Dermott, R., Geminiuc, M., 2003. Changes in the benthic fauna of Lake Ontario 1990–1995, with local trends after 1981. In *State of Lake Ontario (SOLO)—Past, Present, and Future,* M. Munawar, ed., pp. 323-345. Leiden, The Netherlands: Ecovision World Monograph Series, Backhuys Publishers.

Hiltunen, J.K., 1969. The benthic macrofauna of Lake Ontario. Great Lakes Fish. Comm. Tech. Rep. 14, 39-50.

Golini, V.I., 1979. Benthic macro-and meioinvertebrates of Lake Ontario 1977: distribution and relative abundance. Fish. Environ. Can., Fish. Mar. Serv. MS Rep 1519.

Griffiths, R.W., Schloesser, D.W., Leach, J.H., Kovalak, W.P., 1991. Distribution and dispersal of the zebra mussel (*Dreissena polymorpha*) in the Great Lakes region. Can. J. Fish. Aquat. Sci. 48, 1381-1388.

Karatayev, A.Y., Burlakova, L.E., Mehler, K., Daniel, S.E., Elgin, A.K., Nalepa, T.F., 2020. Lake Huron Benthos Survey Cooperative Science and Monitoring Initiative 2017. Technical Report. USEPA-GLRI GL00E02254. Great Lakes Center, SUNY Buffalo State, Buffalo, NY. Available at: http://greatlakescenter.buffalostate.edu/sites/greatlakescenter.buffalostate.edu/files/uploads/Documents/Publications/LakeHuronBenthosSurveyCSMI2017FinalReport.pdf.

Lozano, S.J., Scharold, J.V., Nalepa, T.F., 2001. Recent declines in benthic macroinvertebrate densities in Lake Ontario. Can. J. Fish. Aquat. Sci. 58, 518-529.

Mehler, K., Burlakova, L.E., Karatayev, A.Y., Elgin, A.K., Nalepa, T.F., Madenjian, C.P., Hinchey, E., 2020. Long-term trends of Lake Michigan benthos with emphasis on the southern basin. J. Great Lakes Res. 46, 528-537.

Mills, E.L., Dermott, R.M., Roseman, E.F., Dustin, D., Mellina, E., Corm D.B., Spidle, A.P., 1993. Colonization, ecology, and population structure of the "quagga" mussel (Bivalvia: Dreissenidae) in the lower Great Lakes. Can. J. Fish. Aquat. Sci. 50, 2305-2314.

Nalepa, T.F., and Thomas, N.A. 1976. Distribution of microbenthic species in Lake Ontario in relation to sources of pollution and sediment parameters. J. Great Lakes Res. 2:150-163.

Nalepa, T.F., Baldridge, A.K., 2016. Benthos. Lake Ontario Cooperative Science and Monitoring Initiative (CSMI) 2013. Summary Report.

Nalepa, T.F., Burlakova, L.E., Elgin, A.K., Karatayev, A.Y., Lang, G.A., and Mehler, K., 2017. Major Findings from the CSMI Benthic Macroinvertebrate Survey in Lake Michigan in 2015 with an Emphasis on Temporal Trends. Chapter 3. In: Lake Erie and Lake Michigan Benthos: Cooperative Science and Monitoring Initiative. Final Report. USGS-GLRI G14AC00263. Great Lakes Center, SUNY Buffalo State, Buffalo, NY. Available at: https://greatlakescenter.buffalostate.edu/sites/greatlakescenter.buffalostate.edu/files/uploads/Documents/Publications/LakeErieandMichiganBenthosCSMI2014-2015FinalReport.pdf

Nalepa, T.F., Burlakova, L.E., Elgin, A.K., Karatayev, A.Y., Lang, G.A., Mehler, K., 2020. NOAA Tech memo GLERL-175. Abundance and biomass of benthic macroinvertebrates in Lake Michigan in 2015, with a summary of temporal trends. Tech. Memo, NOAA Great Lakes Environmental Research Laboratory, NOAA Great Lakes environmental Research Laboratory, Ann Arbor MI. doi:10.25923/g0d3-3v41.

Watkins, J.M., Dermott, R., Lozano, S.J., Mills, E.L., Rudstam, L.G., Scharold, J.V., 2007. Evidence for remote effects of dreissenids mussels on the amphipod *Diporea*: analysis of Lake Ontario benthic surveys, 1997-2003. J. Great Lakes Res. 33, 642-657.

# CHAPTER 2. UNDERWATER VIDEO IMAGE ANALYSIS OF *DREISSENA* DISTRIBUTION IN LAKE ONTARIO IN 2018

## INTRODUCTION

Incorporation of underwater image analysis into the designs of benthic surveys allows for the assessment of much larger lakebed areas, independently of substrate, in a cost- and time-effective manner. Such analysis can provide valuable information about the abundance, distribution patterns, and structure of *Dreissena* beds at various spatial scales, and it may significantly increase the precision of population size estimates (Karatayev et al., 2018).

Underwater video methods have been previously used in the Great Lakes; however, these studies were largely limited to the nearshore zone and analyzed relatively few video images per station (Custer and Custer, 1997; Ozersky et al., 2009, 2011; Lietz et al., 2015; Mehler et al., 2018). We conducted the first lake-wide *Dreissena* studies incorporating video transects in Lake Michigan in 2015, followed by Lake Huron in 2017. At each station (47 and 43 in lakes Michigan and Huron, respectively), we collected continuous video footage from 500 m-long transects along the lakebed. In 2018, we used video transects coupled with traditional grab sampling to estimate *Dreissena* coverage, density, and biomass in Lake Ontario, using procedures previously developed for Lake Michigan (Karatayev et al., 2018).

## METHODS

We analyzed bottom video images taken during the 2018 CSMI study in Lake Ontario to study *Dreissena* spatial distributions and aggregation patterns along depth gradients (Fig. 2.1). Video images were obtained from a GoPro Hero 4 Black camera (hereafter GoPro) mounted on the Ponar grab and from a GoPro mounted on a benthic sled towed behind the R/V *Lake Guardian* for approximately 500 m.

Before the analysis, the quality of both Ponar and sled videos were classified as either acceptable or unacceptable for assessment of *Dreissena* density, biomass, and aggregations (Karatayev et al., 2018), and only videos of acceptable quality were used in further analysis. More than 80% of the Ponar videos and almost 60% of the sled videos had acceptable quality (Table 2.1). Half of the sled videos categorized as unacceptable had controllable issues (camera not in focus, insufficient light, sled not on bottom, etc.) while the other half had uncontrollable reasons such as algae cover or *Dreissena* buried in sediment.

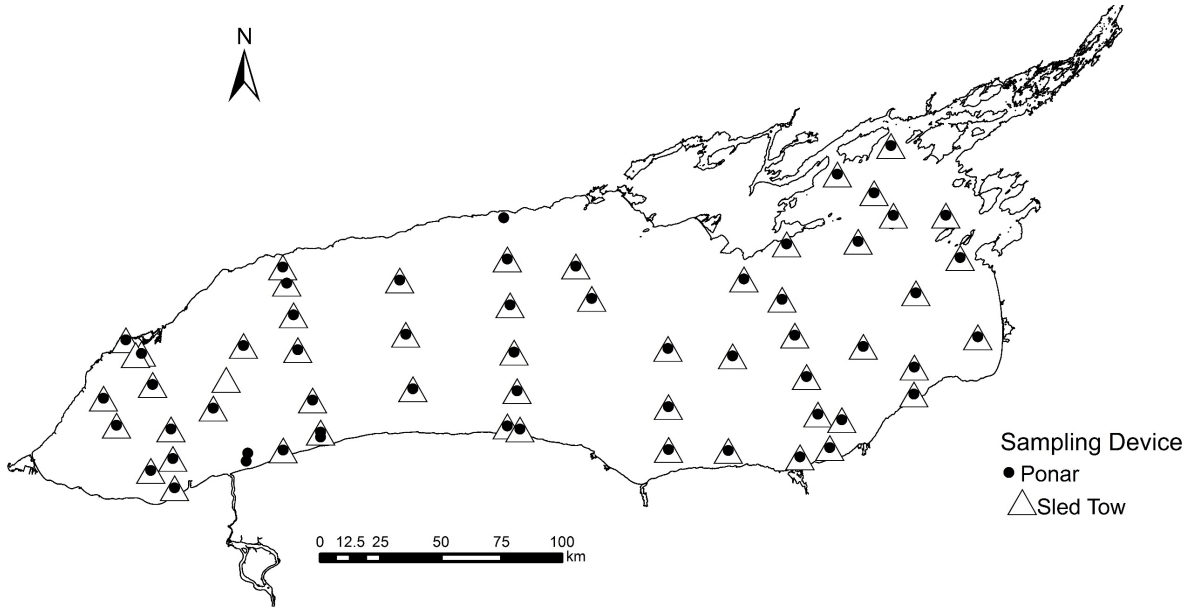


**Figure 2.1.** Location of stations in Lake Ontario sampled in 2018 with Ponar grabs with videos (black filled circles) and sled tows (open triangles).

**Table 2.1.** Number of acceptable (percent of total in parenthesis) and unacceptable bottom images collected in Lake Ontario in 2018 using GoPro cameras attached to Ponar grab and benthic sled. Unacceptable images were classified as controllable (e.g. equipment malfunction or human error) or uncontrollable (e.g. high turbidity, macrophyte coverage, etc.).

| Parameters | Ponar videos (3 still images per video) | Sled videos (100 still images per video) |
|---|---|---|
| Number of stations (CSMI + LTM) with videos | (52 + 7) | (49 + 8) |
| Number of acceptable still images | 123 (86%) | 3300 (58%) |
| Number of unacceptable still images | 54 (14%) | 2400 (42%) |
| Controllable | 47 | 900 |
| Uncontrollable | 7 | 1500 |

Videos from Ponar grabs were stopped shortly before the lake bottom was hit and a screenshot was taken. *Dreissena* mussels in each screen shot from the Ponar deployments (3 replicates at each station) were digitized in Photoshop CS6. *Dreissena* coverage was determined as percentage of each screenshot covered with mussels. To convert *Dreissena* percent coverage obtained from sled video images into density and biomass, we compared the density and biomass of *Dreissena* in three replicate Ponar samples with the mussel coverage estimated from the video images of the exact same Ponar replicate. *Dreissena* density and biomass from each Ponar replicate was paired with the coverage from still images, and the relationship between coverage and density and biomass was estimated using polynomial regression. We removed outliers using Grubbs test for outliers, which is calculated as the ratio of the largest absolute deviation from the sample mean to the sample standard deviation (Grubbs, 1969). We then used the relationship to convert *Dreissena* coverage from sled images into *Dreissena* density and biomass. We used t-tests to compare coverage among lakes using data from same depth zones, and to contrast density and biomass estimations from sled video transects with Ponar densities, and between lakes. For all tests effects were considered significant at $P < 0.05$, and marginally significant at $P < 0.10$.

## RESULTS AND DISCUSSION

### *Benthic Sled Videos*

The *Dreissena* distribution across depths estimated from sled tows had a skewed bell shape, with relatively, low average coverage in the nearshore (10 – 30 m) depth zone, the highest average density in the intermediate (>30 – 100 m) depth zone, and the lowest densities in the deepest part of the lake (>100 m) (Fig. 2.2, Table 2.2). The highest absolute coverage (98.7%) was found on a rocky substrate at station ON66 (16.6 m depth).

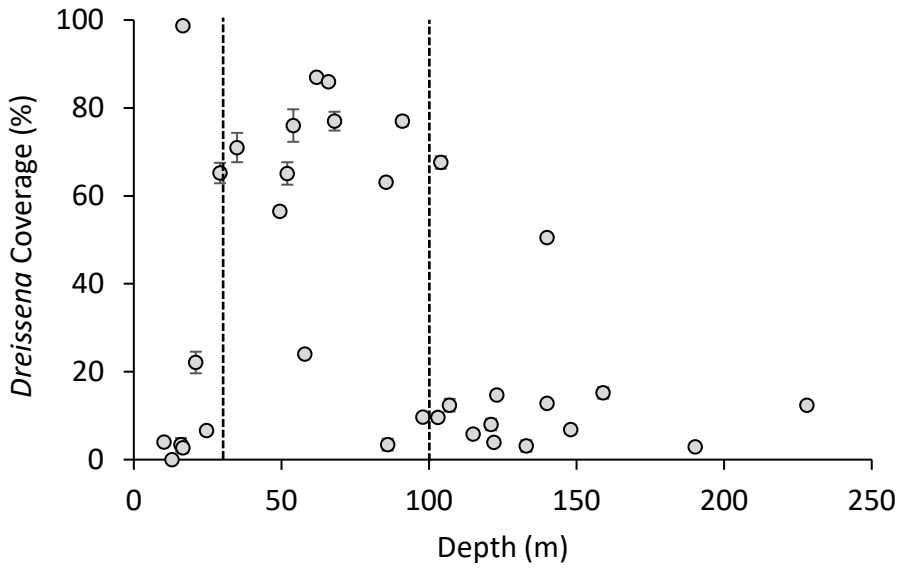


**Figure 2.2.** *Dreissena* percent coverage along depth gradient in of Lake Ontario in 2018. Error bars represent ±1 standard error. Dashed lines denote 30 m and 100 m depth ranges.

A similar bell-shaped distribution pattern of *Dreissena* coverage was found in our previous studies in Lake Michigan in 2015 and Lake Huron 2017 (Fig. 2.3). At the >30 – 100 m depth zone, *Dreissena* coverage was significantly higher in lakes Ontario and Michigan than in Lake Huron ($P < 0.001$ for both t-tests), but the *Dreissena* coverage was not different between lakes Ontario and Michigan ($P = 0.39$). At the >100 m depth zone, *Dreissena* coverage was significantly higher in Lake Ontario compared to Lake Michigan ($P < 0.01$), but no difference was found between lakes Ontario and Huron ($P = 0.29$) or lakes Michigan and Huron ($P = 0.26$). Lake-wide *Dreissena* coverage was significantly higher in lakes Ontario and Michigan compared to Lake Huron ($P < 0.001$ for both tests), but there was no difference in coverage between lakes Ontario and Michigan (33% vs. 34%, $P = 0.42$).

Similar to other Great Lakes, in Lake Ontario there is an abundant food supply for *Dreissena* in the shallow, warm, and well mixed nearshore environment, but physical disturbance (wave and currents) limits *Dreissena* to areas with suitable substrate for attachment (e.g., gravel, rocks, bedrock). Therefore, the distribution of *Dreissena* in such areas is typically very heterogeneous, with higher densities on stable rocky substrates compared to areas with less stable substrates (Fig. 2.4A).

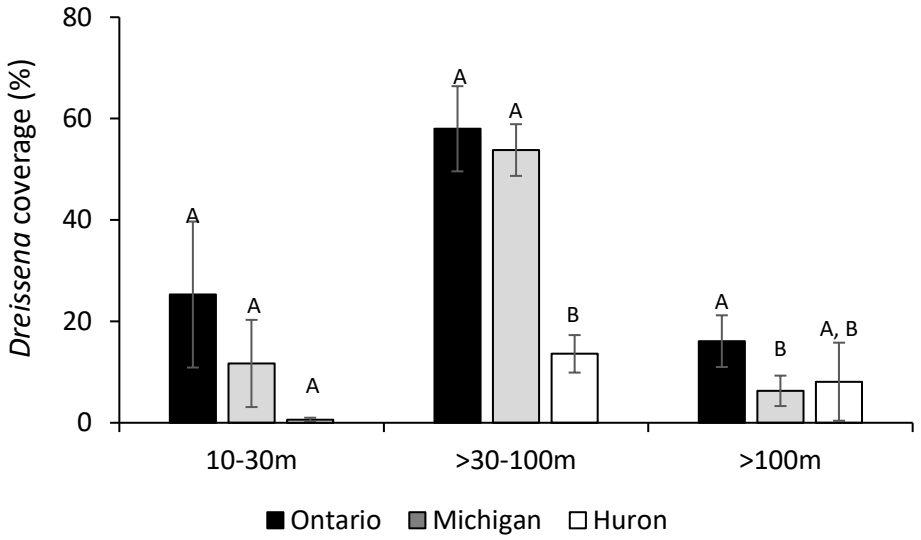


**Figure 2.3.** Comparison of *Dreissena* coverage in sled tows between lakes Ontario, Michigan and Huron. Different letters above each bar indicate a significant difference ($P < 0.05$) between lakes in each depth zone.

In the mid-depth zone, where food is still available but physical disturbance is lower, *Dreissena* forms the largest aggregations (Fig. 2.4B). In the deepest zone, *Dreissena* densities are lower and individuals are almost evenly distributed on the surface of bottom sediments; this distribution pattern is likely beneficial to mussels in the profundal zone because it reduces food competition where resources are scarce (Fig 2.4C). In the deepest zones of the lake, *Dreissena* only forms sizable aggregations along ridges, trenches, or rocks emerging above the sediment surface. These irregularities in the bottom floor create turbulence that can deliver additional food to the area, thus supporting higher densities of mussels than the flat bottom areas.

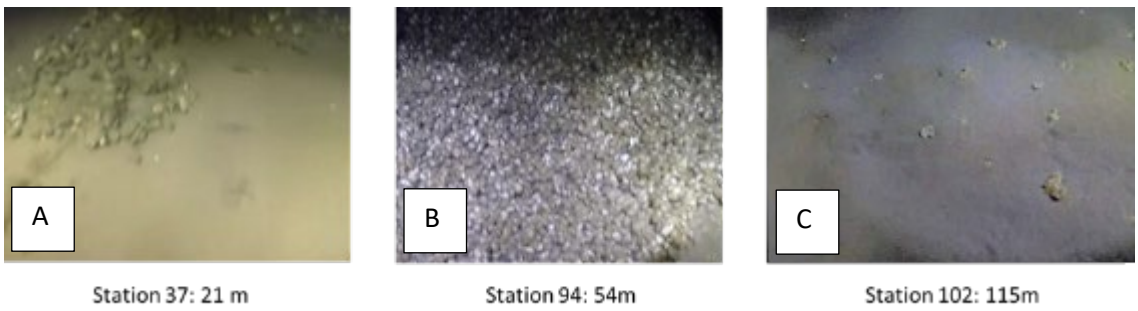


**Figure 2.4.** *Dreissena* representative screen shots for 10 – 30 m (A), >30 – 100 m (B), and >100 m depth zones (C). Station numbers and depth are provided for each screen shot.

### *Ponar Videos*

*Dreissena* areal coverage from 123 Ponar videos (3 replicates per Ponar grab) ranged from 0% to 100% (Mean ± SE: 26.1% ± 2.8). Similar to observations based on sled tow data, the mean *Dreissena* coverage based on Ponar videos was significantly higher (52.8% ± 5.0) at intermediate depths (>30 – 100 m) compared to shallow areas (7.1% ± 2.0, t-test, $p < 0.001$) and deeper areas (>100 m) (12.4% ± 2.1, t-test, $p < 0.001$). There was a strong relationship between coverage and mean *Dreissena* length (Fig. 2.5A). The average shell length of *Dreissena* was larger (15.6 ± 1.0 mm) in areas with the highest coverage in mid-depths (>30 – 100 m) compared to mussels from shallow depths (10 – 30 m, 5.2 ± 1.5 mm) and mussels from >100 m (8.2 ± 0.9 mm), likely due to combined effects of depth-related recruitment, density-dependence, and goby consumption (Fig. 2.5B). The abundance of 5 to 12 mm dreissenids, the size range most commonly consumed by round goby, was low except at >100 m depths. Although these size distributions indicate that round goby is affecting mussel recruitment, we did not find a decline in dreissenid density in the nearshore and mid-depth ranges where goby have been abundant since 2005 (Karatayev et al., accepted, Appendix 3).

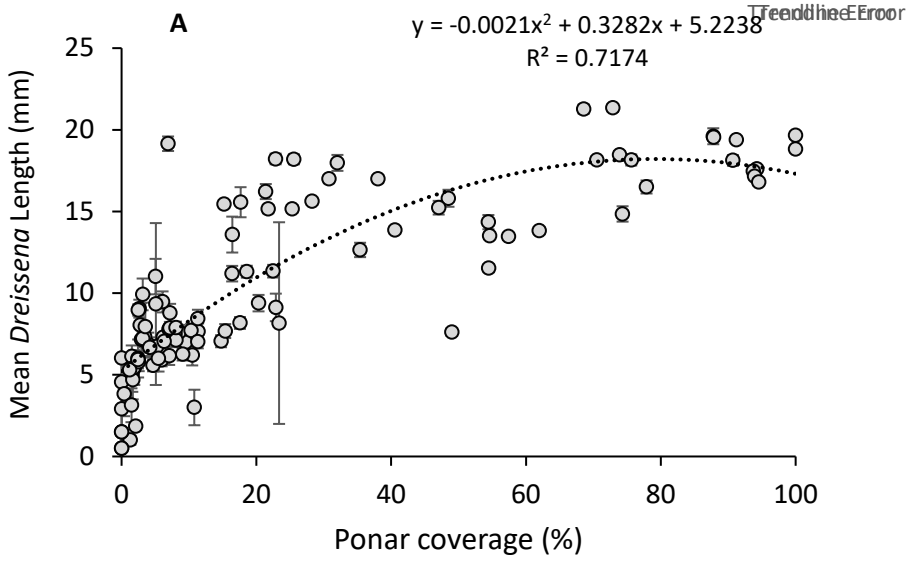

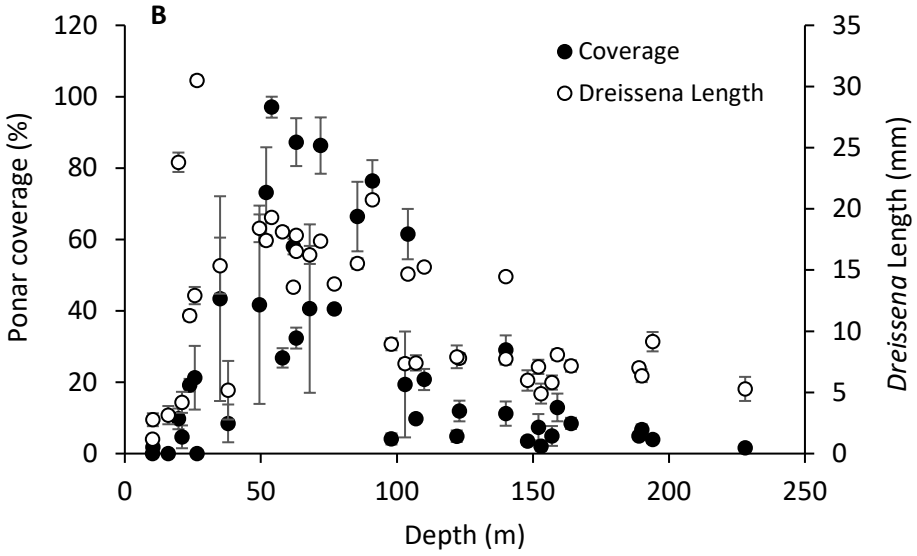


**Figure 2.5.** Power regression between average (+SE) *Dreissena* coverage and *Dreissena* mean length at each station collected from replicate Ponars (A) and relationship between *Dreissena* coverage, mean *Dreissena* size, and depth in Lake Ontario 2018 (B).

### *Dreissena Density: Ponar vs. Video Images*

The relationships between mussel density and biomass measured in Ponar grab samples and *Dreissena* percent coverage obtained from Ponar video images were best explained by second degree polynomial regression:

$$\boldsymbol{Density = -1.0068(coverage)^2 + 138.22(coverage) + 1174.1},$$

multiple $R^2 = 0.53$, $p < 0.01$ (Fig. 2.6A);

$$\boldsymbol{Biomass = -0.2186(coverage)^2\, x\, 44.223(coverage) + 136.53},$$

multiple $R^2 = 0.66$, $p < 0.01$ (Fig. 2.6B).

These coefficients were used to convert *Dreissena* coverage in sled tows into density and biomass. The polynomial relationships were due to the larger average *Dreissena* sizes in areas of intermediate depths and high coverage. *Dreissena* densities increased with increasing coverage up to 60%. Thereafter the curve flattened (biomass) and slightly declined (density) up to a coverage of 100%, respectively.

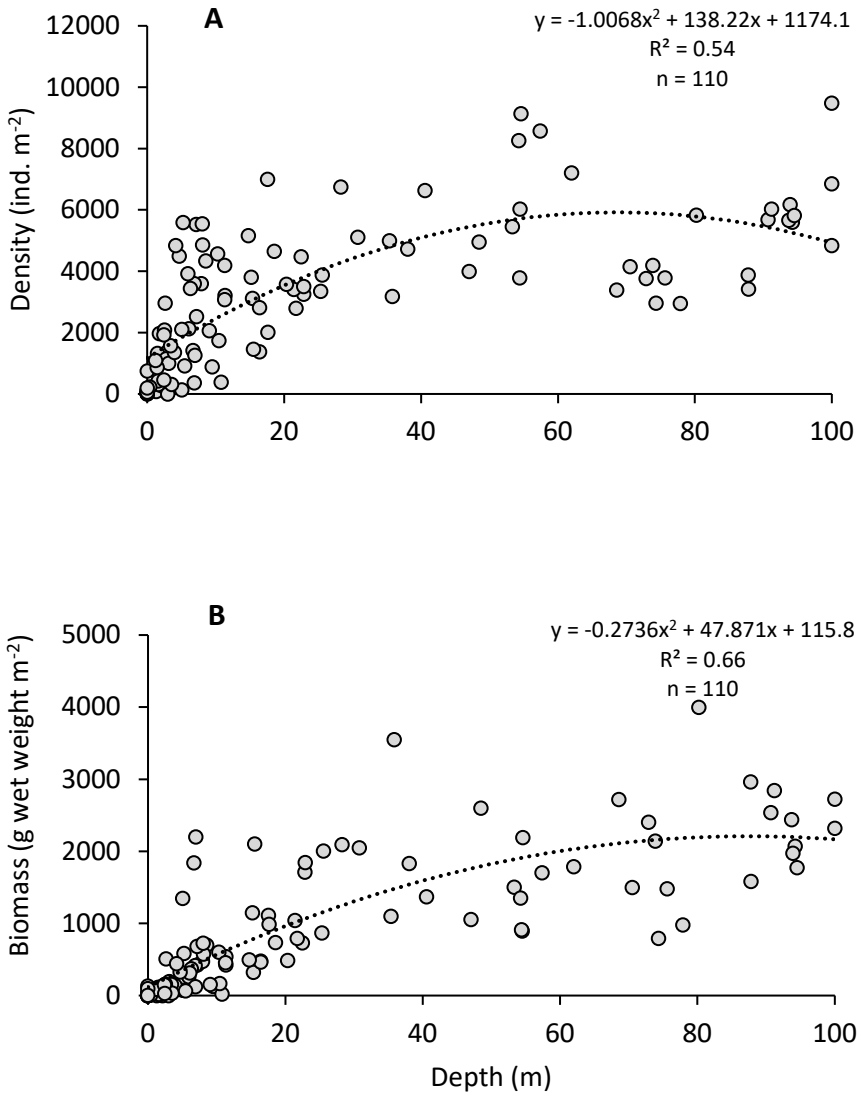


**Figure 2.6.** Relationship between *Dreissena* coverage in video, and density (ind. $m^{-2}$) and biomass (g $m^{-2}$) obtained from the same Ponar grabs in Lake Ontario in 2018.

We compared density and biomass estimated from benthic sled video transects with Ponar samples for 33 stations where we had useable data from both bottom grabs and sled tows (Table 2.2). There was a large but non-significant difference between mean *Dreissena* density estimated for sled tows and Ponar grabs within the 10 – 30 m depth zone (P = 0.23) and the >100 m depth zones (P = 0.06). *Dreissena* densities in the 10 – 30 m and >30 – 100 m depth zones were similar between sled tows and Ponar grabs (P = 0.23). Differences between mean *Dreissena* biomass based on sled tows and Ponar grabs were almost negligible for all three depth zones (0.42 > P > 0.27) due to high densities of small *Dreissena* (<10 mm) in those depth zones (compared to lakes Michigan and Huron), which contributed strongly to

overall density but not to biomass due to their minute weight (Fig. 2.7A). At the 10 – 30 m depth zone, almost half of the total counts were very small mussels (<10 mm), while in the >100 m depth zone, only one third of the mussels were <10 mm in length (Fig. 2.7B).

**Table 2.2.** Average *Dreissena* percent coverage (% ± standard error), average density ($m^{-2}$) and average total wet biomass (g $m^{-2}$, shell plus tissue) across depth zones (m) from Ponar samples and estimated from video transects sampled in lakes Ontario in 2018, Huron in 2017, and Michigan in 2015. N represents the number of stations per depth zone. Data for lakes Michigan and Huron from Karatayev et al. (2018) and Karatayev et al. (2020), respectively. Asterisks indicate significate difference (t-test, $p < 0.05$) between Lake Ontario and other lakes in estimated density and biomass of *Dreissena* by depth zone.

| Depth zone (m) | N | Coverage Sled (%) | Transect video density ($m^{-2}$) | Ponar density ($m^{-2}$) | Transect video biomass (g $m^{-2}$) | Ponar biomass (g $m^{-2}$) |
|---|---|---|---|---|---|---|
| Lake Ontario | | | | | | |
| 10-30 | 7 | 25.3 ± 3.2 | 2885 ± 90 | 4982 ± 3382 | 913 ± 36 | 1115 ± 644 |
| >30-100 | 12 | 58 ± 8.4 | 4665 ± 63 | 5208 ± 1495 | 1719 ± 32 | 1855 ± 1072 |
| >100 | 14 | 16.1 ± 5.1 | 2724 ± 69 | 4368 ± 1782 | 703 ± 26 | 700 ± 405 |
| Lake Huron | | | | | | |
| 10-30 | 12 | 0.6 ± 0.4 | 82 ± 52* | 65 ± 32 | 16 ± 10* | 17 ± 12 |
| >30-100 | 28 | 13.6 ± 3.7 | 1814 ± 484* | 1567 ± 645 | 350 ± 143* | 291 ± 111 |
| >100 | 7 | 8.1 ± 7.7 | 1049 ± 996 | 1150 ± 724 | 202 ± 124 | 207 ± 124 |
| Lake Michigan | | | | | | |
| 10-30 | 9 | 11.7 ± 8.6 | 1930 ± 1418 | 2034 ± 931 | 336 ± 247 | 543 ± 281 |
| >30-100 | 23 | 53.8 ± 5.1 | 8867 ± 849* | 7201 ± 1105 | 1544 ± 148 | 1232 ± 140 |
| >100 | 10 | 6.3 ± 3.0 | 1045 ± 500 | 1544 ± 1091 | 182 ± 87* | 90 ± 46 |

**A**

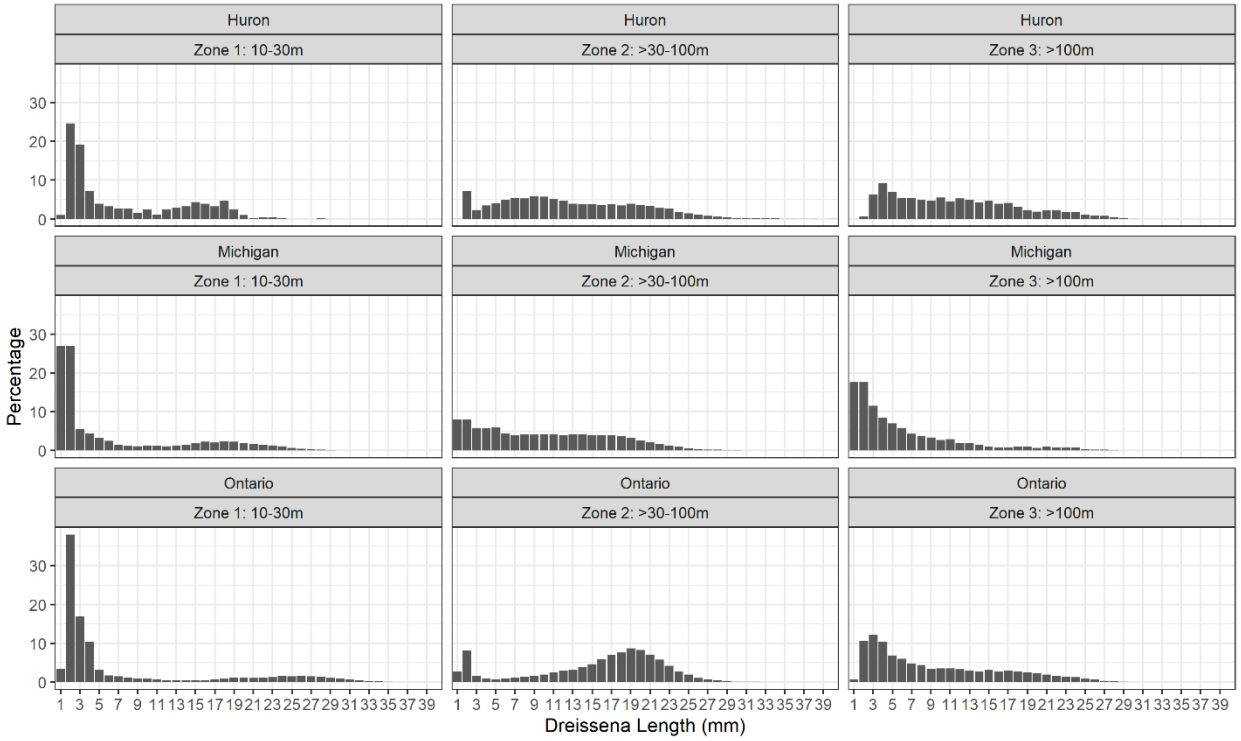


**B**

| Depth zone (m) | N | Percent *Dreissena* <10 mm | Percent *Dreissena* <5 mm |
|---|---|---|---|
| 10 - 30 | 11 | 48 ± 28 | 44 ± 11 |
| >30 - 100 | 16 | 22 ± 12 | 15 ± 16 |
| >100 | 18 | 65 ± 38 | 43 ± 3 |

**Figure 2.7.** Size frequency distribution of *Dreissena* mussels in lakes Huron, Michigan, and Ontario (A) and percent contribution of mussels <10 mm and <5 mm to the total *Dreissena* numbers within each depth zone in Lake Ontario (B). 1 mm and 2 mm mussels were grouped together when measured for Lake Michigan samples. Therefore, the 1 mm and 2 mm size groups in Lake Michigan each represent half of the 1 - 2 mm size group.

We also compared *Dreissena* densities and biomass based on sled tows among depth zones in Lake Ontario and between Lake Ontario and lakes Huron and Michigan using t-test (Table 2.2). In Lake Ontario, the mean *Dreissena* density within the >30 – 100 m depth zone was higher but not significantly different than in both the 10 – 30 m depth zone ($p = 0.18$) and the > 100 m depth zone ( $p = 0.19$). Mean *Dreissena* biomass, however, was marginally significant in >30 – 100 m depth zone compared to the 10 – 30 m depth zone ($p = 0.08$) and was significantly higher than in the > 100 m depth zone ($p < 0.001$). Lake

Ontario *Dreissena* densities within 10 – 30 m and >30 – 100 m depth zones were significantly higher compared to densities for the respective zones in Huron (Table 2.2). Compared to Lake Michigan, Lake Ontario *Dreissena* densities were higher, albeit not significantly, within the 10 – 30 m and >100 m depth zones, but were significantly lower at the 30 – 100 m depth zone. Correspondingly, depth-wise *Dreissena* biomass in Lake Ontario was higher compared to Lake Huron and Lake Michigan, but the difference was not always significant due to large dispersion in data (Table 2.2).

Use of the video transects greatly increases the number of replicates collected at each site (100 replicates/station for a video transect compared to 3 replicates/station for Ponars), which improves the quality of density and biomass estimates via increases in precision and the statistical power of testing (Karatayev et al., 2018). Due to larger sample sizes, the standard error of the station mean in video transects of Lake Ontario was on average 7.3 times lower in sled tows compared to Ponar samples, resulting in an increase in precision of the average estimation of density and biomass at the local (station) scale (Fig. 2.8A and B). At most stations, differences between *Dreissena* densities and biomass were not significant due to usually large standard errors in Ponar grab sample data because of large local patchiness in distribution and low sample size. Therefore, both methods were likely accurate in estimations of the population mean. Only at six stations we did find significant differences in *Dreissena* density and biomass values for sled tows compared to Ponar grabs. Two of those stations (O17, ON64) had a large percentage of small *Dreissena* (>80% were <10 mm), which were difficult to detected in the sled images; this detection error ultimately caused significantly lower densities and biomass in sled tows than the Ponar grabs (ON17 density: $P < 0.0001$, biomass: $P < 0.0001$; ON64 density: $P < 0.05$, biomass: $P < 0.0001$, t-tests). At four other stations, significant differences in either *Dreissena* densities, biomass, or both were the result of unusually low standard error (<10% from mean) in Ponar grab samples (ON27 biomass: $P < 0.01$; ON28 density: $p < 0.05$; ON58 density and biomass: $P < 0.05$; ON94 biomass: $P < 0.05$, t-tests) in contrast to other sites where standard error was high. These stations, all located at the 30 – 100 m depth zone, were quite homogeneously covered by large aggregations of *Dreissena* (Fig. 2.5B) likely resulting in small differences among replicates.

Similar to our previous studies (Karatayev et al., 2018; Karatayev et al., 2020), we found that at a large spatial scale (depth zone), the average *Dreissena* density and biomass were not significantly different between Ponar and video transects. The lack of significant differences between averages obtained by traditional Ponar sampling and video transects have at least two important implications: (1) Ponar grabs provide reliable estimates of *Dreissena* density; (2) the gain in precision by using video transects will be at the station scale, which is the scale used as a target in GLNPO Biology Monitoring Program to monitor changes in benthic species densities. Used in concert with traditional sampling, video

sampling has the potential to greatly expand benthic monitoring capabilities. Information from underwater videos can be used to better describe small scall heterogeneity not only of biological but also physical characteristics of the benthic habitat, such as substrate and lake bottom reliefs. Additionally, information from videos are not restricted to *Dreissena* mussels, but can be used to detect other benthic-dwelling organisms such as round gobies or mysids.

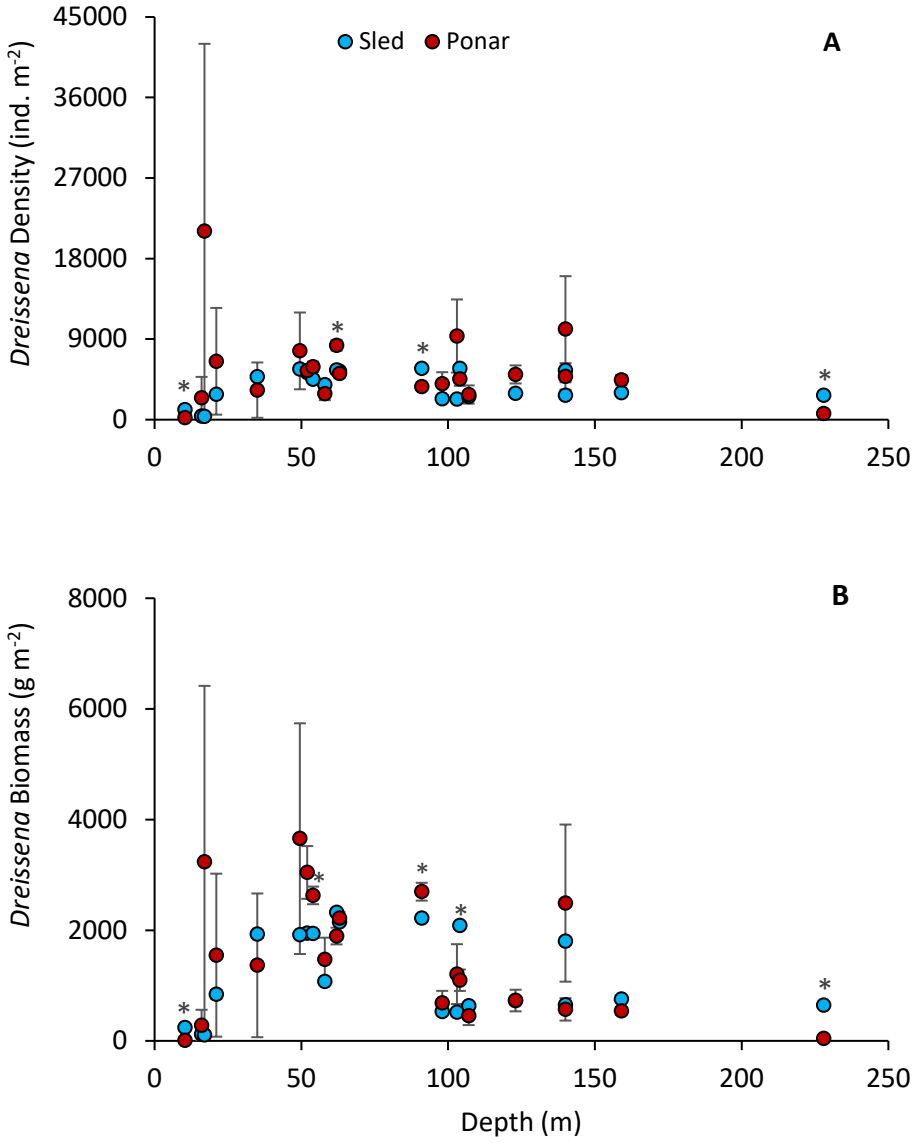


**Figure 2.8.** Mean *Dreissena* density (ind. $m^{-2}$, panel A) and mean biomass (g wet weight $m^{-2}$, panel B) estimated from video transects (100 screen shots analyzed per station, blue circles) and Ponar grab (3 grabs processed per station, red circles). Error bars represent ± 1 standard error. Asterisk above error bars

indicate significant differences between density and biomass based on sled tows and Ponar grabs. Only stations where *Dreissena* were found in both Ponar grabs and video transects are included.

**REFERENCES**


Custer, C.M., Custer, T.W., 1997. Occurrence of zebra mussels in nearshore areas of western Lake Erie. J. Great Lakes Res. 23, 108-115.

Grubbs, F., 1969. Procedures for detecting outlying observations in samples. Technometrics 11: 1-21.

Karatayev, A.Y., Mehler, K., Burlakova, L.E., Hinchey, E.K., Warren, G.J., 2018. Benthic video image analysis facilitates monitoring of *Dreissena populations* across spatial scales. Journal of Great Lakes Research 44: 629-638.

Karatayev, A.Y., Burlakova, L.E., Mehler, K., Daniel, S.E., Elgin, A.K., Nalepa, T.F., 2020. Lake Huron Benthos Survey Cooperative Science and Monitoring Initiative 2017. Technical Report. USEPA-GLRI GL00E02254. Great Lakes Center, SUNY Buffalo State, Buffalo, NY. Available at: http://greatlakescenter.buffalostate.edu/sites/greatlakescenter.buffalostate.edu/files/uploads/Documents/Publications/LakeHuronBenthosSurveyCSMI2017FinalReport.pdf.

Lietz, J.E., Kelly, J.R., Scharold, J.V., Yurista, P.M., 2015. Can a rapid underwater video approach enhance the benthic assessment capability of the national coastal condition assessment in the Great Lakes? Environ. Manag. 55, 1446-1456.

Mehler, K., Burlakova, L.E., Karatayev, A.Y., Biesinger, Z., Valle-Levinson, A., Castiglione, C., Gorsky, D., 2018. Sonar technology and underwater imagery analysis can enhance invasive *Dreissena* distribution assessment in large rivers. Hydrobiologia 810, 119-131.

Ozersky, T., Malkin, S.Y., Barton, D.R., Hecky, R.E., 2009. Dreissenid phosphorus excretion can sustain *C. glomerata* growth along a portion of Lake Ontario shoreline. J. Great Lakes Res. 35, 321-328.

Ozersky, T., Barton, D.R., Depew, D.C., Hecky, R.E., Guildford, S.J., 2011. Effects of water movement on the distribution of invasive dreissenids mussels in Lake Simcoe. Ontario. J. Great Lakes Res. 37, 46-54.

## SUMMARY

In 2018, we conducted a lake-wide survey of benthic macroinvertebrates in Lake Ontario and compared the current status of the community with historic data. We found 87 taxa (species, genera or higher taxa) of benthic macroinvertebrates, and the most diverse were Oligochaeta (33 species and higher taxa), Insecta (Chironomidae, 28), Malacostraca (6 species), and Bivalvia (3). The most widely abundant species throughout the lake was the exotic bivalve *Dreissena r. bugensis*, which was found at 98% of all 55 benthic stations sampled, followed by Oligochaeta, *Mysis*, and chironomids. Among the major long-term changes in densities of benthic macroinvertebrates in Lake Ontario, the most important were the declines in *Diporeia* and Sphaeriidae at all depth zones, which started in the mid-1990s after a period of elevated densities in the late 1980s – early 1990s. Currently, *Diporeia* is only present at depths >90 m at extremely low densities (<1 $m^{-2}$). The highest densities of Oligochaeta were observed in 1964 (app. 10,000 $m^{-2}$), and they declined in the 1970s and 1980s, mostly due to the large decrease in pollution tolerant Tubificidae in shallow zone. Oligochaeta densities then increased during the 1990s, likely due to dreissenid invasion. Although they declined somewhat in the late 2000s, their densities have again been increasing over the past five years. The only taxa that showed long-term increases in density were *Dreissena* and Chironomidae, especially at intermediate (>30 – 90 m) depths. Contrary to our prediction, we found continued significant increases in *Dreissena* lake-wide density and biomass in 2018, suggesting that the mussel population in Lake Ontario is still increasing. The lake-wide average *Dreissena* biomass was the highest ever observed in Lake Ontario to date (at 25.2±3.3 g $m^{-2}$ of ash-free dry tissue weight). During the 2018 CSMI survey for Lake Ontario, videos from 59 Ponar stations and 57 sled tows were used to estimate *Dreissena* distribution in the lake and were compared to results from standard Ponar sampling. *Dreissena* coverage was higher at intermediate depths (between 30 and 100 m) than at both shallow (< 30 m) and deep (> 100 m) areas. Compared to previous surveys in lakes Michigan and Huron, *Dreissena* populations in Lake Ontario had higher abundance of small *Dreissena*, especially in the shallowest depth zone (<30 m). Very small mussels (< 10 mm) were difficult to detect in underwater images, resulting in lower *Dreissena* densities in sled tows compared to Ponar grabs when high abundances of small mussels were present. However, *Dreissena* biomass estimated from Ponar and video transects were almost identical. Moreover, at the larger scale (i.e., depth zones), difference in density and biomass estimations were non-significant between sled tows and Ponar grabs. These results underscore the value that may be added to *Dreissena* monitoring efforts by incorporating underwater video imagery in monitoring, especially in areas where Ponar sampling would not be possible (e.g., rocky bottom).

## ACKNOWLEDGEMENTS

This study was funded by US EPA through the Great Lakes Restoration Initiative under Prime Agreement with Cornell University, Department of Natural Resources Award GL00E02254 "Great Lakes Long-Term 447 Biological Monitoring 2017-2022" (PI Lars Rudstam) and Subaward # 82839-10916 to SUNY Buffalo State. We appreciate the assistance of the Captain and crew of the U.S. EPA R/V *Lake Guardian*, Kathleen Hastings (SUNY Buffalo State, Great Lakes Center), Elizabeth Hinchey (U.S. EPA GLNPO), Leon Katona (Wright State University), Paul Glyshaw (NOAA GLERL), and Michelle Wensman (University of Michigan CIGLR) for help with sample collection. We thank Great Lakes Center technician Erik M. Hartnett and SUNY Buffalo State student technicians Akshay Sharma, Asif Muqtadir, Christina Perry, Joshua Allan, Kyle Glenn, Lauren Martinek, Martens Dorcely, Megan Kocher, and Shania Jean-Pierre for help with sample processing. We are grateful to Anne Scofield, Rae-Ann Maclellan-Hurd, and Elizabeth Hinchey Malloy (U.S. EPA GLNPO) for helpful edits of the report, and Susan Dickinson (Great Lakes Center) for help in report preparation.

## APPENDICES

**Appendix 1.**

**Table A1.** All 61 stations sampled on Lake Ontario in 2018, with information on lake basins, location (decimal coordinates), proposed (historic) and actual water depth, and main substrate.

**Appendix 2.**

**Table A2.** Long-term dynamics of density (mean ± SE, ind./$m^{-2}$) of major benthic taxa in Lake Ontario from 1964 to 1997 by depths zones.

**Table A3.** Long-term dynamics of density (mean ± SE, ind./$m^{-2}$) of major benthic taxa in Lake Ontario from 1998 to 2018 by depths zones.

Data sources: 1964 – Hiltunen, 1969; 1972 – Nalepa and Thomas, 1976; 1977 – Golini, 1979; 1990, 1995 – Dermott and Geminiuc, 2003; 1994, 1997 – Lozano et al., 2001; 1997, 1998, 2003 – Watkins et al., 2007; 2008 – corrected Birkett et al., 2015; 2013 – Nalepa and Baldridge, 2016; 2018 – our data.

**Appendix 3.** Karatayev, A. Y., L. E. Burlakova, K. Mehler, A. K. Elgin, L.G. Rudstam, J.M. Watkins, and M. Wick. Accepted. *Dreissena* in Lake Ontario 30 years post-invasion. Journal of Great Lakes Research.

**Appendix 4.** Burlakova, L.E., A.Y. Karatayev, A.R. Hrycik, S.E. Daniel, K. Mehler, L.G. Rudstam, J.M. Watkins, R. Dermott, J. Scharold, A.K. Elgin, and T. Nalepa. In review. Six decades of Lake Ontario ecological history according to benthos. Journal of Great Lakes Research.

## Appendix 1.

**Table A1.** All 61 stations sampled on Lake Ontario in 2018 (including 52 Cooperative Science and Monitoring Initiative (CSMI) stations sampled September 10-18, 2018 and 9 GLNPO Long-term Monitoring stations sampled in August 2018), with information on lake basins, location (decimal coordinates), proposed (historic) and actual water depth, and main substrate. Three replicate Ponar samples were successfully collected at 55 of the planned 61 stations, excluding 6 stations (#29, 42, 43, 62, 66, and 71B, highlighted in grey) where samples were not collected due to hard substrate. All stations were sampled aboard US EPA R/V *Lake Guardian* with Ponar bottom grab (sampling area 0.0523 $m^2$).

| Station | Basin | Latitude | Longitude | Proposed depth (m) | Sampling depth (m) | Substrate |
|---|---|---|---|---|---|---|
| Cooperative Science and Monitoring Initiative (CSMI) stations | | | | | | |
| 6 | West | 43.46644 | -79.5351 | 62 | 61.5 | silty sand |
| 8 | West | 43.62203 | -79.45365 | 15.6 | 13.8 | silt |
| 9 | West | 43.58705 | -79.39673 | 58 | 56.6 | silt |
| 12 | West | 43.50327 | -79.35188 | 104.8 | 103.2 | silt |
| 14 | West | 43.39395 | -79.48627 | 98 | 95.8 | silt |
| 16 | West | 43.27054 | -79.36514 | 66 | 62.4 | silty clay |
| 17 | West | 43.225 | -79.27148 | 14.4 | 11.1 | silt |
| 18 | West | 43.3034 | -79.27782 | 85.5 | 83.6 | silty clay |
| 19 | West | 43.38353 | -79.28575 | 107 | 104.1 | silt, *Dreissena* |
| 22 | West | 43.2968 | -79.00629 | 11 | 11 | silt, sand |
| 24 | West | 43.43912 | -79.1283 | 120/96 | 119 | silt, clay |
| 26 | West | 43.60797 | -79.01602 | 120 | 116.5 | silty clay |
| 27 | West | 43.68984 | -78.8309 | 114/100 | 101.3 | silt |
| 28 | West | 43.77517 | -78.8546 | 65/61 | 60.6 | sand |
| 29 | West | 43.81742 | -78.86992 | 32 | 29.5 | no sample collected, hard substrate |
| 32 | Central | 43.78277 | -78.4377 | 78 | 75.3 | silty clay |
| 33 | West | 43.59593 | -78.81265 | 138 | 135.3 | silt |
| 34 | West | 43.46135 | -78.75918 | 136 | 134.7 | silty clay |
| 35 | West | 43.36185 | -78.729 | 28 | 27 | silt |
| 36 | Central | 43.45847 | -78.38702 | 140/160 | 158 | silt |
| 37 | Central | 43.39145 | -78.03646 | 19 | 21.7 | silty clay |

| Station | Basin | Latitude | Longitude | Proposed depth (m) | Sampling depth (m) | Substrate |
|---|---|---|---|---|---|---|
| 38 | Central | 43.38287 | -77.9897 | 20 | 16.5 | silty sand |
| 39 | Central | 43.48562 | -77.99746 | 154 | 152.7 | silty clay |
| 40 | Central | 43.58959 | -78.01297 | 190 | 181 | silt |
| 42 | Central | 43.83995 | -78.03722 | 65 | 64.7 | no sample collected, hard substrate |
| 43 | Central | 43.94909 | -78.04914 | 19 | 12.6 | no sample collected, hard substrate |
| 45 | Central | 43.82074 | -77.78242 | 80 | 78.2 | sand, clay |
| 58 | East | 43.328 | -77.43791 | 156/90 | 87.9 | silty sand |
| 61 | East | 43.78645 | -77.15828 | 54 | 51.3 | silty sand, gravel |
| 62 | East | 44.88005 | -76.99859 | 18 | 8.5 | no sample collected, hard substrate |
| 64 | East | 43.52495 | -76.92603 | 214 | 211.1 | silt |
| 65 | East | 43.30797 | -76.95077 | 155 | 144.8 | silt |
| 66 | East | 43.34019 | -76.83732 | 18.5 | 16.5 | no sample collected, hard substrate |
| 67 | East | 43.4054 | -76.79116 | 71 | 69.3 | silty sand |
| 69 | East | 43.60522 | -76.71612 | 15.8 | 184.7 | silt |
| 72 | East | 43.54915 | -76.52569 | 113 | 106.6 | silt |
| 73 | East | 43.63077 | -76.2888 | 40 | 38.1 | fine sand |
| 74 | East | 43.74834 | -76.51604 | 69 | 67.25 | silt |
| 75 | East | 43.84225 | -76.35555 | 32 | 29.3 | silty sand |
| 77 | East | 43.95633 | -76.4082 | 29 | 76 | sand |
| 80 | East | 44.14225 | -76.61178 | 19 | 20.2 | sand |
| 81 | East | 44.0164 | -76.67477 | 36.3 | 34.3 | silty sand |
| 82 | East | 44.06617 | -76.81075 | 27 | 25.2 | silty sand |
| 84 | East | 43.8871 | -76.73356 | 37 | 35 | sand |
| 94 | East | 43.32509 | -77.21652 | 45 | 52.4 | silty sand |
| 101 | Central | 43.63765 | -78.41327 | 146 | 145.5 | silt |
| 102 | Central | 43.7341 | -77.72325 | 130 | 111.4 | silty clay |
| 106 | East | 43.95619 | -76.60317 | 133 | 28.5 | silt |
| 715 | East | 43.63573 | -76.9696 | 151 | 152.3 | silt |

| Station | Basin | Latitude | Longitude | Proposed depth (m) | Sampling depth (m) | Substrate |
|---|---|---|---|---|---|---|
| 716 | East | 43.60093 | -77.4406 | 151 | 146.1 | silt |
| 71B | East | 43.47727 | -76.52705 | 11.6 | 10.7 | no sample collected, hard substrate |
| 93A | West | 43.32743 | -78.86768 | 19 | 17.4 | sand |
| GLNPO Long-term Monitoring Stations | | | | | | |
| ON25 | West | 43.51667 | -79.0800 | 133 | 133 | silt, hard clay on top |
| ON41 | Central | 43.7167 | -78.0269 | 128 | 128 | silt |
| ON55 | East | 43.4439 | -77.4389 | 192 | 198 | silt, few *Dreissena* |
| ON60 | East | 43.58 | -77.2000 | 186/152 | 152 | silt, few *Dreissena* |
| ON63 | East | 43.7317 | -77.0169 | 87 | 87 | silt, live *Dreissena* |
| ON65B | East | 43.30833 | -76.9500 | 25.5 | 25.5 | coarse sand, lots of *Dreissena* |
| ON67B | West | 43.37500 | -78.7294 | 54.5 | 54 | silt, lots of *Dreissena* |
| ON68B | West | 43.58333 | -79.4167 | 51.6 | 51.6 | silt, *Dreissena* |
| ON69B | West | 43.31833 | -79.0000 | 15.8 | 13 | very fine sand |

## Appendix 2.

**Table A2.** Long-term dynamics of density (mean ± SE, ind./$m^{-2}$) of major benthic taxa in Lake Ontario from 1964 to 1997 by depths zones. N – number of stations sampled. n.r. – data were not reported. All groups had significant P-values ($P < 0.001$) for year and depth zone in ANOVAs. Data sources: 1964 – Hiltunen, 1969; 1972 – Nalepa and Thomas, 1976; 1977 – Golini, 1979; 1990, 1995 – Dermott and Geminiuc, 2003; 1994, 1997 – Lozano et al., 2001; 1997 – Watkins et al., 2007. Lake-wide density was calculated as a weighted average using means of stations located at 4 depth zones considering the proportion of the total lake area represented by each zone (21.6, 11.7, 18.5, and 48.2%, respectively).

| **Taxa (by depth zone)** | **1964** | **1972** | **1977** | **1990** | **1994** | **1995** | **1997** |
|---|---|---|---|---|---|---|---|
| **<30 m** | **N = 13** | **N = 20** | **N = 13** | **N = 7** | **N = 4** | **N = 15** | **N = 13** |
| Amphipoda | 551±169 | 113±59 | 0±0 | 105±102 | 63±51 | 330±131 | n.r. |
| *Diporeia* | 1611±689 | 1412±401 | 1763±575 | 24±13 | 75±75 | 22±9 | 34±33 |
| Oligochaeta | 8930±3435 | 8426±2944 | 2229±531 | 10760±3863 | 4200±2079 | 3853±1246 | 1334±477 |
| Chironomidae | 533±195 | 166±67 | 417±109 | 184±77 | 155±100 | 532±208 | n.r. |
| Dreissenidae | 0±0 | 0±0 | 0±0 | 14±9 | n.r. | 4948±1717 | 2033±757 |
| Sphaeriidae | 3339±728 | 989±302 | 1736±405 | 1617±645 | 219±75 | 594±281 | 244±92 |
| Gastropoda | 353±129 | 168±90 | 35±15 | 97±48 | 224±82 | 892±387 | n.r. |
| All Benthos | 16047±3164 | 11372±3258 | 6486±1167 | 12938±3867 | 5475±2367 | 11408±2646 | 4169±975 |
| Benthos w/o *Dreissena* | 16047±3164 | 11372±3258 | 6486±1167 | 12925±3865 | 5475±2367 | 6460±1502 | 2136±643 |
| **31-50 m** | **N = 3** | **N = 5** | **N = 16** | **N = 0** | **N = 2** | **N = 4** | **N = 11** |
| Amphipoda | 5±5 | 10±10 | 0±0 | n.r. | 0±0 | 5±5 | n.r. |
| *Diporeia* | 8708±633 | 3045±821 | 2042±535 | n.r. | 6073±6066 | 58±58 | 163±162 |
| Oligochaeta | 3081±626 | 3185±1575 | 1016±241 | n.r. | 3806±1931 | 1447±762 | 629±260 |
| Chironomidae | 147±126 | 7±4 | 64±27 | n.r. | 42±42 | 34±34 | n.r. |
| Dreissenidae | 0±0 | 0±0 | 0±0 | n.r. | n.r. | 44±37 | 1316±619 |
| Sphaeriidae | 3360±372 | 421±220 | 1549±486 | n.r. | 1955±427 | 673±374 | 496±340 |
| Gastropoda | 45±40 | 3±2 | 3±2 | n.r. | 0±0 | 0±0 | n.r. |
| All Benthos | 15452±991 | 6677±2452 | 4702±1086 | n.r. | 11986±4701 | 2314±1100 | 3243±1074 |
| Benthos w/o *Dreissena* | 15452±991 | 6677±2452 | 4702±1086 | n.r. | 11986±4701 | 2270±1125 | 1927±987 |
| **51-90 m** | **N = 0** | **N = 10** | **N = 31** | **N = 4** | **N = 10** | **N = 11** | **N = 16** |
| Amphipoda | n.r. | 11±11 | 0±0 | 0±0 | 0±0 | 2±2 | n.r. |
| *Diporeia* | n.r. | 2042±572 | 2661±580 | 5883±1646 | 8784±1140 | 3154±683 | 3533±106 |

| Taxa (by depth zone) | 1964 | 1972 | 1977 | 1990 | 1994 | 1995 | 1997 |
|---|---|---|---|---|---|---|---|
| **<30 m** | **N = 13** | **N = 20** | **N = 13** | **N = 7** | **N = 4** | **N = 15** | **N = 13** |
| Oligochaeta | n.r. | 5908±4499 | 1601±304 | 1006±427 | 1404±174 | 1793±544 | 1028±221 |
| Chironomidae | n.r. | 19±13 | 182±79 | 0±0 | 39±29 | 100±49 | n.r. |
| Dreissenidae | n.r. | 0±0 | 0±0 | 5±5 | n.r. | 11±6 | 150±77 |
| Sphaeriidae | n.r. | 101±62 | 675±140 | 624±172 | 839±150 | 1237±382 | 314±65 |
| Gastropoda | n.r. | 0±0 | 0±0 | 0±0 | 0±0 | 0±0 | n.r. |
| All Benthos | n.r. | 8093±4388 | 5127±889 | 7532±2178 | 11208±1091 | 6390±1171 | 5444±1127 |
| Benthos w/o *Dreissena* | n.r. | 8093±4388 | 5127±889 | 7527±2177 | 11208±1091 | 6379±1170 | 5294±1142 |
| **>90 m** | **N = 8** | **N = 20** | **N = 91** | **N = 13** | **N = 35** | **N = 11** | **N = 28** |
| Amphipoda | 0±0 | 0±0 | 0±0 | 0±0 | 0±0 | 4±4 | n.r. |
| *Diporeia* | 1253±358 | 780±139 | 391±68 | 2071±548 | 2994±322 | 3191±478 | 2168±292 |
| Oligochaeta | 773±129 | 371±56 | 599±122 | 521±162 | 742±89 | 671±158 | 224±29 |
| Chironomidae | 211±38 | 5±2 | 38±9 | 10±5 | 16±5 | 9±5 | n.r. |
| Dreissenidae | 0±0 | 0±0 | 0±0 | 7±7 | n.r. | 0±0 | 0±0 |
| Sphaeriidae | 287±80 | 20±12 | 103±15 | 235±114 | 207±88 | 83±28 | 62±15 |
| Gastropoda | 0±0 | 0±0 | 0±0 | 1±1 | 0±0 | 0±0 | n.r. |
| All Benthos | 2537±516 | 1228±171 | 1131±180 | 2932±676 | 4050±301 | 4016±566 | 2600±301 |
| Benthos w/o *Dreissena* | 2537±516 | 1228±171 | 1131±180 | 2925±673 | 4050±301 | 4016±566 | 2599±301 |
| **Lake-wide** | **N = 24** | **N = 55** | **N = 151** | **N = 25** | **N = 51** | **N = 41** | **N = 68** |
| Amphipoda | 146±45 | 27±13 | 0±0 | 23±NA | 13±11 | 74±28 | 12±11 |
| *Diporeia* | 2416±294 | 1415±180 | 1300±179 | 2512±NA | 3798±755 | 2136±263 | 1727±243 |
| Oligochaeta | 3262±916 | 3462±1064 | 1185±143 | 3275±NA | 1967±504 | 1655±310 | 888±143 |
| Chironomidae | 287±59 | 42±15 | 149±28 | 45±NA | 53±23 | 141±46 | 59±28 |
| Dreissenidae | 0±0 | 0±0 | 0±0 | 7±NA | n.r. | 1074±370 | 619±179 |
| Sphaeriidae | 1535±205 | 290±71 | 730±108 | 884±NA | 531±73 | 476±104 | 198±46 |
| Gastropoda | 100±35 | 37±19 | 8±3 | 22±NA | 48±18 | 192±83 | 0±0 |
| All Benthos | 7961±902 | 5323±1115 | 3443±338 | 6841±NA | n.r. | 5851±681 | 3538±353 |
| Benthos w/o *Dreissena* | 7961±902 | 5323±1115 | 3443±338 | 6834±NA | 6610±789 | 4777±494 | 2920±314 |

**Table A3.** Long-term dynamics of density (mean ± SE, ind./$m^{-2}$) of major benthic taxa in Lake Ontario from 1998 to 2018 by depths zones. N – number of stations sampled. n.r. – data were not reported. All groups had significant P-values ($P < 0.001$) for year and depth zone in ANOVAs. Data sources: 1998, 2003 – Watkins et al., 2007; 2008 – corrected Birkett et al., 2015; 2013 – Nalepa and Baldridge, 2016; 2018 – our data. Lake-wide density was calculated as a weighted average using means of stations located at 4 depth zones considering the proportion of the total lake area represented by each zone (21.6, 11.7, 18.5, and 48.2%, respectively).

| | **1998** | **1999** | **2003** | **2008** | **2013** | **2018** |
|---|---|---|---|---|---|---|
| **<30 m** | **N = 25** | **N = 9** | **N = 9** | **N = 13** | **N = 8** | **N = 13** |
| Amphipoda | 138±47 | n.r. | n.r. | 1±1 | 48±41 | 33±16 |
| *Diporeia* | 1±1 | 202±138 | 0±0 | 0±0 | 0±0 | 0±0 |
| Oligochaeta | 1501±472 | 2100±495 | n.r. | 808±272 | 2738±1158 | 3681±940 |
| Chironomidae | 252±83 | 663±313 | n.r. | 154±61 | 486±261 | 569±116 |
| Dreissenidae | 5867±1972 | 1913±333 | 9193±3419 | 2366±1161 | 3302±1387 | 5037±2132 |
| Sphaeriidae | 235±96 | 375±150 | n.r. | 0±0 | 0±0 | 0±0 |
| Gastropoda | 271±86 | n.r. | n.r. | 143±143 | 27±26 | 57±57 |
| All Benthos | 8382±2285 | n.r. | n.r. | 3471±1251 | 6614±1108 | 9401±2919 |
| Benthos w/o *Dreissena* | 2515±592 | n.r. | n.r. | 1106±378 | 3312±1108 | 4364±977 |
| **31-50 m** | **N = 15** | **N = 6** | **N = 5** | **N = 4** | **N = 8** | **N = 3** |
| Amphipoda | 6±2 | n.r. | n.r. | 9±5 | 10±9 | 0±0 |
| *Diporeia* | 67±67 | 9±7 | 1±1 | 0±0 | 0±0 | 0±0 |
| Oligochaeta | 651±350 | 1911±1380 | n.r. | 1025±240 | 1552±653 | 5494±4300 |
| Chironomidae | 289±114 | 241±138 | n.r. | 278±248 | 125±60 | 74±49 |
| Dreissenidae | 1755±548 | 3907±1059 | 10949±5195 | 4419±1936 | 4366±1271 | 4587±1964 |
| Sphaeriidae | 213±70 | 160±76 | n.r. | 0±0 | 0±0 | 0±0 |
| Gastropoda | 3±2 | n.r. | n.r. | 0±0 | 14±13 | 0±0 |
| All Benthos | 2994±722 | n.r. | n.r. | 5732±1824 | 6067±1854 | 10212±6256 |
| Benthos w/o *Dreissena* | 1239±412 | n.r. | n.r. | 1313±351 | 1701±649 | 5626±4295 |
| **51-90 m** | **N = 34** | **N = 24** | **N = 9** | **N = 15** | **N = 8** | **N = 16** |
| Amphipoda | 2±1 | n.r. | n.r. | 1±1 | 0±0 | 2±1 |
| *Diporeia* | 1301±429 | 764±275 | 97±86 | 6±6 | 0±0 | 0±0 |

| | 1998 | 1999 | 2003 | 2008 | 2013 | 2018 |
|---|---|---|---|---|---|---|
| Oligochaeta | 564±57 | 995±120 | n.r. | 631±81 | 1002±218 | 1516±263 |
| Chironomidae | 123±33 | 77±16 | n.r. | 210±70 | 212±72 | 408±90 |
| Dreissenidae | 336±123 | 4487±1397 | 6526±2022 | 7149±1177 | 5504±700 | 4749±532 |
| Sphaeriidae | 280±36 | 231±40 | n.r. | 4±2 | 2±2 | 2±2 |
| Gastropoda | 0±0 | n.r. | n.r. | 0±0 | 0±0 | 0±0 |
| All Benthos | 2630±444 | n.r. | n.r. | 8003±1187 | 6721±750 | 6711±665 |
| Benthos w/o *Dreissena* | 2294±453 | n.r. | n.r. | 855±114 | 1216±184 | 1963±259 |
| **>90 m** | **N = 40** | **N = 28** | **N = 13** | **N = 19** | **N = 21** | **N = 23** |
| Amphipoda | 0±0 | n.r. | n.r. | 0±0 | 0±0 | 0±0 |
| *Diporeia* | 2343±336 | 2181±335 | 545±111 | 41±18 | 0±0 | 0±0 |
| Oligochaeta | 274±49 | 543±109 | n.r. | 169±52 | 381±61 | 426±79 |
| Chironomidae | 13±3 | 54±17 | n.r. | 63±39 | 80±16 | 88±29 |
| Dreissenidae | 2±1 | 35±24 | 1099±614 | 655±361 | 2044±456 | 3554±501 |
| Sphaeriidae | 108±17 | 104±22 | n.r. | 16±4 | 23±6 | 17±5 |
| Gastropoda | 0±0 | n.r. | n.r. | 0±0 | 0±0 | 0±0 |
| All Benthos | 2788±361 | n.r. | n.r. | 965±406 | 2529±496 | 4131±580 |
| Benthos w/o *Dreissena* | 2786±360 | n.r. | n.r. | 310±76 | 485±69 | 577±88 |
| **Lake-wide** | **N = 114** | **N = 67** | **N = 36** | **N = 51** | **N = 45** | **N = 55** |
| Amphipoda | 31±10 | 0±0 | n.r. | 1±1 | 12±9 | 7±4 |
| *Diporeia* | 1380±181 | 1238±172 | 281±56 | 21±9 | 0±0 | 0±0 |
| Oligochaeta | 647±113 | 1122±201 | n.r. | 492±71 | 1141±266 | 1921±545 |
| Chironomidae | 99±21 | 224±68 | n.r. | 135±39 | 197±59 | 249±34 |
| Dreissenidae | 1532±430 | 1717±296 | 4999±1067 | 2667±438 | 3228±420 | 4215±576 |
| Sphaeriidae | 180±25 | 192±36 | n.r. | 8±2 | 11±3 | 9±2 |
| Gastropoda | 59±19 | 0±0 | n.r. | 31±31 | 7±6 | 12±12 |
| All Benthos | 3999±535 | 4513±421 | n.r. | 3366±453 | 4599±425 | 6455±1011 |
| Benthos w/o *Dreissena* | 2467±237 | 2796±305 | n.r. | 700±101 | 1371±255 | 2239±547 |

# Quantifying Lake Ontario Coregonine Habitat Use Dynamics Across Space and Time to Inform Assessment and Restoration

**Brian Weidel, U. S. Geological Survey, Great Lakes Science Center**
**Taylor Brown, Cornell University**
**Michael Connerton, New York State Department of Environmental Conservation**
**Jeremy Holden, Ontario Ministry of Natural Resources**
**Dimitry Gorsky, U.S. Fish and Wildlife Service, Lower Lakes Office**

Contact:
Brian Weidel
bweidel@usgs.gov
315 343 3951 ext 6519
Lake Ontario Biological Station
17 Lake St
Oswego, NY 13126

## Background from (Brown, et al., in review)

Lake Ontario fisheries management objectives seek to conserve and restore remnant coregonine spawning populations (Stewart et al., 2017), but the spatial extent of current coregonine spawning is unknown, as are the mechanisms maintaining existing populations and those limiting the resurgence of historical populations. Historically, spawning areas included embayments, the nearshore zone of the main lake, and tributary habitats (Goodyear et al., 1982), however, by the early 2000's, the known spawning populations were associated with the Bay of Quinte (Ontario), the shores and embayments of Prince Edward County (Ontario) and Chaumont Bay (New York) (Connerton et al., 2014; Hoyle, 2005). Some studies have suggested coregonine spawning in Lake Ontario's eastern habitats is expanding (George et al., 2018b, 2017; McKenna and Johnson, 2009) however the lack of more spatially explicit sampling limits our understanding of potential expansion. It is unclear why the remaining spawning stocks are located within the eastern basin or what factors regulate lake-wide recruitment success (Weidel et al., in press). Understanding the contemporary distribution and relative abundance of coregonine spawning populations at a lake-wide scale is needed to facilitate the design and allocation of coregonine restoration efforts in Lake Ontario (Connerton et al., 2017; Hoyle et al., 2011; Stewart et al., 2017).

In Spring 2018, we conducted a lake-wide binational ichthyoplankton survey in Lake Ontario to describe the contemporary spatial extent of coregonine spawning habitat and to quantify biotic and abiotic drivers of spawning success. This multi-organization, standardized effort was facilitated through the 2018 EPA Cooperative Science and Monitoring Initiative (CSMI) field year in Lake Ontario. We assume that larval abundance provides an integrated metric of spawning success within a specific region including survival to the larval stage. The study objectives were to 1) use observed larval presence and relative abundance to infer the

contemporary spatial extent of successful coregonine spawning, and 2) quantify the relative importance of hypothesized environmental drivers of successful coregonine recruitment to the larval stage.

By identifying the current status, spatial extent, and species-specific environmental drivers of Cisco and Lake Whitefish, our results support the implementation and evaluation of binational coregonine restoration, conservation, and management actions in Lake Ontario. This work was designed to address stated objectives of fisheries and other ecological management plans.

This project directly informs the Lake Ontario Committee's Fish Community Objectives (Stewart et al., 2017) specifically FCO's 2.3 and 3.2:

> *2.3 Increase prey-fish diversity—maintain and restore a diverse prey-fish community that includes Alewife, Lake Herring, Rainbow Smelt, Emerald Shiner, and Threespine Stickleback.*
>
> - *Status/trend indicator: Maintaining or increasing populations and increasing species diversity of the pelagic prey-fish community, including introduced species (Alewife and Rainbow Smelt) and selected native prey-fish species (Threespine Stickleback, Emerald Shiner, and Lake Herring [Cisco]).*
>
> - *Status/trend indicator: Increasing spawning populations of Lake Herring [Cisco] in the Bay of Quinte, Hamilton Harbor, and Chaumont Bay.*
>
> *3.2 Increase Lake Whitefish abundance—increase abundance in northeastern waters and re-establish historic spawning populations in other areas.*
> - *Status/trend indicator: Increasing populations of Lake Whitefish across a range of age-groups sufficient to maintain self-sustaining populations and increasing spawning populations in the Bay of Quinte and eastern Lake Ontario.*

This work also specifically informs stated elements of the basin wide Coregonine Adaptative Management Framework adopted by the Council of Lake Committees including:
- *Gap Analysis describe and map the contemporary populations and habitats*
- *Identify threats and impediments for extant populations*

The project also directly informs the Lake Ontario Biodiversity Conservation Strategy (Lake Ontario LAMP working group, 2011) that, for a variety of regions throughout Lake Ontario, seeks to:
- *Restore populations of Lake Whitefish, lake herring (Cisco)*
- *Explore feasibility of restoring whitefish and lake herring (Cisco)*
- *Reduce sediment runoff into river mouths – rocky shoals are important for herring (Cisco)/whitefish spawning*
- *Evaluate restoration potential for lake herring (Cisco)*

Finally, this project directly informs the Lake Ontario LAMP Priority Science and Monitoring Activities (Environment and Climate Change Canada and the U.S. Environmental Protection Agency, 2018) under point number four:

- *improve understanding of fish dynamics*

## Data availability

All data from this study will be made publicly available through USGS Sciencebase website. Development of the data tables and metadata are underway and we expect these data to be released by May 2021.

## Impact

The lake wide coregonine larval survey results have already influenced Lake Ontario coregonine management. The presence of larvae outside of the eastern basin's Chaumont Bay and Bay of Quinte indicates successful spawning is occurring in those regions, albeit limited. This finding has resulted in U.S. managers reevaluating the need for experimental Cisco stocking in south shore Lake Ontario embayments (Steven LaPan, NYSDEC, personal communication).

One possible interpretation of the larval results is that the extant coregonine populations are sufficiently abundant to recolonize historic spawning regions but that spawning and egg incubation conditions (e.g., substrate, physical conditions, ice cover) are limiting reproduction in regions outside the primary spawning locations. The results from this project and other related coregonine projects have resulted in new GLRI funded projects to quantify the habitat and environmental conditions necessary for successful coregonine egg incubation which will inform management and potential restoration actions.

## Project 1: Contemporary spatial extent and environmental drivers of larval coregonine distributions across Lake Ontario

This project funded Taylor Brown's Master's thesis at Cornell University under the supervision of Suresh Sethi, Lars Rudstam and Brian Weidel. We have reproduced notable excerpts from the MS thesis (T. Brown, 2020) as well as the journal manuscript in review (Brown, et al., in review); however we encourage readers to use the original texts for additional detail and citation.

### *Brown et al. (in review) Abstract*

Coregonine fishes are important to Laurentian Great Lakes food webs and fisheries and are central to basin-wide conservation initiatives. In Lake Ontario, binational management objectives include conserving and restoring spawning stocks of Cisco (*Coregonus artedi*) and Lake Whitefish (*C. clupeaformis*), but the spatial extent of contemporary coregonine spawning habitat and the environmental factors regulating early life survival are not well characterized. In Spring 2018, we conducted a binational ichthyoplankton assessment to describe the spatial extent of coregonine spawning habitat across Lake Ontario. We then quantified the relative importance of a suite of biophysical variables hypothesized to influence coregonine early life success using generalized additive mixed models and multimodel inference. Between April 10 – May 14, we conducted 1,092 ichthyoplankton tows and captured 2,350+ coregonine larvae across 17 sampling areas. Although 95% of catches were in the eastern basin, coregonine larvae were also found in historical south shore spawning areas. Most coregonine larvae were Cisco; less than 6% were Lake Whitefish. Observed catches of both species across sampling areas were strongly and similarly associated with ice cover duration, but the importance of site-specific characteristics varied, such as distance to shore and site depth for Cisco and Lake Whitefish, respectively. These results suggest that regional-scale climatic drivers and local environmental habitat characteristics interact to regulate early life stage success. Furthermore, strong regional and cross-species variation in larval distributions emphasize the importance of lake-wide assessments for monitoring both the current eastern basin populations and potential expansions into western Lake Ontario habitats.

### *Results (Brown, et al., in review)*

-1,092 standardized ichthyoplankton tows from April 10 – May 14, 2018, with 2,354 *Coregonus* larvae captured over the sampling period (Figs. 1, S2, S3, S4, Table 1).

- genetic barcoding identified 1,001 coregonine larvae, with 840 Cisco and 58 Lake Whitefish successfully identified to species and the remainder comprising failed genetic assays (n = 90) or non-coregonine species (n = 13).

- Highest CPUE was observed in Chaumont Bay, Henderson Harbor, Black River Bay, Bay of Quinte, Fox and Grenadier (eastern basin), and West Lake (north shore), collectively comprising almost 98% of all captured coregonine larvae (Figure 1). Of the total 2,354 coregonine larvae captured, approximately half were collected in Chaumont Bay alone.

- Although at low observed abundances, larval coregonines were also detected in sampling areas across the south shore (Irondequoit, Sodus, Little Sodus, and Port bays), western basin (Niagara River, Olcott), north shore (Prince Edward Bay, Presqu'ile, Wellers), and Rochester basin (Stony Creek, northern Mexico Bay).

- No coregonine larvae were observed at offshore sites.

- The observed coregonine assemblage was dominated by larval Cisco, with Lake Whitefish individuals representing less than 6% of the total larval coregonine catch (Figs. 1, S2).

- High collinearity was identified among some of the candidate predictor variables, particularly for the climatic and substrate covariates. This required dropping some covariates from consideration.

- Multimodel inference results indicated that day-of-year, distance to shore, and ice cover duration were most strongly supported as being associated with larval Cisco catches and these predictors were included in the final Cisco model (Figure 2).

- Multimodel inference found that water temperature, site depth, and ice cover duration were most strongly supported as being associated with larval Lake Whitefish catches, all of which were included in the final Lake Whitefish model (Figure 2).

- Other captured larval fish species included percids (n = 24,970, primarily Yellow Perch *Perca flavescens*), catostomids (n = 625), Burbot (n = 57), Deepwater Sculpin (n = 6, *Myoxocephalus thompsonii*) and Rainbow Smelt (n = 30, *Osmerus mordax*, offshore only).

- Burbot and Deepwater Sculpin are species of conservation interest and this project is the first to illustrate larval catches of these species in Lake Ontario (Figure 3)

Table 1. Number of ichthyoplankton tows and mean species-specific catch-per-unit-effort (CPUE, larval catch per minute of towing) ± standard deviation (SD) for each sampling area. Failed assays represent *Coregonus* spp. larvae that were unable to be genetically identified to species. Sampling area acronyms defined here correspond to Figure 1 sampling area labels.

| Sampling Area | Tows Collected | Mean CPUE ± SD | | |
|---|---|---|---|---|
| | | Cisco | Lake Whitefish | Failed Assay |
| Chaumont Bay (CB) | 60 | 6.47 ± 20.5 | 0.01 ± 0.09 | 0.09 ± 0.51 |
| Henderson Harbor (HE) | 44 | 1.76 ± 4.34 | 0.03 ± 0.11 | 0.02 ± 0.08 |
| Black River Bay (BRB) | 29 | 1.12 ± 2.54 | 0.01 ± 0.06 | 0.05 ± 0.12 |
| Bay of Quinte (BQ) | 291 | 0.57 ± 4.89 | 0.05 ± 0.25 | 0.11 ± 0.75 |
| Fox and Grenadier (FG) | 55 | 0.39 ± 0.96 | 0.05 ± 0.19 | 0.04 ± 0.18 |
| West Lake (WL) | 32 | 0.33 ± 1.56 | - | 0.11 ± 0.56 |
| Stony Creek (SC) | 9 | 0.27 ± 0.39 | - | - |
| Little Sodus Bay (LSB) | 36 | 0.21 ± 1.00 | - | 0.02 ± 0.08 |
| Presqu'ile (PR) | 22 | - | 0.01 ± 0.06 | 0.01 ± 0.06 |
| Sodus Bay (SB) | 41 | 0.02 ± 0.09 | 0.01 ± 0.08 | - |
| Niagara River (NR) | 19 | - | - | 0.02 ± 0.08 |
| Olcott (OL) | 20 | - | 0.02 ± 0.07 | - |
| Port Bay (PB) | 20 | 0.02 ± 0.07 | - | - |
| Wellers (WE) | 29 | 0.02 ± 0.07 | - | - |
| Irondequoit Bay (IQT) | 58 | 0.01 ± 0.04 | - | 0.01 ±0.04 |
| Mexico Bay North (MBN) | 31 | 0.01 ± 0.05 | - | - |
| Prince Edward Bay (PEB) | 55 | 0.01 ± 0.04 | - | - |
| Athol Bay (AB) | 9 | - | - | - |
| Braddock Bay (BB) | 16 | - | - | - |
| Charity Shoal | 1 | - | - | - |
| Collins Bay (CO) | 3 | - | - | - |
| False Duck Islands | 8 | - | - | - |
| Genesee River (GR) | 17 | - | - | - |
| Hamilton Harbour (HA) | 20 | - | - | - |
| Main Duck Island (MDI) | 10 | - | - | - |
| Mexico Bay South (MBS) | 16 | - | - | - |
| Nicholson | 7 | - | - | - |
| Oswego (OS) | 22 | - | - | - |
| Point Petre | 5 | - | - | - |
| Popham | 8 | - | - | - |
| Rice Creek | 9 | - | - | - |
| Salmon River | 17 | - | - | - |
| Sandy Pond (SP) | 14 | - | - | - |
| Rocky Point (RP) | 12 | - | - | - |
| St. Lawrence (SL) | 12 | - | - | - |
| Stony Island | 5 | - | - | - |
| Stony Point | 5 | - | - | - |
| Toronto Harbour (TH) | 10 | - | - | - |
| Wilson (WI) | 15 | - | - | - |

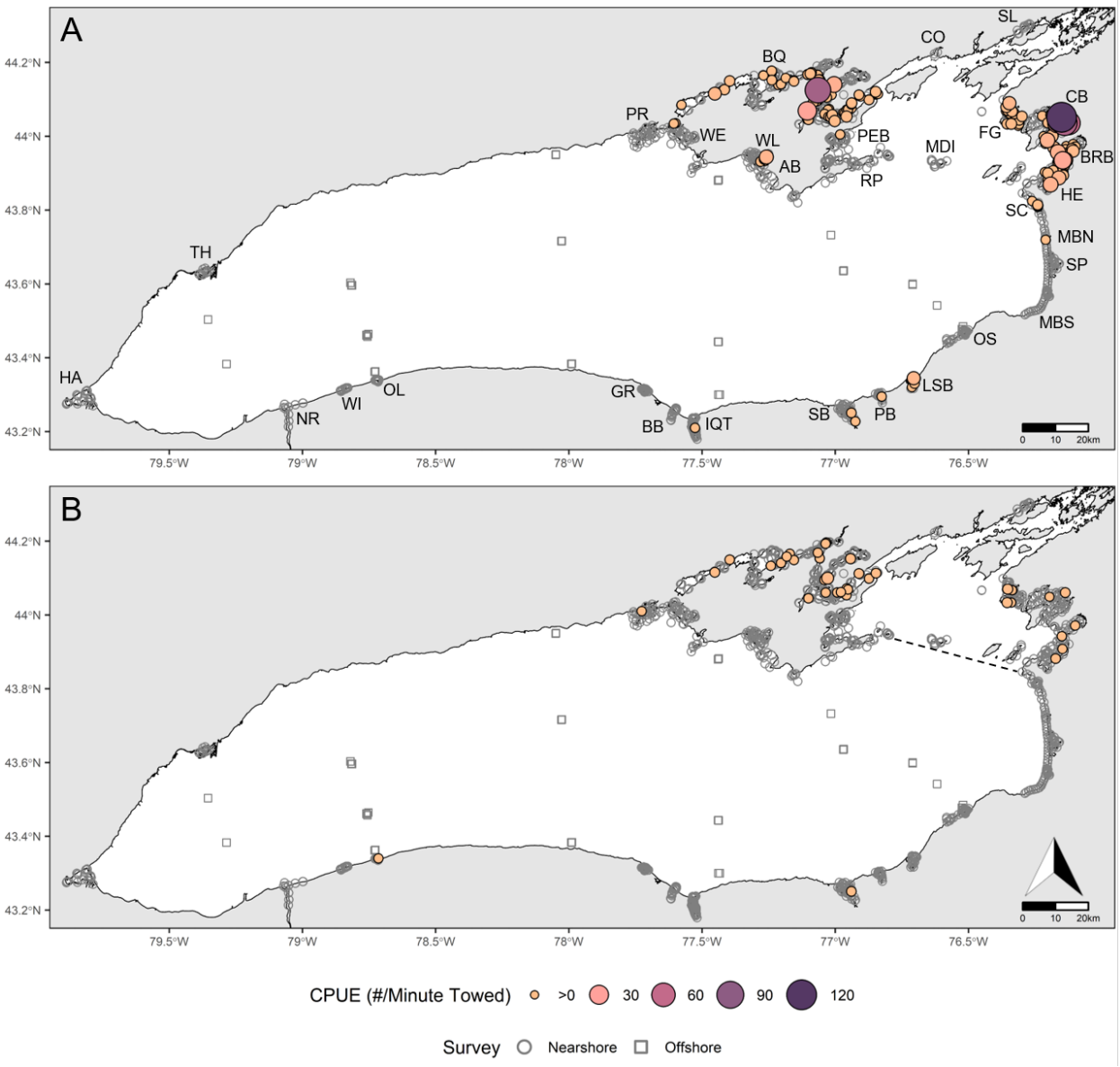


Figure 1. (Brown, et al., in review) Maps of the observed larval A) Cisco and B) Lake Whitefish catch-per-unit-effort (CPUE, larval catch per minute of towing) for each ichthyoplankton tow site. Each point represents a single ichthyoplankton tow. Tows where larval coregonines were present are filled, while open points denote tows where larval coregonines were absent. Points increase in size and darken in fill color with increasing CPUE. Samples collected during the primary nearshore assessment are denoted with circles while offshore samples are denoted with squares. Sampling areas of interest are labeled using the acronyms defined in Table 1. The dashed line in panel B denotes the Duck-Galloo ridge, where the eastern basin is defined as the lake area north of this ridge. Full zoomed in panels are available in the Supplementary Material (Figs. S3 and S4).

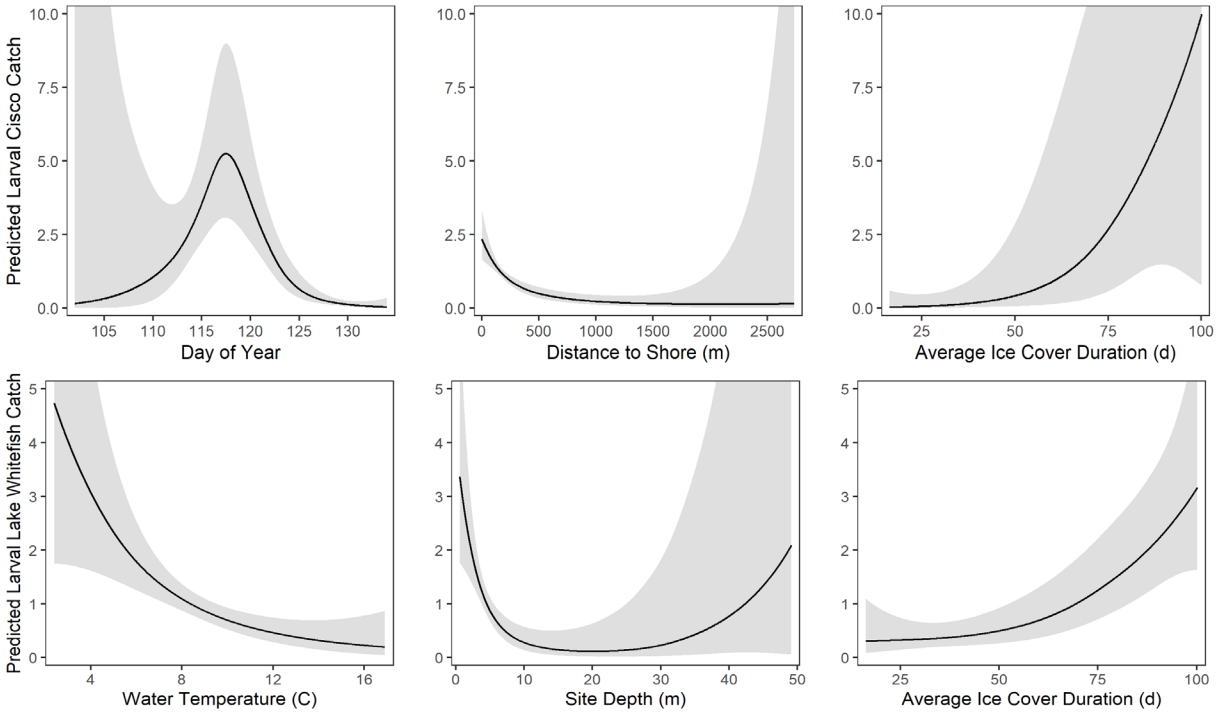


Figures 2 (Brown, et al., in review) Upper three panels illustrate the estimated marginal relationships between best-supported environmental variables and Cisco larval catches from negative binomial generalized additive mixed models. Black lines show predicted, back-transformed larval catches (± 1 standard error in shaded region). Lower three panels represent the same results for Lake White fish larval catches.

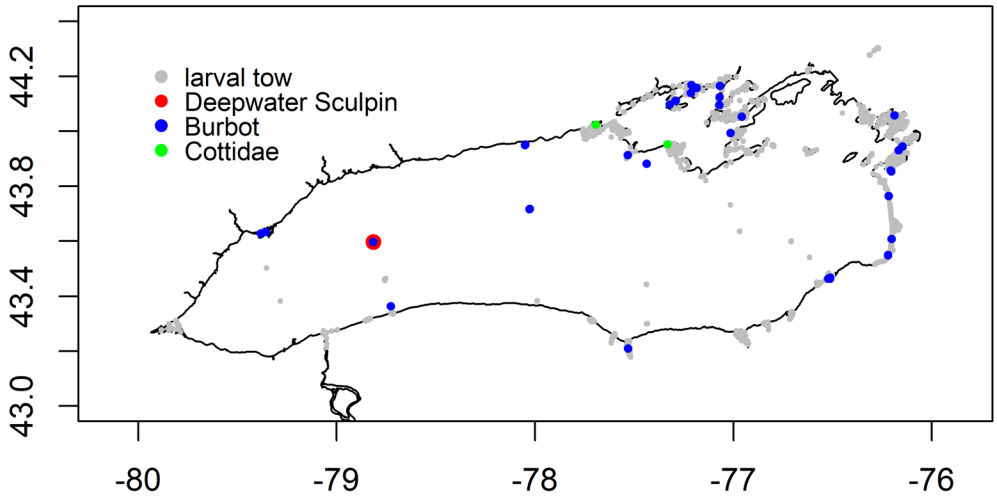


Figure 3. Location of non-coregonine native larval fishes captured as part of the 2018 CSMI larval fish survey.

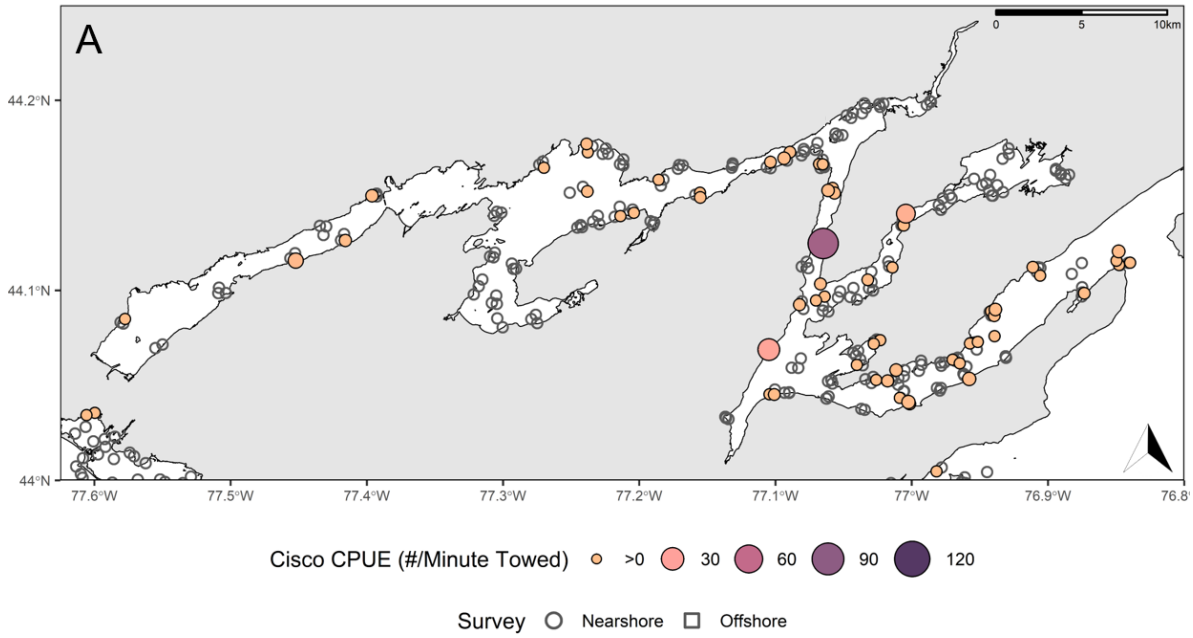


Figure S3(A). (Brown, et al., in review) Larval Cisco catch-per-unit-effort (CPUE, larval catch per minute of towing) for each ichthyoplankton tow site for sampling areas within the Bay of Quinte, Ontario, Canada.

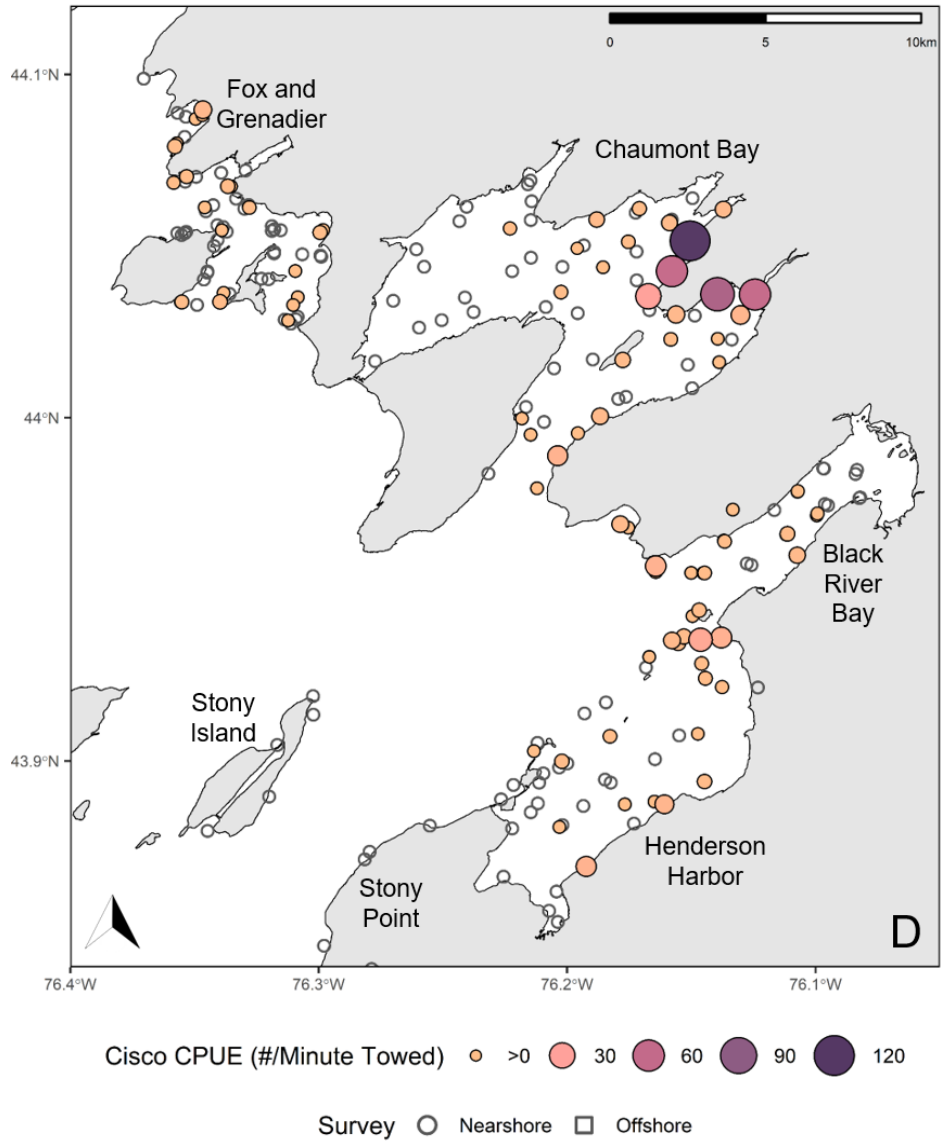


Figure S3(D). (Brown, et al., in review) Larval Cisco catch-per-unit-effort (CPUE, larval catch per minute of towing) for each ichthyoplankton tow site for sampling areas in nearshore New York waters of the eastern basin.

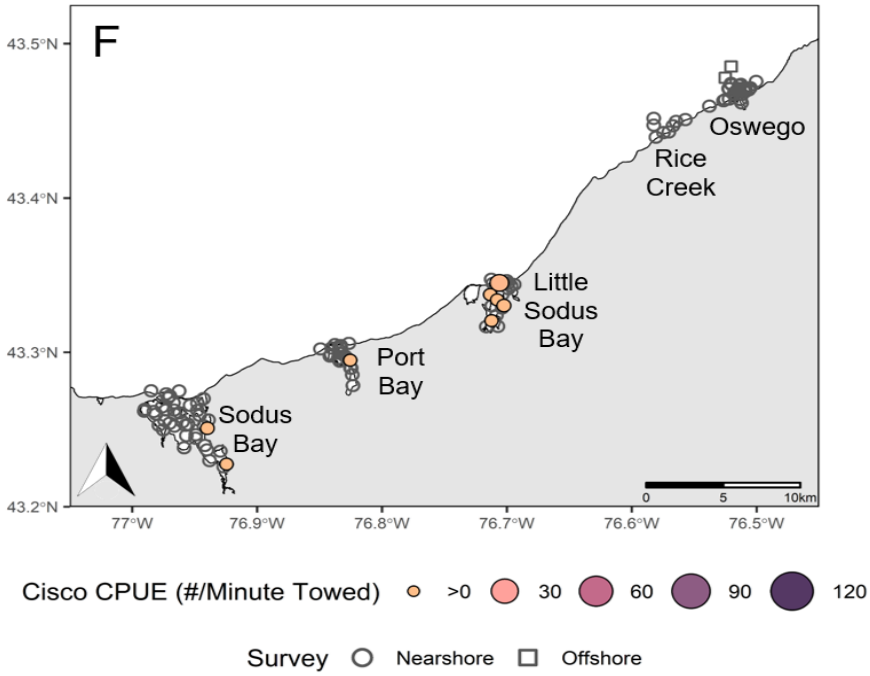


Figure S3(F). (Brown, et al., in review) Larval Cisco catch-per-unit-effort (CPUE, larval catch per minute of towing) for each ichthyoplankton tow site for sampling areas along the southeastern shore of Lake Ontario.

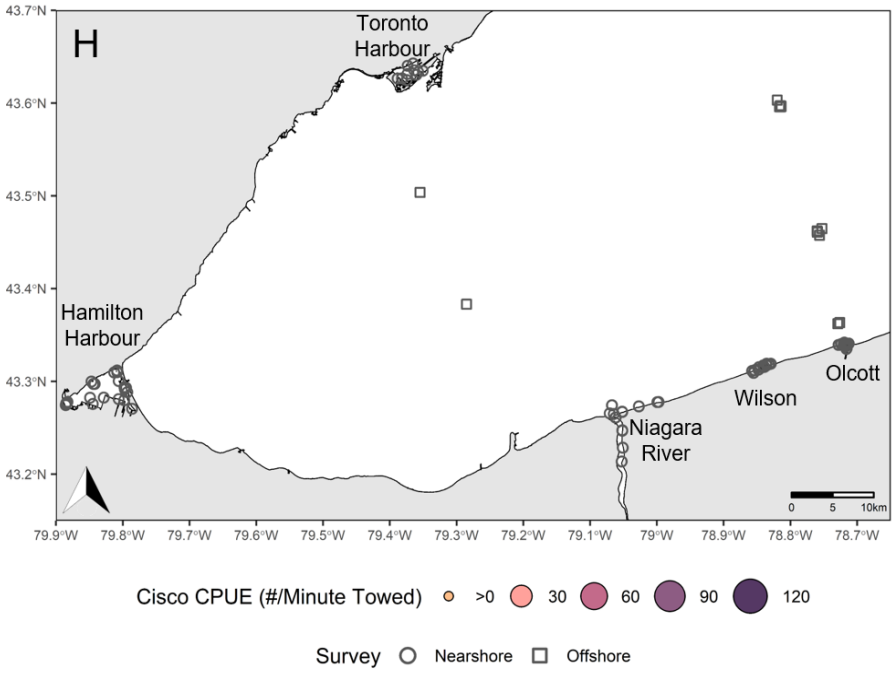


Figure S3(H). (Brown, et al., in review) Larval Cisco catch-per-unit-effort (CPUE, larval catch per minute of towing) for each ichthyoplankton tow site for sampling areas in the western basin of Lake Ontario. No Cisco were observed in these sites

## Acknowledgements

This work was supported by the Great Lakes Restoration Initiative and the Cooperative Science and Monitoring Initiative to B. Weidel (USGS Ecosystems Mission Area Status and Trends Program) and an IAGLR Norman S. Baldwin Fishery Science Scholarship to T. Brown. We thank the vessel crews, biological staff, and support staff that provided essential field, laboratory, and administrative in-kind support for this study, including those from the NYSDEC Cape Vincent Office and Regions 6, 7, 8, and 9; USGS Tunison Lab of Aquatic Science and Lake Ontario Biological Station; OMNRF Lake Ontario Management Unit; USFWS Lower Great Lakes Fish and Wildlife Conservation Office; DFO Burlington; Queen's University; R/V Lake Guardian; Cornell Biological Field Station; and New York Cooperative Fish and Wildlife Research Unit. OMNRF's in-kind support was made possible with funding provided by the Fish and Wildlife Special Purpose Account, the Canada-Ontario Agreement on Great Lakes Water Quality and Ecosystem Health, and Ontario's Great Lakes Strategy. Thank you to S. Ireland and R. DeBruyne (USGS Great Lakes Science Center) for providing their expert guidance in formulating study design and sample processing protocols, and to A. Lau (USGS Lake Ontario Biological Station) for her assistance with field collections and sample processing. Any use of trade, firm, or product names is for descriptive purposes only and does not imply endorsement by the U.S. Government. All USGS sampling and handling of fish during research were carried out in accordance with guidelines for the care and use of fishes by the American Fisheries Society (Use of Fishes in Research Committee, 2014).

## Project 2: Species-Specific Patterns and Biophysical Drivers of Larval Coregonine Spatiotemporal Distributions within Nursery Habitats

*Rationale, Goals, and Hypotheses:*

Coregonine fishes are important components of Laurentian Great Lakes food webs and fisheries and are central to basin-wide conservation initiatives. Recent assessments have suggested that Cisco (*Coregonus artedi*) populations may be expanding, but many Lake Whitefish (*C. clupeaformis*) populations continue to decline or remain at low levels (T. Brown, 2020; Claramunt et al., 2019; Council of Lake Committees, 2018). Cisco and Lake Whitefish eggs and larvae are found in similar habitats, often occurring in sympatry (Goodyear et al., 1982; Schaefer, 2019), but there is increasing evidence that species-specific microhabitat use during early life stages may result in differential interactions with local environmental conditions (T. A. Brown, 2020; McKenna et al., 2020). Understanding the mechanistic drivers of larval Cisco and Lake Whitefish distributions within embayment habitats is critical for understanding species-specific early life-history and spatial ecology. Quantifying which biophysical drivers are important for regulating coregonine early life stages is needed to identify potential recruitment bottlenecks (Zimmerman and Krueger, 2009). Improving our understanding of coregonine spatial ecology is key for designing monitoring programs that accurately reflect population dynamics and can test the effect of potential restoration actions (Cooke et al., 2016; McKenna et al., 2020).

We propose to examine the relationship between larval spatial distributions within individual embayments (e.g., distance from shore, site depth) and how these spatial patterns vary over time, with larval biological attributes (e.g., species identity, total length, developmental stage), and with dynamic physical conditions (e.g., water temperature, wind direction, circulation models). Candidate embayments in Lake Ontario include Chaumont Bay, Bay of Quinte, Black River Bay, Henderson Harbor, and Fox and Grenadier Islands. This research will address multiple hypotheses regarding species-specific life-history and spatial ecology:

1. *Null Model*: Coregonine larvae are randomly distributed within embayment habitats and exhibit no species-specific differences in microhabitat use;
2. *Physical Forcing Hypothesis*: Dynamic physical conditions force planktonic larvae into microhabitats and larvae exhibit no active habitat selection;
3. *Adaptive Habitat Segregation Hypothesis*: Lake whitefish occupy nearshore/shoreline habitats, while Cisco occupy offshore habitats within embayments, which could reduce competitive interactions in these sympatric species (McKenna et al., 2020);
4. *Ontogenetic Habitat Shift Hypothesis*: Both Lake Whitefish and Cisco undergo an ontogenetic transition from offshore to nearshore habitat use over time as larvae grow in body size and swimming ability, allowing larvae to actively select nearshore habitats (Hart, 1931; Pritchard, 1931).

*Expected Methods and Results:*

- This project will use the available 2018 Lake Ontario larval coregonine data as described in above (Figure 1).
- Descriptive statistics for larval catches (species identity, total length, length at age, yolk sac stage, catch per unit effort with respect to time and space

- Analysis relating spatiotemporal patterns of larval catches to hypothesized biophysical drivers
    - Temporal
    - Climatic (wind forcing, days since ice out)
    - Local habitat characteristics (water temperature, shoreline sinuosity, site depth)
    - Life-history (species identity, total length, yolk-sac stage)

This project is currently underway with expected submission during summer of 2021. Data sources from this project follow from Project #1.

## Impact

Quantifying coregonine larval dynamics across time and space is an increasingly important aspect of restoration monitoring as a suite of different actions are evaluated. We expect results from this project to directly inform larval survey sampling design, restoration monitoring, and evaluating restoration actions.

| Region | Habitat | Date | | | | | | | | | | | | | | | | | | | | | | |
|---|---|---|---|---|---|---|---|---|---|---|---|---|---|---|---|---|---|---|---|---|---|---|---|---|
| | | Week 1 | | | Week 2 | | Week 3 | | | | | Week 4 | | | | | Week 5 | | | | | | | |
| | | 4/10 | 4/11 | 4/12 | 4/18 | 4/19 | 4/23 | 4/24 | 4/25 | 4/26 | 4/27 | 4/30 | 5/1 | 5/2 | 5/3 | 5/4 | 5/7 | 5/8 | 5/9 | 5/10 | 5/11 | 5/12 | 5/13 | 5/14 |
| Bay of Quinte | Adolphus Reach | | | | | | | 41 | | | | | 29 | | | | | | | | 11 | | | |
| | Big Bay | | | | | | | | 13 | | | 13 | | | | | | | | | | | | |
| | Hay Bay | | | | | 2 | 77 | | | | | | | | | 8 | | | | | | | | |
| | Long Reach | | | | | | | | | | 362 | 4 | | | 7 | | | | | | | | | |
| | Trenton | | | | | | | | | 37 | | | | | | | | | | | | | | |
| Chaumont | Black River Bay | | | | | | 20 | | 7 | | | 64 | | | | | | | | | | | | |
| | Chaumont Bay | | | | | | | | | | | 658 | | 515 | 11 | | | | | | | | | |
| | Fox and Grenadier | | | | | | | 48 | | | | | 19 | | | | | 12 | | | | | | |
| | Henderson Harbor | | | | | | | | 15 | 21 | | | 1 | 242 | | | | | | | | | | |
| | Stony Island | | | | | | | | | | | | | | | | | | | | | | | |
| | Stony Point | | | | | | | | | | | | | | | | | | | | | | | |
| Main Lake | Charity Shoal | | | | | | | | | | | | | | | | | | | | | | | |
| | Main Duck Island | | | | | | | | | | | | | | | | | | | | | | | |
| Mexico Bay | Mexico Bay Central | | | | | | | | | | | | | | | | | | | | | | | |
| | Mexico Bay North | | | | | | | | | | | | 1 | | | | | | | | | | | |
| | Mexico Bay South | | | | | | | | | | | | | | | | | | | | | | | |
| | Salmon River | | | | | | | | | | | | | | | | | | | | | | | |
| | Sandy Pond | | | | | | | | | | | | | | | | | | | | | | | |
| | Stony Creek | | | | | | | | | | | | 4 | | 4 | | | | | | | | | |
| North Shore | Athol Bay | | | | | | | | | | | | | | | | | | | | | | | |
| | Nicholson | | | | | | | | | | | | | | | | | | | | | | | |
| | Point Petre | | | | | | | | | | | | | | | | | | | | | | | |
| | Presquile | | | | | | | | | | | | | | | | | | | | 2 | | | |
| | Prince Edward Bay | | | | | | | | | | | | | | | | | | 4 | | | | | |
| | Southshore Rocky Point | | | | | | | | | | | | | | | | | | | | | | | |
| | Wellers | | | | | | | | | | | | | | | | | | | | | 3 | | |
| | Wellington and West Lake | | | | | | | | | | | | | | | | | | | 49 | | | | |
| Southcentral | Braddock Bay | | | | | | | | | | | | | | | | | | | | | | | |
| | Genesee River | | | | | | | | | | | | | | | | | | | | | | | |
| | Irondequoit Bay | | | | | | | | | | | | 1 | | | | | | | | | | | |
| | Little Sodus Bay | | | | | | | | | | 4 | | | | | | | | | | | | | |
| | Oswego | | | | | | | | | | | | | | | | | | | | | | | |
| | Port Bay | | | | | | | 1 | | | | | | | | | | | | | | | | |
| | Sodus Bay | | | | | | | | | 4 | | | | | | | | | | | | | | |
| St Lawrence | Collins Bay | | | | | | | | | | | | | | | | | | | | | | | |
| | St Lawrence | | | | | | | | | | | | | | | | | | | | | | | |
| West | Hamilton Harbour | | | | | | | | | | | | | | | | | | | | | | | |
| | Niagara River | | | | | | | | | | | | 1 | | | | | | | | | | | |
| | Olcott | | | | | | | 1 | | | | | | | | | | | | | | | | |
| | Toronto Inner Harbour | | | | | | | | | | | | | | | | | | | | | | | |
| | Wilson | | | | | | | | | | | | | | | | | | | | | | | |

Figure 1. Summary of effort and coregonine catches over time for each sampling area during the 2018 CSMI Lake Ontario Larval Coregonine Assessment. A filled square indicates a sampling event on that day. Blue indicates that no coregonine larvae were captured. Green indicates that coregonine larvae were captured, and the numbers denote how many individuals were collected.

## Literature Cited


Brown, T., 2020. Contemporary spatial extent and environmental drivers of larval coregonine distributions across Lake Ontario. Cornell University.

Brown, T., Sethi, S.A., Rudstam, L.G., Holden, J.P., Connerton, M.J., Gorsky, D., Chalupnicki, M.A., Sard, N., Roseman, E.F., Prindle, S.E., Sanderson, M., Evans, T., Cooper, A., Reinhart, D., Weidel, B.C., in review. Contemporary spatial extent and environmental drivers of larval coregonine distributions across Lake Ontario. J. Gt. Lakes Res.

Brown, T.A., 2020. Contemporary spatial extent and environmental drivers of larval coregonine distributions across Lake Ontario (Master's Thesis). Cornell University, Ithaca, NY.

Claramunt, R.M., Smith, J., Donner, K., Povolo, A., Herbert, M.E., Galarowicz, T., Claramunt, T.L., DeBoe, S., Stott, W., Jonas, J.L., 2019. Resurgence of Cisco (*Coregonus artedi*) in Lake Michigan. J. Gt. Lakes Res. S0380133019300760. https://doi.org/10.1016/j.jglr.2019.04.004

Cooke, S.J., Martins, E.G., Struthers, D.P., Gutowsky, L.F.G., Power, M., Doka, S.E., Dettmers, J.M., Crook, D.A., Lucas, M.C., Holbrook, C.M., Krueger, C.C., 2016. A moving target—incorporating knowledge of the spatial ecology of fish into the assessment and management of freshwater fish populations. Environ. Monit. Assess. 188, 239. https://doi.org/10.1007/s10661-016-5228-0

Council of Lake Committees, 2018. Developing research priorities for Lake Whitefish in the Upper Great Lakes. Great Lakes Fishery Trust and Great Lakes Fisheries Commission, Michigan State University.

Environment and Climate Change Canada and the U.S. Environmental Protection Agency, 2018. Lake Ontario Lakewide Action and Management Plan, 2018-2022.

Goodyear, C.S., Edsall, T.A., Ormsby Dempsey, D.M., Moss, G.D., Polanski, P.E., 1982. Atlas of the spawning and nursery areas of Great Lakes fishes, FWS/OBS-82/52. ed. U.S. Fish and Wildlife Service, Washington, DC.

Hart, J.L., 1931. The spawning and early life history of the whitefish, *Coregonus clupeaformis* (Mitchell) on the bay of Quinte, Ontario. Contrib. Can. Biol. Fish. 6, 165–214. https://doi.org/10.1139/f31-007

Lake Ontario LAMP working group, 2011. Implementing a Lake Ontario LaMP Biodiversity Conservation Strategy.

McKenna, J.E., Stott, W., Chalupnicki, M., Johnson, J.H., 2020. Spatial segregation of Cisco (Coregonus artedi) and Lake Whitefish (C. clupeaformis) larvae in Chaumont Bay, Lake Ontario. J. Gt. Lakes Res. S0380133020301295. https://doi.org/10.1016/j.jglr.2020.06.007

Pritchard, A.L., 1931. Spawning habits and fry of the Cisco (*Leucichthys artedi*) in Lake Ontario. Contrib. Can. Biol. Fish. 6, 225–240. https://doi.org/10.1139/f31-009

Schaefer, H., 2019. Predicting spawning habitat for Lake Whitefish *Coregonus clupeaformis* and Cisco *Coregonus artedi* in the Lake Erie and Lake Ontario regions using classification

and regression tree (CART) and random forest models (Master's Thesis). University of Michigan, Ann Arbor, MI.
Stewart, T.J., Todd, A., Lapan, S., 2017. Fish community objectives for Lake Ontario (Great Lakes Fisheries Commission Special Publication). Ann Arbor, MI.
Zimmerman, M.S., Krueger, C.C., 2009. An ecosystem perspective on re-establishing native deepwater fishes in the Laurentian Great Lakes. North Am. J. Fish. Manag. 29, 1352–1371. https://doi.org/10.1577/M08-194.1

## Paired Contaminants, Fatty Acids and Stable Isotopes in the Lake Ontario Food Web

**Bernard Crimmins, AEACS, LLC/Clarkson University**
**Junda Ren, Clarkson University**
**Sadjad Fakouri Baygi, Clarkson University**
**Adam Point, Clarkson University**
**Sujan Fernando, Clarkson University**
**Philip Hopke, Clarkson University**
**Thomas Holsen, Clarkson University**

**Contact:**
**Bernard Crimmins**
Email: bernard.crimmins@aeacsllc.com
Phone: 202-368-6926

Address:
AEACS, LLC
New Kensington, PA 15068

## Brief Description

Monitoring the trends of contaminants in the Great Lakes has been performed for decades. The U.S. EPA Great Lakes Fish Monitoring and Surveillance Program (GLFMSP) utilizes lake trout and walleye (Erie only) as bioindicators of chemical contamination to track the temporal trends throughout the Great Lakes region. As a top predator, the temporal concentration changes detected in the fish are used as an ecosystem health indicator. Periodic contaminant transport assessments within the system (food web) are needed to monitor the flow of contaminants through the aquatic system. This is especially true for emerging contaminants such as polyfluoroalkyl substance (PFAS) where our understanding of the bioaccumulation throughout the food web dynamics is limited.

As part of the GLFMSP, an intensive sampling campaign is performed on one of the five lakes following the Cooperative Science Monitoring Initiative (CSMI) lake of the year (LOY) schedule. Lake Ontario (LO) was the 2018 LOY and a series of paired contaminant/food web marker measurements were performed to assess the trophic transfer of contaminants in LO for summer/fall of 2018. The overreaching goal of this effort was to develop a "snapshot" of contaminant burdens in fish and macro-invertebrates and then develop predator/prey relationships using complementary trophodynamic metrics. Stable isotopes and fatty acids were employed to trace the flow of the contaminants throughout the aquatic system. This snapshot provides a contemporary picture of the relationship between primary producer, prey fish and top predator fish species to develop potential exposure pathways to chemicals affecting the lake and aquatic species.

Stable isotopes and fatty acids have been employed as trophodynamic markers for decades (Kidd et al. 1995; Hebert, Arts, and Weseloh 2006; Sierszen, Keough, and Hagley 1996). Stable isotopes of nitrogen ($^{14}N$ and $^{15}N$) provide insight into the trophic position. The $^{15}N$ is enriched with increasing trophic levels and the $\delta\ ^{15}N$ (‰) value can be used to locate where a particular species is feeding within the aquatic food web. Similarly, stable isotopes of carbon ($^{12}C$ and $^{13}C$) are indicative of carbon origins (benthic vs. pelagic) and the $\delta\ ^{13}C$ values are used as a metric to catalog species utilizing similar carbon (or energy) sources; pelagic sources tend to be more negative than benthic sources (Zanden and Rasmussen 2001).

Fatty acids in a consumer reflect their diet and the fatty profiles can be used to complement $\delta^{13}C$ and $\delta^{15}N$ analyses in developing food web linkages. The stable isotope signatures provide insight into the feeding levels and carbon sources integrated over the lifetime of the organism. Fatty acids signatures reflect a more contemporary feeding habit that is integrated over several months and can be used to develop more recent potential predator/prey relationships (Hebert, Arts, and Weseloh 2006). Combined, these metrics provide insight into the potential sources and movement of bioacumulative chemical contaminants in the Lake Ontario food web.

The analyte list for the GLFMSP is expansive containing legacy contaminants such as mercury, polychlorinated biphenyls (PCBs), organochlorine pesticides (OCPs) and brominated diphenyl ethers (PBDEs) that are routinely monitored in top predator fish (Zhou et al. 2019; Zhou et al. 2018; Zhou et al. 2017). While these classes of compounds continue to drive the fish consumption advisories in the Great Lakes, the focus of the 2018 CSMI campaign and this report was to understand burdens of polyfluoroalkyl substances (PFAS) in the Lake Ontario food web. A detailed description of the PFAS, stable isotopes and fatty acids relationships has been submitted the Journal of Great Lakes Research Lake Ontario CSMI Special Issue (Ren et al., submitted). The current report summarizes these data with the addition of dissolved PFAS and food web Hg concentrations in Lake Ontario.

## Methods

**Collection.** Biological samples were collected at the GLFMSP Base Monitoring Program (BMP) sites near North Hamlin, NY and Oswego, NY, respectively (Table 1). Fish were collected in the fall by USGS Great Lakes Science Center (Oswego, NY). Lake trout (*Salvelinus namaycush*) were collected using a gill net, while alewife (*Alosa pseudoharengus*), round goby **(***Neogobius melanostomus*), rainbow smelt (*Osmerus mordax*), and deepwater sculpin (*Myoxocephalus thompsonii*) were collected using bottom trawls. Zooplankton were collected in bulk using a combination of vertical and horizontal tows then fractionated by size (63 µm, 118 µm, 243 µm and 500 µm) using sieves aboard the US EPA's *R/V Lake Guardian* in the summer of 2018 by Clarkson University and USGS. Water grab samples were collected using 1 L polypropylene bottles by Clarkson University only for the North Hamlin site concurrent with the macroinvertebrates.

**Analysis.** Stable isotopes of carbon ($^{12}C$ and $^{13}C$) and nitrogen ($^{14}N$ and $^{15}N$) were determined by Environmental Isotope Laboratory, University of Waterloo (https://uwaterloo.ca/environmental-isotope-laboratory/). Fatty acids were determined using a variant of the method described by Folch et al., (Folch, Lees, and Stanley 1957) using a 2:1 chloroform:methanol extraction followed by esterification using 10% BF3 in methanol and analysis using a gas chromatograph coupled to a flame ionization detector (Ren et al., submitted). Specifics on the determination of PFAS and Hg concentrations in the biological media can be found in previous publications from our laboratory (Point et al. 2019; Zananski et al. 2011).

## Results

**Stable Isotopes.** A summary of the stable isotope measurements is provided in Figure 1**.** North Hamlin zooplankton δ $^{15}N$ values (11.5 ± 2.02‰) were significantly greater than observed the at the Oswego site (7.08 ± 0.39‰, p = 0.001, t-test). Conversely, lake trout displayed a significantly greater δ $^{15}N$ at the Oswego site (17.4 ± 0.44‰) compared to North Hamlin (16.5 ± 0.41‰, p<0.001, t-test). Deepwater sculpin displayed the highest δ $^{15}N$ of the prey fish with similar values detected at the both sites (~16‰). The trophic level of the round goby was significantly greater at the Oswego site (14.4 ± 0.24‰ vs. 13.2 ± 0.05‰, p <0.001, t-test), but alewife values were similar among sites (~12‰). Oligochaetas and quagga mussels collected at the north Hamlin sites were similar to the deepwater sculpin (16 ‰ and 18 ‰, respectively).

Zooplankton δ $^{13}C$ values were significantly less negative at the Oswego site relative to North Hamlin (-30.4 $\pm$ 1.0 ‰ and 35.1 $\pm$ 0.69‰, respectively). Lake trout displayed the least negative value with no difference among sites (22‰). The prey species at each site had similar δ $^{13}C$ values ( -24‰) with the alewife exhibiting the largest (least negative) value (-21‰).

**Fatty acids.** Figure 2 provides a summary of the total fatty acid concentration and fraction of saturated, monounsaturated and polyunsaturated fatty acids in each of the species collected at North Hamlin and Oswego. At the Oswego site, lake trout contained the highest fatty acid content followed by alewife and deepwater sculpin. Lake trout at the North Hamlin site also had the highest concentration total fatty acids, but similar levels were also observed for the deepwater sculpin with slightly lower amount in the alewife.

Individually, the highest concentrations were observed for palmitic acid (16:0), cis-7-hexadecenoic acid (16:1n-7), oleic acid (18:1n-9), and docosahexaenoic acid (DHA) consistent

with previous work (Happel et al. 2017). Elevated concentrations of eicosapentaenoic acid (EPA) were observed in zooplankton at Oswego (30 ± 20%) relative to North Hamlin (12 ± 6.5%, p =0.0082, t-test). Alewife and round goby had elevated levels of 18:1n-9 and 16:1n-7, respectively. These two fatty acids are indicative of plant tissue (pelagic) and bacteria (benthic) and can be used as a marker for predators (Happel et al. 2020; Happel et al. 2017). Deepwater sculpin fatty acids profiles were dominated by 18:1n-9, 16:1n-9 and DHA.

**Food web.** For the 2018 LO summer/fall sampling, the stable isotope and FA analyses suggested lake trout fed primarily on alewife (Ren et al., 2021). The combination of stable isotopes and FA results also indicated *Mysis* as a food source for rainbow smelt and deepwater sculpin. Moreover, the $\delta^{15}N$ and $\delta^{13}C$ data supported a strong relationship between rainbow smelt and *Mysis*, with *Mysis* feeding on zooplankton based on the FA analysis.

**PFAS.** Dissolved PFAS were sampled in triplicate at the North Hamlin site in June 2018 (Table 2). Perfluorobutane, perfluoroheptane and perfluorooctane carboxylic acids (PFBA, PFHpA and PFOA, respectively) were observed at 2.7 $\pm$ 0.28, 2.1 $\pm$ 0.10 and 2.8 $\pm$ 0.6 ng/L, respectively. Similarly, the perfluoroalkyl sulfonic acids (PFBS, PFHxS and PFOS, respectively) were observed at 1.2 $\pm$ 0.1, 1.57 $\pm$ 0.04 and 2.6 $\pm$ 0.5. The > C11 carboxylic acids and C10 sulfonate were below detection limits in the dissolved phase collected at North Hamlin. These levels are ~ 10-fold lower than values reported in 2004 (Boulanger et al. 2004), but consistent with more recent values reported in 2019 (Gewurtz et al. 2019).

In the biological samples at least one PFAS congener was detected above the method detection limits (MDLs). Perfluorooctane sulfonic acid (PFOS) was detected in all of the samples, while perfluoropentanoic acid, perfluorobutane sulfonic acid, perfluoroheptanoic acid and perfluorohexandecanoic acid were below the MDLs in >80% of the media collected. The sulfonic acids accounted for > 60% of the PFAS with perfluorooctane sulfonic acid (PFOS) as the dominant congener.

The highest total PFAS concentration (∑PFAS) was observed in deepwater sculpin followed by lake trout > alewife ~ rainbow smelt > round goby > *Mysis* > zooplankton (Figure 3). Deepwater sculpin PFOS concentrations at North Hamlin (143 $\pm$ 109 ng/g) and Oswego (91 $\pm$ 19 ng/g) were lower than previous food web studies (Martin et al. 2004). Lake trout concentrations (54 $\pm$ 18

and 46 ± 10 ng/g for North Hamlin and Oswego, respectively) were ~1/2 of those observed for deepwater sculpin, but greater than the remaining forage fish (≤ 20ng/g).

**Hg.** Mercury concentrations followed a traditional bioaccumulation trend with levels increasing with trophic level at the Oswego and North Hamlin sites (Figure 4). Lake trout contained the highest levels followed by deep water sculpin, alewife, goby and smelt, respectively. Concentrations were greater in Oswego for the prey fish while the lake trout contained higher concentrations in North Hamlin.

## Summary

Macroinvertebrates, prey fish, top predator fish and water was collected as part of the U.S. EPA Great Lakes Fish Monitoring Surveillance Program in support of the 2018 CSMI program to assess the contaminant burdens in the Lake Ontario foodweb. Dissolved PFAS levels were found to be similar to those reported by Canadian researchers in Lake Ontario during the same time period, but significantly lower than values reported in 2004.

Fatty acids and stable isotope measurements resolved linkages between lake trout and alewife at both sites with minor contributions from round goby. PFAS concentrations were highest in the deepwater sculpin even though they are not top predator feeders. This is in contrast to the Hg distribution where lake trout contained significantly higher levels than all of the prey fish species. This dichotomy highlights the need to perform periodic emerging contaminant transport studies in the Great Lakes aquatic food web.

**Table 1.** Biological Sample Summary

| Species | Site | Collection Month | Collection Method |
|---|---|---|---|
| Zooplankton | Oswego | July | Vertical Trawl |
| Mysis | Oswego | July | Horizontal Trawl |
| Water Flea | Oswego | July | Benthic Sled |
| Alewife | Oswego | November | Bottom Trawl |
| Deepwater sculpin | Oswego | November | Bottom Trawl |
| Rainbow Smelt | Oswego | November | Bottom Trawl |
| Round Goby | Oswego | November | Bottom Trawl |
| Lake Trout | Oswego | October | Gill Net |
| Zooplankton | North Hamlin | June | Vertical Trawl |
| Mysis | North Hamlin | June | Vertical Tow |
| Dressenid Mussel | North Hamlin | June | Benthic Sled |
| Oligochaeta | North Hamlin | June | Benthic Sled |
| Alewife | North Hamlin | October | Bottom Trawl |
| Deepwater sculpin | North Hamlin | October | Bottom Trawl |
| Rainbow Smelt | North Hamlin | October | Bottom Trawl |
| Round Goby | North Hamlin | October | Bottom Trawl |
| Lake Trout | North Hamlin | October | Gill Net |

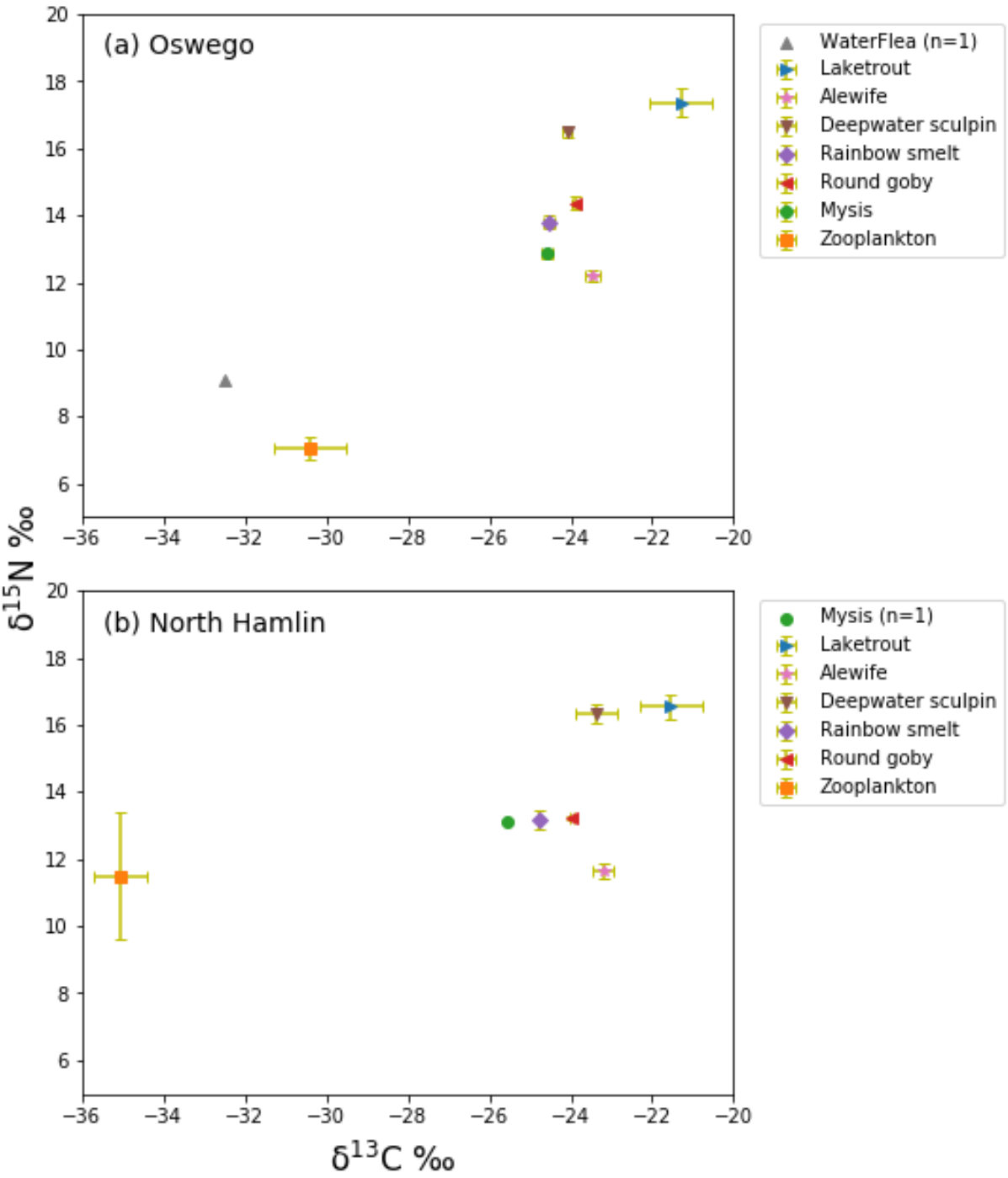


**Figure 1.** Relative stable isotopes of carbon and nitrogen observed in the Lake Ontario food web.

**Figure 2**. Total fatty acid concentrations observed at the Oswego and North Hamlin sites in Lake Ontario separated into saturated (SFA), monounsaturated (MUFA) and polyunsaturated (PUFA) fatty acid classes.

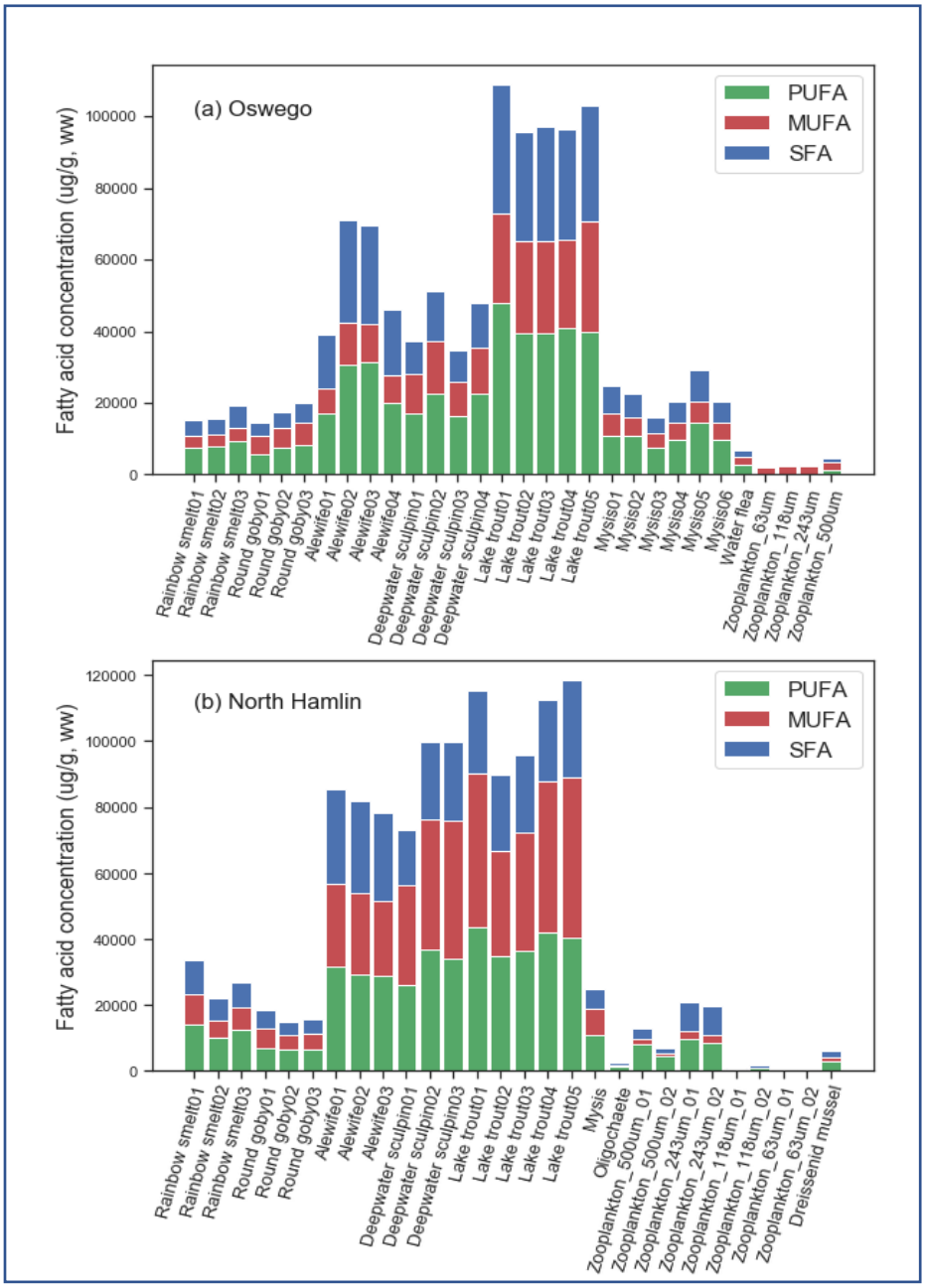

**Table 2**. Dissolved PFAS Concentrations at the North Hamlin Site

| PFAS | Abbreviation | Mean | SD |
|---|---|---|---|
| perfluorobutanoic acid | PFBA | 2.70 | 0.28 |
| perfluoropentanoic acid | PFPeA | 1.80 | 0.10 |
| perfluorohexanoic acid | PFHxA | 1.26 | 0.04 |
| perfluoroheptanoic acid | PFHpA | 2.07 | 0.10 |
| Perfluorooctanoic acid | PFOA | 2.79 | 0.64 |
| perfluorononanoic acid | PFNA | 0.59 | 0.05 |
| perfluorodecanoic acid | PFDA | 0.14 | 0.04 |
| perfluoroundecanoic acid | PFUnA | 0.03 | 0.01 |
| perflourododecanoic acid | PFDoA | <MDL | |
| perfluorotridecanoic acid | PFTrA | <MDL | |
| perfluorotetradecanoic acid | PFTeA | <MDL | |
| perfluorohexadecanoic acid | PFHxDA | <MDL | |
| | | | |
| perfluorobutane sulfonate | PFBS | 1.21 | 0.14 |
| perfluorohexane sulfonate | PFHxS | 1.57 | 0.04 |
| perfluorooctane sulfonate | PFOS | 2.63 | 0.46 |
| perfluorodecane sulfonate | PFDS | <MDL | |

SD – Standard deviation

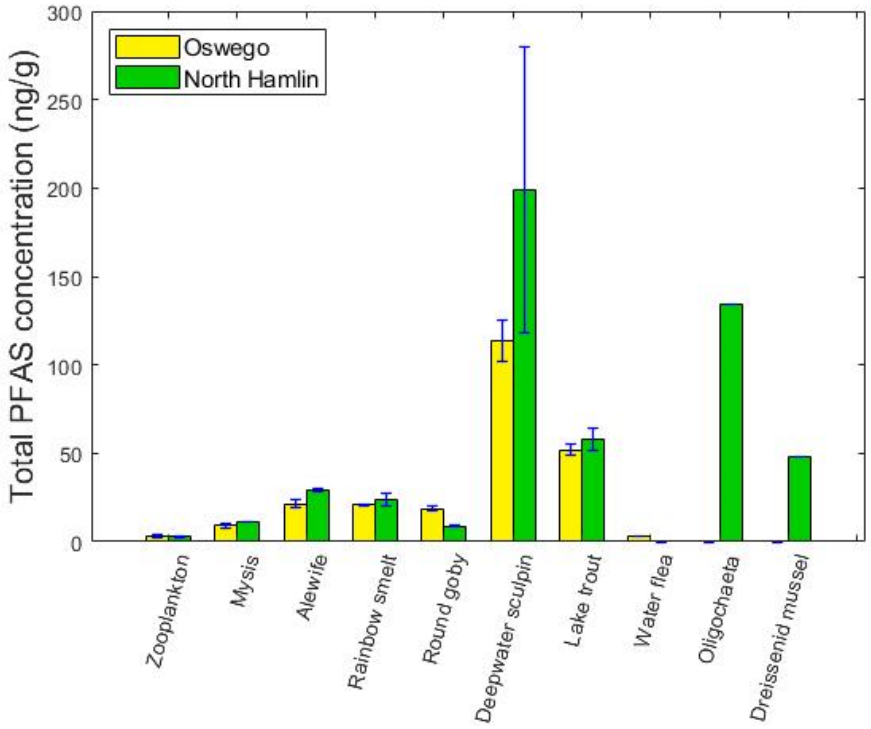


**Figure 3.** Total PFAS concentrations observed in biological media in Lake Ontario. Total PFAS is defined as the sum of the individual values for the analytes listed in Table 2

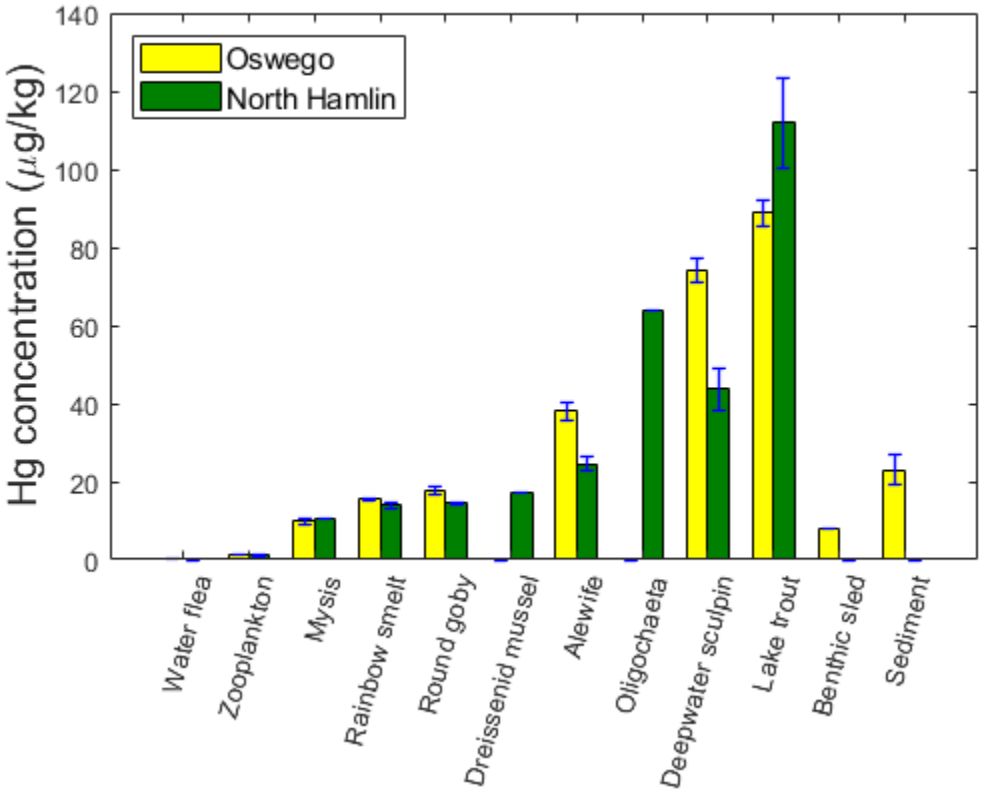


**Figure 4.** Hg concentrations observed in fish collected at the Oswego and North Hamlin Site in Lake Ontario.

## *References*


Boulanger, Bryan, John Vargo, Jerald L. Schnoor, and Keri C. Hornbuckle. 2004. 'Detection of Perfluorooctane Surfactants in Great Lakes Water', *Environmental Science & Technology*, 38: 4064-70.

Folch, J., M. Lees, and G.H.S. Stanley. 1957. 'A simple method for the isolation and purification of total lipids from animal tissues', *Journal of Biological Chemistry*, 226: 497-509.

Gewurtz, Sarah B., Lisa E. Bradley, Sean Backus, Alice Dove, Daryl McGoldrick, Hayley Hung, and Helena Dryfhout-Clark. 2019. 'Perfluoroalkyl Acids in Great Lakes Precipitation and Surface Water (2006–2018) Indicate Response to Phase-outs, Regulatory Action, and Variability in Fate and Transport Processes', *Environmental Science & Technology*, 53: 8543-52.

Happel, Austin, Robert Pattridge, Maureen Walsh, and Jacques Rinchard. 2017. 'Assessing diet compositions of Lake Ontario predators using fatty acid profiles of prey fishes', *Journal of Great Lakes Research*, 43: 838-45.

Happel, Austin, Craig P. Stafford, Jacques Rinchard, and Sergiusz Czesny. 2020. 'Fatty acid profiles of lake trout reveal the importance of lipid content for interpreting trophic relationships within and across lakes', *Journal of Great Lakes Research*, 46: 188-97.

Hebert, Craig E., Michael T. Arts, and D. V. Chip Weseloh. 2006. 'Ecological Tracers Can Quantify Food Web Structure and Change', *Environmental Science & Technology*, 40: 5618-23.

Kidd, K., D. Schindler, R. Hesslein, and D. Muir. 1995. 'Correlation between stable nitrogen isotope ratios and concentrations of organochlorines in biota from a freshwater food web', *The Science of the total environment*, 160-161: 381-90.

Martin, Jonathan W., D. Michael Whittle, Derek C. G. Muir, and Scott A. Mabury. 2004. 'Perfluoroalkyl Contaminants in a Food Web from Lake Ontario', *Environmental Science & Technology*, 38: 5379-85.

Point, Adam D., Thomas M. Holsen, Sujan Fernando, Philip K. Hopke, and Bernard S. Crimmins. 2019. 'Towards the development of a standardized method for extraction and analysis of PFAS in biological tissues', *Environmental Science: Water Research & Technology*, 5: 1876-86.

Sierszen, Michael E., Janet R. Keough, and Cynthia A. Hagley. 1996. 'Trophic Analysis of Ruffe (Gymnocephalus cernuus) and White Perch (Morone americana) in a Lake Superior Coastal Food Web, Using Stable Isotope Techniques', *Journal of Great Lakes Research*, 22: 436-43.

Zananski, Tiffany J., Thomas M. Holsen, Philip K. Hopke, and Bernard S. Crimmins. 2011. 'Mercury temporal trends in top predator fish of the Laurentian Great Lakes', *Ecotoxicology*, 20: 1568-76.

Zanden, M. Jake Vander, and Joseph B. Rasmussen. 2001. 'Variation in δ15N and δ13C trophic fractionation: Implications for aquatic food web studies', *Limnology and Oceanography*, 46: 2061-66.

Zhou, Chuanlong, Mark D. Cohen, Bernard A. Crimmins, Hao Zhou, Timothy A. Johnson, Philip K. Hopke, and Thomas M. Holsen. 2017. 'Mercury Temporal Trends in Top Predator Fish of the Laurentian Great Lakes from 2004 to 2015: Are Concentrations Still Decreasing?', *Environmental Science & Technology*, 51: 7386-94.

Zhou, Chuanlong, James Pagano, Bernard S. Crimmins, Philip K. Hopke, Michael S. Milligan, Elizabeth W. Murphy, and Thomas M. Holsen. 2018. 'Polychlorinated biphenyls and organochlorine pesticides concentration patterns and trends in top predator fish of Laurentian Great Lakes from 1999 to 2014', *Journal of Great Lakes Research*, 44: 716-24.

Zhou, Chuanlong, James Pagano, Daryl J. McGoldrick, Da Chen, Bernard S. Crimmins, Philip K. Hopke, Michael S. Milligan, Elizabeth W. Murphy, and Thomas M. Holsen. 2019. 'Legacy Polybrominated Diphenyl Ethers (PBDEs) Trends in Top Predator Fish of the Laurentian Great Lakes (GL) from 1979 to 2016: Will Concentrations Continue to Decrease?', *Environmental Science & Technology*, 53: 6650-59.

# Zooplankton Sampling Efforts in CSMI Lake Ontario 2018

Jim Watkins and Lars Rudstam, Cornell University

## Collaborators

A team from Cornell University led by Jim Watkins and Lars Rudstam collected and analyzed zooplankton and mysid samples collected on the R/V Lake Guardian with the support of US EPA Great Lakes Program Office and CESU/USGS from lakewide surveys in April, June, August, and September. Canada Department of Fisheries and Oceans (Warren Currie and Kelly Bowen) provided samples from a Canadian lakewide sampling effort in July and from the far western transect for all seasons. US EPA MED from Duluth also collected samples and LOPC transects in July. The Biomonitoring Program collected net samples in the nearshore and offshore on a monthly basis on the south shore.

## Relevance

Zooplankton and mysid shrimp represent a key link between primary production and fish. They are a key diet for planktivorous fish such as Alewife and coregonids as well as for larval fish for a range of species. Thus, they support important salmonids. Over recent decades zooplankton biomass has steadily decreased in response to lower nutrients. Vertical redistribution and community shifts are also key observations seen in the upper Great Lakes. Invasive species have a major impact, particularly the large predatory cladocerans spiny waterflea (*Bythotrephes*) and fishhook waterflea (*Cercopagis*) that are commonly seen in late summer. Dreissenid mussels release small but abundant veliger larvae. Large mysids migrate from the lake bottom to the metalimnion at night and represent an important component of the zooplankton community that both supports and competes with planktivorous fish.

## Objectives

- Build on the long term (since 1997) time series of offshore zooplankton biomass with an emphasis in the CSMI year of expanding spatial and seasonal coverage. This consists of standard whole water column (to 100 m) net sampling with 153 micron mesh nets.

- Use finer mesh nets (64 micron) in the epilimnion (0-20 m) to track microzooplanton such as rotifers, copepod nauplii, and dreissenid veligers. These small organisms are poorly sampled by larger mesh nets but can be important.

  Use closing nets (also 64 micron) to sample discrete strata such as the metalimnion and hypolimnion in the day and night to describe vertical distribution and diel vertical migration.

Use whole water column large mesh mysid nets to expand monitoring of the abundance, cohort growth, and life history parameters of mysid shrimp. As with the offshore zooplankton series the CSMI year significantly expands the seasonal coverage.

Use advanced technologies (Laser Optical Plankton Counter) undulating along two offshore 10 km transects from 0-60 m in several seasons to track fine scale vertical distribution of different size groups of zooplankton and their diel vertical migration.

Use consistent counting and measurement methods, taxonomic specificity of species list, and length-dry weight conversions in compilation of net tow data.

Make zooplankton data easily available in a comprehensive relational database that includes water column profiles and water chemistry.

Compare and contrast offshore zooplankton data with long term nearshore (10 m depth) zooplankton data to better understand nearshore-offshore gradients.

## Preliminary Results

### *Zooplankton Biomass and Composition*

The status of offshore zooplankton in Lake Ontario is "good" relative to that of Lake Huron that experienced a food web collapse in 2004. (Figure 1, SOGL 2019). Biomass in Lake Ontario did decline from 1997 to 2019 with a shift in the community away from cladocerans and cyclopoid copepods in favor of calanoid copepods, a trend also seen in the upper Great Lakes. However, total zooplankton biomass is still sufficient to support preyfish populations at this time.

CSMI 2018 sample coverage was extensive both spatially and temporally due to the large collaborative effort (Figure 2). This comprehensive data series track the seasonal development of zooplankton biomass to fill the typical sampling gap between annual April and August GLNPO sampling (Figure 3). These patterns closely follow the timing of surface water warming and stratification (Figure 4). The seasonal coverage confirms the importance of August sampling as the "biomass peak", but also indicates that features are missed by this narrow window of time including cladoceran development and predatory cladoceran dynamics.

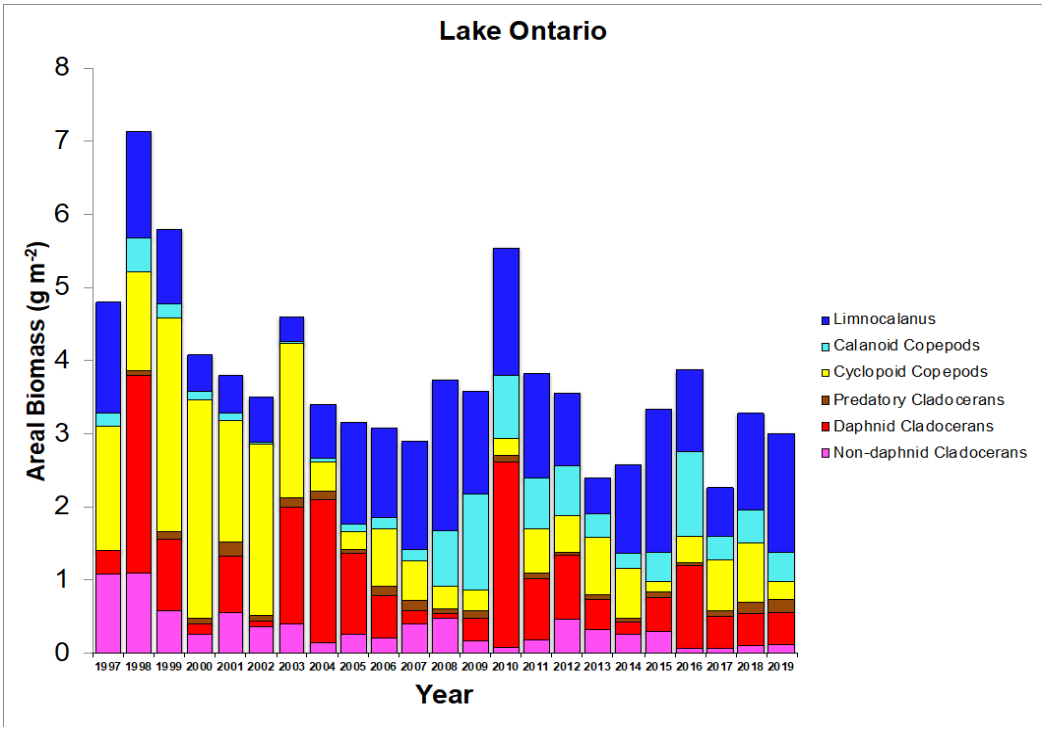


Figure 1. Long term areal biomass (g m-2) for deep tow summer zooplankton from GLNPO time series. Zooplankton groups identified by color in legend.

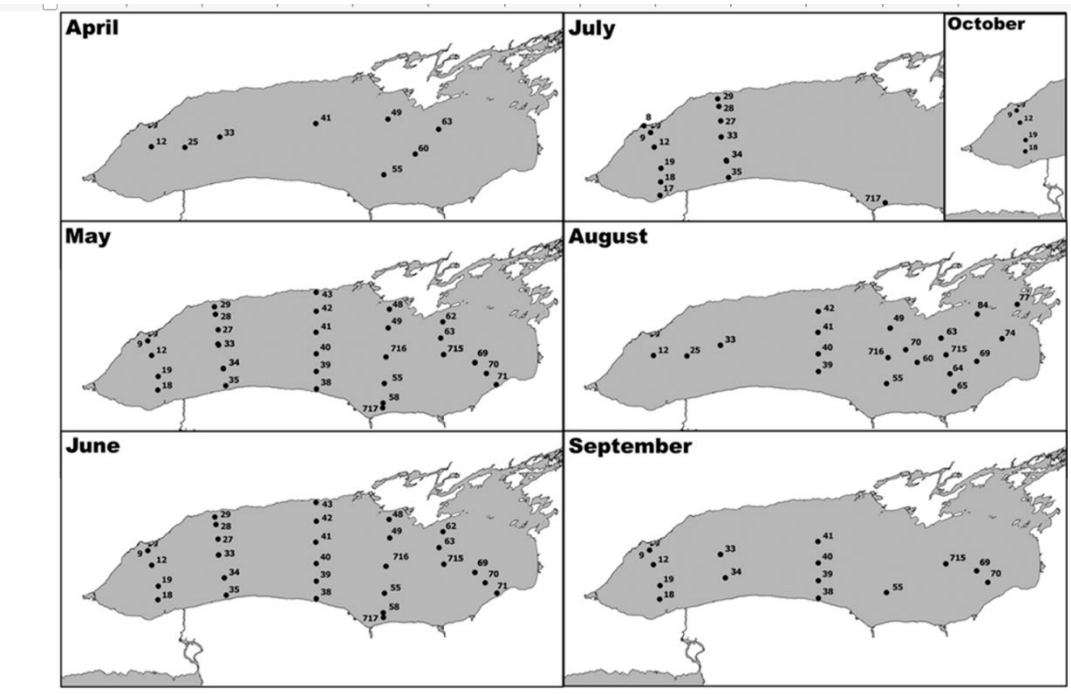


Figure 2. Zooplankton samples collected in Lake Ontario during each month in 2018.

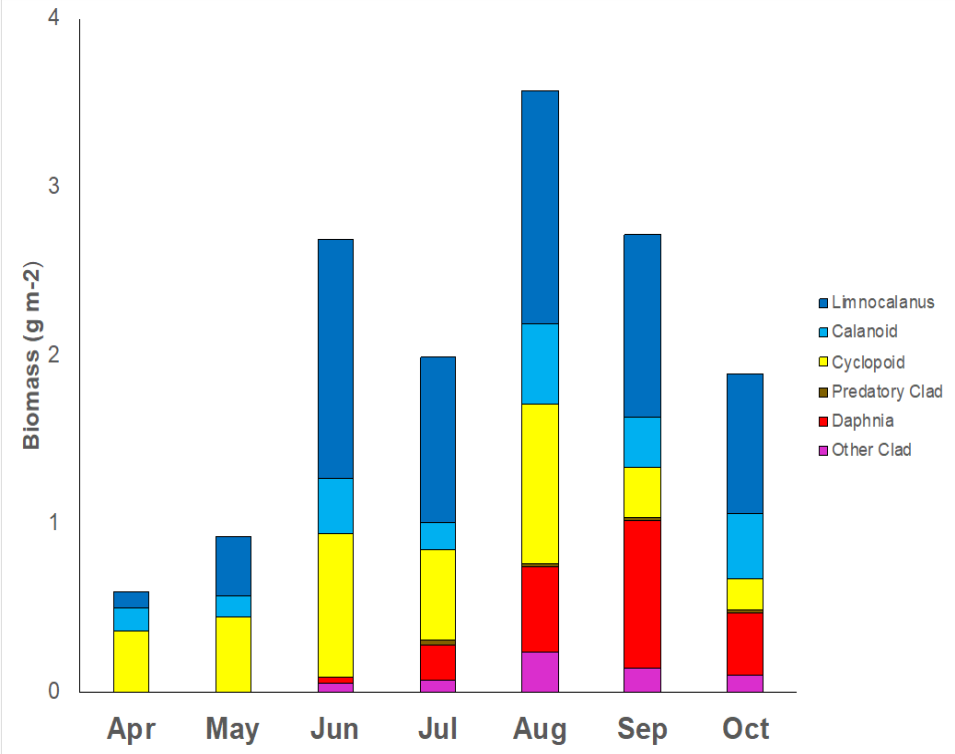


Figure 3. Seasonal progression of areal biomass for deep tow samples for Lake Ontario in 2018. Note that April and August are GLNPO surveys.

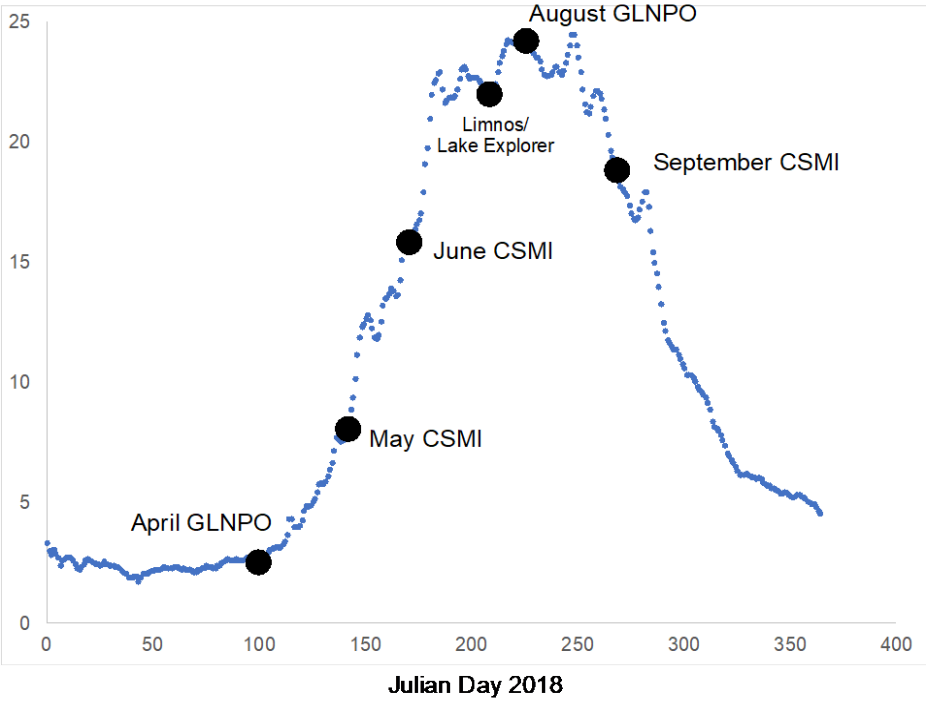


Figure 4. Seasonal progression of GLSEA surface water temperature and timing of seasonal surveys.

## Invasive species

As previously mentioned, *Bythotrephes* and *Cercopagis* each have a unique seasonal development that is often missed by midsummer surveys. They are relatively large zooplankton that are predators of smaller zooplankton as well as preferred prey for fish. The seasonal coverage of CSMI sampling pinpointed a peak abundance of *Cercopagis* in July and *Bythotrephes* in September 2018 that was also identified by the Biomonitoring program. The timing in the release of dreissenid veliger larvae was also identified with this seasonal coverage, with a particularly high epilimnetic density of veligers in October in the western end of the lake. Two nonnative microcrustacean species new to Lake Ontario were detected in 2018 - the benthic harpacticoid copepod species *Schizopera borutzkyi* and *Heteropsyllus nunni*. These two species have been found elsewhere in the Great Lakes and *S. borutzkyi* and other harpactacoids have been found in ballast tanks (Duggan et al. 2005), but neither previously recorded from Lake Ontario (Connolly in prep).

## Fine mesh Sampling

Analysis of the microzooplankton rotifer community throughout the year was a new addition in 2018. This clearly tracked seasonal succession of rotifer taxa, as well as their density and biomass relative to larger zooplankton (Figure 5 and 6, Marshall, in prep). Microzooplankton abundance decreased sharply with depth, so most were within the top 20 m. As mentioned earlier, seasonal dynamics of veligers were also tracked.

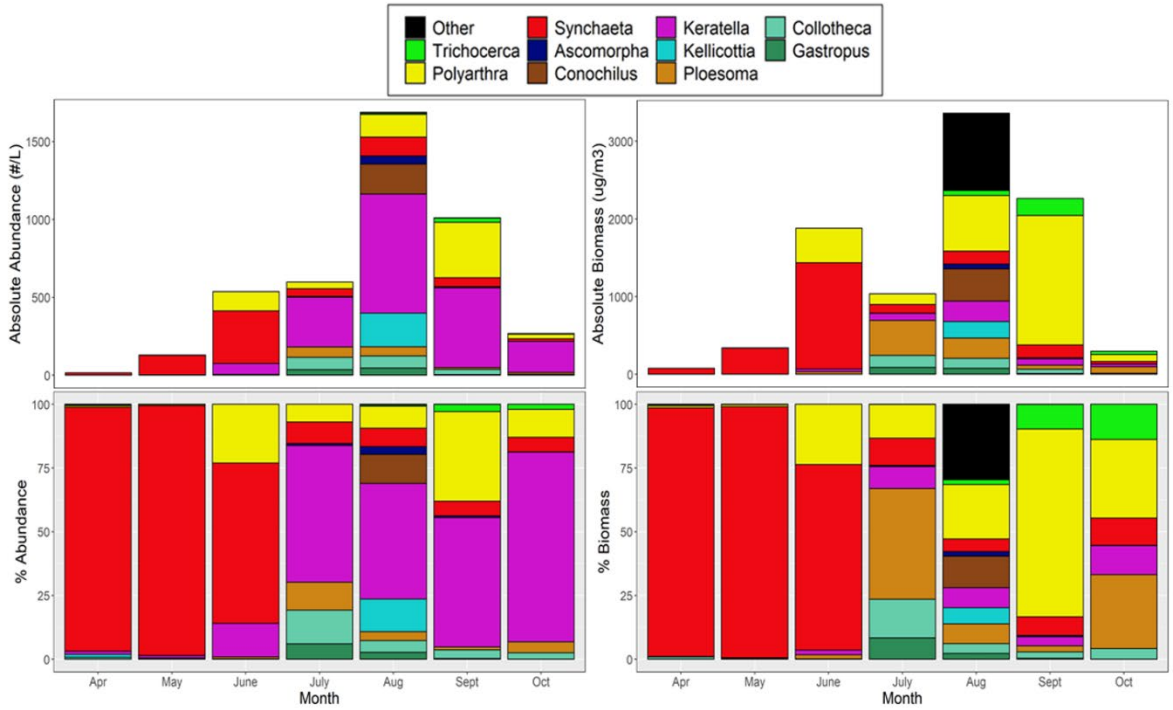


Figure 5. Upper Panel: Stacked bar graphs representing average epilimnion abundance (#/L) and average epilimnion biomass (ug/m3) for common rotifer genera per month. Lower Panel:

Corresponding % abundance and % biomass for each rotifer genera in a given month. (Marshall et al. in prep)

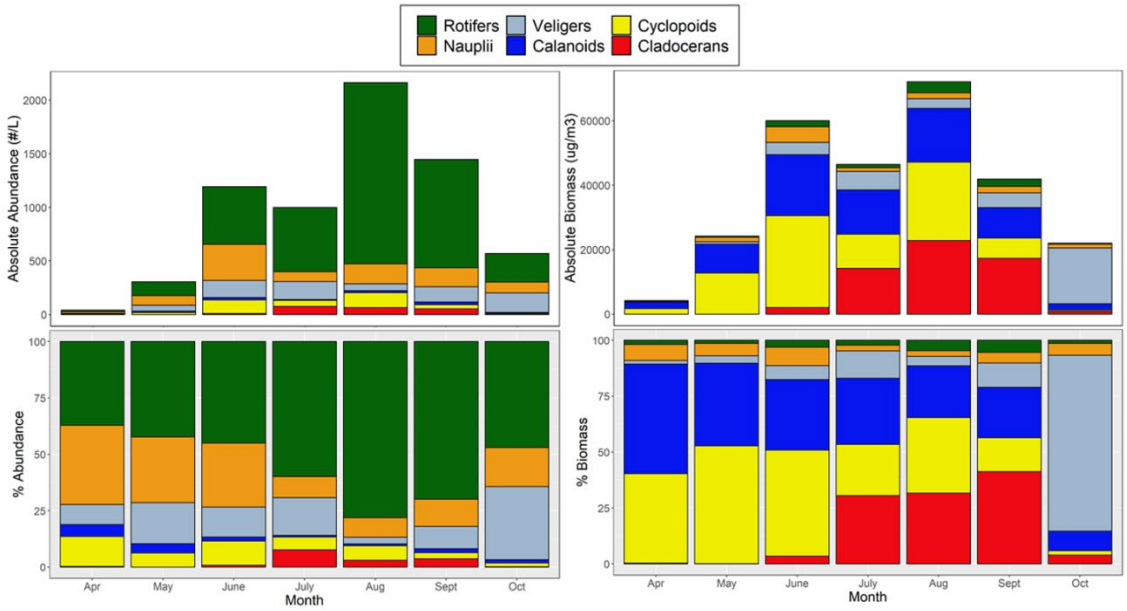


Figure 6. Upper Panel: Stacked bar graphs representing average epilimnion abundance (#/L) and average epilimnion biomass (ug/M3) for both micro (rotifers, nauplii, veligers) and macro (calanoids, cyclopoids, cladocerans) crustaceans for each month. Lower Panel: Corresponding % abundance and % biomass for each taxa in a given month. Marshall et al. in prep.

## Mysids

Mysids were collected at 13 offshore sites from April-September, 2018, adding to and incorporated with the April and August monitoring by GLNPO (Chapina et al. in prep). The two mysid cohorts (age 0 and age 1) were tracked using length distributions over the year (Figure 7). Overall density was calculated at 264 m-2 and biomass 540 mg m-2. Growth rates were estimated at 0.028 mm/day. Over the past decade mysid density in Lake Ontario has been stable and high relative to other Great Lakes, particularly compared to Lakes Huron and Michigan (Holda et al. in prep)

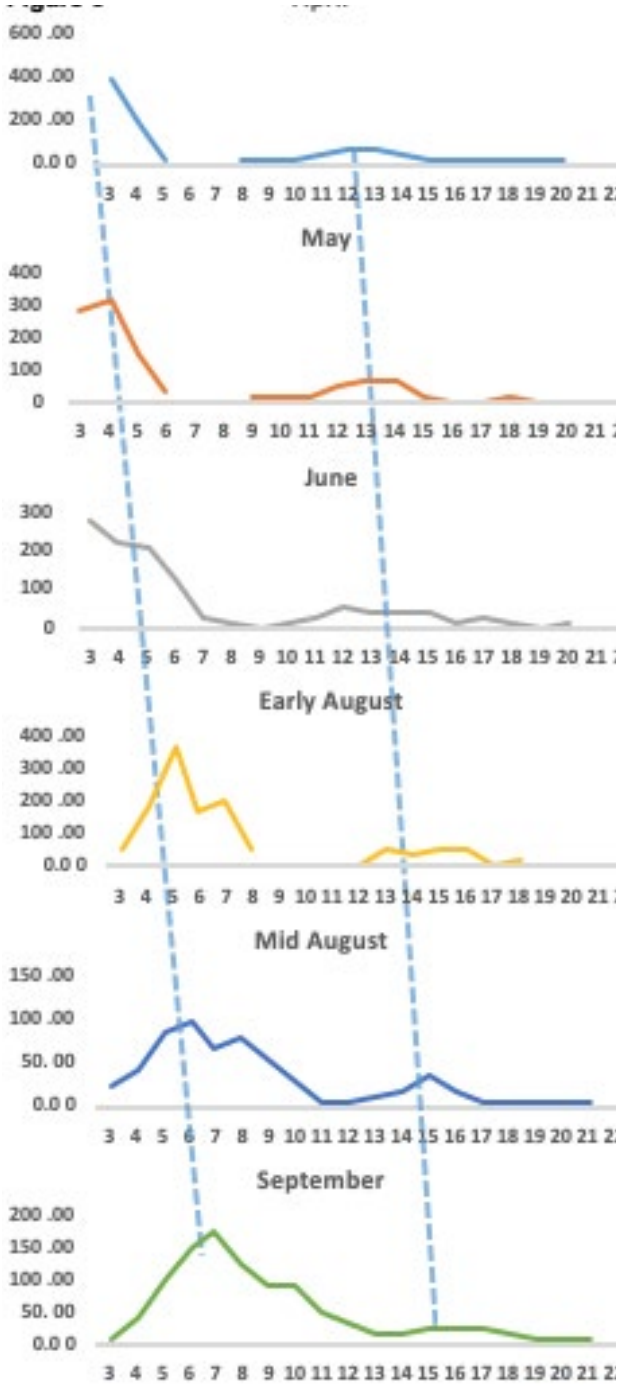


Figure 7. Cohort development of age 0 and age 1 mysids during 2018 in Lake Ontario. The x-axis is length in mm of individual mysids.(Boynton, poster presentation IAGLR 2019)

## New technologies

Successful deployment of the LOPC mounted with other sensors on the Triaxus vehicle was completed in May, June, July, and September 2018. These were run offshore on transect 2 (west) and 5 (east) often for both day and night. June and July sampling confirms close correspondence of zooplankton biomass with the deep chlorophyll layer, and upward migration of zooplankton from the day to night. Deep zooplankton biomass maxima were often observed within the metalimnion (Figure 8, Watkins et al. in prep). Larger zooplankton generally had a deeper distribution than smaller zooplankton restricted to the surface mixed layer.

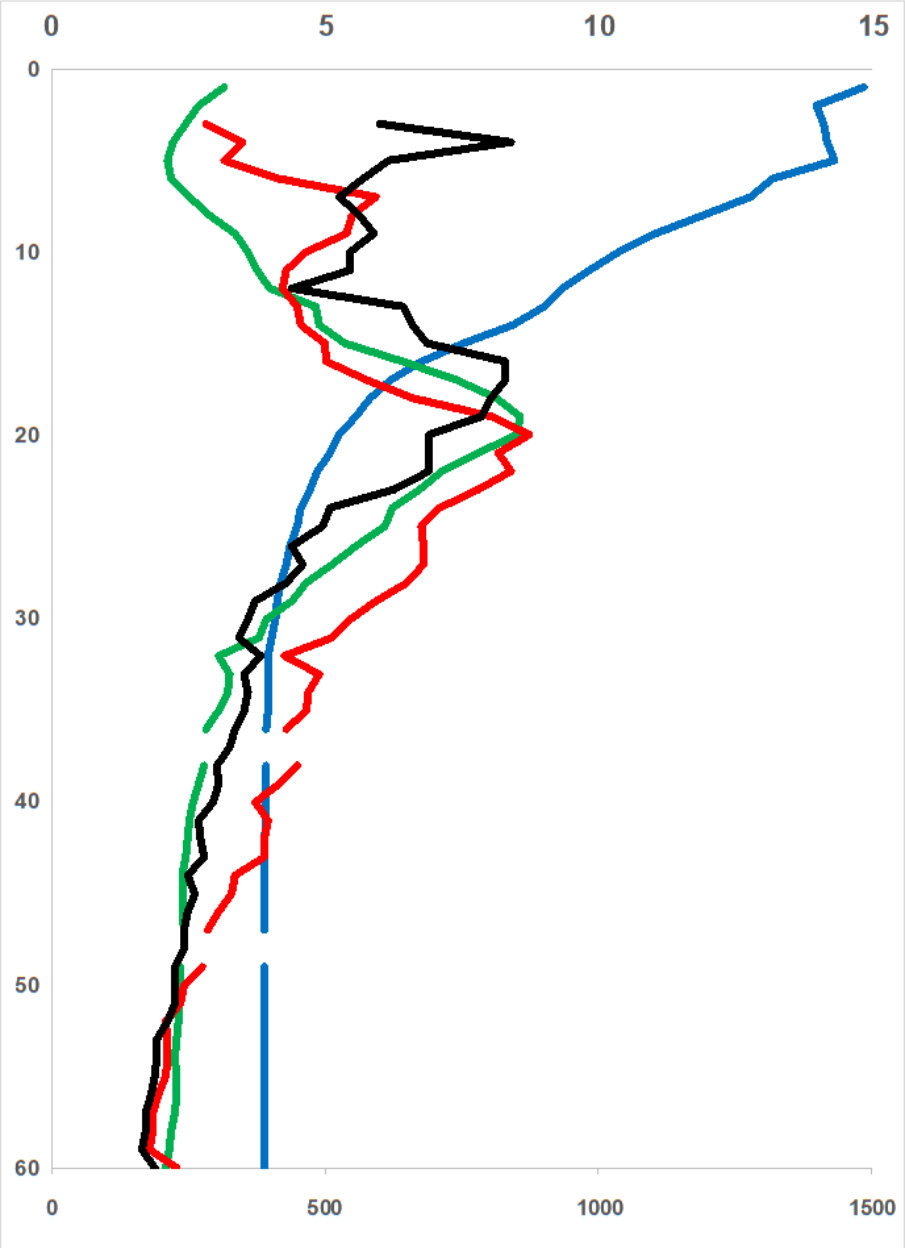

Figure 8. Composite vertical profile of temperature (blue, top axis), chlorophyll (green, top axis) and LOPC determined zooplankton biomass (wet biomass ug/m3, bottom axis) during the day (red) and night (black). Note close correspondence of zooplankton peak to deep chlorophyll layer within the metalimnion at 20 m and evidence of upward migration. Data presented at 1 m resolution. This is a compilation of 13 undulations during the day and 15 undulations during the night. Watkins et al. (in prep)

## Database

A key advance for 2018 was the development of a comprehensive relational Access database developed by EPA Region 2 Cayla Sullivan and Dan Gurdak. This will be the model for future CSMI efforts for all five Great Lakes. This database includes all water column profiles and water chemistry measurements. It also includes phytoplankton, zooplankton, and mysid data. These components are all linked by an event table. Previous efforts are based on only a single component. Annual monitoring data for 2018 by GLNPO and Biomonitoring were also included with CSMI efforts.

## Nearshore/Offshore Dynamics

Cornell Graduate student Stephanie Figary is comparing the zooplankton data from the nearshore Biomonitoring program to the offshore EPA GLNPO program. Her approach is to start with stations that overlap between the programs, towards combining data from these efforts. The foundation of the Biomonitoring program are biweekly collections at 8 nearshore (10 m depth) stations, supplemented by long term offshore stations, some of which overlap with the 8 routine GLNPO stations. CSMI efforts in 2013 and 2018 provide additional spatial and temporal coverage that contribute to this effort.

# Classification of *Typha*-dominated wetlands using airborne hyperspectral imagery along Lake Ontario, USA.

**Glenn M. Suir[a*], Douglas A. Wilcox[b], and Molly Reif[a]**
**[a] U.S. Army Engineer Research and Development Center, Environmental Laboratory, Geospatial Data Analysis Facility, ATTN: CEERD-EE-C, 3909 Halls Ferry Road, Vicksburg, MS 39180-6199, USA**

**[b] Department of Environmental Science and Ecology, SUNY Brockport, 350 New Campus Drive, Brockport, New York 14420**

**Corresponding Author: Email: Glenn.M.Suir@usace.army.mil**
**Phone: 225-368-5749**
**Fax: 225-578-7157**
**https://orcid.org/0000-0002-6080-3644**

Date of the manuscript draft: February, 2021
Manuscript word count (including text and captions): 6,308

*Abstract*

Shoreline wetlands along Lake Ontario are valuable, multi-functional resources that have historically provided large numbers of important ecosystem goods and services. However, alterations to the lake's natural hydrologic regime have impacted traditional meadow marsh in the wetlands, resulting in competition and colonization by dense and aggressive *Typha angustifolia* and *Typha* x *glauca* (cattails). The shift to a *Typha*-dominated landscape resulted in an array of negative impacts, including increased *Typha* density, substantial decreases in plant species richness and diversity, and altered habitat and changes in associated ecosystem services. Successful long-term adaptive management of these wetland resources requires timely and accurate monitoring. Historically, wetland landscapes have been surveyed and mapped using field-based surveys and/or photointerpretation. However, given their resource- and cost-intensive nature, these methods are often prohibitively time- and labor-consuming or geographically limited. Other remote sensing applications can provide more rapid and efficient assessments when evaluating wetland change trajectories or analyzing direct and indirect impacts across larger spatial and temporal scales. The primary goal of this study was to develop and describe methodology using U.S. Army Corps of Engineers National Coastal Mapping Program hyperspectral imagery, light detection and ranging data, and high-spatial resolution true-color imagery to provide updated wetland classifications for Lake Ontario coastal wetlands. This study used existing field-collected vegetation survey data (Great Lakes Coastal Wetland Management Program), ancillary imagery, and existing classification information as training data for a supervised classification approach. These data were used along with a generalized wetland schema (classes based on physical and biological gradients: elevation, *Typha*, meadow marsh, mixed emergent, upland vegetation) to generate wetland classification data with Kappa values near 0.85. Ultimately, these data and methods provide helpful knowledge elements that will allow for more efficient inventorying and monitoring of Great Lake resources, forecasting of resource condition and stability, and adaptive management strategies.

*Keywords:* Wetland Classification; *Typha*; Hyperspectral Imagery; Maximum Likelihood Classifier; Wetland Monitoring; Lake Ontario

## Introduction

Wetland plants provide habitat and food for wildlife and aquatic organisms, increase sedimentation rate and shoreline stability, and regulate water quality through the assimilation of nutrients (Brix and Schierup, 1989; Poirrier et al., 2010). While indigenous plant species typically provide these and other biological, chemical, and physical benefits, non-native plant species can cause severe ecological and economic damage (Office of Technology Assessment, 1993; Environmental Protection Agency 2008; Smart et al., 2009).

The shoreline wetlands of Lake Ontario are valuable, multi-functional resources that provide unique biological diversity and serve as habitat for numerous wildlife and fish (Wilcox et al., 2005). However, these wetlands, which require seasonal water-level fluctuations to maintain ecological function and stability and retain an early successional stage, have been impacted by management of lake level (Wilcox et al., 2005; Wilcox et al., 2008; Howard et al., 2016) contributing to an invasion by non-native plants. Water-level regulation, which began in the early 1960s under Plan 1958DD, compressed the natural hydrologic range (reducing high water levels and increasing low water levels), resulting in competition and colonization by dense and aggressive *Typha angustifolia* and *Typha* x *glauca* (cattails) into traditional meadow marsh (Wilcox et al., 2008; Wilcox and Bateman, 2018). Wilcox et al. (2005) estimated that *Typha* displaced more than 50% of the total Lake Ontario meadow marsh wetland area, and for some wetlands, more than 80% reductions have occurred since the 1960s. This shift to a *Typha*-dominated landscape resulted in an array of negative impacts, including increased *Typha* density and litter mass (Vaccaro et al., 2009), substantial decreases in plant species richness and diversity, increases in soil organic matter and organic matter depth, and altered habitat and changes in associated ecosystem services (Mitchell et al., 2011). This loss in habitat heterogeneity and diversity, and the increasing dominance of *Typha*, has and will continue to be, magnified by cumulative natural and human stresses (Mortsch, 1998; Wilcox et al., 2005).

Generally, wetlands have long been managed for environmental protection, recreation and aesthetics, and production of renewable resources (Mitsch and Gosselink, 2000). Successful, long-term adaptive management of wetland resources requires timely and accurate monitoring (Robles et al., 2006). Historically, wetland landscapes have been surveyed and mapped with field-based reconnaissance and/or photointerpretation (Kowalski and Wilcox, 1999; Wilcox et al., 2008; Wilcox and Bateman, 2018). However, given their resource- and cost-intensive nature, these methods can be prohibitively time-consuming and inefficient (Vis et al., 2003). These limitations may be overcome with the use of other remote sensing data and techniques, which provide spatial, spectral, and temporal perspectives on ecological phenomena that would otherwise be difficult to study (Anderson and Gaston, 2013). Remote sensing data from air- and space-borne sensors that are more rapidly and efficiently collected can be used to classify, map, and analyze changes across larger geographic areas (Jakubauskas et al., 2002; Robles et al., 2010). Previous studies have demonstrated that such remote sensing can be an effective tool for mapping wetland species locations, densities, and impacts from natural and anthropogenic drivers and can provide critical knowledge for more efficient inventorying and monitoring of wetland resources (Jensen et al., 1992; Jakubauskas et al., 2002; Robles et al., 2006; Allen and Suir, 2014; Suir et al., 2018). These tools and techniques can ultimately provide capabilities for assessing significant biophysical and ecological parameters, monitoring the short- and long-term effectiveness of management activities, and predicting location and severity of future invasive wetland plant infestations (Thiago et al., 2008; Bourgeau-Chavez et al., 2009; DigitalGlobe, 2010; Allen and Suir, 2014; Bourgeau-Chavez et al., 2015).

The primary goal of this study was to develop and describe the use of hyperspectral imagery (HSI), light detection and ranging (lidar) data, and high-spatial resolution true-color (RGB) imagery to provide updated wetland classifications for Lake Ontario coastal wetlands and establish methods for future use of these tools. This study used existing field-collected vegetation survey data, ancillary imagery, and existing classification information as training data for a supervised classification algorithm. The study objectives were to 1) demonstrate the utility of airborne HSI for the classification and monitoring of

*Typha* extent and encroachment into other wetland zones and 2) provide a more efficient method for updating previously measured wetland extent and community dynamics along Lake Ontario.

## Study sites

The study area consists of 25 *Typha* spp. (cattail) dominated wetlands that are located along the southern and eastern shoreline of Lake Ontario and along the southern banks of the upper St. Lawrence River. The sites stretch from Brush Creek (77.8°W, 43.34°N; located northwest of Rochester, New York) in the west to Crooked Creek (75.8°W, 44.4°N; located west of Schermerhorn Landing, New York) in the east (Figure 1). These sites are high priority for the International Joint Commission's (IJC) Great Lakes – St. Lawrence River Adaptive Management (GLAM) Committee, and have been used for previous lake level elevation studies (16 sites as part of the Lake Ontario-St. Lawrence River (LOSLR) 2003 study; 16 sites as part of the Great Lakes Restoration Initiative (GLRI) 2012-2014 study; combined accounting for all 25 sites).

Of the study sites, six are classified as barrier beach lagoons, six as drowned-river-mouth wetlands, seven as open embayments, and six as protected embayments (**Appendix Table A1**) (Ingram et al., 2004; Albert et al., 2005; Wilcox et al., 2008; Wilcox and Bateman, 2018). Fifteen were part of an array of Lake Ontario wetlands that have been extensively evaluated through traditional wetland measures, photointerpretation, and general wetland classification assessments (spanning assessment periods from 1954 to 2015; Wilcox et al., 2005, 2008; Wilcox and Xie, 2007, 2008; Wilcox and Bateman, 2018), thus providing longer term data for evaluation of our results.

## Methods

### *Air-borne collection*

#### *CZMIL system*

HSI, lidar, and true-color imagery were collected by the Joint Airborne Lidar Bathymetry Technical Center of Expertise (JALBTCX) in September 2018 using the Coastal Zone Mapping and Imaging Lidar (CZMIL) system for 25 Lake Ontario wetland sites. The CZMIL is a sensor- and data-fusion-based system, comprising a low-altitude airborne lidar sensor (400 m flying height) that is tightly integrated with a spectrographic imager and a true-color digital frame camera (Wozencraft and Lillycrop, 2006). Low-altitude (400 m) data collection is standard for CZMIL; however, imagery-specific collection at high altitude (2000 m) is possible within a time-frame when illumination imbalances occur at low-altitude. The CZMIL system collects concurrent data that are routinely used for physical and environmental characterization of beaches, wetlands, marshes, estuaries, and barrier islands (Reif et al., 2013).

#### *Hyperspectral imagery*

Hyperspectral sensors, which typically collect imagery in hundreds of narrow and contiguous spectral bands along the electromagnetic spectrum, are often used in remote sensing to measure the spectral reflectance of objects on the Earth's surface (Reif et al., 2011). The primary advantage that HSI data have over more common coarse spectral resolution sensors is the narrowness of HSI spectral bands (Lillesand et al., 2008). The JALBTCX CZMIL system uses the programmable Itres Compact Airborne Spectrographic Imager (CASI)-1500, which is a pushbroom hyperspectral sensor featuring up to 288 bands (375 to 1050 nanometer [nm]) at 1.9 nm intervals and a nominal nadir orientation with a total field of view of approximately 40 degrees (Reif et al., 2011). For the Lake Ontario collection, the programmable CASI sensor was configured to measure 48 spectral bands in the 380- to 1050-nm spectral range (visible to near-infrared portion of the electromagnetic spectrum) (Figure 2A). The CZMIL system uses Teledyne's HydroFusion software suite to perform radiometric calibration processing, which includes conversion of DN to at-sensor radiance, glint/ripple correction to smooth water surface effects due to glint and wind driven ripples, and atmospheric corrections to surface radiance to provide surface

reflectance prior to mosaicking into 1-meter spatial resolution imagery (Schowengerdt, 2007; Park and Tuell, 2010; Reif et al., 2013).

### *Lidar and true-color imagery*

Topographic/bathymetric data were collected using lidar - a remote-sensing technology that actively emits light pulses and uses the time of flight between the sensor and target to measure the elevation of the ground and surface features (Lefsky et al., 2002; Reif et al., 2011, 2013). The CZMIL system employs a 10-kHz bathymetric full waveform lidar (green laser in the 532 nanometer wavelength) with a segmented detector that increases measurement rate to 70 kHz on land and in optically shallow water (i.e., where the water-leaving reflectance signal is primarily from the seafloor; Fuchs and Tuell, 2010). This system, which has a fixed incidence angle of about 20 degrees, is able to achieve simultaneous topographic and bathymetric (topo/bathy) operations through waveform processing (Reif et al., 2013). The lidar data were collected at the standard 400-m altitude. However, illumination imbalances occurred early in the data-collection window; therefore, the HSI and true-color imagery were collected at a 2,000-m altitude. This higher altitude allowed for extended coverage in fewer flight lines, maximizing time in the air, and providing more consistent illumination conditions. With a 10,000 pulse-per-second laser, the lidar sensor collected data with shot spacing of 0.7 m (topographic) to 2 m (bathymetric) and a vertical root mean square (RMS) error of 15 cm for bathymetric data and 10 cm for topographic data. Seamless topo/bathy geo-referenced high-resolution images (1 meter spot spacing and approximately 19.5-cm elevation accuracy at 95% confidence level) were produced through CZMIL processing (Wozencraft and Lillycrop, 2006; Park and Tuell, 2010). JALBTCX generated first return elevation data (Figure 2B1), which were used to identify tree and shrub heights and other over-story vegetation and structures. JALBTCX also generated bare earth data (Figure 2B2) by removing over-story vegetation elevations from the last-return data. Bare earth data were used to differentiate dominant vegetation zones and verify wetland classifications. The true-color three band (RGB) collection returned higher spatial resolution imagery (approximately 5 cm and 20 cm ground resolution for 400 and 2000 m altitude collection, respectively), which were used as ancillary data for feature and species identification and verification (Figure 2C).

## *Ground verification data*

In remote sensing, ground verification data refers to the traditional on-site gathering of reference data and information that characterize states, conditions, and parameters associated with the Earth's surface (Short and Robinson, 1999). These ground verification data are critical components of wetland classifications because they are necessary for training supervised classification algorithms, validating classified areas, and performing error evaluations (Jensen, 2015). Most remote sensing classifiers rely on the statistical distributions of the reflectance values of the target classes as defined by the training data provided for each class (Broussard et al., 2018). For this study, the training data consisted of vegetation survey information collected as part of the Great Lakes Coastal Wetland Monitoring Program (CWMP). The CWMP conducts vegetation sampling in Great Lakes coastal wetlands for the purposes of identification of important wetlands for protection or acquisition and characterization of wetlands for restoration and management (Uzarski et al., 2017). CWMP vegetation sampling is conducted along transects for the purpose of identifying physical gradients and corresponding biological gradients or zones (i.e., wet meadow, emergent, and submergent vegetation) (Uzarski et al., 2017). The CWMP uses 1m × 1m quadrats along transects in each zone to identify surface and subsurface plant species and determine percent coverage (Uzarski et al., 2017).

## *Wetland Classification*

Wetland classification refers to the designation and mapping of different wetland types, often on the basis of vegetation type and as a function of elevation, hydrology, and soils (Tiner, 1996). The typical remote sensing wetland classification process consists of three primary steps. These include pre-processing, classification, and post-processing (Schowengerdt, 2007) (**Appendix Figure A).**

### *Pre-processing*

Once remote sensing data have been collected, they must undergo a preparatory pre-processing phase to remove image irregularities prior to processing and analysis. The most common pre-processing steps include radiometric calibration (transformation of digital numbers to physical radiance or reflectance units), atmospheric correction (accounting for atmospheric scattering and absorption), and geometric correction (correcting geometric distortions) (Schott, 2007). CZMIL used Teledyne's HydroFusion software suite and the standard National Research Council's Committee on Data Management and Computation (CODMAC) levels for HSI and lidar data pre- and post-processing and product generation. The true-color imagery processing was performed using PhaseOne's COPE engine and Simactive's Correlator 3D.

### *Classification*

The classification process consists of four primary sub-processes: feature extraction, classification schema, training, and labeling (**Appendix Figure A**). Feature extraction is a technique used to acquire the "essential elements" of an HSI data cube by reducing the very high-dimensional data space to a manageable low-dimensional space in which data analysis can be performed more effectively (Jollineau and Howarth, 2008; Chang, 2013). This feature extraction, or dimensionality reduction (DR) can reduce the number of channels or bands and reduce computational demands. For this study, the Minimum Noise Fraction (MNF) transformation was performed to retain most relevant bands and maximize spectral information available for the analysis. The MNF transformation applies principal component analyses and variance-covariance matrices to denoise and retain coherent HSI data (Jensen, 2015). This process allowed for the selection of effective bands for discriminating classes of interest, thereby increasing the accuracy of the supervised classification (Jollineau and Howarth, 2008; Campbell and Wynne, 2011). In this case, the hyperspectral data were reduced from 48 bands to between 19 and 22 for each of the study sites. Figure 3 provides an example of the MNF-transformed data for the Point Vivian Bay study area, where the first three MNF bands are loaded into the RGB channels.

In vegetation mapping, remotely sensed imagery and classification schemas are typically used to delineate the geographic distribution, extent, and landscape patterns of vegetation types and structural characteristics (Nelson et al., 2015; Verma and Jana, 2019). To establish a meaningful classification schema, a survey of local experts and resource managers was used to identify and evaluate established schemas, as well as target wetland species and classes of interest. Existing schemas (e.g., CWMP, Environment and Climate Change Canada [ECCC], and the Great Lakes Research Center [GLRC]) are based on dominant vegetation zones and their associated plant species and elevation ranges (Wilcox et al., 2005). The classification schema selected for use in this study consists of land-cover types in the urban, upland, and water environments but primarily focuses on wetland zones that range from aquatic vegetation at low elevations, and move to mixed emergent, *Typha* sp, meadow marsh, and upland vegetation, with increasing elevation (**Appendix Table A2).**

The Maximum Likelihood Classifier (MLC) was the classifier selected for use in this study. The MLC is a universally accepted and used classifier for multispectral and hyperspectral imagery due to its ease of implementation and wide availability in popular software packages (Suir, 2018). This parametric classifier uses statistical distributions of target class reflectance values, as defined by the class specific "on the ground" training data (Carle, 2013), to establish decision boundaries that partition the feature space and label each pixel (Schowengerdt, 2007). Training data for this study consisted of the dominant vegetation (>50% cover) at each CWMP site or were generated using the high resolution true-color imagery, other ancillary data (recent classification data), and a "heads-up" digitizing method to create additional training sites. For the MLC, each pixel was assigned to the class with the highest probability (unless "unclassified" thresholds are provided), and all pixels in the image were labelled as one of the

target classes (Carle, 2013). Each of the MNF images from the 25 study wetlands was classified using the MLC and associated training data.

### *Post-processing*

For MLC classifications, the initial output typically generates classification data that are highly pixelated ("salt-and-pepper" appearance) with spurious pixels. Majority filtering, which is a simple and standard process by which pixels are clumped and sieved to increase classification accuracy (Kwang, 1996), was used to remove or reduce non-target classes and spurious pixels from the preliminary classification data. Initially, a Majority filter was used iteratively to remove an interim "shadow" class from the preliminary MLC data. A Majority 3 × 3 kernel filter then removed spurious pixels from non-wetland classes, which typically consisted of structures and long and linear features like roads. Additionally, a Majority 5 × 5 kernel filter removed spurious pixels from the remaining vegetation- and water-based classes. Another important consideration in wetland classification is the Minimum Mapping Unit (MMU). An MMU, which is defined as "the smallest size areal entity to be mapped as a discrete area" (Lillesand et al. 2008), is typically operationally defined, based on application needs, and is not necessarily related to the sensors utilized for the classification (Bourgeau-Chavez et al., 2015; Draksler et al., 2017). Given the high spatial resolution of the CZMIL data, the size of features of interest, and the desire to compare the classification data to previous photo-interpreted data, the MMU for this project was set to 4 $m^2$. Lidar data and the higher resolution true-color imagery were used to verify the precision of the filtered classification results, and misclassified features were reclassified based on elevation gradients and image attributes (i.e., size, shape, tone, texture, and pattern). The Edit Classification Image tool in ENVI v5.5 (L3Harris Geospatial, Boulder, Colorado) was used, in conjunction with ancillary data (i.e., lidar and the true-color imagery), to verify (qualitatively) and edit misclassified pixels in the classified and filtered images. A quantitative classification accuracy was performed using validation sites and traditional error matrix methods (Jollineau and Howarth, 2008).

### *Wetland area change*

Finally, the total area (hectares) and percentage of total area were calculated for each primary wetland community type and used to update and compare to existing data from Lake Ontario wetlands (data prior to 2015 are from Wilcox et al. (2008) and Wilcox and Bateman (2018)). However, some of the CZMIL data collection did not provide complete coverage across the previously established study sites (Wilcox et al., 2008; Wilcox and Bateman, 2018). In most cases, the areas were similar, but our 2018 collection omitted a small section at the perimeter of a site. Therefore, to make comparisons to the existing photointerpretation-based data, the area of target wetland vegetation types (floating/aquatic vegetation, meadow marsh, mixed emergent, and *Typha*) are provided as percentages of the total area from the associated study site.

## Results and Discussion

### *Maximum likelihood classification*

The MLC process used HSI and ancillary data from 2018 to produce 25 wetland and land-cover maps. This classification schema focused on target wetland zones (i.e., aquatic plants, meadow marsh, mixed emergent, and *Typha*) but also included upland vegetation, shrub, forested areas, agriculture, water, and other developed or managed cover types. Figure 4 provides an example of the final classification data from a portion of the Point Vivian Bay wetland study area, where wetland and land-cover classes are color-coded based on the classification schema. This area consists largely of *Typha* vegetation, with interspersed areas of water/aquatic plant and regions of mixed emergent, as well as a larger area of meadow marsh to the northwest. Classification maps for all study sites are provided in **Appendix Figure B.**

## *Accuracy assessment*

The average Overall Accuracy (OA) and Kappa values for final classifications across all study sites were 88.68 and 0.85, respectively. The OA ranged from a low of 72.95 at The Isthmus site, to 98.67 at the Port Bay site. The Kappa values, which are provided in Tables 3 to 6, ranged from a low of 0.614 at the Black River Bay – South Muskellunge site, to a high of 0.983 at the Port Bay site. A majority (20 of 25) of classifications returned Kappa values within the range of 0.75 to 1.0 (Tables 1 to 4). Those with Kappa values between 0.6 and 0.75 consisted of landscapes with greater percentages of aquatic plants or contained areas with higher occurrences of mixed classes (i.e., intermixing of *Typha* and mixed emergent classes).

## *Wetland classification and area percentages*

### *Barrier Beach wetlands*

Of the six barrier beach wetland sites, four were previously studied (Wilcox et al., 2008, Wilcox and Bateman, 2018) and are field- and photointerpretation-based, while two (Buck Pond and Second Creek) only contain our data from 2018 (Table 1). *Typha* experienced substantial increases in total area within the study site wetlands since the 1950s. However, much of the increase in *Typha* occurred from the mid-1960s to the late 1970s. Mixed emergent vegetation in the barrier beach sites experienced similar but smaller change trends. Conversely, the barrier beach sites experienced reductions in meadow marsh area across the 1950s to 2014/2015 period. During this same period, the floating vegetation experienced incremental increases and decreases in percentages of total area at different dates within each site.

The 2018 percentage of barrier beach sites consisting of *Typha* ranged from 4.5 (Second Creek) to 73.0 (Round Pond) (Table 1). Of the barrier beach sites with complete records over time, all experienced nominal decreases in percent *Typha* from 2014/2015 to 2018, except for Round Pond, which experienced a nominal increase in *Typha* (71.9% to 73.0%). There were considerable differences in aquatic vegetation percentages between 2018 and previous dates. These differences are due to classification differences, where the previous classifications consisted of only floating aquatics, and the 2018 classification scheme combined all aquatic vegetation into one class – resulting in higher percentages.

### *Drowned-river-mouth wetlands*

Three of the six drowned-river-mouth wetland sites were also studied previously (Wilcox et al., 2008; Wilcox and Bateman, 2018) (Table 2). Similar to the barrier beach sites, the drowned-river-mouth sites experienced substantial increases in the total *Typha* area since the 1950s. Much of the increase in *Typha* occurred after the late 1950s and mid-1960s. Mixed emergent vegetation in the drowned-river-mouth sites experienced nominal change, while the percentages of meadow marsh decreased. The floating vegetation experienced nominal increases for all drowned-river-mouth sites within the same period. From our study, the 2018 percentage of drowned-river-mouth sites consisting of *Typha* ranged from 6.7 (North Buck Bay) to 50.7 (Crooked Creek) (Table 2). Of the three drowned-river-mouth sites with complete period of record, two (Brush Creek and Crooked Creek) experienced nominal decreases in percent *Typha* from 2015 to 2018, while Kents Creek experienced a slight increase in *Typha* (29.7% to 31.0%).

### *Open embayment wetlands*

The open embayment wetlands differ from the barrier beach and drowned-river-mouth wetland sites in that three of the four sites studied previously (Wilcox et al., 2008; Wilcox and Bateman, 2018) experienced decreasing percentages of *Typha* across the 1950s to 2014/2015 period of record (Table 3). The mixed emergent vegetation at the open embayment sites experienced nominal change, while the percentages of meadow marsh generally decreased. From our study, the 2018 percentage of open embayment sites consisting of *Typha* ranged from 12.5 (Black River Bay – North Perch) to 51 (Buttonwood Creek) (Table 3). The four open embayment sites with complete period of record, Black

River Bay – North Perch, Braddock Bay – Salmon Creek North, Eel Bay – Flatiron, and The Isthmus, experienced -2.66, -3.57, -1.79, -5.45 percent per year decreases in percent *Typha*, respectively, from 2014/2015 to 2018.

### *Protected embayment wetlands*

For the protected embayment wetlands, three of the four sites studied previously (Wilcox et al., 2008; Wilcox and Bateman, 2018) experienced increasing percentages of *Typha* from 1959 to 2014/2015 (Table 4), with most increases from the mid-1960s to late 1970s. Point Vivian Bay experienced an overall decrease but was subject to cattail-control restoration efforts. The mixed emergent vegetation and meadow marsh at these protected embayment sites all experienced loss during the same time period. The percentage of protected embayment sites consisting of *Typha* in our 2018 study ranged from 1.17 for Grass Point, to 37.64 at Point Vivian Bay (Table 4). From 2014/2015 to 2018, Black River Bay – South Muskellunge, Goose Bay, and North Pond experienced -0.65, -1.06, and -0.06 percent per year decreases in percent *Typha*, respectively, while Point Vivian Bay experienced a 0.07 percent per year increase.

Overall, the average total area in percentage for meadow marsh, mixed emergent, and *Typha* (floating/aquatic vegetation class omitted from this assessment, details provided below) for all sites in 2014/2015 was 14.67%. When comparing these photo interpreted data to the HSI-derived percentages, the difference between our 2018 data and the 2014/2015 data was ±1.21 standard deviation. We assume that the majority of these differences are attributable to shifts in plant communities and differences in the classification methods.

## Conclusions

Although this was not intended to be an eco-hydrologic study, some of the results from our remote sensing data collection should have accompanying explanations, which include the previous studies. The general increases in *Typha* from the 1950s to the 1970s and later were related to regulation of Lake Ontario water levels that began about 1960. Regulation under Plan 158DD compressed the overall range of water-level fluctuations from approximately 2.0 m to 1.3 m in years following 1973. The range of growing season peak water levels was similarly reduced from approximately 1.5 m without regulation to 0.7 m after 1973, mostly due to reduction in low lake levels (Wilcox and Xie, 2007). Lack of years with low waters resulted in greater soil moisture at higher elevations in the wetlands, thus allowing moisture-requiring *Typha* to overcome the competitive advantage of sedges and grasses and to expand into meadow marsh (Wilcox et al., 2008). However, our 2018 results generally showed a decrease in area of *Typha*, which was again related to lake levels. Extreme water levels in the upper Great Lakes in 2017 resulted in increased flows into downstream Lake Ontario and elevated lake levels. Mean high water found in Lake Ontario records in June is 75.06 m (IGLD1985) but reached 75.81 m in June 2017 (https://www.lre.usace.army.mil/Portals/69/docs/GreatLakesInfo/docs/WaterLevels/LTA_GLWL-Metric_2019.pdf?ver=2020-02-04-152044-723). This reduced cover of *Typha* by breaking off sections of the floating cattail mat and flooding rooted cattails. Lake levels were much reduced (74.71 m) for our September 2018 remote sensing data collection, but recovery of *Typha* was not yet evident. These results are supported by Smith et al. (2021), who found decreases in cover of *Typha* from 2009-2016 to 2017 across most elevations in 12 Lake Ontario wetlands, with some recovery occurring in 2018 but not to previous levels.

This study was able to demonstrate the utility of airborne HSI, lidar, and true-color RGB imagery for the classification and monitoring of target wetland species and classes, specifically the dense and aggressive *Typha* community. The classification process provides efficient methods and consistent data products for updating previously photo interpreted wetland extent and community dynamics. Limitations that were encountered with the methods used for this study were the lack of adequate training data at some sites, the time-intensive nature of some reclassifications, and the inability to identify and separate

species/zones in highly mixed landscapes. However, most of these limitations can be overcome with additional data collection and/or remote sensing techniques. In addition, ground verification data for training relied on CWMP data sets. If such data were not available, other means of ground verification would have been required.

Although this study used standard classification techniques, the HSI, lidar, and true-color suite provided ancillary data and additional products that are ideal for more objective and automated approaches to wetland classifications and resource management. Future work should include the use of Unmanned Aircraft Systems (UAS) data collection to increase the establishment of training data, rule-based methods for more rapid and automated classifications, and spectral un-mixing and/or species-level classifications (Judd et al., 2007) for increased accuracy and raster-based tracking of floristic quality (Suir et al., 2020a). UAS might also be used to generate further verification data, which could be especially helpful in areas with access limitations or constraints (Suir et al., 2020b).

For wetland and ecosystem managers, the higher spatial and spectral resolution of the CZMIL-based classification data can also provide novel products about vegetation distribution, disturbances, resiliency, and recovery. Overall, this study satisfied the objective of using HSI, lidar, and true-color RGB data to more efficiently classify, map, and update wetland zones along Lake Ontario, USA.

## Acknowledgments

Permission to publish this information was granted by the Chief of Engineers and the Great Lakes Coastal Wetland Monitoring Program. The authors thank the Great Lakes Coastal Wetland Monitoring Program for providing advice and data for this study. The authors thank Scott Borne, Sam Jackson, Christopher Macon, Joseph Harwood, and Jennifer Wozencraft for review of the paper.

## Funding

Funding for this research and paper was provided by the US Army Corps of Engineers Buffalo District and the National Coastal Mapping Program.

### *Literature Cited*

Albert, D.A., Wilcox, D.A., Ingram, J.W., Thompson, T.A., 2005. Hydrogeomorphic classification for Great Lakes coastal wetlands. J. Great Lakes Res. 31 (Suppl. 1), 129–146.

Allen, Y.C., Suir, G.M., 2014. Using high-resolution, regional-scale data to characterize floating aquatic nuisance vegetation in coastal Louisiana navigation channels. ERDC/TN-APCRP-EA-27. Vicksburg, MS: U.S. Army Research and Development Center.

Anderson, K., Gaston, K.J., 2013. Lightweight unmanned aerial vehicles will revolutionize spatial ecology. Frontiers in Ecology and the Environment, 11(3), pp.138-146.

Bourgeau-Chavez, L.L, Endres, S., Battaglia, M., Miller, M.E., Banda, E., Laubach, Z., Higman, P., Chow-Fraser, P. and Marcaccio, J., 2015. Development of a bi-national Great Lakes coastal wetland and land use map using three-season PALSAR and Landsat imagery. Remote Sensing, 7(7), pp.8655-8682.

Bourgeau-Chavez, L.L., Riordan, K., Powell, R.B., Miller, N. and Nowels, M., 2009. Improving wetland characterization with multi-sensor, multi-temporal SAR and optical/infrared data fusion. In Advances in geoscience and remote sensing. IntechOpen.

Brix, H., Schierup, H.H., 1989. The use of aquatic macrophytes in water-pollution. Ambio 18, 100–107.

Broussard, W.I., Suir, G.M., Visser, J.M., 2018. Unmanned Aircraft Systems (UAS) and satellite imagery collections in a coastal intermediate marsh to determine the land-water interface, vegetation types, and Normalized Difference Vegetation Index (NDVI) values. United States Army Engineer Research and Development Center, Vicksburg, Mississippi.

Campbell, J.B., Wynne, R.H., 2011. Introduction to Remote Sensing, 5th edition. New York: The Guildford Press.
Carle, M.V. 2013. Spatial structure and dynamics of the plant communities in a Pro-Grading River Delta: Wax Lake Delta, Atchafalaya Bay, Louisiana. PhD Dissertation, Louisiana State University, Baton Rouge, LA, USA.
Chang, C.I. 2013. Hyperspectral data processing: algorithm design and analysis. John Wiley & Sons
DigitalGlobe. 2010. The benefits of the 8 spectral bands of WorldView-2. In White Paper Longmont, CO: DigitalGlobe.
Draksler, A., Cron, J. and Meng, I.L., 2017. The Effect of Satellite Image Resolution and Minimum Mapping Unit on the Accuracy of Forest Cover Maps. Technische Universität München, Munich, Germany.
Environmental Protection Agency. 2008. Effects of climate change on aquatic invasive species and implications for management and research. National Center for Environmental Assessment Office of Research and Development U.S. Environmental Protection Agency Washington, DC.
Howard, T.G., Feldmann, A.L., Spencer, E., Ring, R.R, Perkins, K.A., Corser, J., 2016. Wetland monitoring for Lake Ontario adaptive management. New York Natural Heritage Program, Albany, NY.
Jakubauskas, M.E., Peterson, D.L., Campbell, S.W., deNoyelles, F., Campbell, S.D., Penny, D., 2002. Mapping and monitoring invasive aquatic plant obstructions in navigable waterways using satellite multispectral imagery. FIEOS 2002 Conference Proceedings.
Jensen, J.R. 2015. Introductory digital image processing: a remote sensing perspective. Prentice Hall Press.
Jollineau, M.Y., Howarth, P.J., 2008. Mapping an inland wetland complex using hyperspectral imagery, Int. J. Remote Sens. 29, 3609–3631. DOI: 10.1080/01431160701469099.
Judd, C., Steinberg, S., Shaughnessy, F. and Crawford, G., 2007. Mapping salt marsh vegetation using aerial hyperspectral imagery and linear unmixing in Humboldt Bay, California. Wetlands, 27(4), pp.1144-1152.
Kowalski, K.P., Wilcox, D.A. 1999. Use of historical and geospatial data to guide the restoration of a Lake Erie coastal marsh. Wetlands 19, 858-868.
Kwang, E.K. 1996. Adaptive majority filtering for contextual classification of remote sensing data, Int. J. Remote Sens. 17, 1083–1087. DOI: 10.1080/01431169608949070
Lefsky, M.A., Cohen, W.B., Parker, G.G., Harding, D.J., 2002. Lidar remote sensing for ecosystem studies. BioScience, 52(1), 19-30.
Lillesand, T.M., Kiefer, R.W., Chipman, J.W., 2008. Remote sensing and image interpretation, 6th edition. John Wiley & Sons, Hoboken, NJ.
Mitchell, M.E., Lishawa, S.C., Geddes, P., Larkin, D.J., Treering, D., Tuchman, N.C., 2011. Time-dependent impacts of cattail invasion in a Great Lakes coastal wetland complex. Wetlands 31, 1143–1149.
Mitsch, W.J., Gosselink, J.G., 2000. Wetlands. John Wiley & Sons. Inc., New York, NY.
Nelson, M.L., Brewer, C.K., Solem, S.J., 2015. Existing vegetation classification, mapping, and inventory technical guide, version 2.0. Gen. Tech. Rep. WO–90. Washington, DC, U.S. Department of Agriculture, Forest Service, Ecosystem Management Coordination Staff.
Office of Technology Assessment. 1993. Harmful non-indigenous species in the United States. U.S. Congress Office of Technology Assessment; OTA-F-565. Available online at http://govinfo.library.unt.edu/ota/Ota_1/DATA/1993/9325.pdf
Park, J.Y., Tuell, G., 2010. Conceptual design of the CZMIL data processing system (DPS): algorithms and software for fusing lidar, hyperspectral data, and digital images. Proc. SPIE 7695, Algorithms and Technologies for Multispectral, Hyperspectral, and Ultraspectral Imagery XVI, 769510. doi: 10.1117/12.851976
Poirrier, M.A., Burt-Utley, K., Utley, J.F., Spalding, E.A., 2010. Submersed aquatic vegetation of the Jean Lafitte National Historical Park and Preserve. Southeast. Nat. 9, 477–486.

Reif, M.K., Macon, C.L., Wozencraft, J.M., 2011. Post-Katrina land-cover, elevation, and volume change assessment along the south shore of Lake Pontchartrain, Louisiana, USA. J. Coastal Res. 62, 30–39.
Reif, M.K., Wozencraft, J.M., Dunkin, L.M., Sylvester, C.S., Macon, C.L., 2013. A review of US Army Corps of Engineers airborne coastal mapping in the Great Lakes. J. Great Lakes Res. 39, 194–204.
Robles, W., Madsen, J.D., Mathur, A., Bruce, L.M., 2006. Ground-truthed hyperspectral data for remote sensing of waterhyacinth. Proc. Southern Weed Science Soc. 59, 194.
Robles, W., Madsen, J>D., Wersal, R.M., 2010. Potential for remote sensing to detect and predict herbicide injury on waterhyacinth (*Eichhornia crassipes*). Inv. Plant Sci. Manage. 3, 440–450.
Schott, J.R. 2007. Remote sensing: the image chain approach. Oxford University Press on Demand.
Schowengerdt, R.A. 2007. Remote sensing: models and methods for image processing. Elsevier.
Short, N.M., Robinson, J.W., 1999. Remote sensing and image interpretation and analysis. (J. W. Robinson, Ed.) Greenbelt, Maryland, USA, USA: NASA's Goddard Space Flight Center.
Smart, R.M., Dick, G.O., Snow, J.R., Honnell, D.R., Smith, D.H., Smith, J.K., 2009. Ecological effects of exotic and native aquatic vegetation. ERDC/EL TR-09-10. Vicksburg, MS: US Army Engineer Research and Development Center.
Smith, I.M., Fiorino, G.E., Grabas, G.P., Wilcox, D.A. 2021. Wetland vegetation response to record-high Lake Ontario water levels. Journal of Great Lakes Research 47, 160-167.
Suir, G.M., 2018. Sediment and Plant Dynamics in a Degrading Coastal Louisiana Landscape. Louisiana State University Doctoral Dissertations. 4504. Baton Rouge, LA.
Suir, G.M., Carle, M.M., Harris, J.M., Sasser, C.E., Saltus, C.L., 2020a. Raster-Based Floristic Quality Index: Proof of Concept. ERDC/EL TN20-1. Vicksburg, MS: US Army Engineer Research and Development Center.
Suir, G.M., Saltus, C.L., Sasser, C.E., Harris, J.M., Reif, M.K., Diaz, R., Giffin, G., 2020b. Evaluating 'Drone Truthing' as an Alternative to Ground Truthing: An Example with Wetland Plant Identification. APCRP Technical Notes Collection. ERDC TN-APCRP. Vicksburg, MS: U.S. Army Engineer Research and Development Center.
Thiago, S.F.S., Costa, M.P.F., Melack, J.M., Novo, E.M.L.M., 2008. Remote sensing of aquatic vegetation: theory and applications. Environ. Monit. Assess. 140, 131–145.
Tiner, RW. 1996. Technical aspects of wetlands: wetland definitions and classifications in the United States. US Geological Survey Water-Supply Paper, Report: W, 2425.
Vaccaro, L., Bedford, B.L., Johnston, C.A., 2009. Litter accumulation promotes dominance of invasive species of cattail (*Typha* spp.) in Lake Ontario wetlands. Wetlands 29, 1036–1048.
Uzarski, D.G., Brady, V.J., Cooper, M.J., Wilcox, D.A., Albert, D.A., Axler, R.P., Bostwick, P., Brown, T.N., Ciborowski, J.J., Danz, N.P., Gathman, J.P., 2017. Standardized measures of coastal wetland condition: implementation at a Laurentian Great Lakes basin-wide scale. Wetlands, 37(1), pp.15-32.
Verma, D., Jana, A., 2019. LULC classification methodology based on simple Convolutional Neural Network to map complex urban forms at finer scale: Evidence from Mumbai. arXiv preprint arXiv:1909.09774.
Vis, C., Hudon, C., Carignan, R., 2003. An evaluation of approaches used to determine the distribution and biomass of emergent and submerged aquatic macrophytes over large spatial scales. Aquatic Botany, Vol. 77, 187–201.
Wilcox, D.A., Bateman, J.A., 2018. Photointerpretation analysis of plant communities in Lake Ontario wetlands following 65 years of lake-level regulation. J. Great Lakes Res. 44, 1306–1313.
Wilcox, D.A., Ingram, J.W., Kowalski, K.P., Meeker, J.E., Carlson, M.L., Xie, Y., Grabas, G.P., Holmes, K.L., Patterson, N.J., 2005. Evaluation of water-level regulation influences on Lake Ontario and Upper St. Lawrence River coastal wetland plant communities. Report to the International Joint Commission, Washington, DC and Ottawa, ON.

Wilcox, D.A., Kowalski, K.P., Hoare, H.L., Carlson, M.L., Morgan, H.N., 2008. Cattail invasion of sedge/grass meadows in Lake Ontario: photointerpretation analysis of sixteen wetlands over five decades. J. Great Lakes Res. 34, 301–323.
Wilcox, D.A., Xie, Y., 2007. Predicting wetland plant community responses to proposed water-level-regulation plans for Lake Ontario: GIS-based modeling. J. Great Lakes Res. 33, 751–773.
Wilcox, D.A., Xie, Y., 2008. Predicted effects of proposed new regulation plans on sedge/ grass meadows of Lake Ontario. J. Great Lakes Res. 34, 745–754.
Wozencraft, J.M., Lillycrop, W.J., 2006. JALBTCX coastal mapping for the USACE. The International hydrographic review.

**Figure 1**. Location map of the Lake Ontario wetland classification sites.

**Figure 2.** Example HSI (panel A), first return lidar (panel B1), bare earth lidar (panel B2) and high resolution true-color RGB data (panel C) from the Point Vivian Bay study area.
**Figure 3**. Example MNF data from the Point Vivian Bay study area.
**Figure 4**. Example MLC wetland classification data from the Point Vivian Bay study area.

Table 1. Area in percentages for wetland vegetation types (Floating/Aquatic Vegetation, Meadow Marsh, Mixed Emergent, and Cattail) from the 1950s to 2018 in Lake Ontario barrier beach wetlands. Data prior to 2018 are from Wilcox et al. (2008) and Wilcox and Bateman (2018).

| Barrier Beach Wetland Site | Year | Kappa | Community Type | | | | |
|---|---|---|---|---|---|---|---|
| | | | Total | Floating / (Aquatic Vegetation) | Meadow Marsh | Mixed Emergent | Cattail |
| | | | Area | Area Percentage of Total | Area Percentage of Total | Area Percentage of Total | Area Percentage of Total |
| | | | (ha) | (%) | (%) | (%) | (%) |
| Buck Pond | 2018 | 0.871 | 321.38 | (9.16) | 1.51 | 1.43 | 50.95 |
| Lakeview Pond (Floodwood) | 1959 | | 148.57 | 1.12 | 7.06 | - | 33.38 |
| | 1966 | | 148.57 | 8.16 | 6.06 | - | 34.08 |
| | 1979 | | 148.57 | 0.04 | 0.03 | 0.05 | 38.85 |
| | 1988 | | 148.57 | 8.65 | 2.65 | 1.00 | 38.02 |
| | 2001 | | 148.57 | 14.81 | 0.48 | 0.24 | 40.53 |
| | 2015 | | 148.57 | 8.50 | 0.02 | 1.28 | 40.63 |
| | 2018 | 0.969 | 147.33 | (25.67) | 0.04 | 3.84 | 36.69 |
| Maxwell Bay | 1954 | | 11.86 | 39.63 | 0.51 | 0.00 | 3.79 |
| | 1963 | | 11.86 | 0.59 | 22.26 | 0.00 | 6.75 |
| | 1978 | | 11.86 | 35.33 | 0.67 | 0.00 | 15.85 |
| | 1988 | | 11.86 | 19.22 | 0.00 | 0.00 | 13.49 |
| | 2001 | | 11.86 | 31.87 | 2.02 | 0.25 | 24.79 |
| | 2014 | | 11.86 | 35.16 | 2.78 | 1.60 | 32.97 |
| | 2018 | 0.874 | 11.86 | (46.06) | 1.46 | 8.82 | 25.47 |
| Round Pond | 1958 | | 103.10 | 4.65 | 1.00 | 0.00 | 60.60 |
| | 1966 | | 103.10 | 7.16 | 0.00 | 0.00 | 51.98 |
| | 1980 | | 103.10 | 2.56 | 0.00 | 0.00 | 63.47 |
| | 1988 | | 103.10 | 12.65 | 0.00 | 0.00 | 64.36 |

| | | | | | | | |
|---|---|---|---|---|---|---|---|
| | 2001 | | 103.10 | 4.46 | 0.21 | 0.00 | 70.14 |
| | 2015 | | 103.10 | 3.32 | 0.05 | 0.16 | 71.85 |
| | 2018 | 0.846 | 93.21 | (10.59) | 1.14 | 1.59 | 72.96 |
| Second Creek | 2018 | 0.890 | 1623.31 | (10.83) | 0.29 | 0.39 | 4.54 |
| South Colwell Pond | 1959 | | 78.97 | 2.18 | 22.93 | 2.33 | 10.70 |
| (North Colwell) | 1966 | | 78.97 | 22.73 | 26.92 | 5.48 | 7.53 |
| | 1978 | | 78.97 | 7.71 | 0.73 | - | 29.50 |
| | 1988 | | 78.97 | 16.11 | 0.20 | 1.47 | 30.19 |
| | 2001 | | 78.97 | 16.07 | 2.67 | - | 26.97 |
| | 2015 | | 78.97 | 1.29 | 0.35 | 1.54 | 26.73 |
| | 2018 | 0.894 | 78.97 | (51.06) | 1.67 | 5.27 | 23.04 |

Table 2. Area in percentages for wetland vegetation types (Floating/Aquatic Vegetation, Meadow Marsh, Mixed Emergent, and Cattail) from the 1950s to 2018 in Lake Ontario drowned-river-mouth wetlands. Data prior to 2018 are from Wilcox et al. (2008) and Wilcox and Bateman (2018).

| Drowned River Wetland Site | Year | Kappa | Community Type | | | | |
|---|---|---|---|---|---|---|---|
| | | | Total | Floating / Aquatic Vegetation | Meadow Marsh | Mixed Emergent | Cattail |
| | | | Area | Area Percentage of Total | Area Percentage of Total | Area Percentage of Total | Area Percentage of Total |
| | | | (ha) | (%) | (%) | (%) | (%) |
| Brush Creek | 1958 | | 53.13 | 0.00 | 21.06 | 0.00 | 30.68 |
| | 1966 | | 53.13 | 3.16 | 13.59 | 0.00 | 38.13 |
| | 1979 | | 53.13 | 0.00 | 2.33 | 0.00 | 36.19 |
| | 1988 | | 53.13 | 0.00 | 0.00 | 0.00 | 37.93 |
| | 2001 | | 53.13 | 5.70 | 0.00 | 0.00 | 40.43 |
| | 2015 | | 53.13 | 7.13 | 0.00 | 0.00 | 37.61 |
| | 2018 | 0.944 | 41.97 | (5.97) | 0.47 | 0.06 | 35.14 |
| Crooked Creek | 1959 | | 311.30 | 0.86 | 43.38 | - | 22.25 |
| | 1966 | | 311.30 | 1.05 | 50.36 | - | 15.64 |
| | 1978 | | 311.30 | 1.17 | 17.72 | - | 46.69 |
| | 1990 | | 311.30 | - | 5.96 | - | 55.39 |
| | 2001 | | 311.30 | 10.38 | 5.88 | 0.67 | 56.05 |
| | 2015 | | 311.30 | 10.71 | 4.16 | 0.93 | 52.95 |
| | 2018 | 0.735 | 297.60 | (11.38) | 6.60 | 8.36 | 50.70 |
| Kents Creek (Mud Bay) | 1959 | | 60.60 | - | 37.66 | - | 14.17 |
| | 1966 | | 60.60 | 0.84 | 14.70 | 0.21 | 34.93 |
| | 1978 | | 60.60 | - | 18.71 | - | 32.51 |
| | 1988 | | 60.60 | 6.70 | 26.32 | - | 21.20 |
| | 2001 | | 60.60 | 9.41 | 19.62 | - | 27.10 |
| | 2015 | | 60.60 | 0.05 | 17.05 | - | 29.70 |
| | 2018 | 0.880 | 57.39 | (13.61) | 17.26 | 1.01 | 30.98 |
| North Buck Bay | 2018 | 0.930 | 38.20 | (1.30) | 2.73 | 1.43 | 6.71 |
| Port Bay | 2018 | 0.983 | 415.98 | (9.10) | 1.89 | 1.34 | 21.81 |
| Sterling Wetland Creek | 2018 | 0.830 | 441.79 | (17.18) | 5.85 | 8.10 | 39.94 |

Table 3. Area in percentages for wetland vegetation types (Floating/Aquatic Vegetation, Meadow Marsh, Mixed Emergent, and Cattail) from the 1950s to 2018 in Lake Ontario open embayment wetlands. Data prior to 2018 are from Wilcox et al. (2008) and Wilcox and Bateman (2018).

| Open Embayment Wetland Site | Year | Kappa | Community Type | | | | |
|---|---|---|---|---|---|---|---|
| | | | Total | Floating / Aquatic Vegetation | Meadow Marsh | Mixed Emergent | Cattail |
| | | | Area | Area Percentage of Total | Area Percentage of Total | Area Percentage of Total | Area Percentage of Total |
| | | | (ha) | (%) | (%) | (%) | (%) |
| Black River Bay (North Perch) | 1959 | | 345.95 | - | 0.97 | - | 23.01 |
| | 1966 | | 345.95 | 4.94 | 1.88 | - | 27.22 |
| | 1979 | | 345.95 | 0.10 | 0.94 | - | 14.35 |
| | 1988 | | 345.95 | 11.87 | - | - | 16.86 |
| | 2001 | | 345.95 | 4.58 | - | - | 14.99 |
| | 2014 | | 345.95 | 7.59 | - | 0.09 | 15.20 |
| | 2018 | 0.762 | 326.98 | (11.40) | 0.61 | 1.90 | 12.54 |
| Braddock Bay | 2018 | 0.677 | 18.90 | (8.58) | 3.97 | 0.04 | 39.39 |
| Braddock Bay (Salmon Creek North) | 1958 | | 230.29 | 1.26 | 0.00 | 0.00 | 32.97 |
| | 1966 | | 230.29 | 3.99 | 3.19 | 0.00 | 39.02 |
| | 1978 | | 230.29 | 5.42 | 0.51 | 0.05 | 27.69 |
| | 1988 | | 230.29 | 4.09 | 0.52 | 0.34 | 26.80 |
| | 2001 | | 230.29 | 14.35 | 0.04 | 0.00 | 30.82 |
| | 2014 | | 230.29 | 12.07 | 0.19 | 0.66 | 30.64 |
| | 2018 | 0.885 | 200.21 | (35.50) | 2.21 | 1.32 | 27.06 |
| Buttonwood Creek | 2018 | 0.869 | 91.2 | (9.16) | 1.51 | 1.43 | 50.95 |
| Eel Bay (Flatiron) | 1959 | | 41.34 | 1.43 | 25.88 | - | 12.89 |
| | 1966 | | 41.34 | 8.03 | 11.27 | - | 31.79 |
| | 1978 | | 41.34 | 4.11 | - | - | 34.06 |
| | 1990 | | 41.34 | - | - | 0.12 | 34.13 |
| | 2001 | | 41.34 | 7.28 | 1.43 | 1.43 | 33.89 |
| | 2014 | | 41.34 | 10.72 | 0.60 | 1.89 | 33.84 |
| | 2018 | 0.896 | 41.33 | (3.17) | 0.01 | 3.86 | 32.05 |
| Salmon Creek South | 2018 | 0.885 | 92.28 | (36.44) | 2.58 | 1.69 | 25.99 |

| | | | | | | | |
|---|---|---|---|---|---|---|---|
| The Isthmus | 1959 | | 40.89 | - | 17.41 | - | 28.86 |
| | 1966 | | 40.89 | 0.22 | 14.38 | - | 27.64 |
| | 1978 | | 40.89 | 2.18 | 6.92 | 0.12 | 19.47 |
| | 1988 | | 40.89 | 1.15 | 4.11 | 6.33 | 18.56 |
| | 2001 | | 40.89 | 3.42 | 5.48 | 3.50 | 19.03 |
| | 2014 | | 40.89 | 8.14 | 3.94 | 4.62 | 22.84 |
| | 2018 | 0.677 | 40.03 | (39.67) | 6.80 | 7.36 | 17.39 |

Table 4. Area in percentages for wetland vegetation types (Floating/Aquatic Vegetation, Meadow Marsh, Mixed Emergent, and Cattail) from the 1950s to 2018 in Lake Ontario protected embayment wetlands. Data prior to 2018 are from Wilcox et al. (2008) and Wilcox and Bateman (2018).

| Protected Embayment Wetland Site | Year | Kappa | Community Type | | | | |
|---|---|---|---|---|---|---|---|
| | | | Total | Floating / Aquatic Vegetation | Meadow Marsh | Mixed Emergent | Cattail |
| | | | Area | Area Percentage of Total | Area Percentage of Total | Area Percentage of Total | Area Percentage of Total |
| | | | (ha) | (%) | (%) | (%) | (%) |
| Black River Bay (South Muskellunge) | 1959 | | 92.00 | 5.82 | 5.61 | - | 16.23 |
| | 1966 | | 92.00 | 7.53 | 14.23 | - | 9.04 |
| | 1979 | | 92.00 | - | 2.17 | - | 15.97 |
| | 1988 | | 92.00 | 27.78 | 2.89 | - | 24.04 |
| | 2001 | | 92.00 | 45.68 | 1.82 | 0.20 | 20.83 |
| | 2015 | | 92.00 | 1.57 | 0.87 | - | 24.90 |
| | 2018 | 0.614 | 89.82 | (51.97) | 3.06 | 1.63 | 22.97 |
| Grass Point | 2018 | 0.889 | 86.02 | (1.36) | 0.01 | 0.29 | 1.17 |
| Goose Bay | 1959 | | 76.81 | 2.83 | 39.89 | - | 5.79 |
| | 1966 | | 76.81 | 0.83 | 27.94 | - | 15.28 |
| | 1978 | | 76.81 | 1.11 | 11.91 | - | 31.13 |
| | 1990 | | 76.81 | 0.43 | 8.45 | 5.49 | 32.89 |
| | 2001 | | 76.81 | 3.59 | 11.85 | - | 31.31 |
| | 2015 | | 76.81 | 14.70 | 10.02 | - | 30.23 |

| | | | | | | | |
|---|---|---|---|---|---|---|---|
| | 2018 | 0.692 | 68.41 | (8.38) | 9.26 | 5.72 | 27.06 |
| Hill Island West | 2018 | 0.909 | 46.23 | (14.32) | 0.57 | 0.91 | 11.35 |
| North Pond | 1959 | | 32.59 | 19.70 | 9.57 | - | 6.11 |
| | 1965 | | 32.59 | 15.07 | 13.53 | 16.51 | 5.74 |
| | 1978 | | 32.59 | 34.31 | 3.59 | 7.92 | 10.25 |
| | 1988 | | 32.59 | 30.87 | 9.30 | 4.33 | 21.54 |
| | 2001 | | 32.59 | 22.92 | 8.44 | 6.26 | 19.88 |
| | 2014 | | 32.59 | 30.68 | 4.33 | 2.27 | 30.44 |
| | 2018 | 0.809 | 30.26 | (31.35) | 1.72 | 13.62 | 30.21 |
| Point Vivian Bay | 1959 | | 15.28 | 0.52 | 5.30 | - | 67.47 |
| | 1966 | | 15.28 | 4.25 | 3.21 | - | 70.42 |
| | 1978 | | 15.28 | 12.50 | 3.21 | - | 63.48 |
| | 1990 | | 15.28 | - | 2.95 | - | 60.14 |
| | 2001 | | 15.28 | 18.78 | 4.32 | - | 63.81 |
| | 2015 | | 15.28 | 20.88 | 2.09 | 12.24 | 37.43 |
| | 2018 | 0.921 | 15.28 | (38.87) | 2.16 | 12.98 | 37.64 |

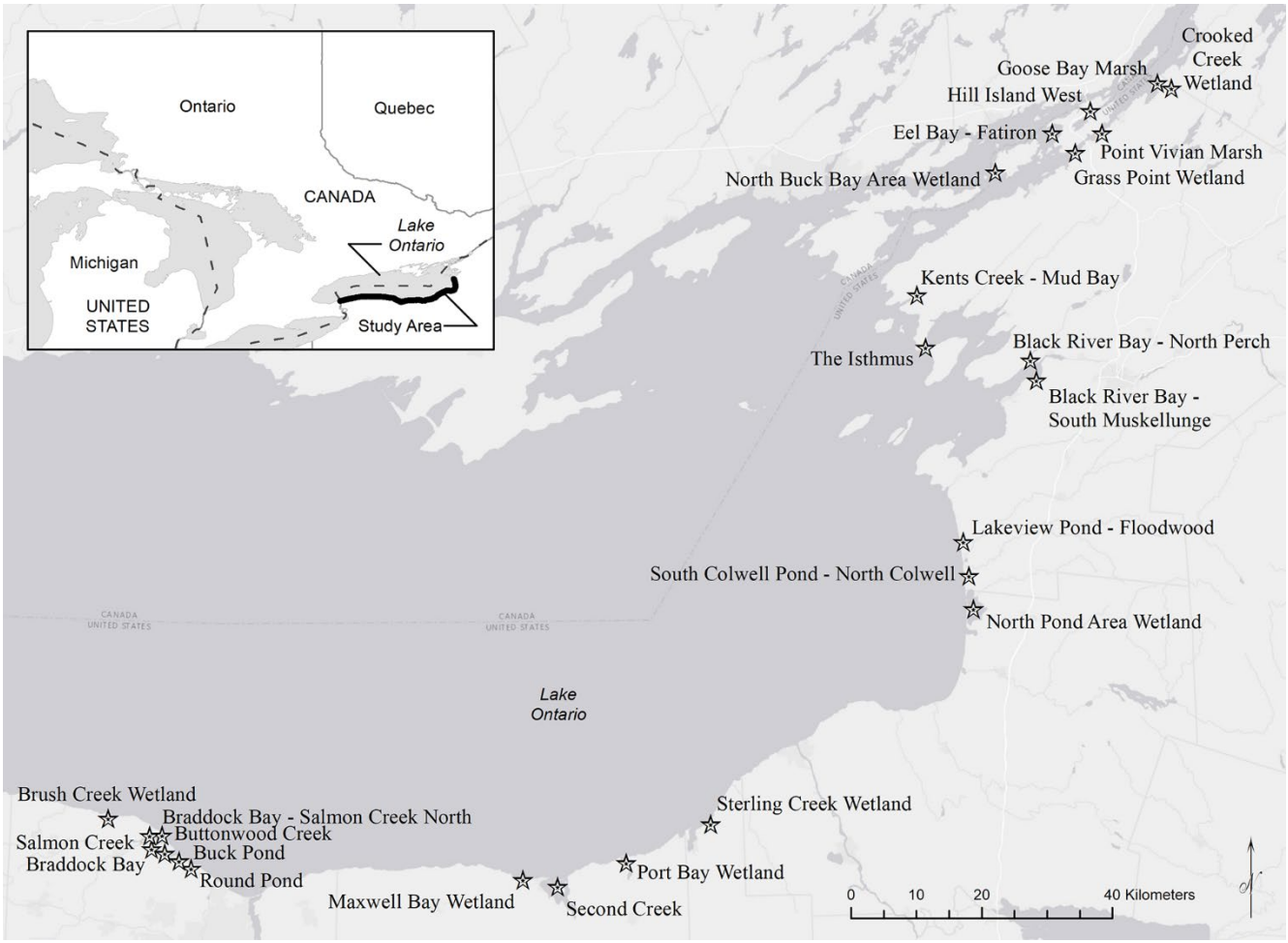
Ontario
Quebec
CANADA
Lake
Ontario
Michigan
UNITED
STATES
Study Area
Crooked
Creek
Wetland
Goose Bay Marsh
Hill Island West
Eel Bay - Fatiron
Point Vivian Marsh
Grass Point Wetland
North Buck Bay Area Wetland
Kents Creek - Mud Bay
The Isthmus
Black River Bay - North Perch
Black River Bay -
South Muskellunge
Lakeview Pond - Floodwood
South Colwell Pond - North Colwell
North Pond Area Wetland
Lake
Ontario
Brush Creek Wetland
Braddock Bay - Salmon Creek North
Salmon Creek
Buttonwood Creek
Buck Pond
Braddock Bay
Round Pond
Maxwell Bay Wetland
Second Creek
Port Bay Wetland
Sterling Creek Wetland
0
10
20
40 Kilometers

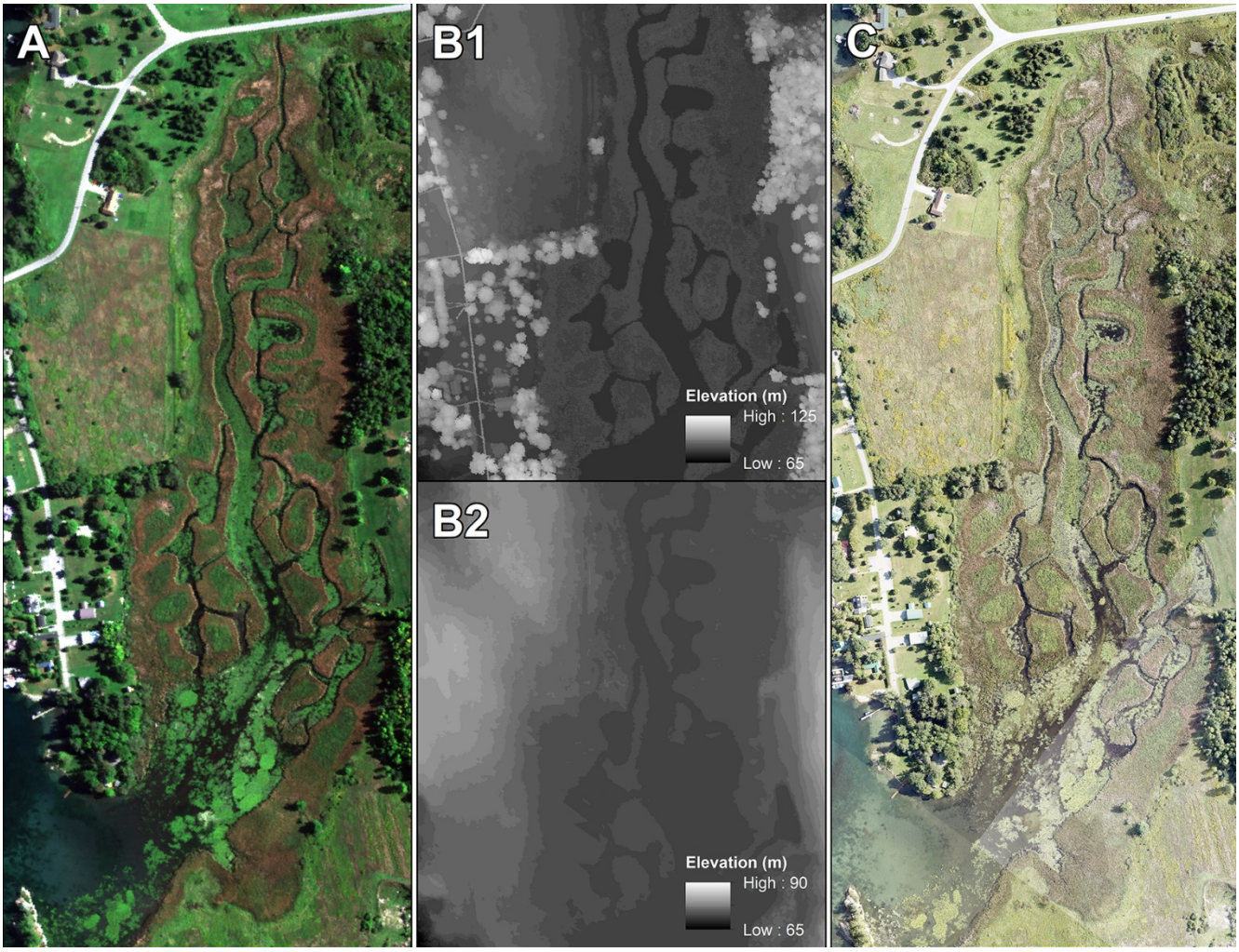
A
B1
Elevation (m)
High : 125
Low : 65
B2
Elevation (m)
High : 90
Low : 65
C

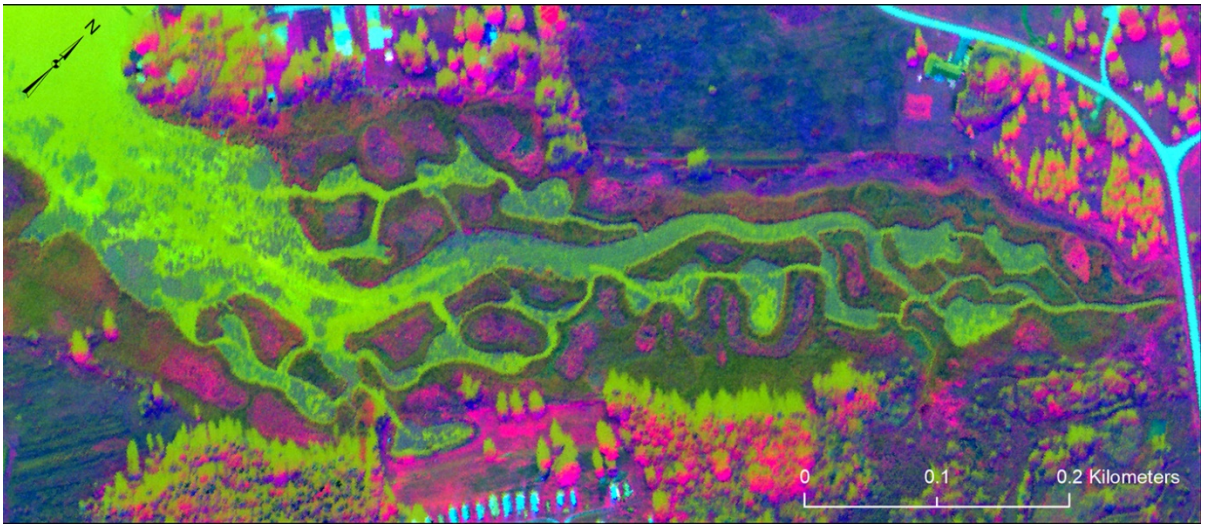
N
0
0.1
0.2 Kilometers

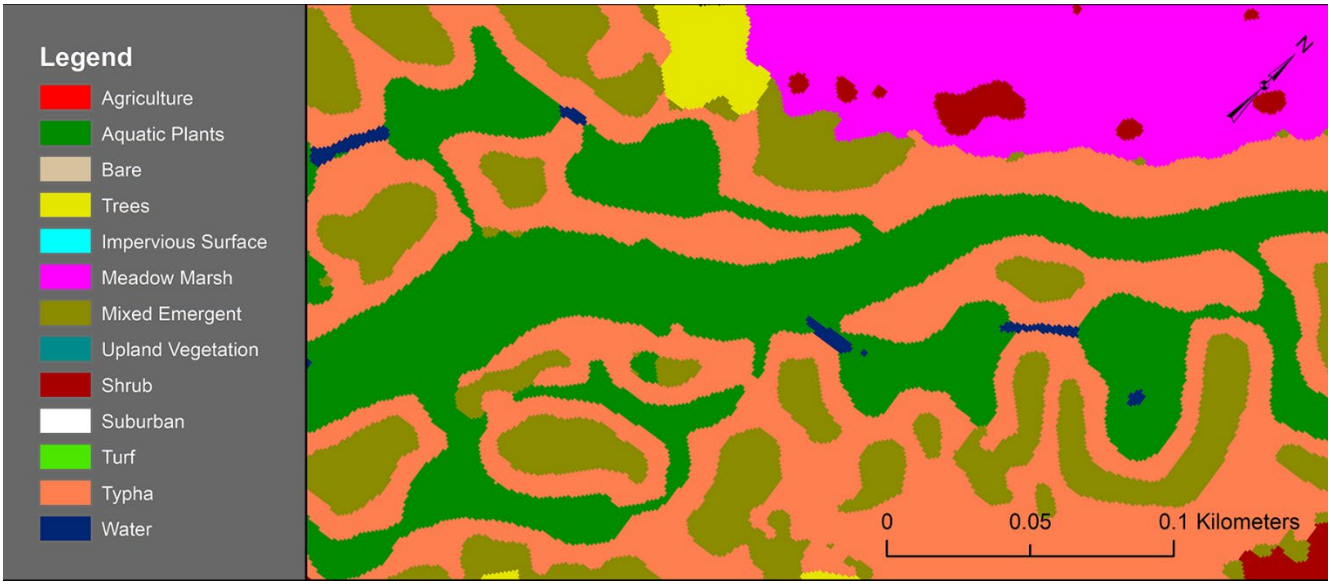
Legend
Agriculture
Aquatic Plants
Bare
Trees
Impervious Surface
Meadow Marsh
Mixed Emergent
Upland Vegetation
Shrub
Suburban
Turf
Typha
Water
N
0
0.05
0.1 Kilometers

**Appendix A**

Table A1. Geomorphological settings and classification periods for each of the study site wetland areas. Classifications prior to 2018 were performed by Wilcox et al. (Wilcox et al., 2005, 2008; Wilcox and Xie, 2007, 2008; Wilcox and Bateman, 2018).

| Geomorphological Setting | Site | Classification Years |
|---|---|---|
| Barrier Beach | Buck Pond | 2018 |
| | Lakeview Pond - Floodwood | 1959 - 2018 |
| | Maxwell Bay | 1954 - 2018 |
| | Round Pond | 1958 - 2018 |
| | Second Creek | 2018 |
| | South Colwell Pond - North Colwell | 1959 - 2018 |
| Drowned River Mouth | Brush Creek | 1958 - 2018 |
| | Crooked Creek | 1959 - 2018 |
| | Kents Creek - Mud Bay | 1959 - 2018 |
| | North Buck Bay | 2018 |
| | Port Bay | 2018 |
| | Sterling Creek Wetland | 2018 |
| Open Embayment | Black River Bay - North Perch | 1959 - 2018 |
| | Braddock Bay | 2018 |
| | Braddock Bay - Salmon Creek North | 1958 - 2018 |
| | Buttonwood Creek | 2018 |
| | Eel Bay - Flatiron | 1959 - 2018 |
| | Salmon Creek | 2018 |
| | The Isthmus | 1959 - 2018 |
| Protected Embayment | Black River Bay - South Muskellunge | 1959 - 2018 |
| | Grass Point | 2018 |
| | Goose Bay | 1959 - 2018 |
| | Hill Island West | 2018 |
| | North Pond | 1959 - 2018 |
| | Point Vivian Bay | 1959 - 2018 |

Table A2. Classification schema (modified from Wilcox et al., 2005; Jollineau and Howarth, 2008).

| Environment | Land Cover | Class Description |
|---|---|---|
| Urban | Impervious Surface | Roads, parking lots, and other impervious features |
| | Suburban | Houses, building, and other structures |
| Upland | Turf/Grassland | |
| | Agriculture | Existing or recently harvested cropland or orchards |
| | Forest | Areas where mixed deciduous species represent >75% of the canopy |
| | Bare | Unvegetated ground |
| | Upland Vegetation | Terrestrial plants above 75.6 meter elevation |
| Wetland | Shrub | Defined as wetland areas that contain (25% tree cover and 0.25% hydrophytic shrub cover) |
| | Meadow Marsh | *Calamagrostis canadensis*, and *Carex* spp. dominated wetlands between 74.85 and 75.6 meter elevation |
| | Typha | Dense patches of *Typha xglauca* and *Typha angustifolia* between 74.7 and 75.25 meter elevation |
| | Mixed Emergent | *Schoenoplectus* spp. and *Sparganium eurycarpum* dominated wetland between 74.7 and 74.85 meter elevation |
| | Aquatic Plants | Floating and submerged aquatic macrophytes between 73 and 74.7 meter elevation |
| Water | Water | Shallow and deep open water |

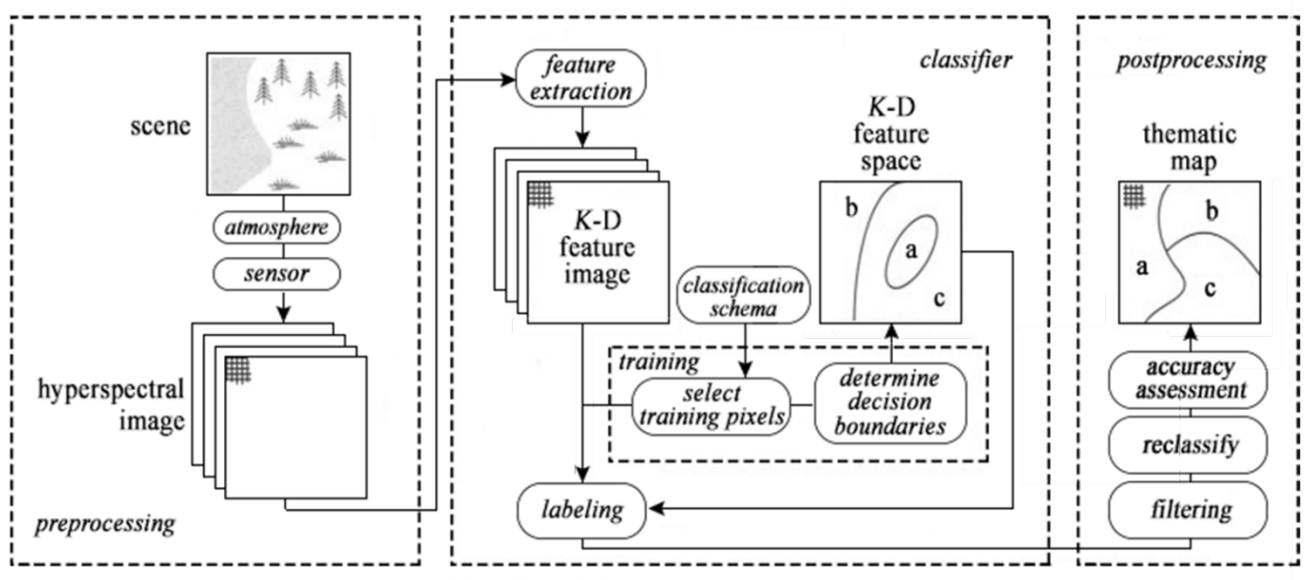


Figure A1. Typical data flow in the hyperspectral image classification process (modified from Schowengerdt 2007).

## Appendix B

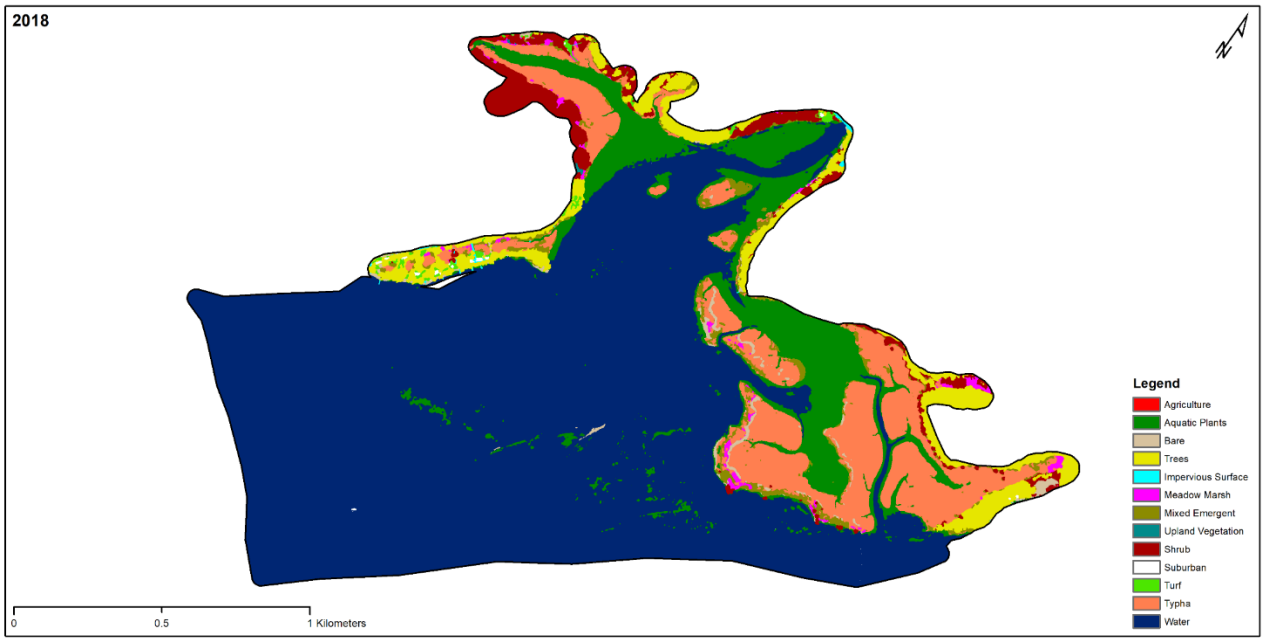


Figure B1. Maximum Likelihood Classifier wetland classification data from the Black River Bay – North Perch study area.

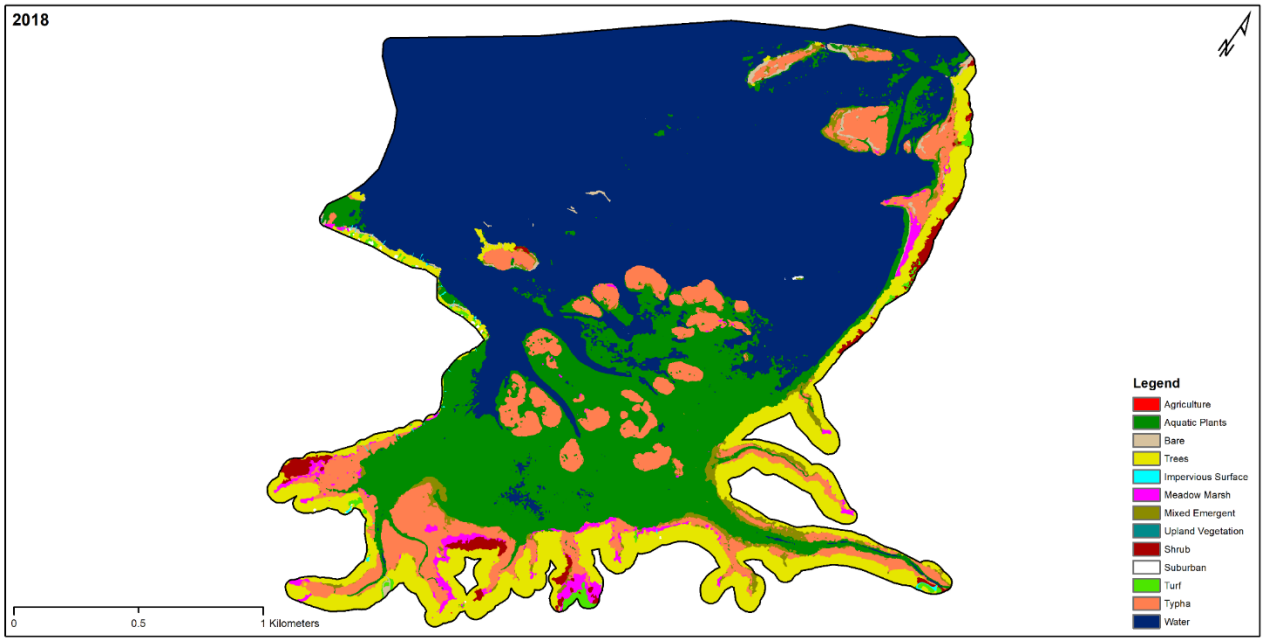

Figure B2. Maximum Likelihood Classifier wetland classification data from the Black River Bay - South Muskellunge study area.

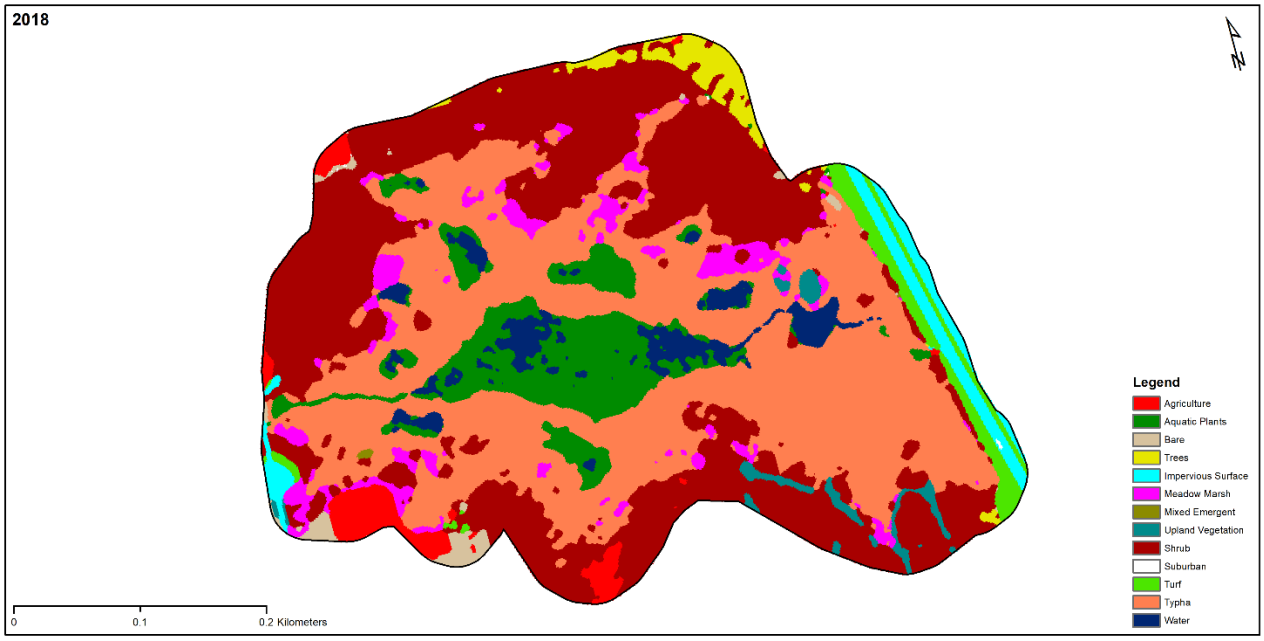


Figure B3. Maximum Likelihood Classifier wetland classification data from the Braddock Bay study area.

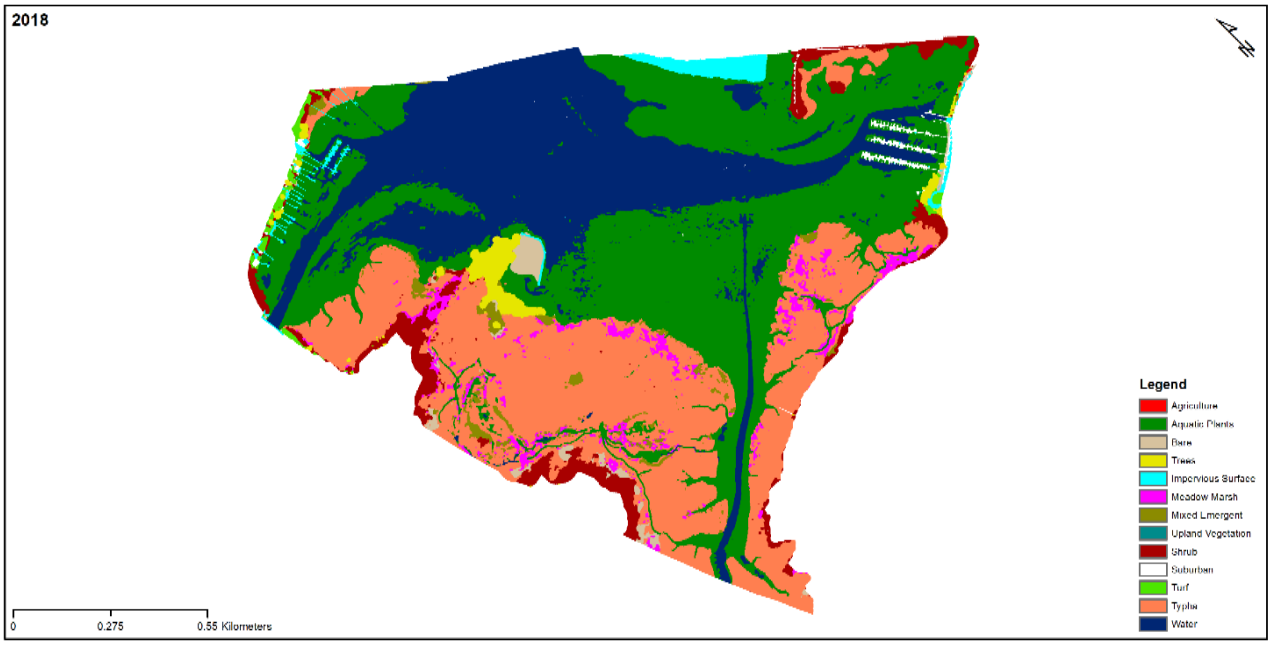

Figure B4. Maximum Likelihood Classifier wetland classification data from the Braddock Bay - Salmon Creek North study area.

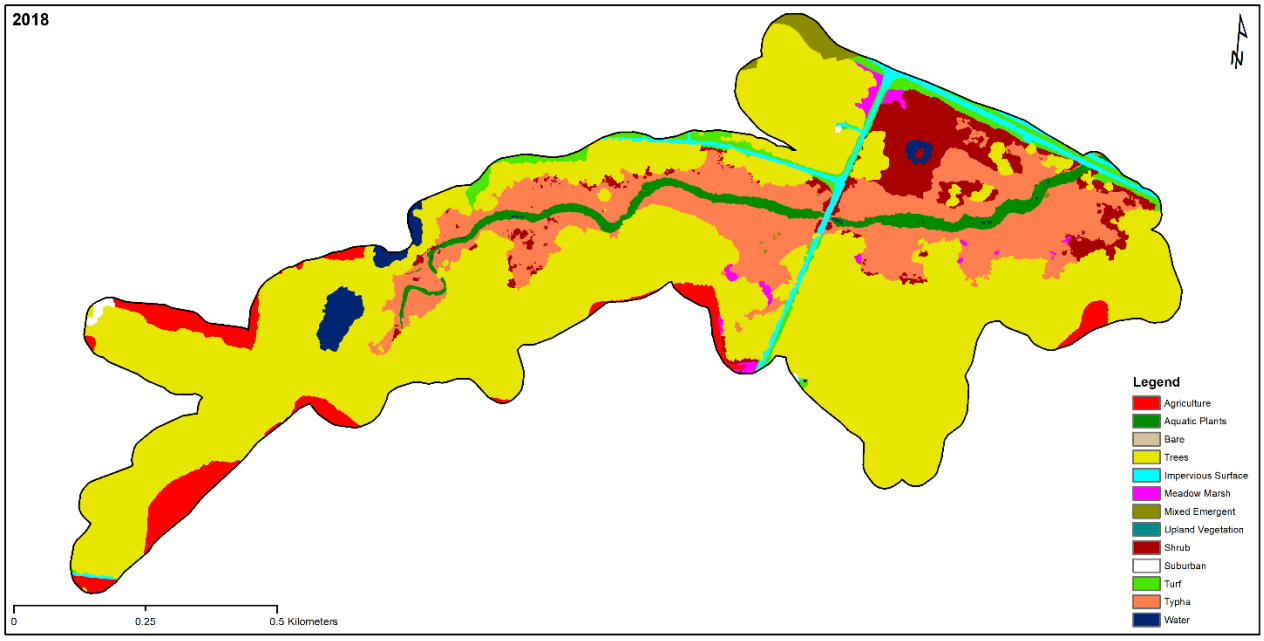


Figure B5. Maximum Likelihood Classifier wetland classification data from the Brush Creek study area.

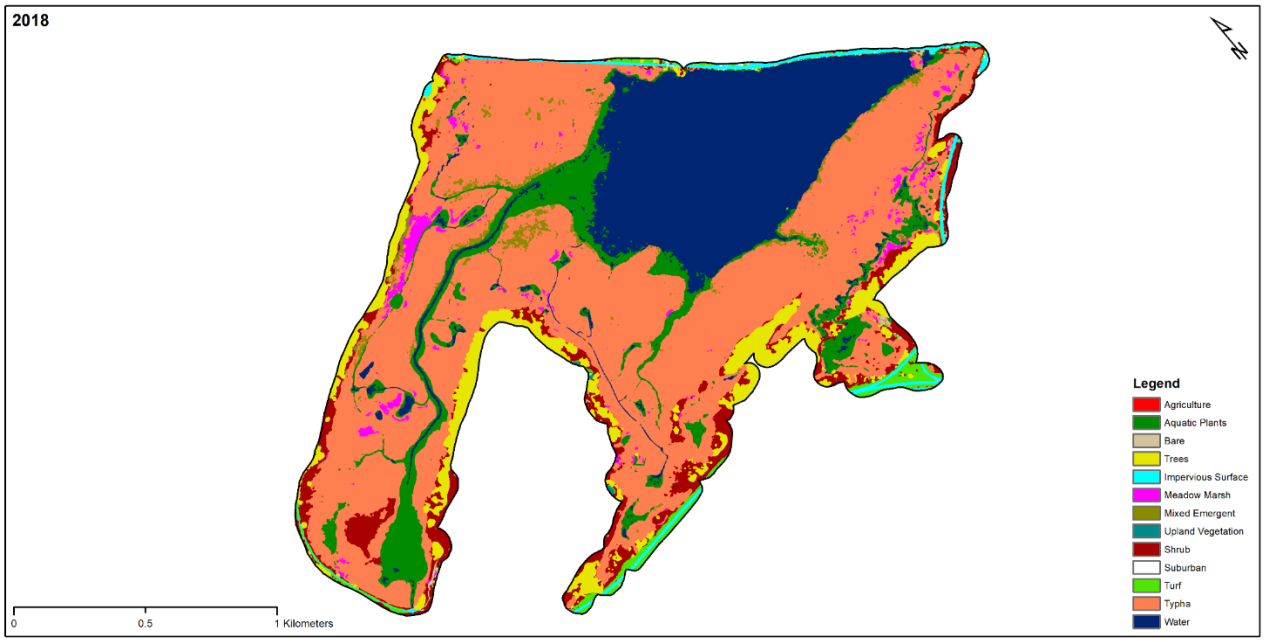

Figure B6. Maximum Likelihood Classifier wetland classification data from the Buck Pond study area.

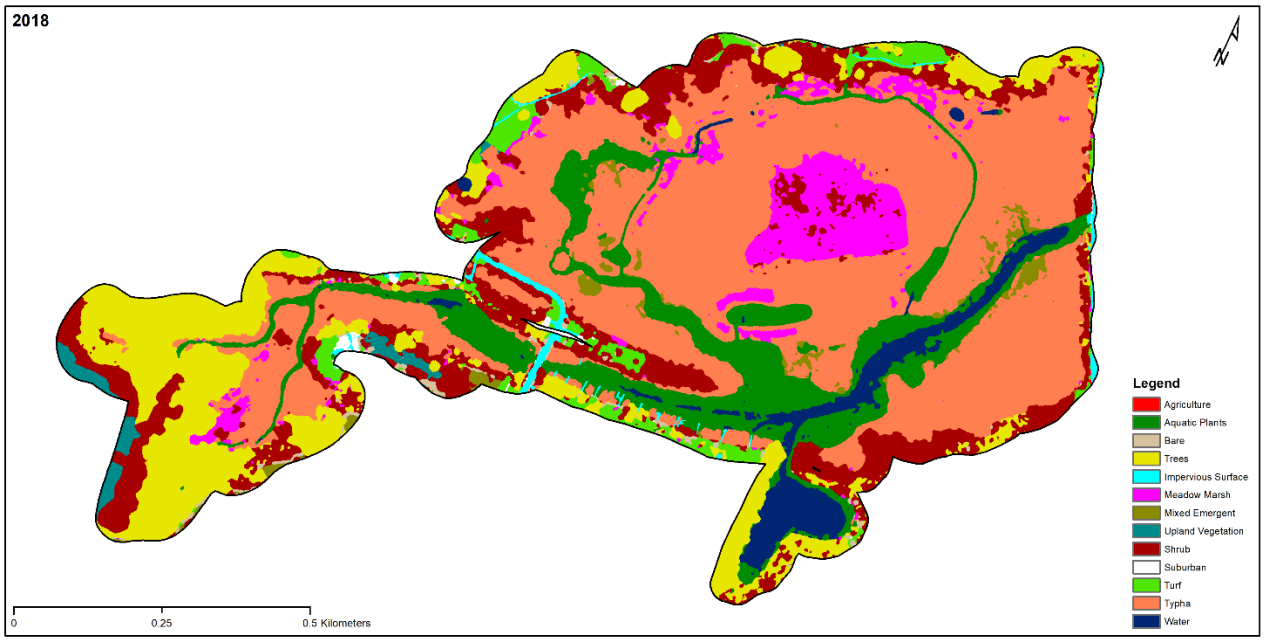


Figure B7. Maximum Likelihood Classifier wetland classification data from the Buttonwood Creek study area.

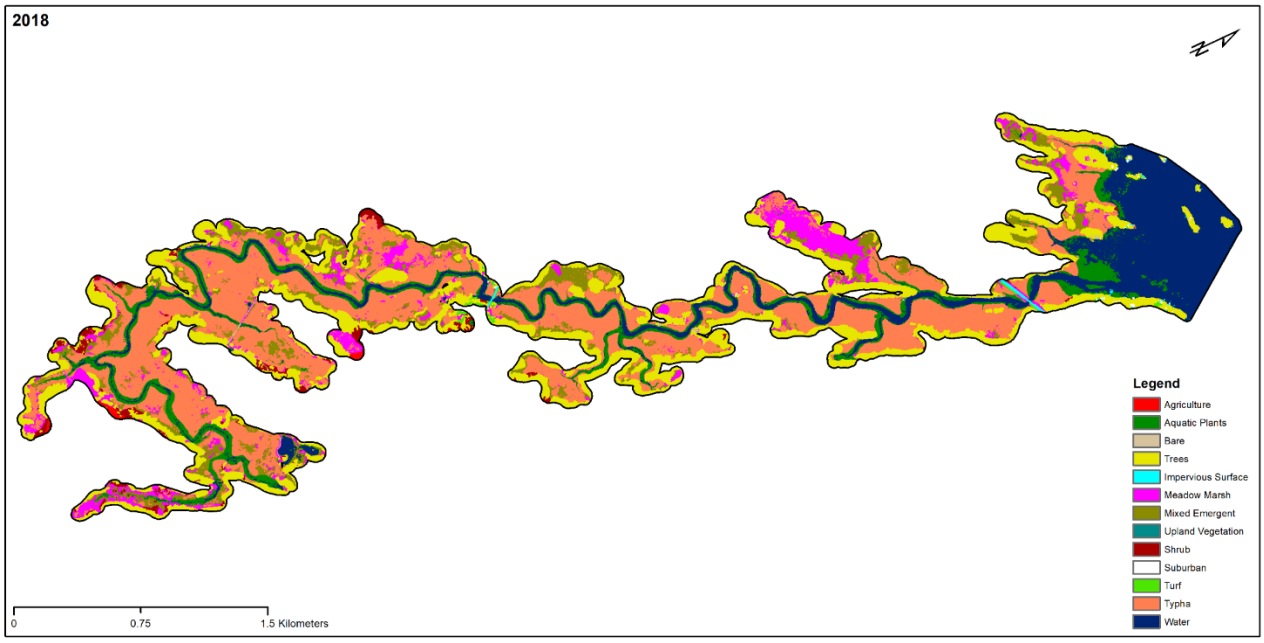

Figure B8. Maximum Likelihood Classifier wetland classification data from the Crooked Creek study area.

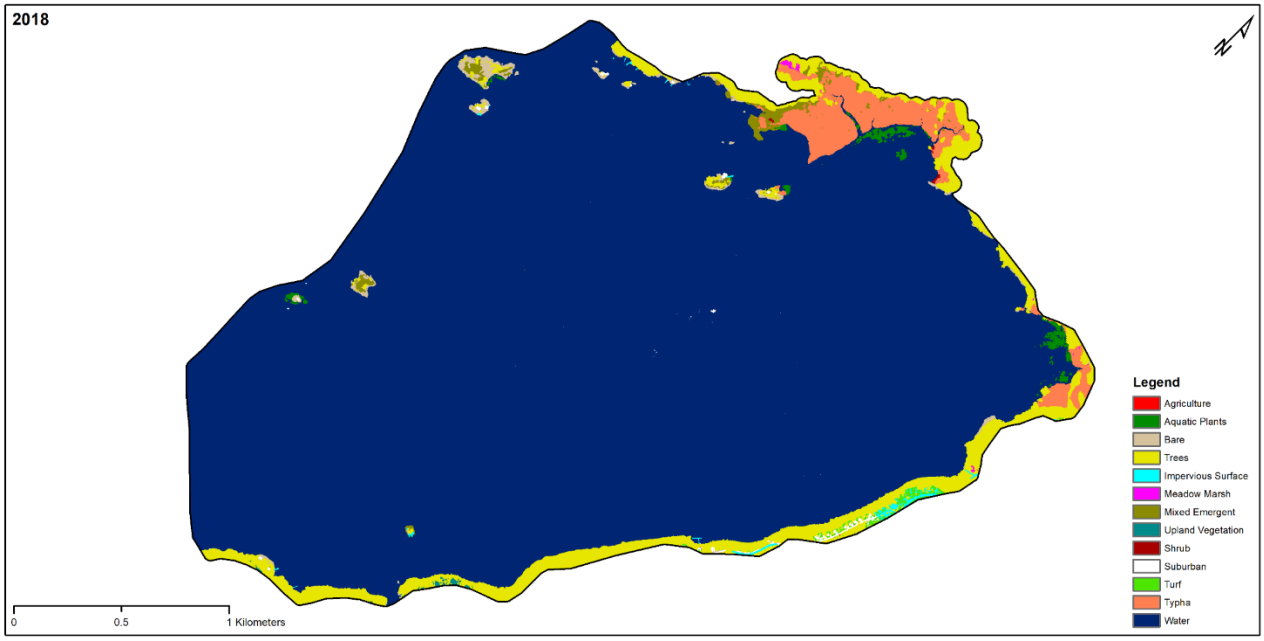


Figure B9. Maximum Likelihood Classifier wetland classification data from the Eel Bay - Flatiron Marsh study area.

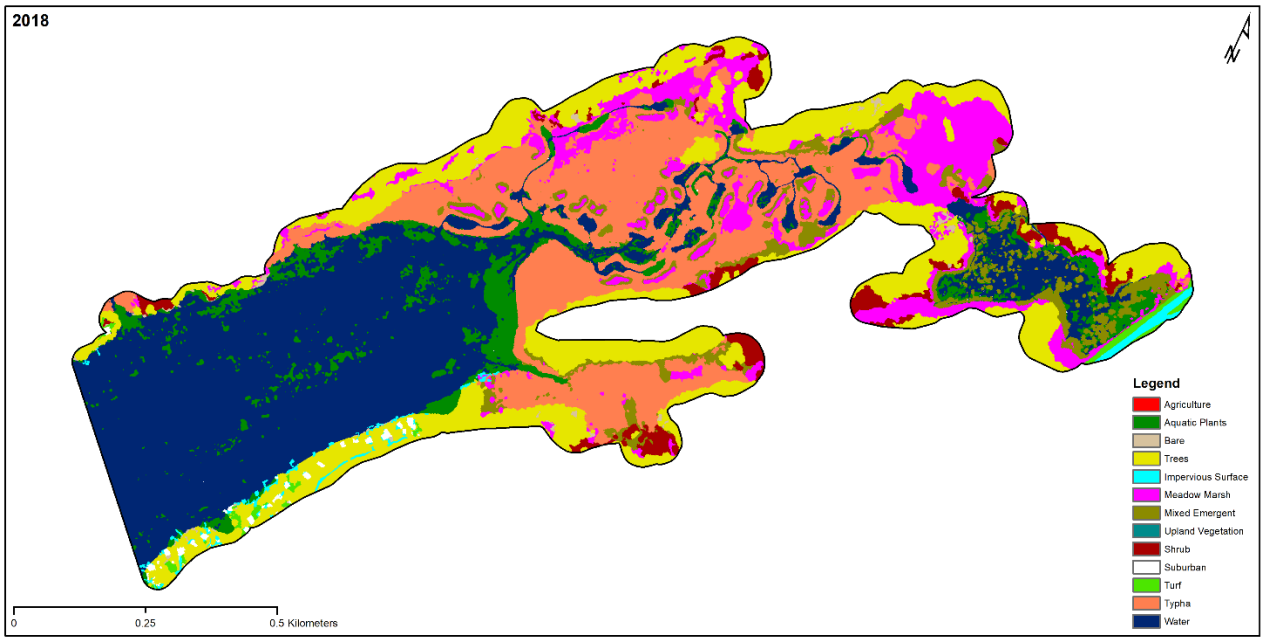

Figure B10. Maximum Likelihood Classifier wetland classification data from the Goose Bay study area.

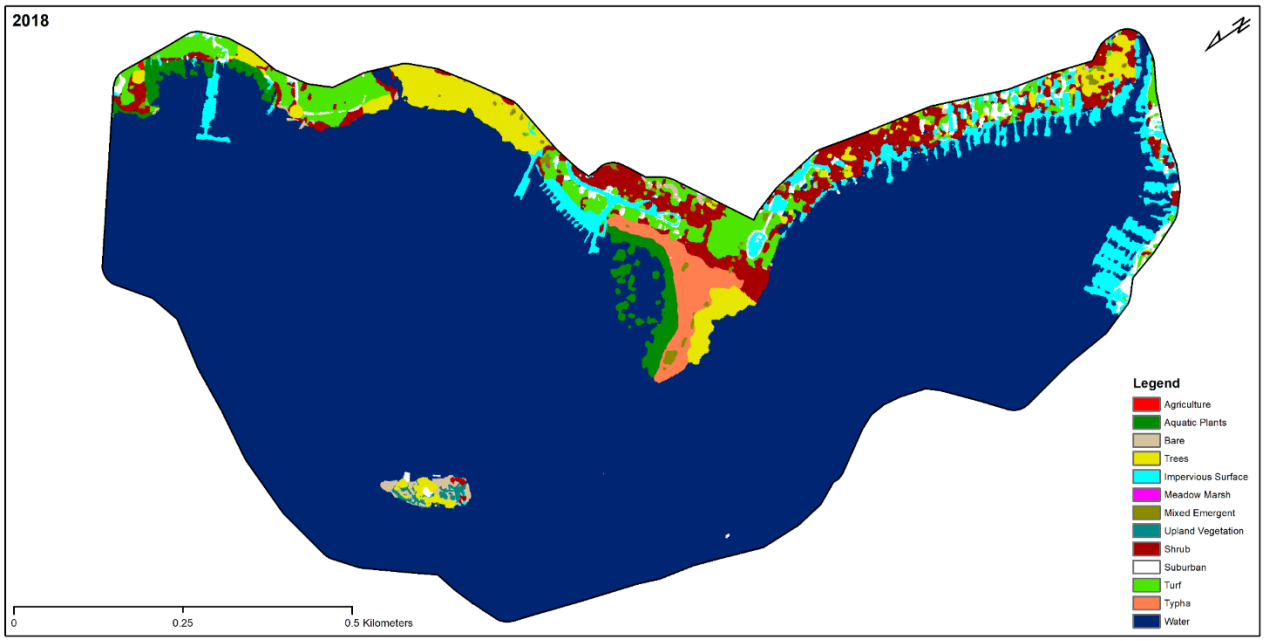


Figure B11. Maximum Likelihood Classifier wetland classification data from the Grass Point study area.

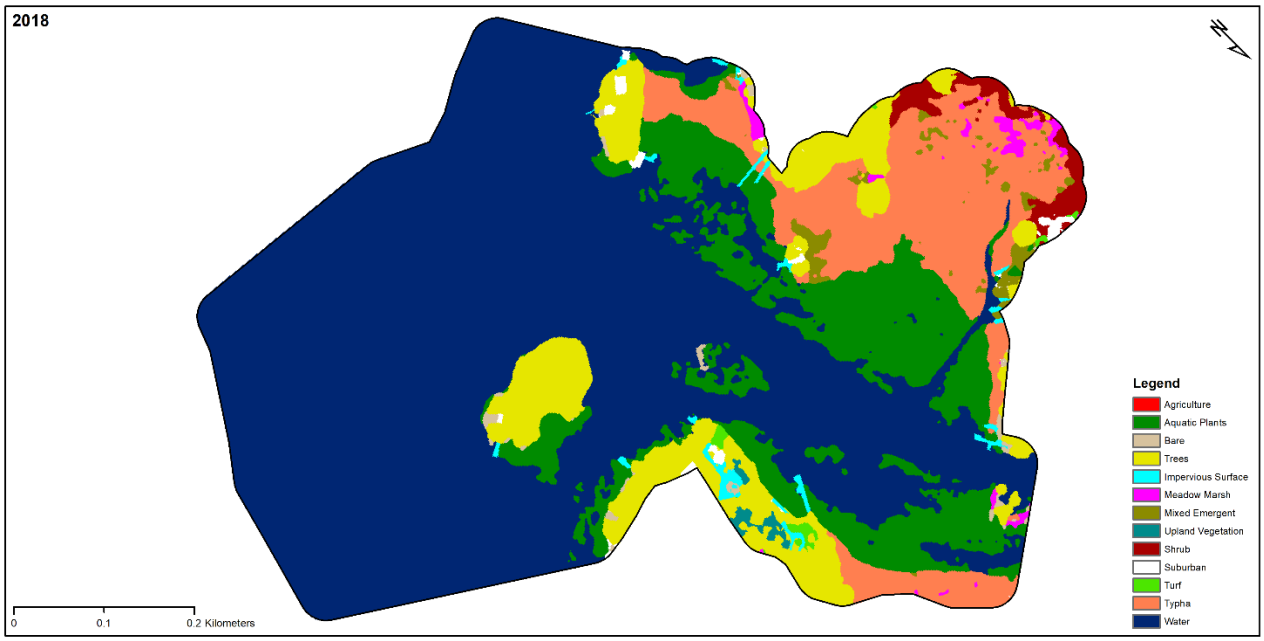


Figure B12. Maximum Likelihood Classifier wetland classification data from the Hill Island West study area.

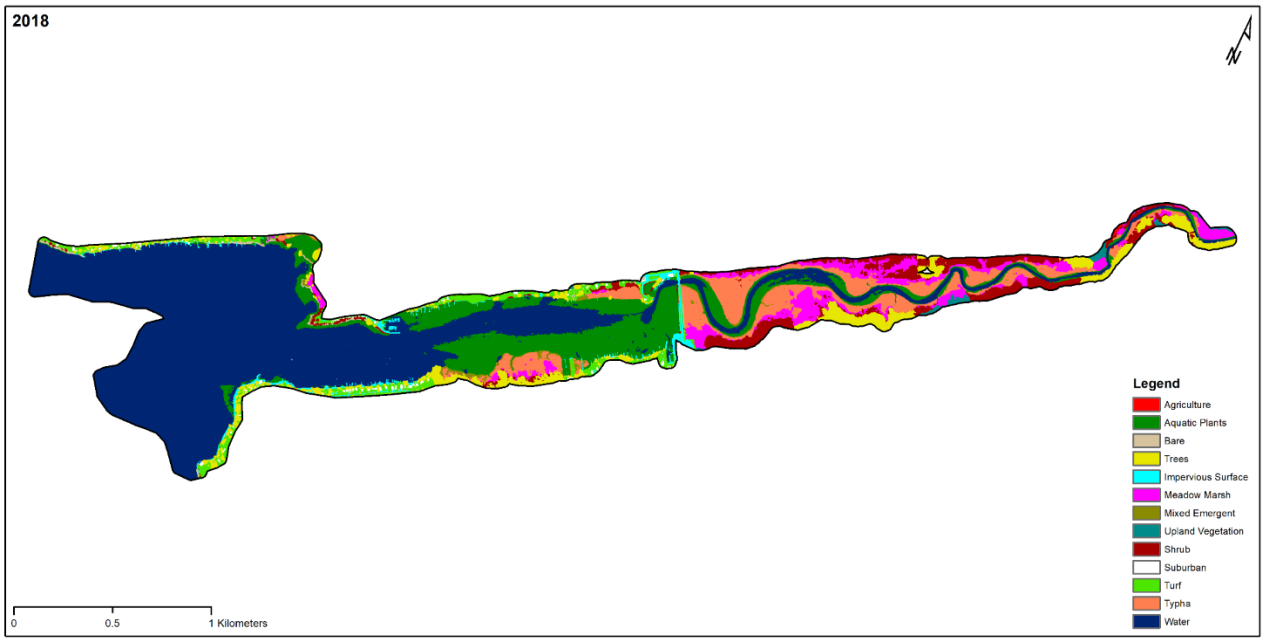


Figure B13. Maximum Likelihood Classifier wetland classification data from the Kents Creek - Mud Bay study area.

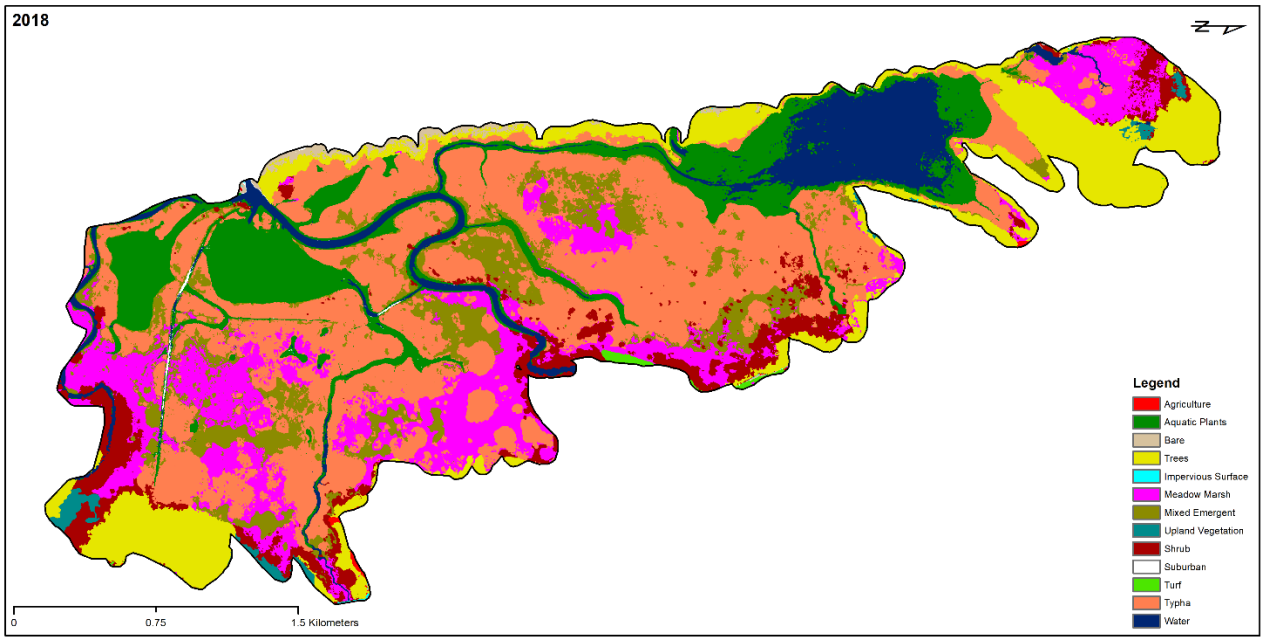


Figure B14. Maximum Likelihood Classifier wetland classification data from the Lakeview Pond - Floodwood Pond study area.

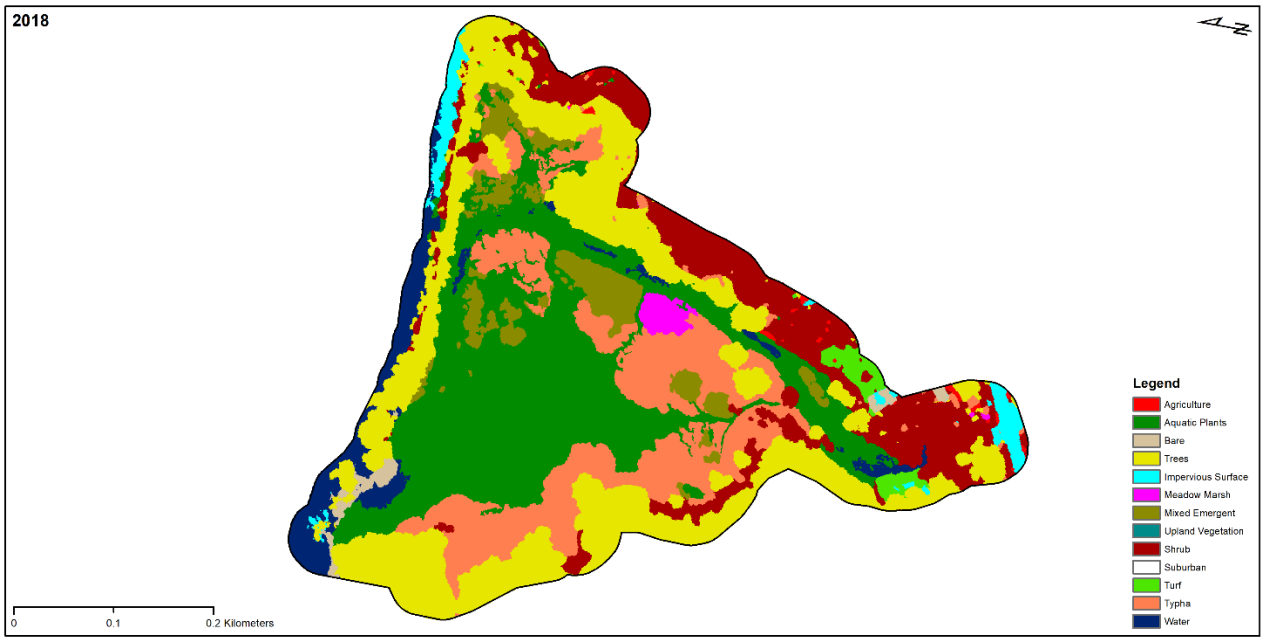


Figure B15. Maximum Likelihood Classifier wetland classification data from the Maxwell Bay study area.

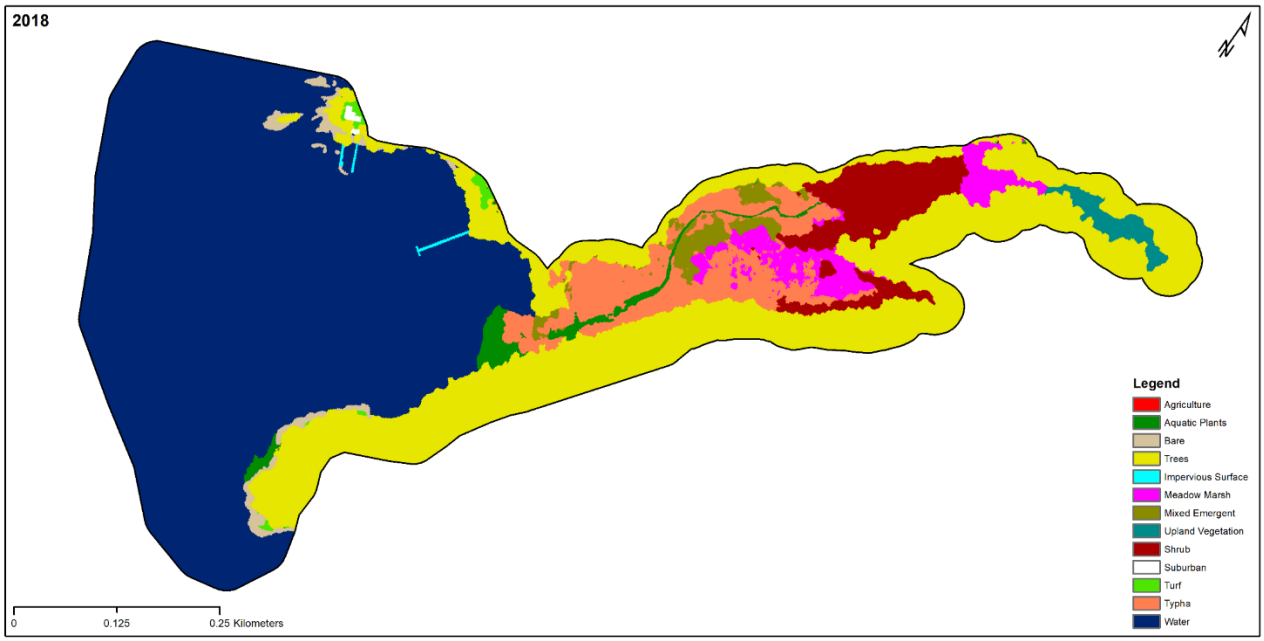

Figure B16. Maximum Likelihood Classifier wetland classification data from the North Buck Bay study area.

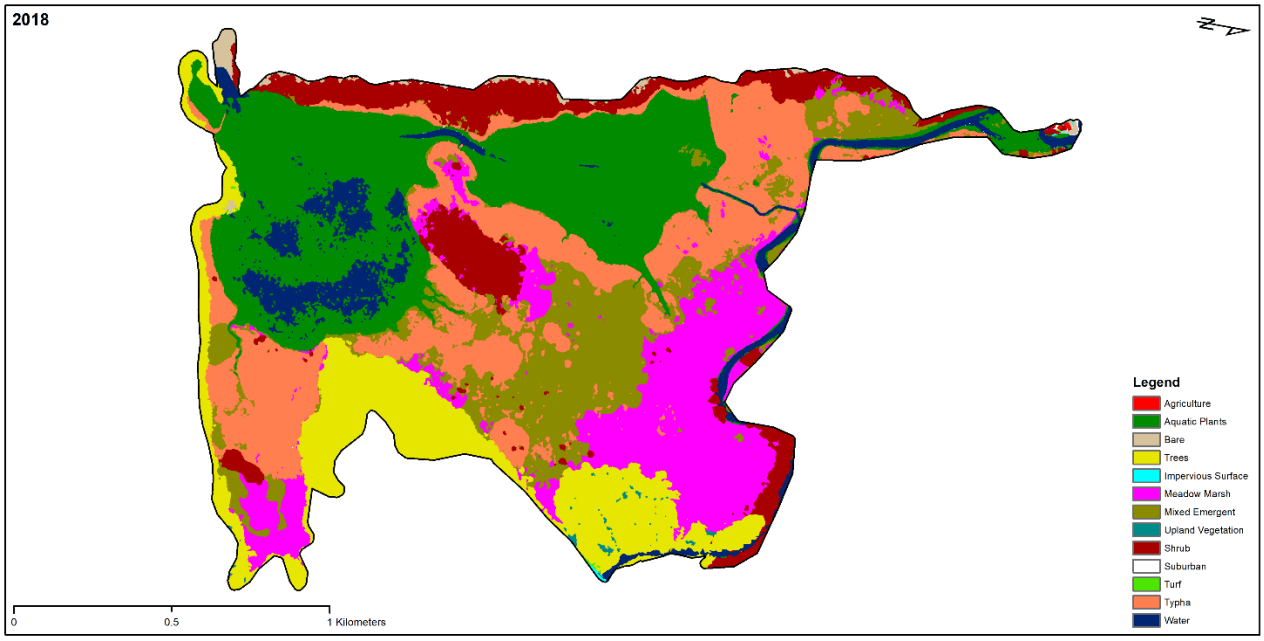


Figure B17. Maximum Likelihood Classifier wetland classification data from the South Colwell Pond – North Colwell study area.

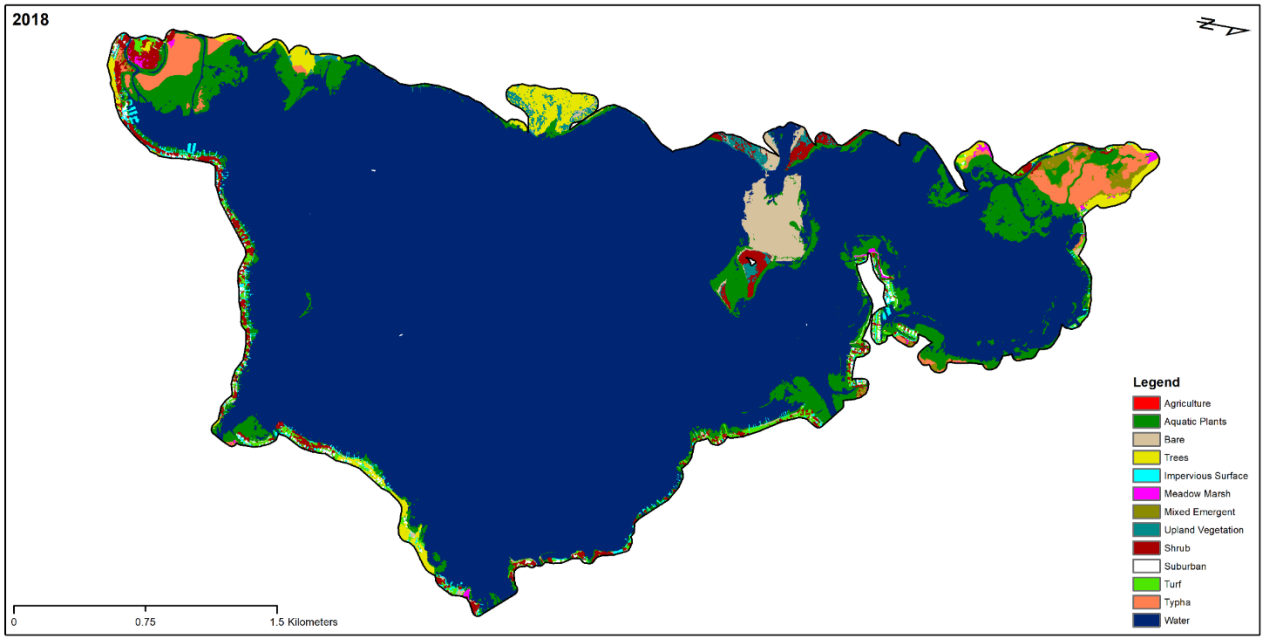


Figure B18. Maximum Likelihood Classifier wetland classification data from the North Pond study area.

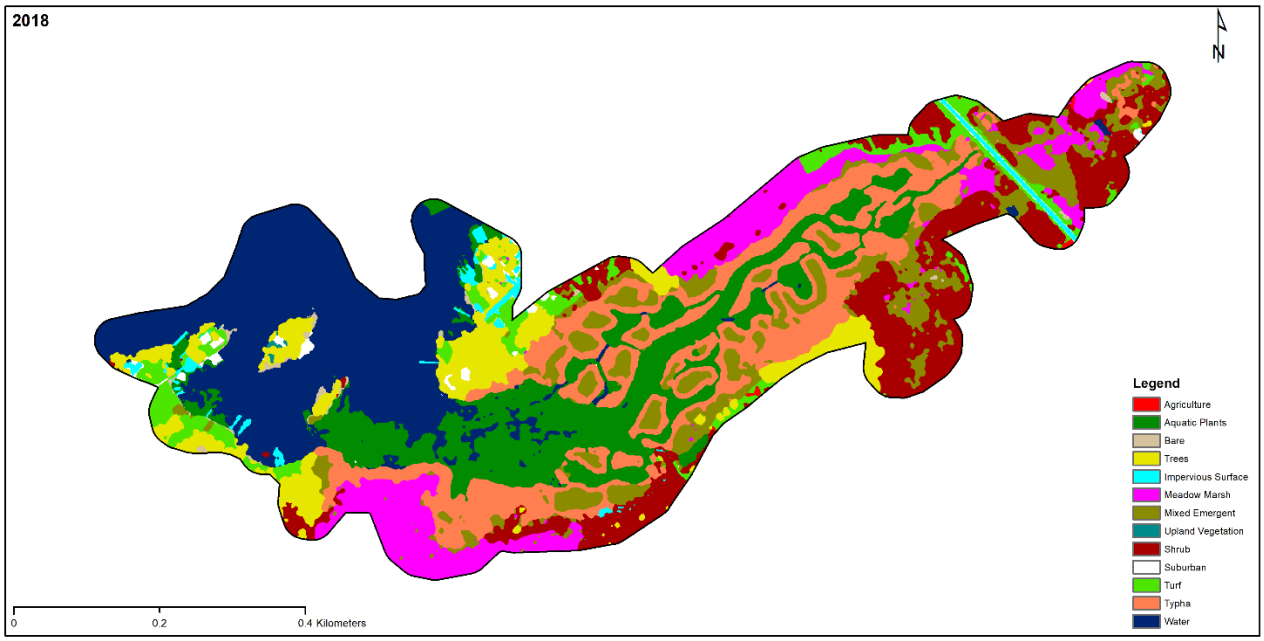


Figure B19. Maximum Likelihood Classifier wetland classification data from the Point Vivian Bay area.

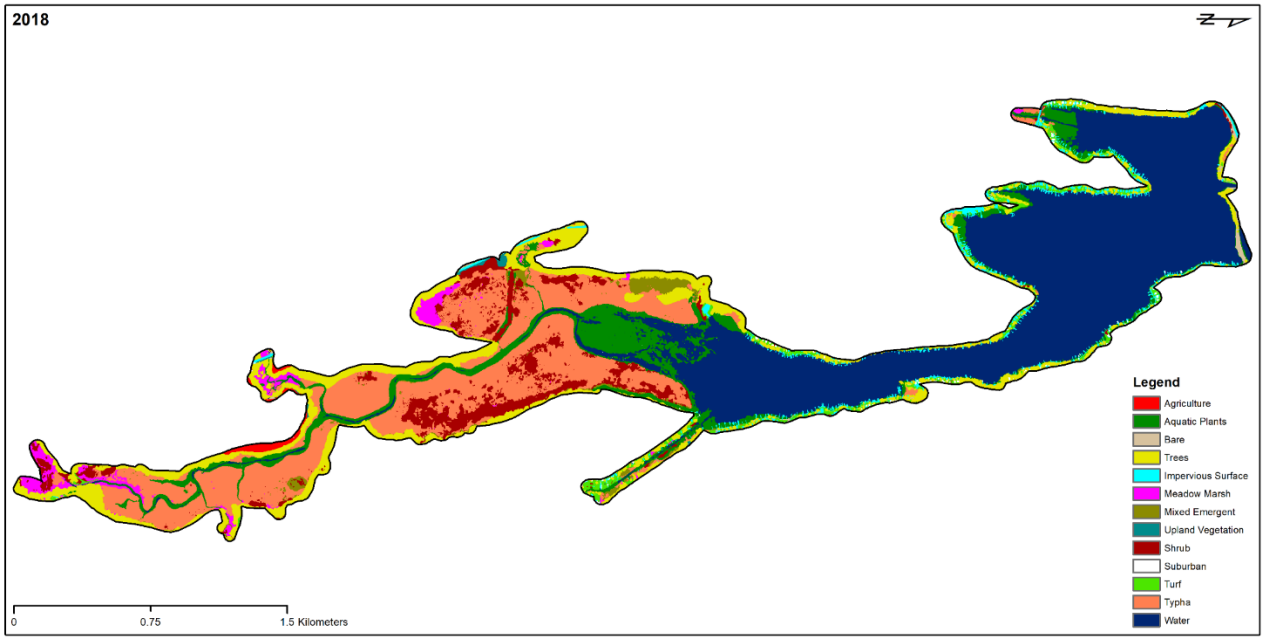


Figure B20. Maximum Likelihood Classifier wetland classification data from the Port Bay study area.

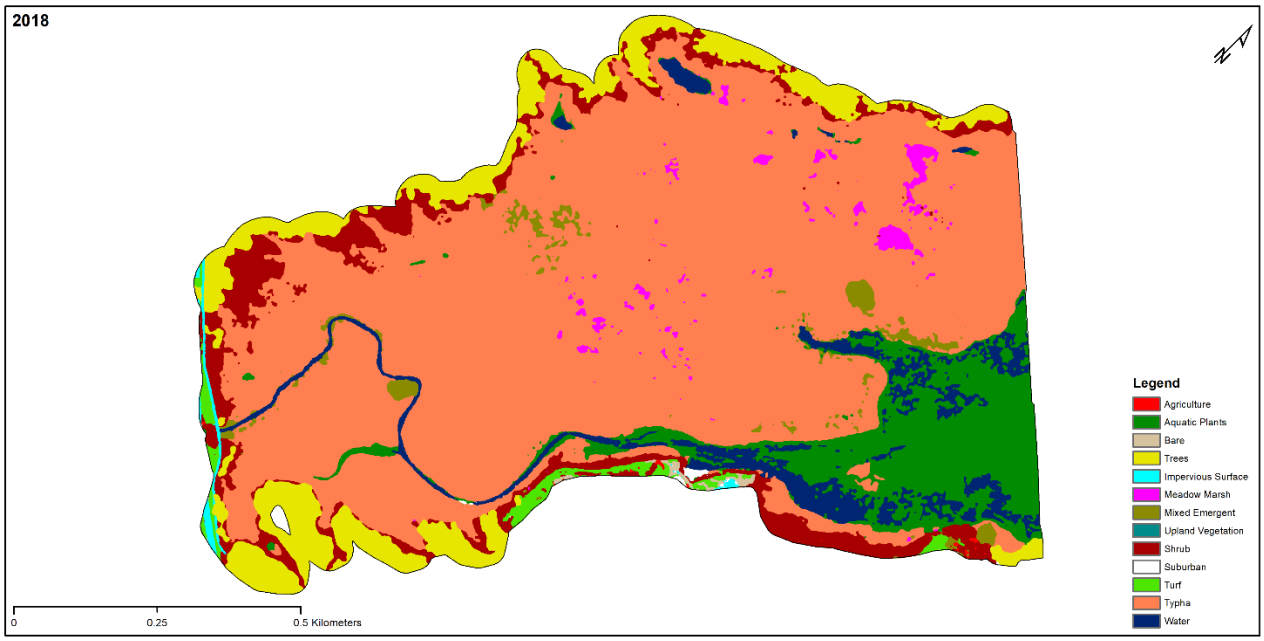


Figure B21. Maximum Likelihood Classifier wetland classification data from the Round Pond study area.

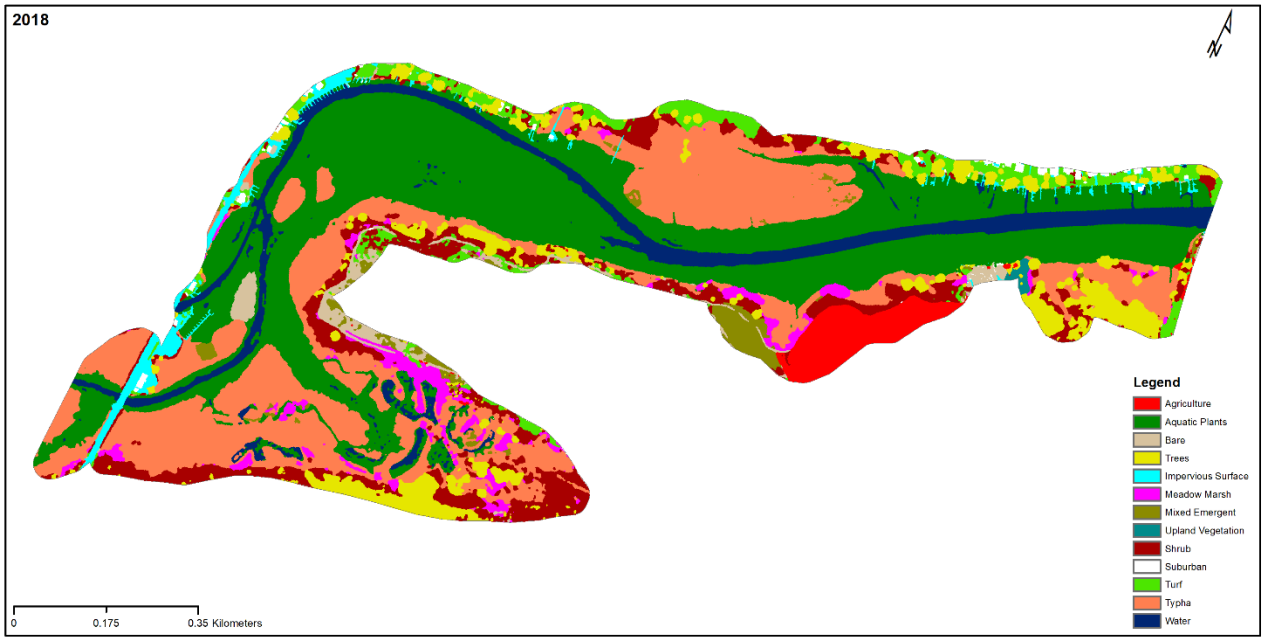


Figure B22. Maximum Likelihood Classifier wetland classification data from the Salmon Creek study area.

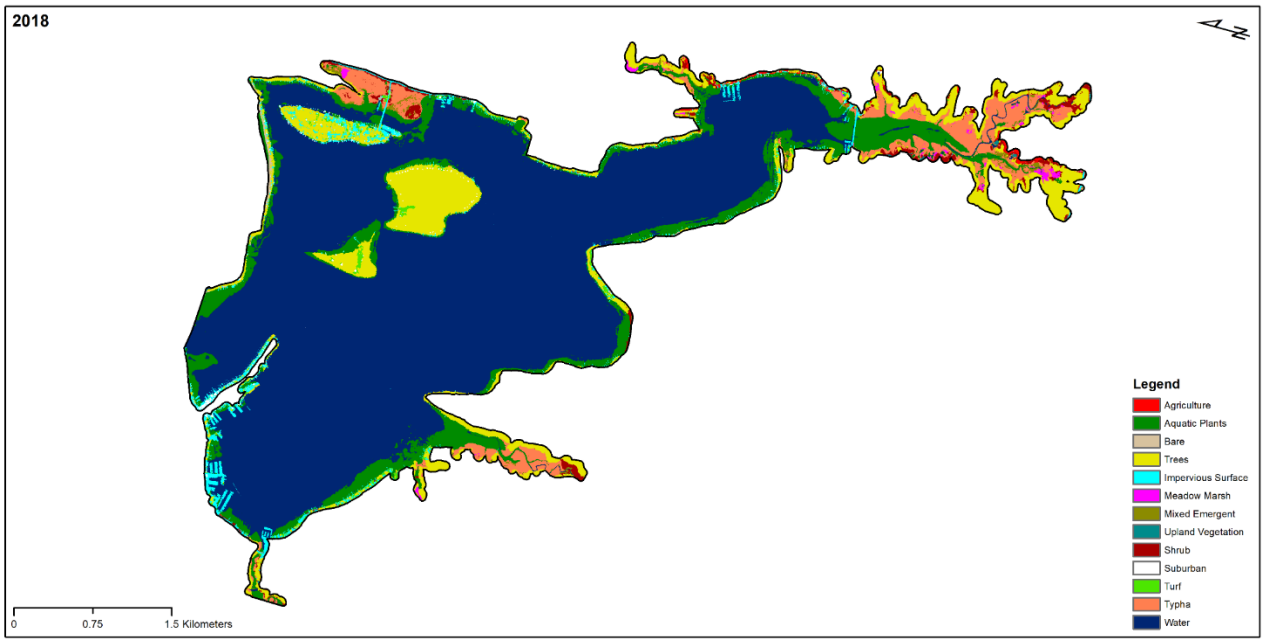


Figure B23. Maximum Likelihood Classifier wetland classification data from the Second Creek study area.

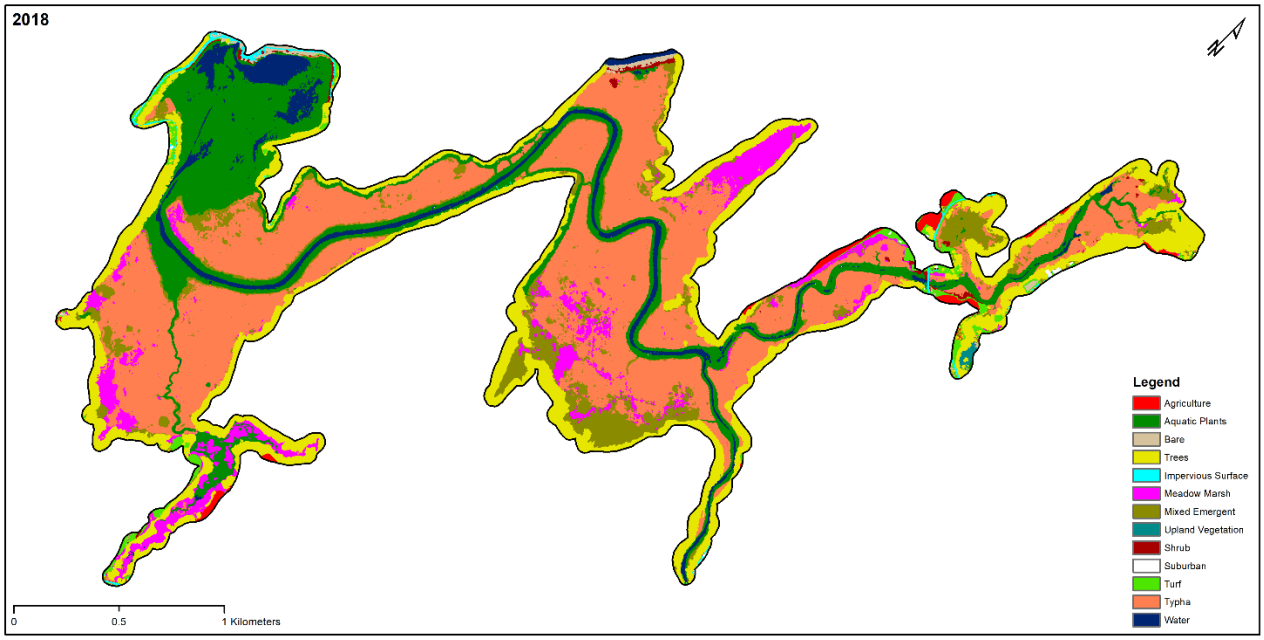


Figure B24. Maximum Likelihood Classifier wetland classification data from the Sterling Creek Wetland study area.

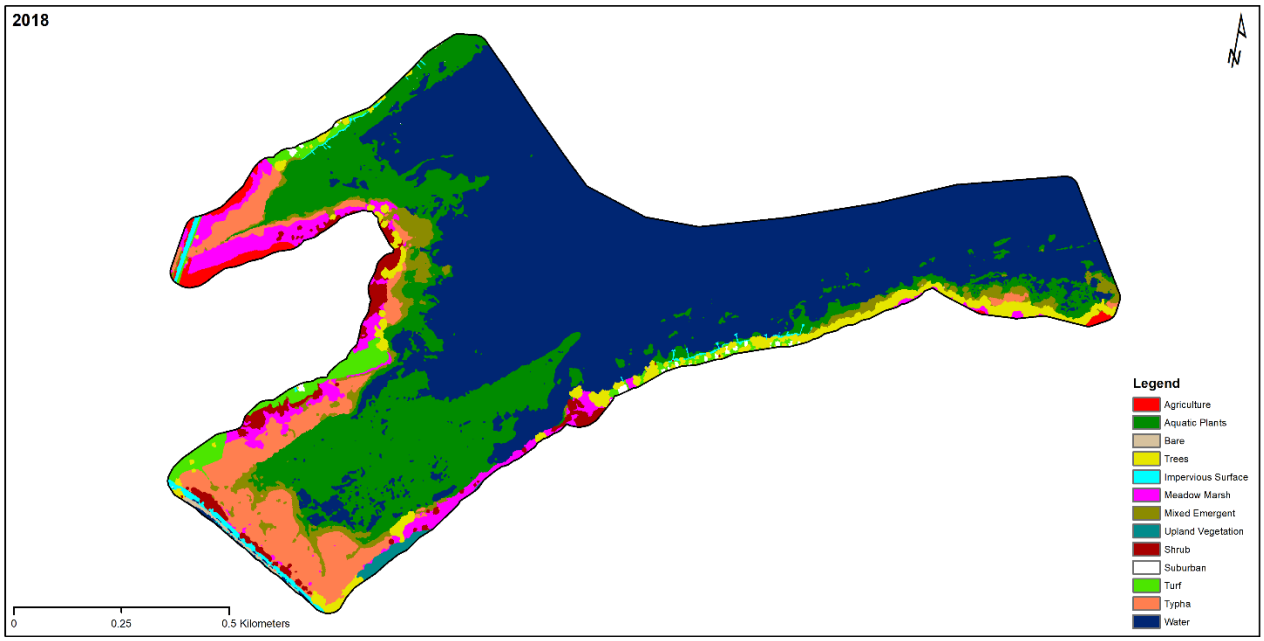


Figure B25. Maximum Likelihood Classifier wetland classification data from the The Isthmus study area.

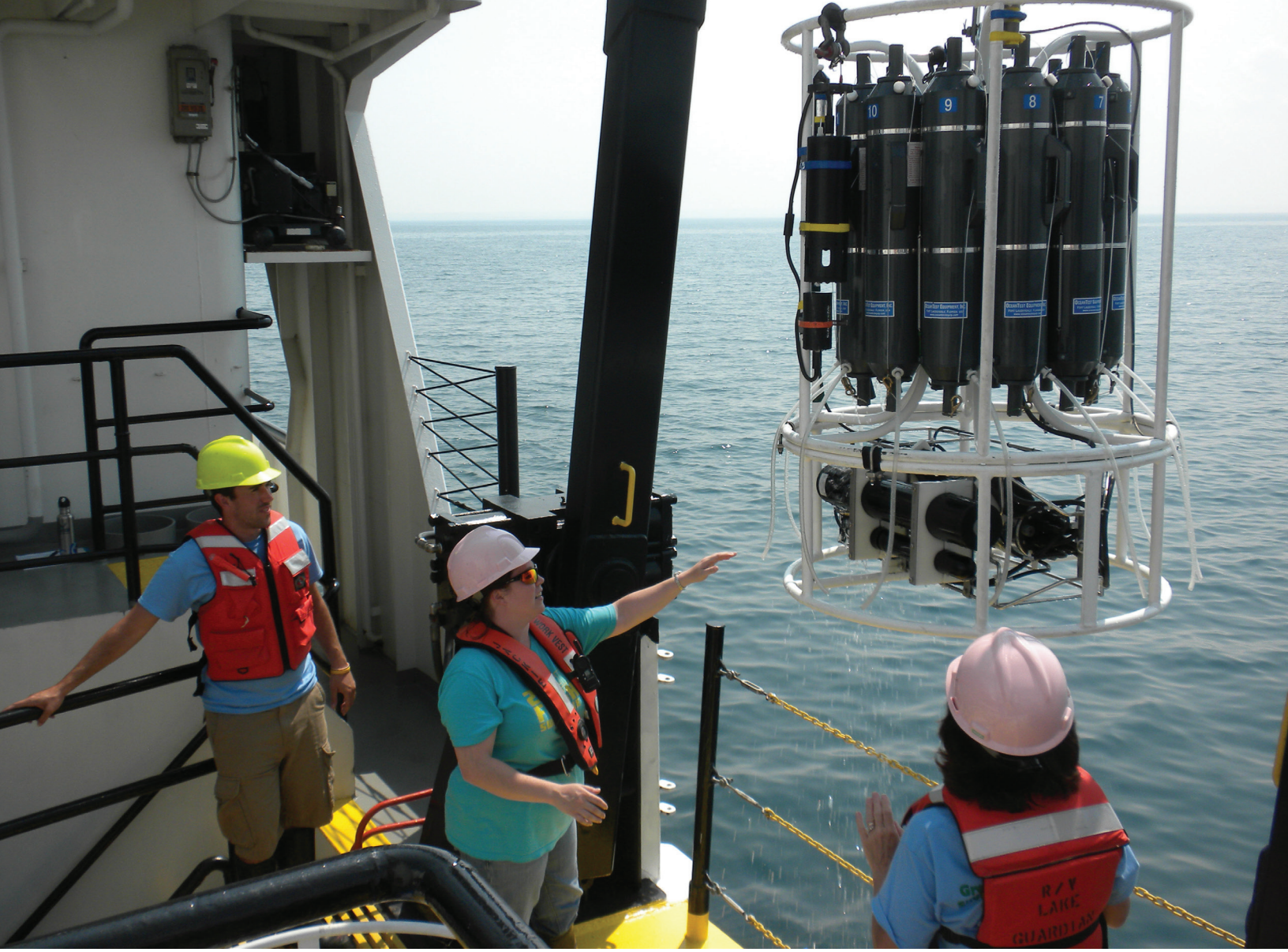


*Photo : Paul C. Focazio/NYSG*